EPRI

Topics:
Spent-fuel storage
Thermal hydraulics models
Heat transfer
Radiation shielding

EPRI NP-4887
Project 2406-4
PNL-5917
UC-85
Interim Report
November 1986

The Castor-V/21 PWR Spent-Fuel Storage Cask: Testing and Analyses

Prepared by
Virginia Power Company
Pacific Northwest Laboratory
and
EG&G Idaho, Idaho National Engineering Laboratory

REPORT SUMMARY

SUBJECTS: Analysis and testing / Waste management / Fuel and core management and development

TOPICS: Spent-fuel storage; Heat transfer; Thermal hydraulics models; Radiation shielding

AUDIENCE: Fuels engineers / R&D scientists

The Castor-V/21 PWR Spent-Fuel Storage Cask: Testing and Analyses

In full-scale tests, the 100-t Castor-V/21 cask proved itself both technically sound and practical for on-site storage of spent PWR fuel—a milestone in the qualification of metal casks for dry storage. Moreover, pretest predictions of the cask's thermal performance demonstrated the accuracy of the advanced HYDRA computer code, soon to be available for utility licensing analyses.

BACKGROUND

Some utilities may have to begin using dry storage systems for spent fuel in the late 1980s, when their present on-site storage basins are full. This testing of the Castor-V/21 cask manufactured by the Gesellschaft fur Nuklear Service is part of a DOE–Virginia Power Company–EPRI demonstration in which large metal casks from three vendors are undergoing performance testing at the Idaho National Engineering Laboratory (INEL).

OBJECTIVES

- To demonstrate the thermal, shielding, and operational performance of the Castor-V/21 cask.
- To demonstrate the ability of the advanced HYDRA computer code to model the cask system and predict its thermal performance.

APPROACH

After 21 spent-fuel assemblies shipped from the Virginia Power Company Surry nuclear power station arrived at INEL, the project team loaded the cask, which they had equipped with temperature and radiation sensors. They ran tests with the cask in both horizontal and vertical positions, with each of three internal environments—vacuum, nitrogen, and helium. Test conditions approached the cask's thermal design limits. Before testing, analysts used the HYDRA heat transfer code, being evaluated at the Pacific Northwest Laboratory, to predict the thermal performance of the cask. After testing, they compared the predictions to the actual measured data and then refined the predictions where appropriate.

RESULTS

The tests showed the Castor-V/21 cask to be well suited to spent-fuel storage. Its heat transfer performance was exceptionally good—peak cladding temperatures in the vertical position were less than the allowable 380°C with both helium and nitrogen backfills and a cask heat load of 28 kW.

The shielding performance of the cask met design expectations except for minor peaks at the sidewall near the top and bottom of the cask.

The HYDRA code accurately predicted both the shapes of the temperature profiles and the actual temperatures: pretest predictions were within 50°C of the test data. The posttest analysis, which corrected for internal dimensional changes and heat transfer conditions at the surface of the cask, agreed to within 25°C.

EPRI PERSPECTIVE

These results represent a major milestone in the qualification of large metal casks for on-site storage of spent nuclear fuel. In addition to confirming the thermal and shielding performance of the Castor-V/21 cask, the tests also showed the handling and loading of these large containers to be a straightforward process that made no unusual demands on personnel or facilities. The testing was also remarkably smooth, despite the involvement of multiple organizations and sites, the employment of complex instrumentation, the shipping of sizable quantities of spent nuclear fuel, and the use of a sophisticated new computer code.

This is the first of six EPRI reports to document large storage cask demonstrations in project RP2406-4. In another part of the same cooperative program, Virginia Power Company has obtained a license to store fuel in the CASTOR-V/21 metal cask at its Surry nuclear power station.

PROJECT

RP2406-4
EPRI Project Manager: Ray W. Lambert
Nuclear Power Division
Contractors: Virginia Power Company; Pacific Northwest Laboratory; EG&G, Idaho National Engineering Laboratory

For further information on EPRI research programs, call EPRI Technical Information Specialists (415) 855-2411.

The Castor-V/21 PWR Spent-Fuel Storage Cask: Testing and Analyses

NP-4887
Research Project 2406-4
PNL-5917
UC-85

Interim Report, November 1986

Prepared by

VIRGINIA POWER COMPANY
Post Office Box 26666
Richmond, Virginia 23261

Principal Investigators
D. Dziadosz
E. V. Moore

PACIFIC NORTHWEST LABORATORY
Battelle Boulevard
Richland, Washington 99352

Principal Investigators
J. M. Creer
R. A. McCann
M. A. McKinnon
J. E. Tanner
E. R. Gilbert
R. L. Goodman

EG&G IDAHO, IDAHO NATIONAL ENGINEERING LABORATORY
550 Second Street
Idaho Falls, Idaho 83415

Principal Investigators
D. H. Schoonen
M. Jensen
C. Mullen

Prepared for

Virginia Power Company

U.S. Department of Energy

and

Electric Power Research Institute
3412 Hillview Avenue
Palo Alto, California 94304

EPRI Project Manager
R. W. Lambert

LWR Fuel and Spent Fuel Storage Program
Nuclear Power Division

ORDERING INFORMATION

Requests for copies of this report should be directed to Research Reports Center (RRC), Box 50490, Palo Alto, CA 94303, (415) 965-4081. There is no charge for reports requested by EPRI member utilities and affiliates, U.S. utility associations, U.S. government agencies (federal, state, and local), media, and foreign organizations with which EPRI has an information exchange agreement. On request, RRC will send a catalog of EPRI reports.

NOTICE

ABSTRACT

A performance test of a Gesellschaft fur Nuklear Service CASTOR-V/21 pressurized water reactor (PWR) spent fuel storage cask was performed. The test was the first of a series of cask performance tests planned under a cooperative agreement between Virginia Power and the U.S. Department of Energy. The performance test consisted of loading the CASTOR-V/21 cask with 21 PWR spent fuel assemblies from Virginia Power's Surry reactor. Cask surface and fuel assembly guide tube temperatures, and cask surface gamma and neutron dose rates were measured. Testing was performed with vacuum, nitrogen, and helium backfill environments in both vertical and horizontal cask orientations. Limited spent fuel integrity data were also obtained.

Results of the performance test indicate the CASTOR-V/21 cask exhibited exceptionally good heat transfer performance which exceeded design expectations. Peak cladding temperatures with helium and nitrogen backfills in a vertical cast orientation and with helium in a horizontal orientation were less than the allowable of 380°C with a total cask heat load of 28 kW. Significant convection heat transfer was present in vertical nitrogen and helium test runs as indicated by peak temperatures occurring in the upper regions of the fuel assemblies. Pretest temperature predictions of the HYDRA heat transfer computer program were in good agreement with test data, and post-test predictions agreed exceptionally well (25°C) with data.

Cask surface gamma and neutron dose rates were measured to be less than the design goal of 200 mrem/hr. Localized peaks as high as 163 mrem/hr were measured on the side of the cask, but peak dose rates of <75 mrem/hr can easily be achieved with minor refinements to the gamma shielding design.

From both heat transfer and shielding perspectives, the CASTOR-V/21 cask can, with minor refinements, be effectively implemented at reactor sites and central storage facilities for safe storage of spent fuel.

ACKNOWLEDGMENTS

The authors acknowledge the support of Virginia Power, the U.S. Department of Energy, the Electric Power Research Institute, EG&G Idaho Inc., the Pacific Northwest Laboratory, Lawrence Livermore National Laboratory, General Nuclear Systems, Inc., and Gesellschaft fur Nuklear Services. The CASTOR-V/21 cask performance test was truly a team effort, and the contributions of the following persons are greatly appreciated.

Technical Management Committee

M. L. Smith, Chairman (VP)
H. S. McKay (VP)
R. W. Lambert (EPRI)
G. H. Beeman (PNL)
J. L. Daily/G. J. Bracken (DOE-RL)

Virginia Power

D. P. Batalo
B. Wakeman
S. M. Bowman
W. A. Peterson
J. Miller
N. Wolfhope
J. G. Fisher

DOE Headquarters

D. Shelor

DOE Richland

P. A. Craig

EPRI

R. F. Williams

LLNL

H. W. Culham
C. F. Smith
V. M. Oversby

DOE Idaho

C. P. Gertz
M. W. Fisher

PNL

C. M. Heeb
D. F. Newman
L. E. Wiles
A. J. Currie

EG&G Idaho, Inc.

G. R. Rodman
L. R. Makey
N. Wilde

GNS

H. Baatz
H. Geiser
D. Rittscher
D. Maitling
J. Migenda

GNSI

V. J. Barnhart
R. T. Anderson
K. R. Kingsley

CONTENTS

ILLUSTRATIONS

TABLES

EXECUTIVE SUMMARY

This report documents a heat transfer and shielding performance test conducted on a Gesellschaft fur Nuklear Service (GNS) CASTOR-V/21 pressurized water reactor (PWR) spent fuel storage cask. Performance testing was conducted, under a cooperative agreement program between Virginia Power (VP) and the U.S. Department of Energy (DOE), by the Pacific Northwest Laboratory (PNL) operated by Battelle Memorial Institute, the Idaho National Engineering Laboratory (INEL) operated by EG&G Idaho, Inc., and VP. The Electric Power Research Institute (EPRI) participated in the cooperative cask testing program via a separate agreement with Virginia Power. Testing was performed at INEL's Test Area North (TAN) cask testing facility and consisted of pretest preparations, performance testing, and post-test activities. Pretest preparations included conducting cask-handling dry (cold) runs and characterizing PWR spent fuel assemblies from VP's Surry Nuclear Power Plant. The performance test matrix included five runs consisting of two cask orientations and three backfill environments. Post-test activities included crud collection and video and photographic scans of selected fuel assemblies.

The CASTOR-V/21 PWR spent fuel storage cask consists of a nodular cast-iron body. The cast-iron/graphite material exhibits good strength and ductility and provides effective gamma shielding. The cask is 4.9 m (16 ft) long and 2.4 m (8 ft) in diameter and weighs approximately 100 tons when loaded with unconsolidated PWR spent fuel. Two concentric rows of polyethylene rods are incorporated in the cask wall to provide neutron shielding. The external surface consists of heat transfer fins oriented circumferentially around the cask surface. The fuel basket within the cask is configured to hold 21 PWR spent fuel assemblies and is constructed of stainless steel and borated stainless steel for criticality control. The Surry spent fuel assemblies used during testing are of a standard Westinghouse 15x15 rod design. The cask is closed with two lids having both elastomer and metallic O-rings to seal the cask cavity from the environment.

Dry (cold) runs of cask handling and fuel loading with a nonirradiated dummy fuel assembly were performed before the Surry spent fuel was loaded in the cask. The objectives of the dry runs were to gain operational experience and to finalize

handling and test procedures. Each dry run was conducted successfully without unusual problems or significant modifications to the cask or handling equipment.

The Surry PWR spent fuel assemblies were characterized using in-basin ultrasonic examinations and video scans. After testing, selected fuel assemblies were videotaped and photographed, and smear samples were collected. The results of these examinations revealed no indication of any failed fuel before or after the CASTOR-V/21 cask performance test.

Based on pretest ORIGEN2 predictions, fuel assembly decay heat generation rates totaled approximately 28 kW at the start of testing and 27 kW at the end of testing (Table S-1). Thirteen of the twenty-one fuel assemblies had decay heat rates near 1 kW; the remaining eight assemblies had decay heat rates of approximately 1.8 kW at the start of the month-long test. The fuel assemblies were loaded in the cask with the hot assemblies in the outer regions of each quadrant, as seen in Figure S-1. Pretest heat transfer predictions using the HYDRA computer program indicated that peak cladding temperatures in nitrogen and helium would be below or near 380°C. The selected fuel loading pattern was predicted to create a relatively flat radial temperature profile across the basket during testing.

Table S-1

SURRY PWR SPENT FUEL CHARACTERISTICS

Assembly	Burnup, GWd/MTU	Cooling Time, Months	Initial Enrichment, wt%	Sept. 1985 Pred. Decay Heat, kW	
				Start	End
V04, V08, V12, V24	31.1	46	2.91	1.00	0.98
V05	31.5	46	2.91	1.02	0.99
T03, T07, T08, T09, T11, T12, T13, T16	35.7	46	3.11	1.11	1.09
V11, V13, V14, V15	29.8	26	2.91	1.79	1.72
V01, V09, V25, V27	30.2	26	2.91	1.83	1.75
			Total	28.4	27.5

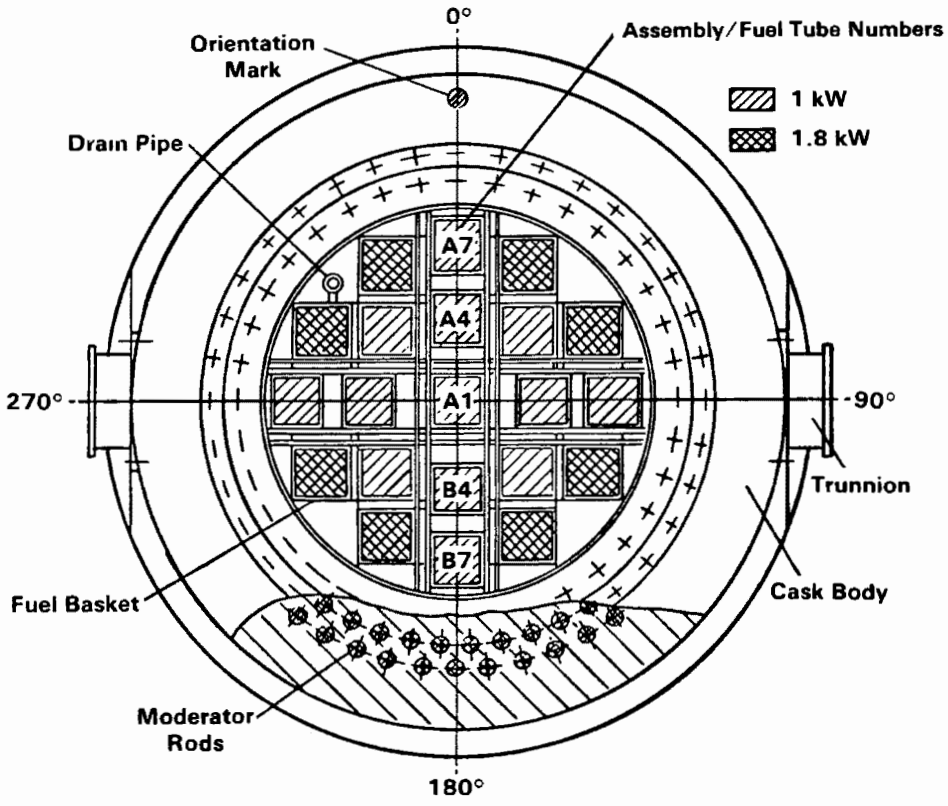

Figure S-1. CASTOR-V/21 Cask Cross Section

Figure S-2 shows the predicted axial decay heat profile assumed for each of the Surry assemblies. Measured axial power profiles for the Surry assemblies were not available for predicting axial decay heat profiles of the assemblies used in the CASTOR-V/21 cask performance test. Axial gamma radiation scans previously obtained on Turkey Point reactor fuel assemblies were used to predict an assembly axial burnup distribution. The Turkey Point and Surry reactors and spent fuel are Westinghouse PWR designs and are essentially the same. ORIGEN2 was used with the assembly axial burnup distribution and the Surry operating history to determine the predicted axial decay heat profile shown in Figure S-2. The dips in the decay heat profile are due to grid spacers. Axial decay heat profiles are important in the placement of fuel rod temperature instrumentation and as input to heat transfer computer codes because they strongly affect the shape of measured axial fuel temperature profiles.

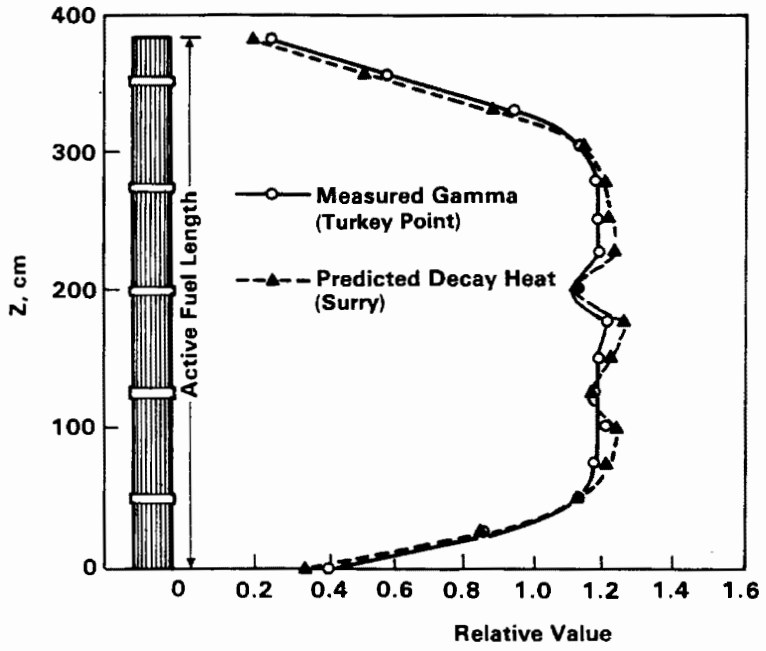

Figure S-2. Measured Gamma and Predicted Decay Heat Axial Profiles

The outer surface of the cask was instrumented with 35 thermocouples (TCs), 69 gamma dose rate sensors, and 69 neutron dose rate sensors. Sixty TCs contained in ten lances (tubes) were inserted through the cask lid into fuel assembly guide tubes or basket void spaces. Of the ten TC lances, eight with six TCs each were inserted into fuel assembly guide tubes, and two with six TCs each were positioned in basket void spaces, as shown in Figure S-3.

The cask test matrix included assessments of performance with a full load of fuel (21 assemblies), vertical and horizontal cask orientations, and vacuum, nitrogen, and helium backfill environments. The test matrix and corresponding measured peak guide tube temperatures and estimated peak cladding temperatures are presented in Table S-2. Peak cladding temperatures were estimated by using calculated guide tube-to-hot rod temperature differences from the HYDRA computer program.

Table S-2 indicates that in a vertical cask orientation with nitrogen and helium backfills, peak cladding temperatures were less than the 380°C allowable. This was also the case for the horizontal helium test run. The vertical vacuum and horizontal nitrogen test runs resulted in peak cladding temperatures over 380°C, but not exceeding 425°C. None of the peak temperatures occurred in the high decay heat

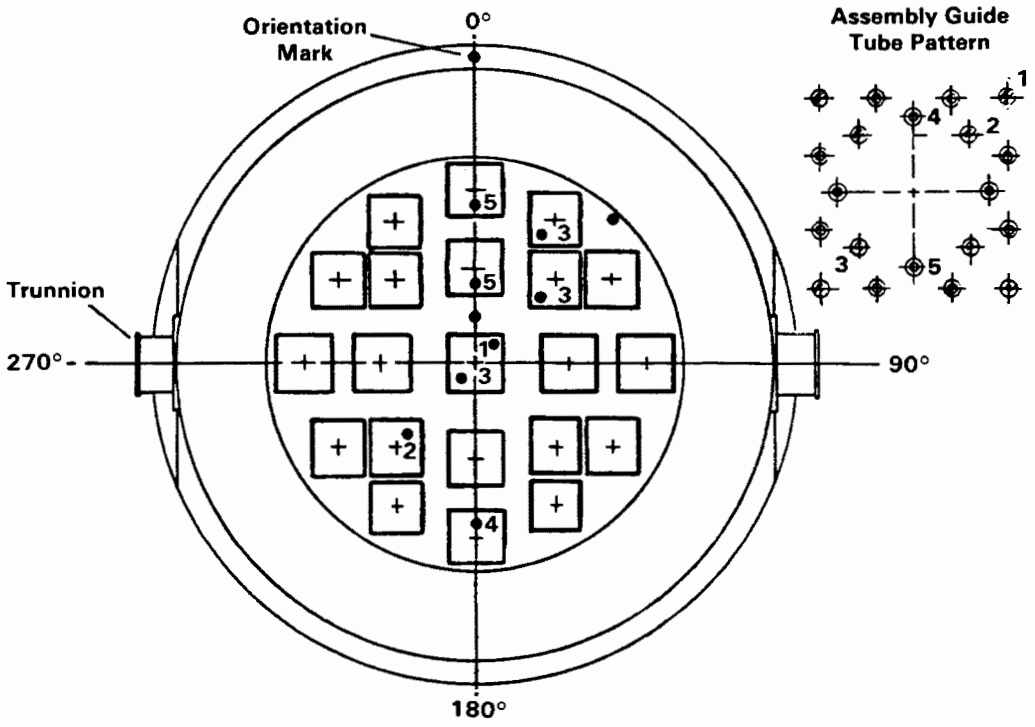

Figure S-3. Thermocouple Lance Locations

Table S-2

CASTOR-V/21 CASK TEST MATRIX AND PEAK TEMPERATURES

Run No	Loading	Orientation	Backfill	Cask Heat Load, kW	Ambient Temp, °C	Measured Guide Tube Temp, °C	Estimated Peak Clad. Temp, °C
1	Full	Vertical	Helium	28.4	27	347	352
2	Full	Vertical	Nitrogen	28.4	24	358	368
3	Full	Vertical	Vacuum	28.4	25	414	424
4	Full	Horizontal	Helium	28.4	24	360	365
5	Full	Horizontal	Nitrogen	28.4	24	395	405

(1.8-kW) outer assemblies (Figure S-1). In general, the cask heat transfer performance was concluded to be exceptionally good because it exceeded design expectations with the peak temperature in helium, when the cask was dissipating approximately 28 kW, being less than that specified for the cask operating limit of 21 kW in the cask topical safety analysis report.

Axial and radial temperature profiles for the five test runs are shown in Figures S-4 and S-5. Attention should be given to data points only, because their corresponding lines are provided for clarity and do not necessarily represent actual profiles. The axial profiles are for the hot center assembly, and the radial profiles are for the axial location at which the temperatures peak in a vacuum and in a horizontal orientation. The axial profiles vividly show the effects of convection in nitrogen and helium in a vertical orientation where peak temperatures are skewed toward the top of the cask. This is in spite of the fact that the density of helium is much less than that of nitrogen; i.e., buoyancy forces in helium are substantially less than they are in nitrogen. Note that the peak temperature in the vertical helium run is not significantly lower than the peak temperature in nitrogen. This suggests that convection in nitrogen may effectively compensate for the relatively high thermal conductivity (five times that of nitrogen) of helium. The

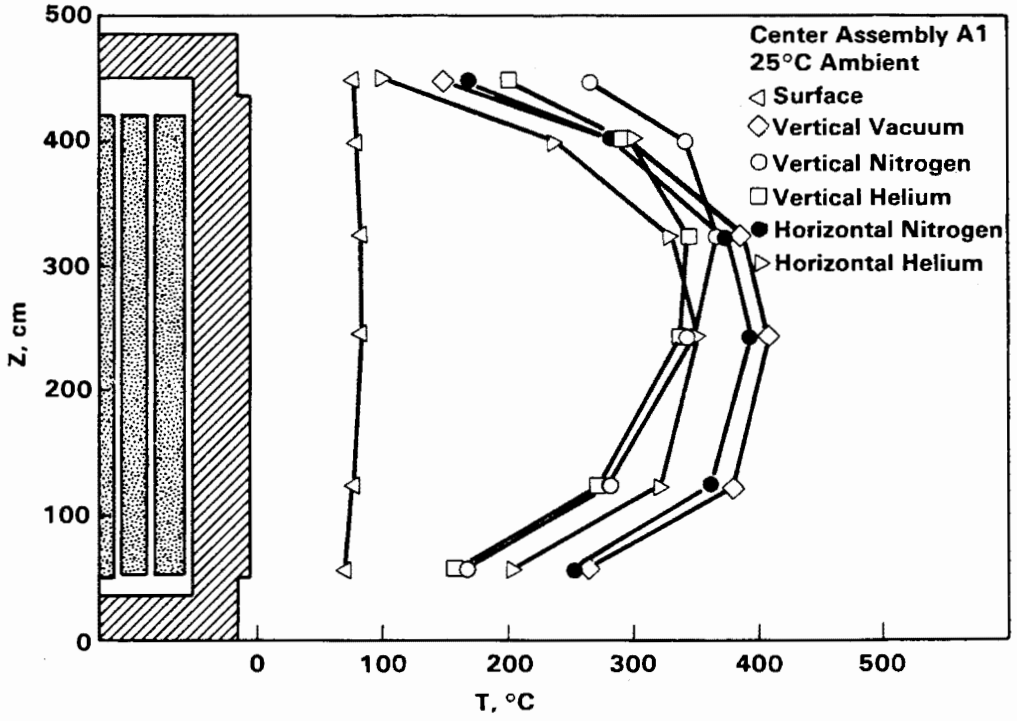

Figure S-4. Center Assembly Axial Temperature Profiles

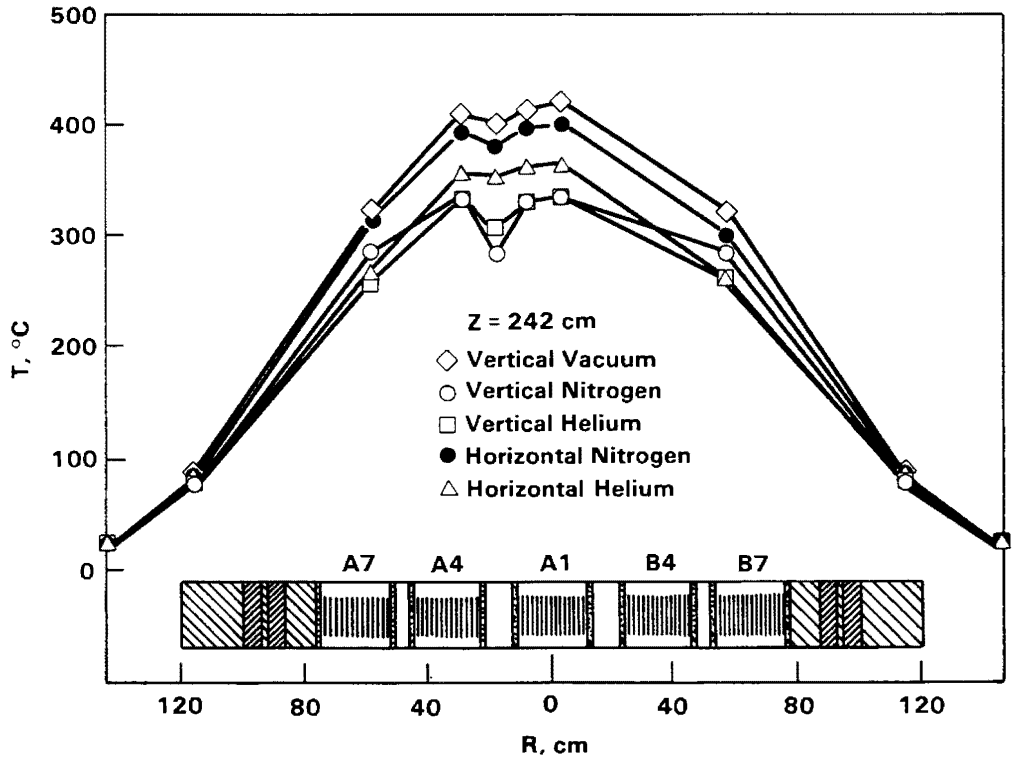

Figure S-5. Radial Temperature Profiles

indication of significant convection in the CASTOR-V/21 cask implies that the basket design permits convection, which is obvious from the relatively "open" design indicated in Figures S-1 and S-3.

Symmetry with respect to the predicted axial decay heat profile over the length of the fuel assemblies in the vertical vacuum and all horizontal axial temperature profiles indicates that axial convection in these runs was negligible (Figure S-4). These profiles are similar to the axial gamma and decay heat profiles previously presented in Figure S-2. The lack of axial convection in vacuum and horizontal runs is reasonable because significant density gradients cannot usually develop in a vacuum or in an orientation with low axial gravitational forces.

Radial temperature profiles for the five test runs shown in Figure S-5 indicate relatively flat profiles across the fuel assemblies, and significant temperature differences between the outer fuel assemblies and the inner cask wall. Predictions from the HYDRA heat transfer computer code confirm that most of the temperature drop exists from outer fuel assemblies to the inner cask wall. HYDRA predictions also

indicate the basket-to-inner wall gap may be important to the heat transfer performance of the cask because temperature gradients across the gap of 8°C/mm in helium and 48°C/mm in nitrogen and vacuum were predicted.

Temperature differences from assemblies A1 and A4 to the gas adjacent to their fuel tubes are seen to be greater in vertical helium and nitrogen test runs than in the vertical vacuum or horizontal runs. This indicates that significant gas flow occurred outside assembly fuel tubes in a vertical orientation (convection heat transfer was significant) and that axial gas flow was relatively low (overall heat transfer by radiation and/or conduction was relatively more important than convection) in vacuum and all horizontal test runs.

The HYDRA heat transfer code was used to select spent fuel assemblies, determine the loading pattern, and identify optimal TC locations. Selected HYDRA pre- and post-test predictions are shown in Figures S-6 and S-7 for vertical test runs. The pretest HYDRA prediction of the axial profile for the helium run is lower (35°C) than data (Figure S-6). In contrast, predictions for nitrogen and vacuum backfills are higher than data by as much as 45°C and 60°C, respectively. The shapes of the temperature profiles are reasonably good for all three backfill environments.

After the test was completed, it was determined that the basket-to-inner cask wall gap approached zero during testing instead of the 1.5 mm (0.059 in.) assumed for the pretest analysis. Changing the gap thickness to essentially zero, adjusting the external surface convection heat transfer coefficient, and including flow resistances of numerous support plates located between basket fuel tubes (Figure S-1) resulted in the post-test predictions shown in Figure S-6. All post-test temperature predictions agree with experimental test data within 25°C.

Pre- and post-test radial temperature predictions are presented in Figure S-7. Both sets of predictions are in satisfactory agreement with the test data and the post-test predictions agree well (25°C) with the data.

Predictions of horizontal nitrogen and helium test data compared with measured temperatures in a manner similar to the way predictions of vertical nitrogen and helium data compared to measured temperatures.

Gamma and neutron dose rates on the top, side, and bottom of the cask are shown in Figures S-8, S-9, and S-10. Only data points should be considered because the corresponding lines are provided for clarity and do not represent actual profiles.

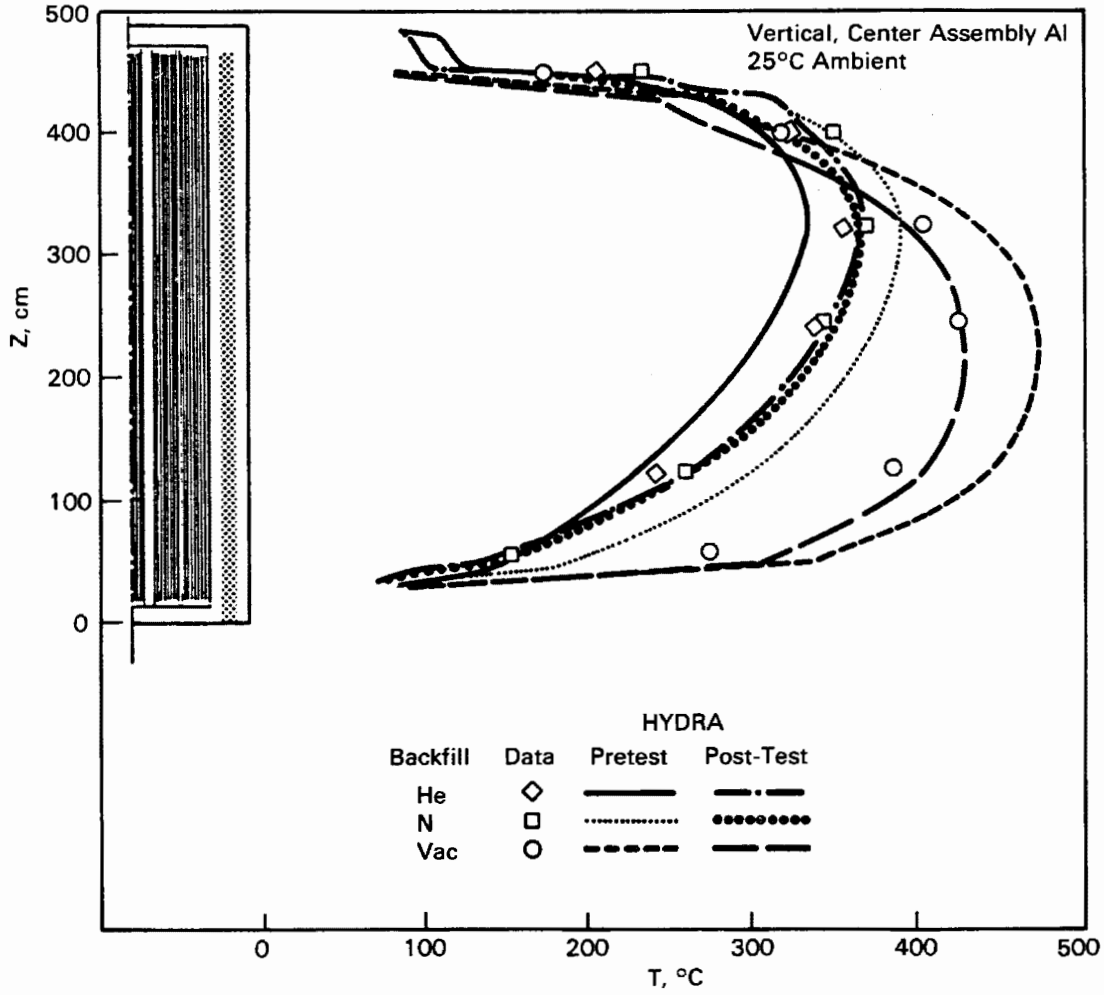

Figure S-6. Pre- and Post-Test Axial Temperature Profile Predictions Compared to Vertical, Vacuum, Nitrogen, and Helium Data

The radiation source strength was higher for the test fuel than fuel considered in the cask topical safety analysis report. A peak gamma dose rate of 56 mrem/hr was measured on the top of the primary lid (Figure S-8) at 90 degrees (the outer lid was not used during testing). The total dose rate (gamma plus neutrons) was approximately 85 mrem/hr at the center of the primary lid. When the secondary lid (90 mm, 3.5 in. thick) is used on the cask during normal operation, these dose rates should be reduced significantly.

The total dose rates along most of the cask side were less than 50 mrem/hr (Figure S-9). There were localized peaks in the gamma and neutron dose rates of up to

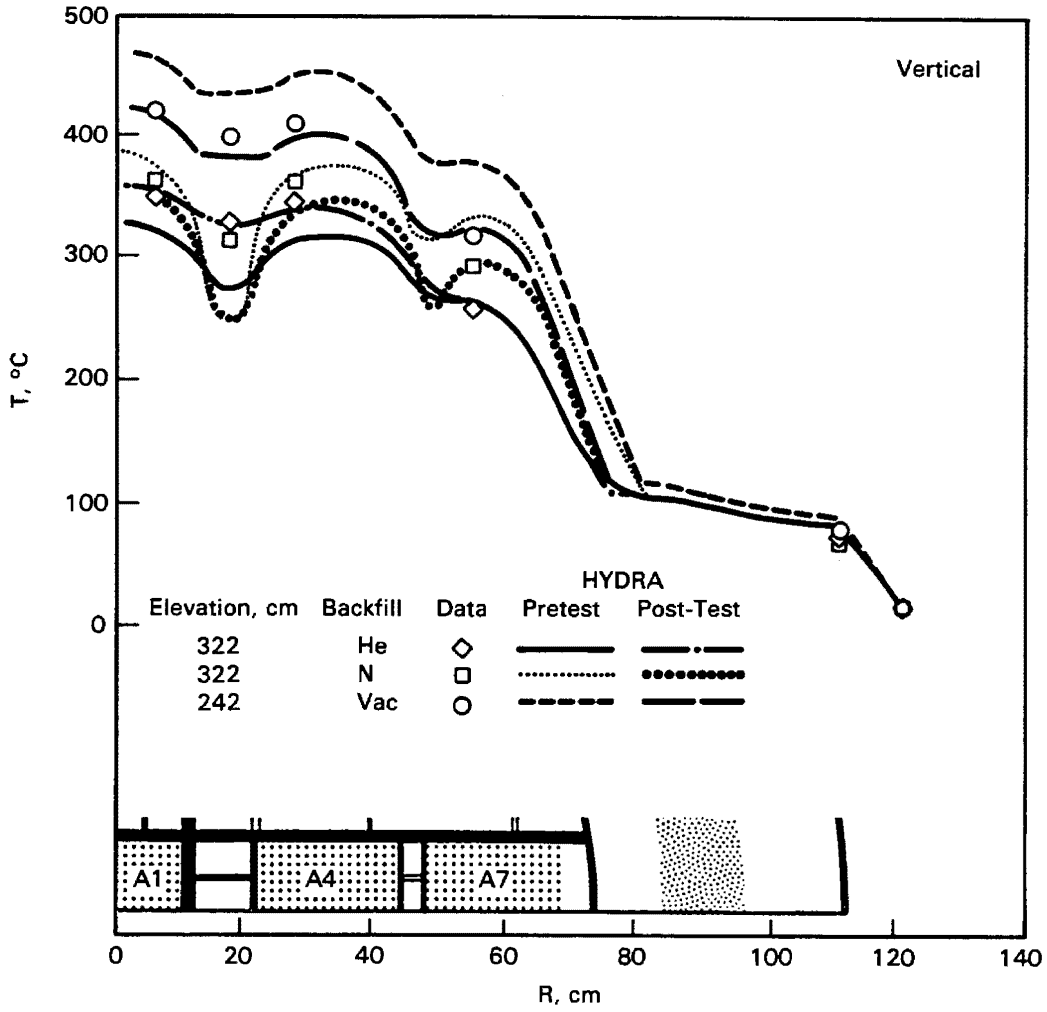

Figure S-7. Pre- and Post-Test Radial Temperature Profile Predictions Compared to Vertical, Vacuum, Nitrogen, and Helium Data

140 mrem/hr and 21 mrem/hr, respectively. The neutron dose rate peaks were relatively low, but the gamma peaks were substantial. The localized peaks occurred at locations adjacent to fuel assembly upper and lower end fittings. However, minor refinements in the gamma shielding design at locations corresponding to the dose rate peaks could reduce the gamma peaks significantly.

Dose rates on the bottom of the cask (Figure S-10) peaked at the center (65 mrem/hr total), but were relatively low and uniform on the remainder of the surface. These relatively low dose rates were not of concern when the cask was oriented horizontally.

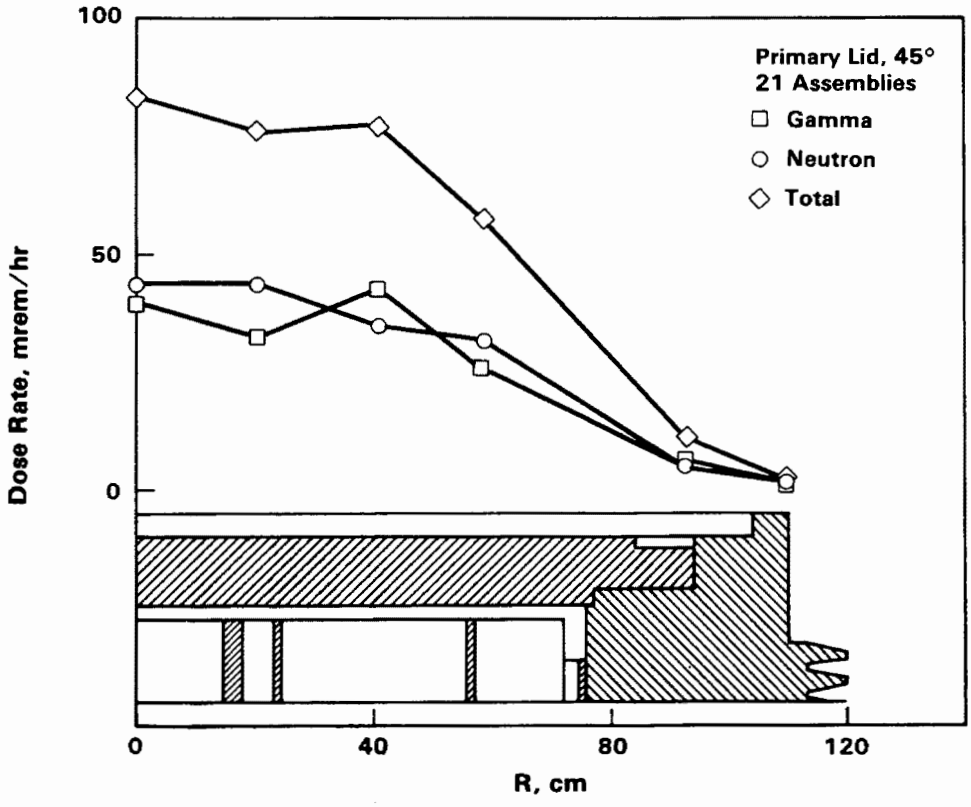

Figure S-8. Gamma and Neutron Dose Rates on Cask Primary Lid

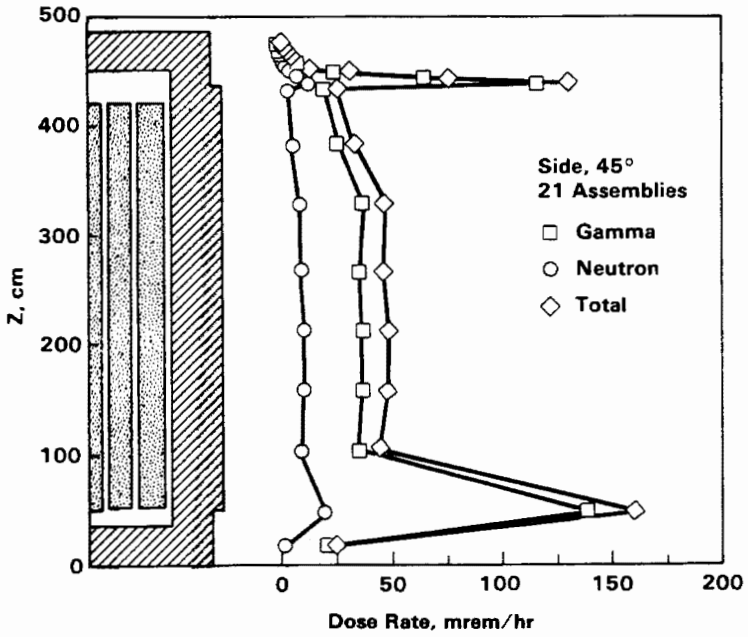

Figure S-9. Gamma and Neutron Dose Rates on Cask Side

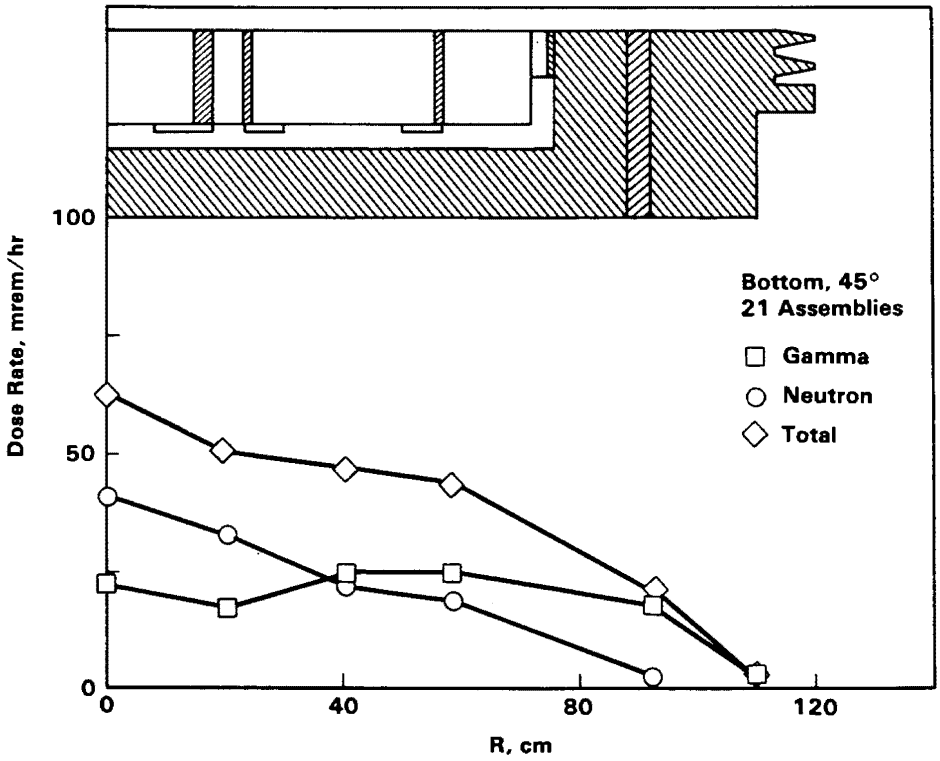

Figure S-10. Gamma and Neutron Dose Rates on Cask Bottom

The overall shielding performance of the CASTOR-V/21 cask was good and met the intended design goal of $\leq$200 mrem/hr, even though the test fuel had a higher source strength than fuel considered in the topical safety analysis report. With a very minor refinement in the gamma shielding design, total dose rates can easily be reduced to less than 75 mrem/hr.

After cask testing was completed, selected fuel assemblies were videotaped and photographed, and smear samples were taken. No unusual anomalies were observed on any of the selected assemblies; however, eight indications of cracks were observed in the CASTOR-V/21 basket. The observed indications had no effect on the ease with which fuel assemblies could be removed or inserted in the basket. Figure S-11 identifies the locations of the crack indications.

The test basket was designed to have a relatively tight fit to provide a precise alignment that would permit the TC lances to pass through the primary lid and into fuel assembly guide tubes. GNS performed a thermal stress analysis of the basket and concluded that the basket expanded and came in contact with the inner wall of the cask (Gap 2). Also, the fuel tubes containing the outer assemblies adjacent to

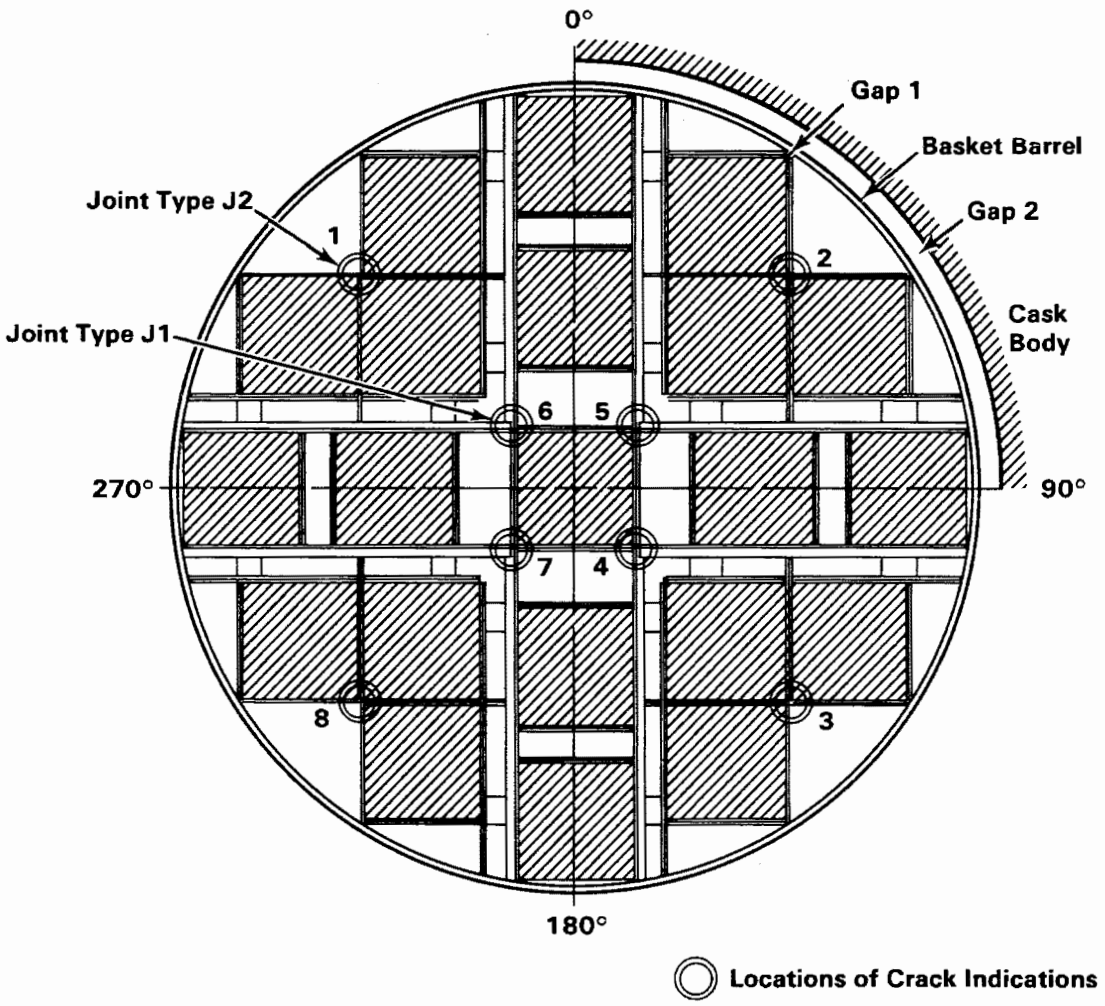

Figure S-11. CASTOR-V/21 Basket Crack Indication Locations

the quadrant bisectors came in contact with the basket barrel (Gap 1). An examination of the measured temperatures, HYDRA temperature predictions, and associated differential thermal expansion between the basket and cask body substantiates the GNS analysis. The cracks in the basket welds did not result in adverse safety implications because the cracked welds have minimal structural requirements.

The cask performance test demonstrated that the CASTOR-V/21 cask could be satisfactorily handled and loaded dry. It was concluded that the heat transfer performance of the cask was exceptionally good and exceeded design expectations. Peak cladding temperatures with helium and nitrogen backfills in a vertical cask orientation and with helium in a horizontal orientation were less than the allowable of 380°C with a total cask heat load of 28 kW. The shielding performance of the cask met design expectations ($\leq$200 mrem/hr), and cask surface dose rate peaks of <75 mrem/hr can

easily be achieved with minor refinements in the gamma shielding design. From both heat transfer and shielding perspectives, the CASTOR-V/21 cask can, with minor refinements, be effectively implemented at reactor sites and central storage facilities for safe storage of spent fuel.

Section 1

INTRODUCTION

Implementation of spent fuel dry storage systems may be required in the late 1980s when several at-reactor storage basins attain maximum capacity (1). The Nuclear Waste Policy Act of 1982 (NWPA) assigns the U.S. Department of Energy (DOE) the responsibility for assisting utilities with their spent fuel storage problems. An additional provision of the NWPA is that DOE, in cooperation with the private sector, enter into demonstration programs of spent fuel dry storage systems at nuclear power reactor sites. The objective of the cooperative demonstrations is to establish one or more storage technologies that the U.S. Nuclear Regulatory Commission (NRC) may, by rule, approve for use at civilian reactor sites without the need for additional site-specific approvals by the NRC. In addition, the NWPA authorizes DOE to establish a research and development (R&D) program at federally-owned facilities as part of the cooperative demonstrations to collect data necessary to assist utilities in their licensing activities.

In May 1983, a solicitation for Cooperative Agreement Proposal (SCAP) was issued to the private sector by DOE-Richland Operations Office (DOE-RL) and proposals were received in August 1983. Virginia Power (VP) proposed that pressurized water reactor (PWR) spent fuel storage cask performance testing be conducted at a federal site in support of their at-reactor licensed demonstration. Virginia Power and DOE signed a Cooperative Agreement in March 1984, and VP signed a separate agreement with the Electric Power Research Institute (EPRI), essentially establishing a three-party cooperative agreement.

A preliminary assessment of candidate federal sites capable of performing dry storage system tests was undertaken by the Pacific Northwest Laboratory (PNL) in parallel with the issuance and response to the SCAP. The three sites evaluated were Idaho, Nevada, and Hanford. In July 1984, DOE selected the Test Area North (TAN) facility located at the Idaho National Engineering Laboratory (INEL) operated by EG&G Idaho, Inc., as the federal cask testing facility, and the VP/DOE cask performance testing effort was initiated.

The primary objective of PWR spent fuel storage cask performance testing to be performed at TAN is to obtain heat transfer and shielding data and limited spent fuel integrity data needed to support VP's at-reactor licensing efforts at its twin Surry reactors. Spent fuel with decay heat generation rates near cask design limits are to be used when practical. Other objectives of the testing effort are to provide data to other utilities; gain cask-handling experience; identify candidate cask design improvements; and obtain heat transfer and shielding data for computer code evaluations.

The technical baseline of the cooperative agreement for cask performance testing at TAN to accomplish the objectives is to test three different cask designs with unconsolidated spent fuel and two of the cask designs with consolidated fuel. Unconsolidated fuel cask testing is planned in 1985 and 1986, and consolidated fuel testing is planned in 1987 and 1988. This report documents the first test using unconsolidated fuel in a CASTOR-V/21 cask designed and manufactured by Gesellschaft fur Nuclear Service (GNS) of the Federal Republic of Germany.

The work began with a revision to TAN's safety analysis documents to permit dry loading of unconsolidated PWR fuel in the CASTOR-V/21 cask. Dry (cold) runs with a nonirradiated dummy fuel assembly were performed to gain operating experience and finalize handling and test procedures. The PWR spent fuel assemblies were ultrasonically examined and videotaped in the Surry reactor basin to ensure integrity. The CASTOR-V/21 cask was delivered to TAN and 21 PWR assemblies were shipped from Surry to TAN using Transnuclear TN-8L shipping casks. The exterior cask surface was instrumented with thermocouples and radiation dose rate sensors. Thermocouples were inserted into selected fuel assembly guide tubes after the cask was loaded with 21 fuel assemblies to monitor temperatures throughout the test. A test station was prepared, comprising of a rail car and a data acquisition system. A total of five runs involving a combination of cover gases and cask orientations were performed during the test. The backfill environments used were vacuum, nitrogen, and helium, and they were sampled and analyzed to detect leaking fuel assemblies. Both vertical and horizontal orientations were investigated and test runs were performed inside under controlled conditions. At the conclusion of testing, selected fuel assemblies were videotaped and photographed, and smear samples were collected and analyzed.

This report documents the first performance test using a CASTOR-V/21 cask. The conclusions and recommendations are presented in Section 2. In Section 3, the CASTOR-V/21 cask, the Surry PWR fuel assemblies, cask and fuel instrumentation,

the TAN cask testing facility, the test plan, and the cask-handling procedures and experience are presented. Heat transfer and shielding data are presented and discussed in Section 4. Pre- and post-test heat transfer predictions obtained with the HYDRA computer program are compared to test data in Section 5.

Section 2

CONCLUSIONS AND RECOMMENDATIONS

Performance testing of a CASTOR-V/21 PWR spent fuel storage cask was successfully completed at TAN. The test demonstrated that the cask could be satisfactorily handled and loaded dry, and demonstrated the heat transfer and shielding performance of the cask when loaded with 21 PWR spent fuel assemblies generating 28 kW. The heat transfer performance of the cask was exceptionally good and exceeded design expectations. Peak cladding temperatures with nitrogen and helium backfill gases with the cask in a vertical orientation and with helium in a horizontal orientation were below the allowable of 380°C. The shielding performance met design expectations ($\leq$200 mrem/hr) and dose rates of <75 mrem/hr can easily be achieved with minor gamma shielding design refinements. Cracks that developed in the basket as a result of an unusually tight fit with the cask inner wall and substantial axial temperature gradients can easily be avoided by opening up critical gaps and welding basket plates only where structural support is absolutely necessary. From both heat transfer and shielding perspectives, the CASTOR-V/21 cask can, with minor refinements, be effectively implemented at reactor sites and central storage facilities for safe storage of spent fuel.

The following sections present specific conclusions and recommendations noted during the testing and analyses effort.

CONCLUSIONS

The results of the cask performance test permit the following conclusions:

Cask Handling and Loading

- The CASTOR-V/21 cask can be satisfactorily handled in many reactor facilities. Only minor modifications to the supplied handling equipment and procedures were required to conduct testing at TAN.
- Dry (cold) runs with a nonirradiated dummy assembly of all steps required to handle and test the cask were valuable in familiarizing personnel with handling characteristics of the cask and finalizing test procedures.
- Approximately 1 hour was required to pump the cask down to 1 mbar and backfill with gas to 600 mbar. During a double pumpdown/

backfill operation, measured guide tube temperatures increased by <20°C during a 2-hour period. It is anticipated that evacuating and backfilling the cask after loading in a water basin will require a longer period and result in higher temperature increases.

- The dual elastomer/metallic O-ring sealing technique used in the CASTOR-V/21 cask performed exceptionally well during many repetitive on/off lid operations. Similar high quality lid gaskets that can withstand repetitive use are desirable if incremental loading is to be performed.

- When loading dry, sealing surface protectors are required to ensure that crud or particles do no lodge on these surfaces and result in blemishes or scratches that could compromise the finish of the sealing surfaces.

- The total personnel radiation exposures during handling, loading, and testing of the CASTOR-V/21 cask were relatively low, being approximately 1.8 man-rem. The exposure at a reactor or storage facility will be even lower because casks will not be incrementally loaded or continuously worked around.

Heat Transfer Performance

- The heat transfer performance of the cask was exceptionally good and exceeded design expectations. Peak temperatures were less than the 380°C allowable with nitrogen and helium backfills in a vertical orientation and with helium in a horizontal orientation when dissipating 28 kW.

- Peak temperatures with vacuum in a vertical orientation were 414°C and with nitrogen in a horizontal orientation were 395°C.

- The relatively open design of the CASTOR-V/21 fuel basket permitted significant convection with both nitrogen and helium backfill gases. Peak temperatures with both backfills occurred in the upper third of the instrumented guide tubes.

- The peak temperature with nitrogen (358°C) in a vertical cask was only slightly higher than with helium (347°C), indicating that convection with nitrogen almost compensated for the higher (five times) thermal conductivity of helium.

- In a horizontal orientation, the added contact conductance between fuel assemblies and basket fuel tubes did not compensate for convection with either nitrogen or helium; i.e., peak temperatures in a horizontal orientation were higher than in a vertical orientation with both backfill gases.

- Large temperature differences (200°C) from the outer assemblies to the cask outer surface indicate the basket-to-inner cask wall interface is important to the heat transfer performance of the cask.

- Peak temperatures of the outer 1.8-kW assemblies were always less than the center 1-kW assembly.

- Eight indications of cracks in the basket were observed in post-test fuel assembly inspections. It was concluded that the relatively

tight fit between the test basket and cask inner wall, along with substantial axial temperature gradients, were the potential causes of cracking. A tight fit was used to align the basket with the lid and permit thermocouple lances to be inserted through the cask lid into selected fuel assembly guide tubes.

HYDRA Heat Transfer Analysis

- HYDRA heat transfer predictions were valuable in planning the CASTOR-V/21 cask performance test, i.e., in selecting spent fuel assemblies, identifying the assembly load pattern, placing temperature sensors, and developing the test matrix.

- Pretest predictions of peak temperatures agreed with data within 50°C. Shapes of temperature profiles were satisfactorily predicted.

- The exterior surface temperature of the cask was consistently overpredicted (up to 20°C) during the pretest analysis, indicating that the exterior surface heat transfer coefficient correlation resulted in conservatively low heat transfer coefficients.

- Post-test predictions were improved (<25°C differences between predictions and data) by 1) reducing the basket-to-inner wall gap from 1.5 mm (0.059 in.) to the actual value of essentially zero, 2) including flow resistances of fuel tube external support plates, and 3) using an improved exterior surface heat transfer coefficient correlation.

- Convection in both nitrogen and helium was predicted to be significant, with mass fluxes in nitrogen being approximately an order of magnitude higher than in helium.

- Heat flux maps obtained from HYDRA indicate that peak heat fluxes were located in the outer basket region near the inner cask wall.

- HYDRA best-estimate predictions of the maximum heat that can be dissipated by a vertical CASTOR-V/21 cask resulted in values of 22 kW for a nitrogen backfill and 25 kW for a helium backfill. These best-estimate predictions assumed 1) each fuel assembly was generating the same amount of heat, 2) a 1-mm (0.039-in.) basket-to-inner wall gap, 3) a 37°C ambient temperature, and 4) a 380°C allowable peak cladding temperature.

Shielding Performance

- Total dose rates (gamma and neutron) on the cask surface were less than the 200 mrem/hr design goal.

- Most total dose rates on the cask surface were less than 100 mrem/hr.

- Peak gamma dose rates as high as 140 mrem/hr were measured on the cask side adjacent to fuel assembly upper and lower end fittings. Minor refinements of the gamma shield at these locations could reduce these peaks to less than 75 mrem/hr.

Fuel Characterization and Integrity

- Results of pretest, in-test, and post-test fuel integrity activities resulted in the conclusion that no failed fuel rods were loaded in the CASTOR-V/21 cask.
- Pre- and post-test inspections of selected assemblies revealed that no noticeable changes occurred during the testing.
- Expected slight rod bowing was observed in some fuel assemblies during video scans and photography before and after cask performance testing.
- Because of uneven rod growth during irradiations, the elevations of the upper ends of some fuel rods in an assembly were different (misaligned) by up to approximately 2.5 cm (1 in.), which could affect future rod consolidation activities.
- Video scans and photography indicated the presence of an intermittent crud layer on the fuel assemblies.
- Smear samples from selected fuel assemblies indicated that large quantities of ^{60}Co were present, but no fission product species were detected.

RECOMMENDATIONS

The results and conclusions of this work led to the following recommendations.

Cask Handling and Loading

- The cask information required prior to handling a cask should include cask design drawings and specifications, operating and maintenance manuals, procedures, and spare parts.
- Dry runs of the cask and associated equipment should be performed for all phases of cask handling and loading including backfilling the cask with a cover gas and gas sampling. Cask vendor representatives should be in attendance for operational and functional checkouts of the cask.
- Cask handling procedures are site-specific, and procedures should be developed for each site. The experience gained during this performance test will be helpful in developing such procedures.
- The cover gas system used to evacuate, backfill, monitor, and obtain gas samples should be carefully designed. The difficulty associated with backfilling the cask with a pure (>99%) cover gas and obtaining gas samples without introducing air should not be underestimated. The cask should be pumped down and backfilled a minimum of two times to ensure purity (>99%) of the final cover gas.

Heat Transfer Performance

- Critical basket gaps should be controlled, and only basket welds absolutely required for structural support should be applied to eliminate the possibility of basket cracking.

HYDRA Heat Transfer Analysis

- HYDRA is an effective code that can be used to accurately predict temperatures in spent fuel dry storage systems and, once successfully evaluated and documented, may be used for design and licensing safety analyses.

- HYDRA predictions of dry storage system temperatures within 25°C can be obtained. Further, if it is desirable to improve this agreement, the following, in order of importance, should be pursued:

  - System geometries, especially gap widths and characteristics of contacting surfaces, must be better known.

  - Emissivities of important basket/cask components should be measured.

  - The effects of free-stream turbulence and mixed convection (free and forced) adjacent to the exterior surface of the cask should be modeled.

  - Velocity fields should be measured in simulated casks, and HYDRA predictions should be evaluated with the measured distributions.

- The heat transfer data contained in this report should be used to evaluate other heat transfer codes.

Shielding Performance

- Minor refinements to the gamma shield adjacent to fuel assembly end fittings should be made to decrease peak dose rates to <75 mrem/hr.

Section 3

CASK PERFORMANCE TESTING

Details of the cask performance test are discussed in this section. The CASTOR-V/21 cask and instrumentation are described, as are the Surry PWR spent fuel assemblies and associated instrumentation. The data acquisition system used to receive and process instrumentation signals is presented. A description of the INEL cask testing facility is provided. The test plan is presented, and the procedures resulting from the plan are summarized. Experiences gained during cask-handling dry runs and testing are described.

CASTOR-V/21 CASK AND ASSOCIATED INSTRUMENTATION

The CASTOR-V/21 cask and associated instrumentation are briefly discussed in this section. A detailed description of the cask can be found in References 2 and 3.

Cask Body

The cask body is a one piece cylindrical structure composed of ductile cast iron in nodular graphite form (3). This material exhibits good strength and ductility, as well as providing effective gamma shielding. The overall external dimensions of the cask body are 4886 mm (16 ft) high and 2385 mm (8 ft) in diameter (Figure 3-1). The external surface has 73 heat transfer fins that run circumferentially around the cask, and is coated with epoxy paint for corrosion protection and ease of decontamination.

The cask body wall, excluding fins, is 380 mm (15 in.) thick. Incorporated within the wall of the body are polyethylene moderator rods to provide neutron shielding. Two concentric rows of these 60-mm (2.3-in.) nominal diameter rods are distributed around the cask perimeter (Figure 3-2). Two lifting trunnions are bolted on each end of the cask body.

The diameter of the inner cavity is 1527 mm (5 ft), and the overall inner cavity length is 4152 mm (163 in.). Precision-machined surfaces are provided at the open end of the cask cavity for positive gasket sealing, and bolt holes are included at

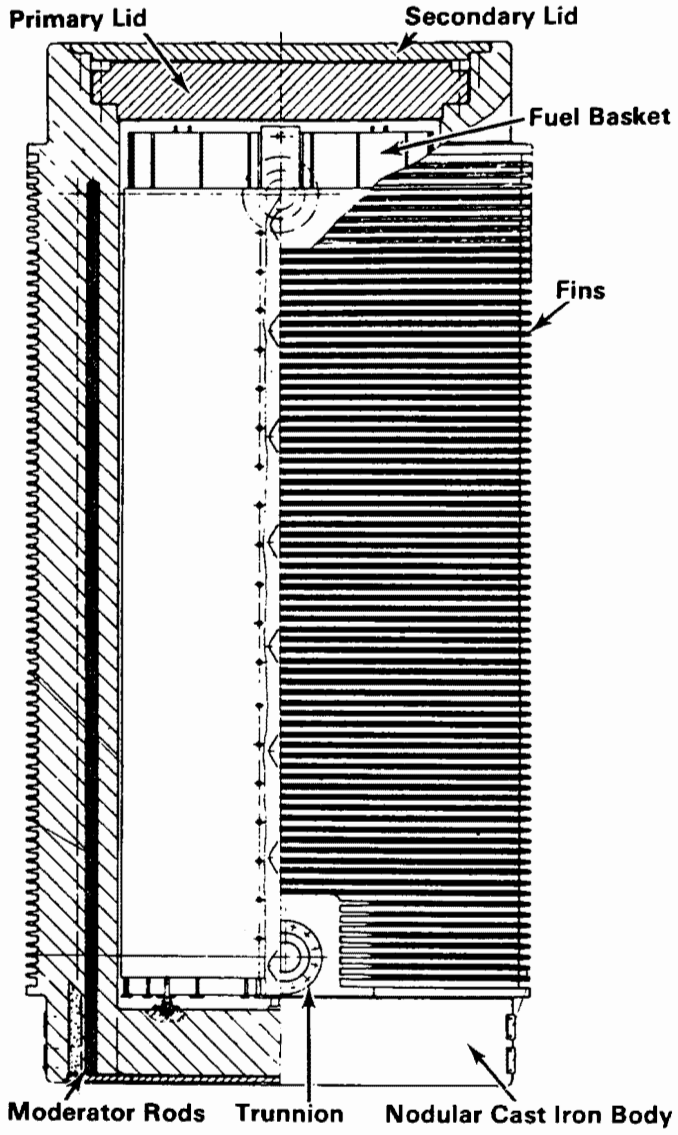

Figure 3-1. CASTOR-V/21 PWR Spent Fuel Storage Cask

these locations to secure the two cask lids. The interior cavity surfaces, including sealing surfaces, have a galvanic applied nickel plating.

Spent Fuel Basket

The spent fuel basket (Figure 3-2) is a cylindrical structure of welded stainless steel plate, and borated stainless steel plate, having a boron content of approximately 1% for criticality control. The basket comprises an array of 21 square fuel tubes/channels that provide structural support and positive positioning of the fuel assemblies. The basket overall height is 4110 mm (13.5 ft) including the four

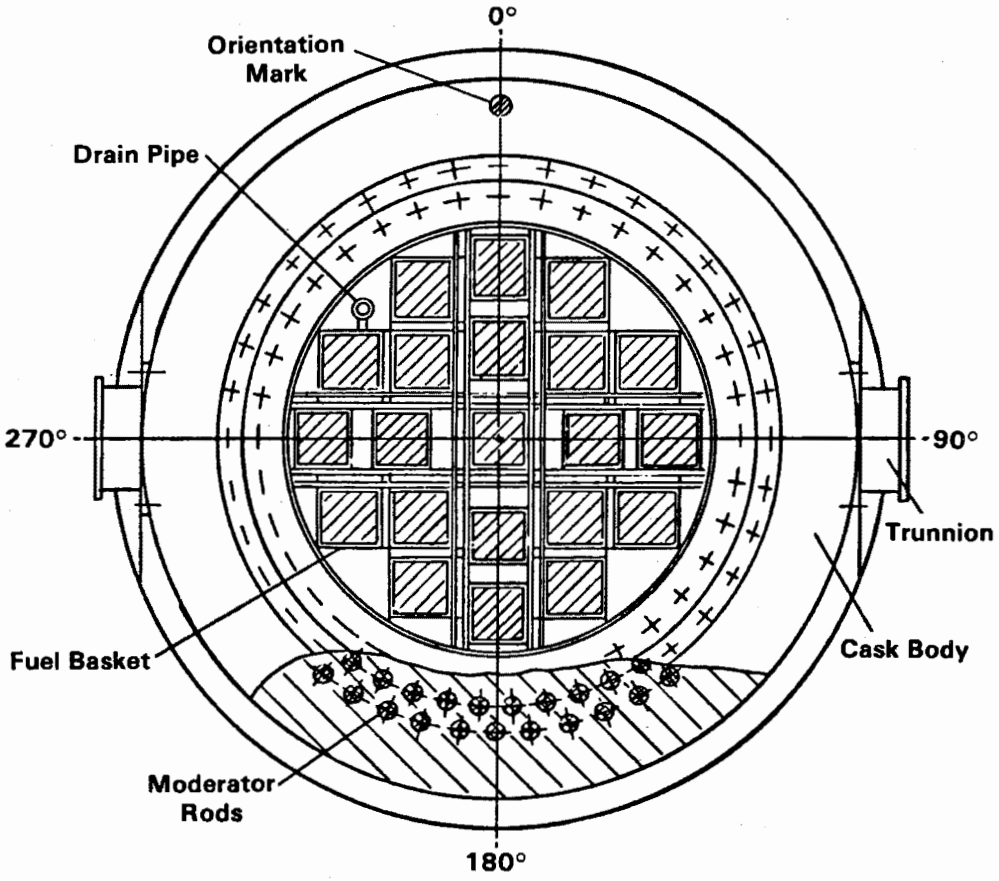

Figure 3-2. CASTOR-V/21 Cask Cross Section

130-mm-diameter (5-in.) pedestals that support the basket and fuel weight on the bottom of the cask cavity. The basket outside diameter of 1524 mm (5 ft) fits tightly in the cask cavity inner diameter of 1527 mm (5 ft). The depth of each fuel tube is 4050 mm (13.3 ft). A spacing of 74 mm (3 in.) is present between the top of the basket cavity and the underside of the primary lid, thus accommodating a fuel assembly length of 4124 mm (162 in.) and supporting convection heat transfer. The final assembly results in a clearance of approximately 60 mm (2.3 in.) between the top of the fuel assemblies and the bottom of the primary lid, for a reference fuel assembly of 4064 mm (160 in.).

The basket layout results in inter-fuel tube spaces that act as flux traps for criticality control and channels to support free convection heat transfer. The basket design ensures a subcritical configuration under worst-case conditions, and the basket structure physically protects the fuel under normal and accident conditions.

A pipe with an inner diameter of 42 mm (1.6 in.) and a lead-in funnel at the top is welded to the side of a fuel tube near the outer circumference of the basket. The pipe location corresponds to a penetration in the primary lid and the low side of the slope in the cask cavity bottom. This pipe provides a path for a flanged pipe used to fill and drain the cask.

Primary Lid

A stainless steel primary lid, 1785 mm (6 ft) in diameter and 290 mm (12 in.) thick, is provided (Figure 3-3). Forty-four bolt holes are machined near the lid perimeter to secure the lid to the cask body. Two grooves machined around the lid underside, inside the bolt circle, are provided for O-ring gaskets (Figure 3-4). The inner groove accepts a metal O-ring, which serves as the first barrier between stored fuel and the environment. The outer groove accepts an elastomer O-ring. A 10-mm-diameter (0.5-in.) penetration through the lid provides access to the annulus between the two seals to perform post-assembly leak testing. This penetration is plugged when not in use.

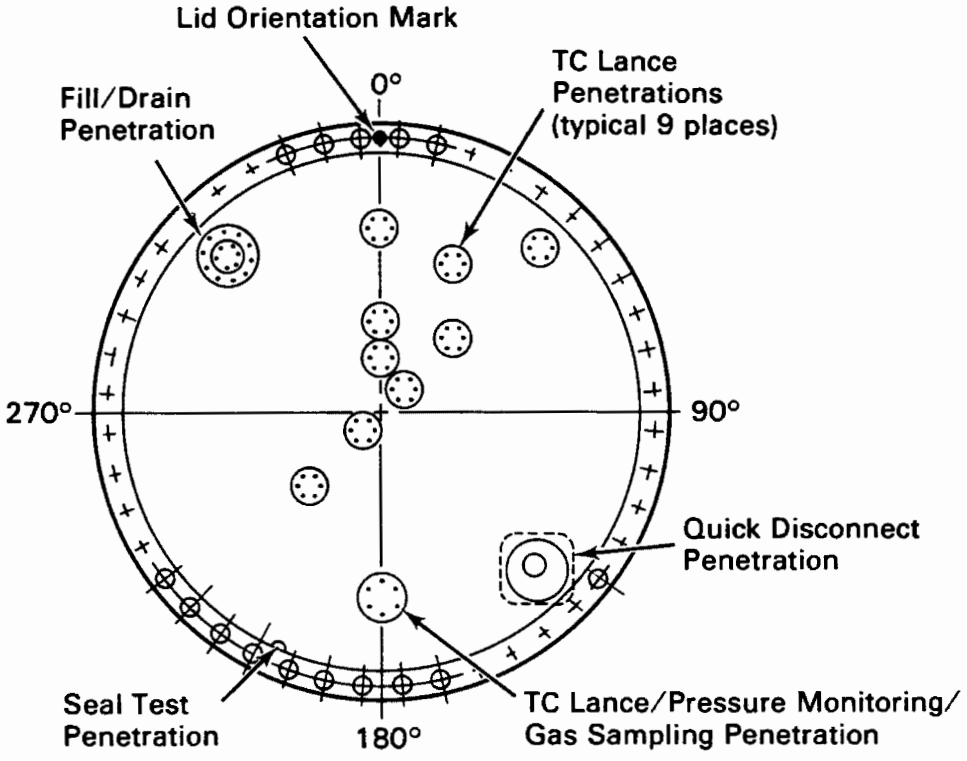

Figure 3-3. CASTOR-V/21 Primary Test Lid

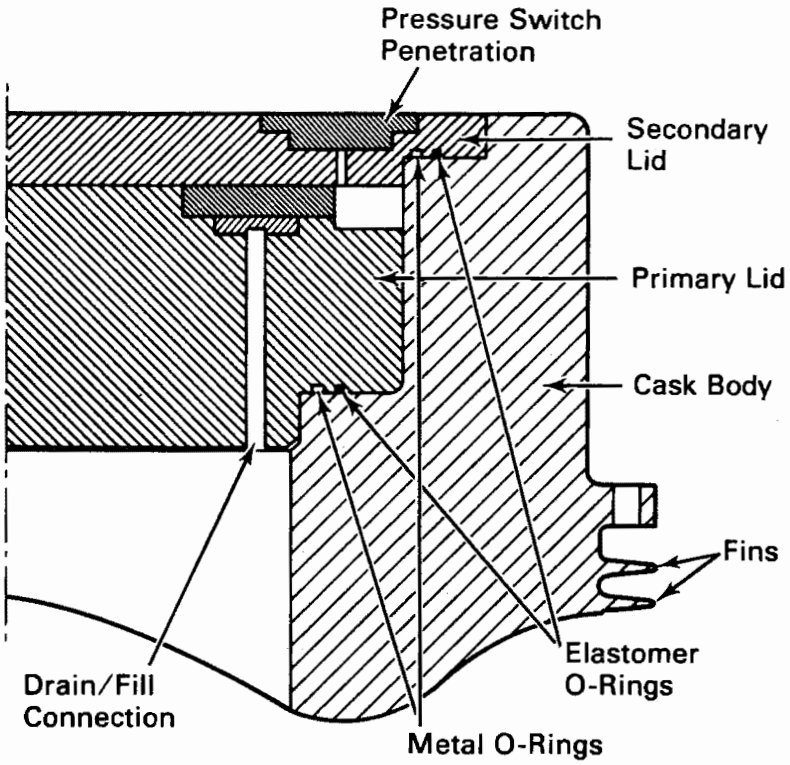

Figure 3-4. CASTOR-V/21 Cask Lid System

Three penetrations through the lid are provided for various cask operations. A 35-mm-diameter (1.4-in.) straight-through penetration is used for water fill/drain operations. This penetration is located near the perimeter of the lid and is normally sealed with two flanges equipped with elastomer O-rings. This location corresponds to the pipe attached to the fuel basket. The other two penetrations, spaced next to each other and covered by a single flange, are also located near the lid perimeter, but 180 degrees from the fill/drain penetration. The through-lid penetration at this location is equipped with a quick-disconnect fitting used for vacuum drying and backfilling with gas. The second penetration at this location leads to the lower edge of the lid. Although not needed for the CASTOR-V/21, this penetration could be used for leak-testing an optional third lid gasket. This penetration is sealed by a gasketed seal plug in addition to the top cover flange.

The primary lid used during testing was not a standard lid and has 10 additional penetrations for fuel assembly guide tube instrumentation [thermocouple (TC) lances] described in detail in the next section. Nine of the penetrations are machined with 18-mm (0.7-in.) holes through the lid and countersunk (20 mm, 0.8 in.) to accept the TC lances and 105-mm-diameter (4-in.) flanges. The tenth penetration has a hole

through the lid for a TC lance and accepts a 140-mm-diameter (5.5-in.) flange. The pattern of the 10 fuel assembly instrumentation penetrations was selected to measure radial temperature profiles across the basket in the spent fuel assemblies. The pattern was developed using pretest temperature predictions of the undocumented HYDRA thermal hydraulics computer program as discussed in Section 5.

Secondary Lid

The stainless steel secondary lid is 2007 mm (79 in.) in diameter and 90 mm (3.5 in.) thick (Figure 3-4). Forty-eight bolt holes are machined near the lid perimeter to secure the lid to the cask body. Two concentric grooves located inside the bolt circle on the underside are provided for a metal O-ring/elastomer O-ring sealing system of the same design as that used on the primary lid. Three normally sealed penetrations are provided for various cask operations (Figure 3-4). A 10-mm-diameter (0.4-in.) penetration through the lid provides access to the annulus between the two seals for post-assembly seal testing. A gasketed seal plug is used to close this penetration.

A second penetration is equipped with a quick-disconnect fitting, which is used for vacuum drying and gas backfilling of the primary/secondary inter-lid space. A 130-mm-diameter (5-in.) cover plate and gasket secured by six 12-mm (0.5-in.) bolts is in place when this penetration is not used. The third penetration provides a pressure sensing port between the inter-lid space and a pressure switch mounted in the secondary lid. The pressure switch is the primary component of the cask seal monitoring system.

The secondary lid was not used during the CASTOR-V/21 cask performance test because of interference with fuel assembly instrumentation leads. Therefore, dose rates discussed in Section 4 were obtained on the primary lid exterior surface. Addition of the secondary lid will greatly reduce measured dose rate values.

Cask Cavity Pressure Measurements

A Leybold Heraeus model MAC 2000 pressure transducer was used to measure cask cavity pressures. The transducer had a range of 0 to 2000 mbar and a stated accuracy of ±0.2% of full scale. The transducer was connected to the quick-disconnect penetration provided in the primary lid of the cask (Figure 3-3) via the valve tree shown in Figure 3-5. The signal from the transducer was conditioned and read out on a digital readout and the data acquisition system (DAS) described in a later section.

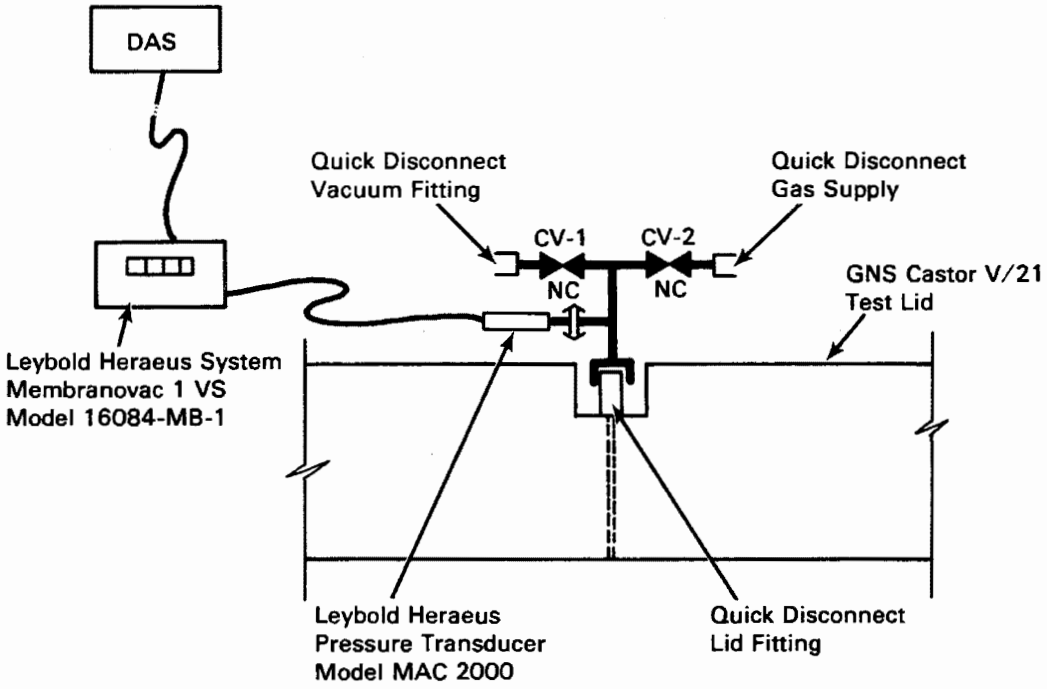

Figure 3-5. Pressure Transducer Valve Tree

Exterior Surface Temperature Instrumentation

The exterior surface of the cask was instrumented with 35 iron/constantan Type J thermocouples (TCs). Figures 3-6 and 3-7 identify the locations of the TCs on the primary lid, barrel, and bottom of the cask. Only during horizontal testing were TCs placed on the bottom of the cask. The TC patterns on each surface were selected to provide appropriate axial, radial, and circumferential temperature profiles. The patterns were developed using pretest predictions of the HYDRA thermal hydraulics computer code discussed in Section 5.

Exterior Surface Dose Rate Instrumentation

Gamma dose rates were measured on the surface of the cask with thermoluminescent dosimeters (TLDs). Neutron dose rates were measured with track etch dosimeters (TEDs). Portable hand-held survey instruments were used to measure both gamma and neutron dose rates. Data obtained from these sources are presented and discussed in Section 4. The dosimeters and hand-held instruments, along with spectra instrumentation required to calibrate the TLDs and TEDs, are briefly discussed in the following sections.

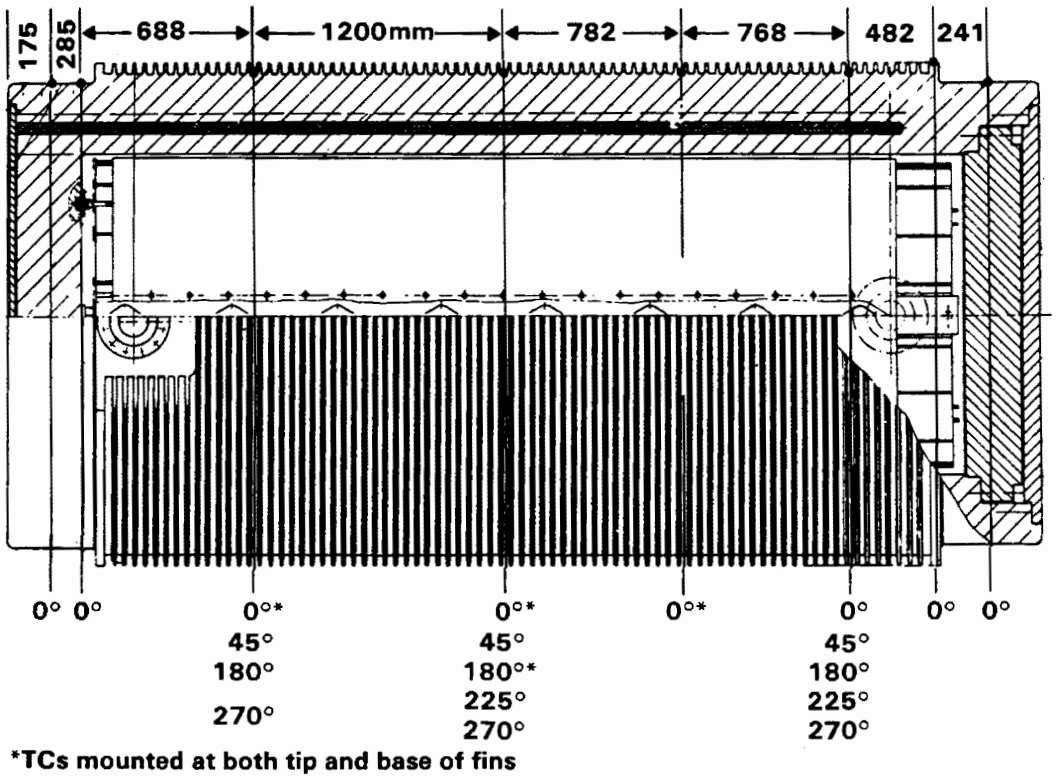

Figure 3-6. Cask Surface Thermocouple Locations

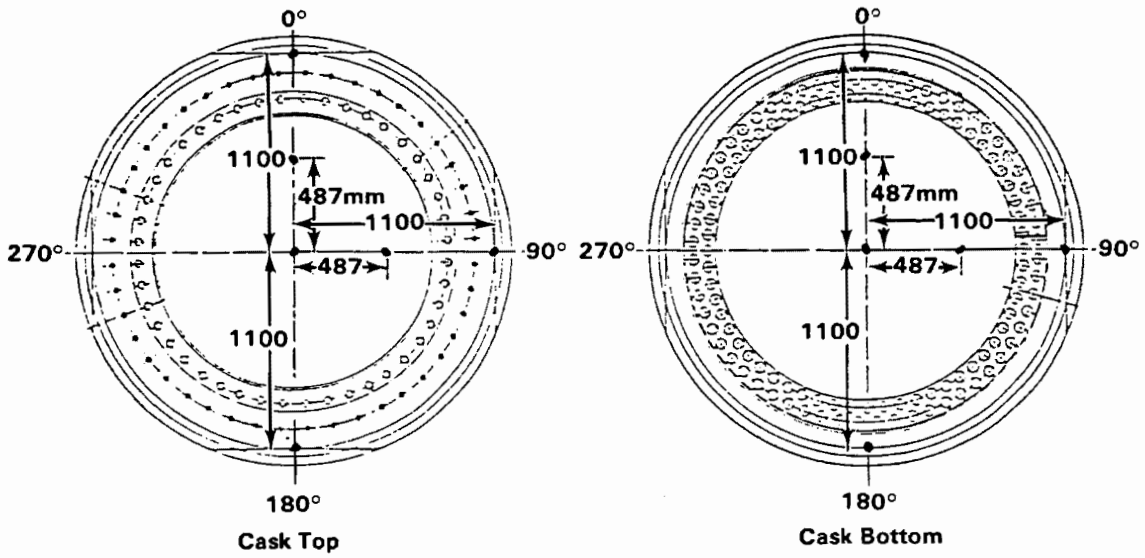

Figure 3-7. Cask Top and Bottom Thermocouple Locations

Energy Spectrum Instruments. Energy spectra measurements were required to determine accurate gamma and neutron dose equivalents from TLD and TED measurements, i.e., to calibrate the TLDs and TEDs. Gamma energy spectra were measured with an intrinsic germanium spectrometer near the surface adjacent to the centers of the cask lid and bottom, and midway up the cask side. The spectrometer, a semiconductor-type radiation detector, and consists of a germanium crystal operated as a reverse biased diode. Gamma rays that interact within the crystal cause ionization, and the resulting charged particles produce an electron current that is collected at the electrodes. The electron current is proportional to the energy deposited within the crystal. A detailed description of the intrinsic germanium spectrometer is provided in (4).

Neutron dose equivalents and energy spectra were measured with a multisphere spectrometer on the surface and 1 m (3.3 ft) from the surface at locations previously indicated for gamma energy spectra measurements. The multisphere spectrometer consists of a ^{6}Li iodide scintillation crystal optically coupled to a photomultiplier tube. The detector is used in conjunction with a cadmium cover and five high-density polyethylene spheres of varying sizes. For a single location, count rate measurements are taken with the bare detector, with a cadmium cover on the detector, and with polyethylene spheres on the detector. The spheres are of five diameters: 76 mm (3 in.), 127 mm (5 in.), 203 mm (8 in.), 250 mm (10 in.), and 305 mm (12 in.). The polyethylene moderates the neutrons, and the resulting slow neutrons produce a distinct measureable peak. The incident neutron energy spectrum can be estimated by using the differences in slow neutron count rates produced by the different sizes of spherical moderators. A detailed discussion of the multisphere spectrometer is presented in (4).

Neutron spectra between thermal and 1 MeV were measured with a ^{3}He spectrometer. The ^{3}He spectrometer provides direct measurements of neutron flux as a function of energy and consists of a proportional counter filled with a mixture of ^{3}He and Ar. The neutrons interact with the ^{3}He to produce a triton and a proton. These charged particles are slowed by the fill gas and deposit some or all of their energy in the detector. When the charged particles are completely stopped in the sensitive volume of the tube, the energy absorbed is directly proportional to the energy of the incident neutron plus 764 keV, the energy released by the nuclear reaction. The ^{3}He detector is most sensitive to thermal neutrons due to the 1/v cross section of ^{3}He for neutron absorption. This results in a large peak at 764 keV, which is used to calibrate the spectrometer. A detailed discussion of the ^{3}He spectrometer is presented in (4).

Thermoluminescent Dosimeters. Axial and radial gamma dose rate profiles on the cask surface were measured using thermoluminescent dosimeters (TLDs) at the 69 locations identified in Figures 3-8 and 3-9. Each TLD consisted of three 7LiF chips placed in a gelatin capsule. Each capsule was attached to a 1-in. styrofoam cube to protect the dosimeter from the high temperatures at the very surface of the cask. Along the side of the cask the styrofoam blocks were attached to paper cards and suspended between the protruding fins to further avoid overheating the dosimeters. The paper cards were attached to the cask with silicone adhesive. When heated, TLDs emit light in quantities proportional to the energy deposited in the material by the incident radiation; hence, the need to protect the dosimeters from high temperatures. The three chips per dosimeter were used to give good statistical results.

The TLDs were left on the cask for several days. The dates and times on and off were recorded for each dosimeter to determine exposure times. After exposure of the TLDs on the storage cask, the chips were removed from the gelatin capsules and read.

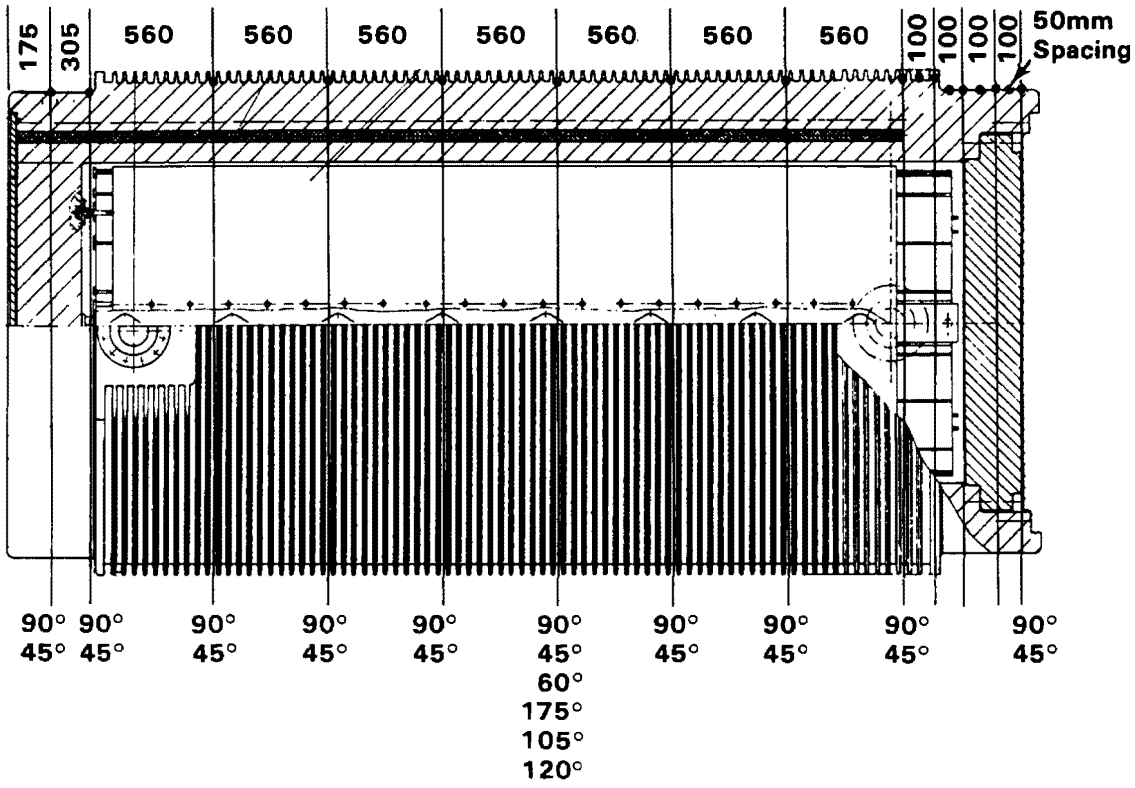

Figure 3-8. Cask Surface Dosimeter Locations

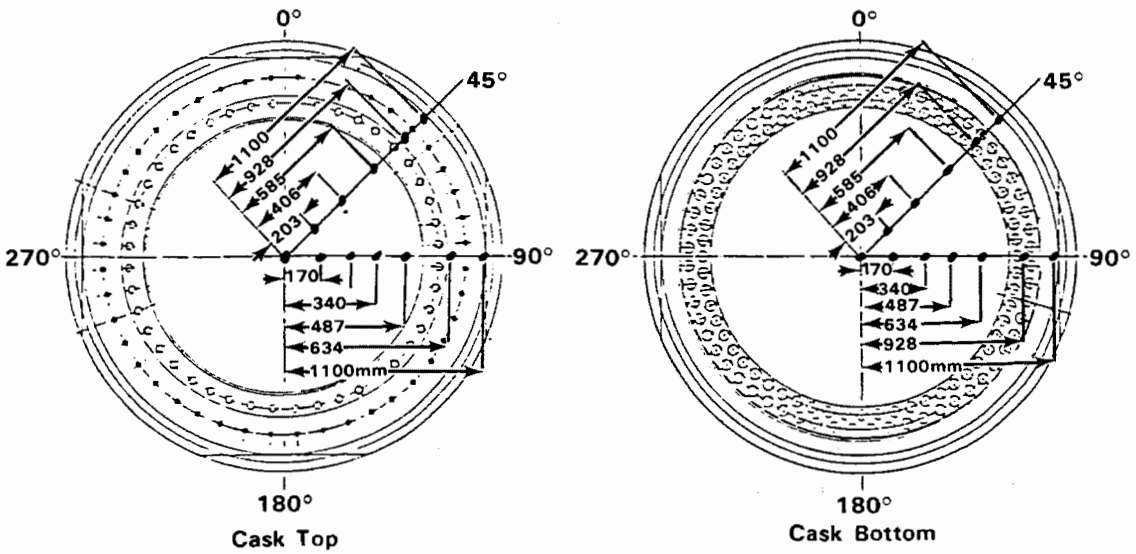

Figure 3-9. Cask Top and Bottom Dosimeter Locations

Gamma dose rates from TLDs are calculated using a calibration factor derived by exposing a set of calibration dosimeters to 1000 mr of radiation from a 10-Ci ^{137}Cs National Bureau of Standards (NBS) certified source. The average of the readouts from all the calibration chips was used to convert the TLD output from nanocoulombs to milliroentgens (mr). The results for the three chips in a given dosimeter capsule were averaged, and the background determined by a set of control TLDs was subtracted out. The resulting total doses in milliroentgens were divided by the length of time the TLDs were on the cask to determine total dose rates in mr/hr.

Track Etch Dosimeters. Track etch dosimeters (TEDs) were used to determine neutron dose equivalent rate profiles. TED measurement locations consisted of 40 points along the side of the cask, 17 on the top, and 12 on the bottom (Figures 3-8 and 3-9). The dosimeters were left on the cask for about 2 days before being removed and processed.

The TEDs were made of strips of CR-39 plastic (allyl diglycol polycarbonate) 29 mm (1.125 in.) by 16 mm (0.625 in.) by 2 mm (0.07 in.). They were covered with an 8-mm (0.003-in.) layer of polyethylene to protect them from background alpha radiation. During dose rate measurements, the TEDs were attached to thick paper cards adhered to the surface of the cask, and the times and locations were individually recorded. Upon exposure to radiation, damage sites were created through neutron bombardment of the polymer, causing proton recoil interactions and breaking some of the polymer crosslinkages. The TEDs were analyzed using a caustic solution and electrochemical

etching to produce visible tracks of the damage sites. The number of tracks was counted, and the visible track density was related to dose rate using predetermined calibration factors.

Several TEDs designated as controls were taken to the site and placed away from the cask to provide an indication of the background radiation received by the dosimeters. The neutron fluences from the TEDs were calculated from the track density (tracks/cm^2) using the energy response for an average neutron energy of 200 keV as given by the spectrometer results. The calibration factor was 5.0×10^{-6} tracks/neutron to convert tracks/cm^2 to neutron fluence (n/cm^2). Neutron dose equivalents were calculated from fluences using 6.11×10^{-6} mrem/(n/cm^2). The total dose equivalent in millirems was then divided by the time the dosimeter was on the cask to get the dose equivalent rate.

Tissue Equivalent Proportional Counter. A tissue equivalent proportional counter (TEPC) was used to directly measure the neutron dose rate at locations indicated in Figures 3-8 and 3-9. The TEPC also provides information about the linear energy transfer and quality factor of the incident neutrons. It consists of a hollow sphere or cylinder of tissue equivalent plastic filled with a low pressure tissue equivalent gas. Neutrons interacting within the wall of the TEPC produce recoil protons and heavy ions that travel through the fill gas, causing ionization. The electronic pulses created by the charged particles are collected on the counter anode. Energy deposited in the gas divided by the mass of the gas is the absorbed dose by definition. Using an appropriate algorithm, it is possible to determine neutron quality factors from the pattern of energy deposited in the counter and, thus, it is possible to determine dose equivalent rates directly from the TEPC data. As a result, the TEPC is an absolute dosimeter and does not require independent calibration, so long as the size of the gas cavity is accurately known. Data taken with the tissue equivalent proportional counter were analyzed with the computer code TACI (5), which is run on an HP-87 desktop computer.

Portable Survey Instruments. Two standard portable survey instruments were used by INEL to measure gamma and neutron dose rates at the same locations that TLD and TED measurements were obtained (Figures 3-8 and 3-9). Gamma dose rate measurements were made using a Eberline RO-3A air ion chamber with a 3.5 mg/cm^2 mylar window. Neutron dose rates were measured with an Eberline PNR-4. The PRN-4 consisted of a BF_3 tube moderated by a 9-in.-diameter polyethylene sphere.

PNL also performed radiation surveys of the cask to corroborate the results from the TLDs, TEDs, and spectrometers. The PNL gamma survey readings were taken with an Eberline RO-3B, which is the same type of instrument as the RO-3A but with a different readout format. The neutron survey was performed using a SNOOPY, which consists of a BF_3 detector moderated by a 8-1/2-in. polyethylene cylinder.

The results of the PNL and INEL surveys provide a valuable comparison and example of how the same types of survey instruments can give consistently different readings depending on the method and source used to calibrate the instrument and the source of radiation being measured. The INEL gamma survey instrument was calibrated using ^{137}Cs and the neutron survey instrument was calibrated with an unmoderated ^{252}Cf source. The PNL gamma survey instruments was also calibrated with a ^{137}Cs source, but the SNOOPY was calibrated against an unmoderated PuBe source.

SURRY PWR SPENT FUEL AND ASSOCIATED INSTRUMENTATION

In this section, the design of the Surry spent fuel assemblies used in the CASTOR-V/21 cask performance test is presented and discussed. Results of predictions of the decay heat rates and associated average axial decay heat profile for the test assemblies are described. A description of the instrumentation used to measure assembly guide tube temperatures is provided. The methods used to determine spent fuel integrity prior to, during, and after testing are discussed, along with results and findings obtained with each method.

Fuel Assembly Design

The fuel assemblies are square in cross section, nominally 214 mm (8.426 in.) on a side, and have a total length of 4058 mm (159.765 in.). The fuel column is 3658 mm (144 in.) long. The overall configuration is shown in Figure 3-10.

The fuel rods in a fuel assembly are arranged in a square array with 15 rod locations per side and a nominal rod-to-rod centerline pitch of 14.3 mm (0.563 in.) as shown in Figure 3-11. Of the total possible 225 rod locations per assembly, 20 are occupied by guide tubes for the control rods and burnable poison rods, and one central thimble is reserved for incore instrumentation. The remaining 204 locations contain fuel rods. In addition to fuel rods, a fuel assembly also includes a top nozzle, a bottom nozzle, and seven grid assemblies.

The 21 guide tubes, in conjunction with the grid assemblies and the top and bottom nozzles, comprise the basic structure of the fuel assembly. The top and bottom ends of the guide tubes are fastened to the top and bottom nozzles, respectively. The

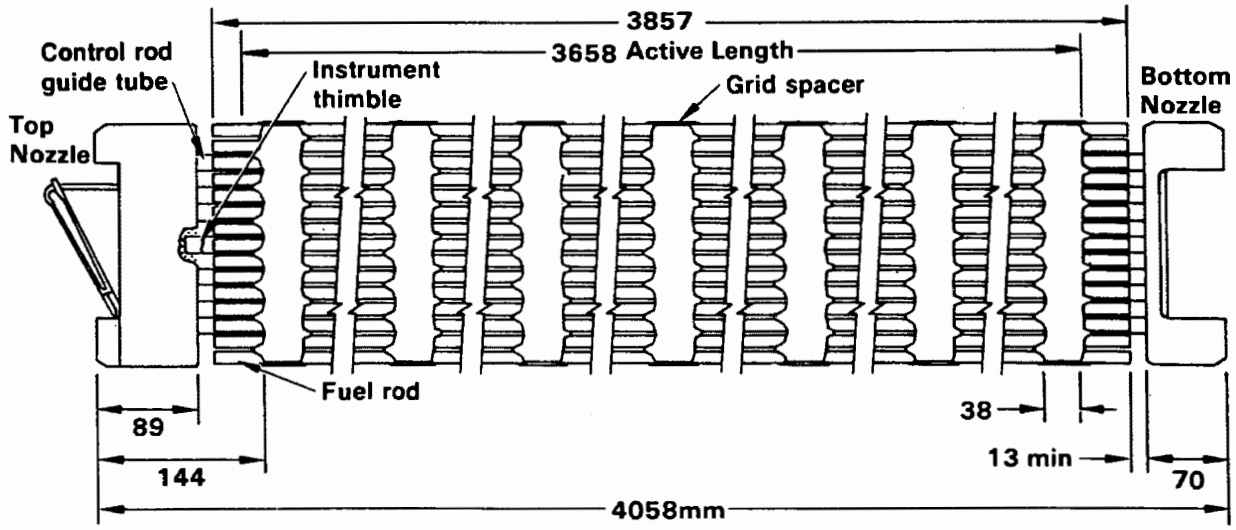

Figure 3-10. Surry 15 x 15 PWR Fuel Assembly

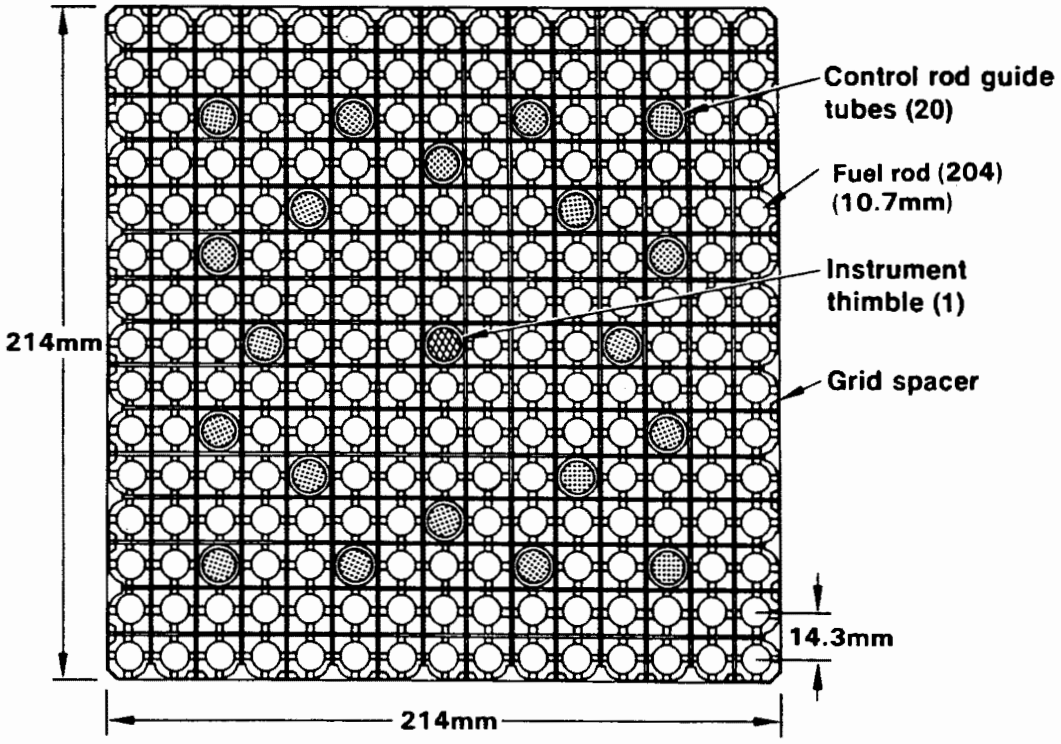

Figure 3-11. Surry 15 x 15 PWR Fuel Assembly Cross Section

grid assemblies are fastened to the guide tubes at each location along the length of the fuel assembly at which lateral support for the fuel rods is required. The fuel rods are contained and supported, and the rod-to-rod centerline spacing is maintained along the assembly within this skeletal framework.

The bottom nozzle is a square pedestal structure that controls the coolant flow distribution to the fuel assembly and functions as the bottom structural element of the fuel assembly. The nozzle is fabricated from type 304 stainless steel parts consisting of a perforated plate, four angle legs, and four pads or feet. The angle legs are welded to the plate to form a plenum space for the inlet coolant flow into the fuel assembly. The bottom support surface for the fuel assembly is formed under the plenum space by the four pads, which are welded to the corner angles.

The guide tubes, which carry axial loads imposed on the assembly, are fastened to the bottom nozzle plate. These loads, as well as the weight of the assembly, are distributed through the nozzle to the lower core support plate. Indexing and positioning of the fuel assembly in the core is fixed by two holes in diagonally opposite pads, which mate with two locating pins in the lower core plate. Lateral loads imposed on the fuel assembly are also transferred to the core support structures through the locating pins.

The top nozzle is a square box-like structure that functions as the fuel assembly upper structural element and forms a plenum space where the heated reactor coolant mixes and is directed toward the flow holes in the upper core plate. The nozzle comprises an adaptor plate, nozzle enclosure, top plate, two clamps, double-leaf holddown springs, and assorted hardware. All parts with the exception of the springs and their holddown bolts are constructed of type 304 stainless steel. The springs are made from age-hardenable Inconel 718, and the bolts from Inconel 600.

The control rod guide tubes in the fuel assembly provide guide channels for the control rods during insertion and withdrawal. The guide tubes are fabricated from a single piece of Zircaloy 4 tubing, which is drawn to two different diameters. The larger inside diameter at the top provides a relatively large annular area for rapid insertion during a reactor trip. It also accommodates a small amount of upward cooling flow during normal operation. The bottom portion of the guide tube has a smaller diameter to cause a dashpot action when the control rods approach the end of travel in the guide tubes. The transition zone at the dashpot section is conical so that there are no sharp changes in diameter in the tube. Flow holes are provided

just above the transition of the two diameters to permit the entrance of cooling water during normal operation, and to accommodate the outflow of water from the dashpot action during reactor trip.

The control rod guide tubes are closed at the bottom with a welded end plug. The end plugs are subsequently fastened to the bottom nozzle during fuel assembly fabrication. Flow holes are provided in the end plugs to permit entrance of cooling water during normal operation and to regulate dashpot action during control rod trip. The instrumentation thimble is left open at the bottom to receive the incore instrumentation.

The spring clip grid spacers consist of individual slotted straps that interlock in an "egg-crate" arrangement. They are furnace-brazed to permanently join the straps at their points of intersection. Details such as spring fingers, support dimples, mixing vanes, and tabs are punched and formed in the individual straps prior to assembly.

Two types of grid spacers are used in the Surry PWR fuel assemblies. Grid mixing vanes that project from the edges of the straps into the coolant stream are used in the high-heat region of the fuel assemblies to promote mixing of the coolant. The grids located at the bottom and top ends of the assembly are of the nonmixing type. They are similar to the mixing type but do not have mixing vanes on the internal straps.

The outside straps on all grids contain mixing vanes that also aid in guiding the grids and fuel assemblies past projecting surfaces during handling or core loading and unloading. In addition, there are small tabs on the outside straps; the irregular contour of the straps is also for guiding.

Inconel 718 is used for the grid material because of its corrosion resistance and high strength properties. After the combined brazing and solution annealing temperature cycle, the grid material is age-hardened to obtain the material strength necessary to develop the required grid spring forces.

The fuel rods consist of uranium dioxide ceramic pellets contained in slightly cold-worked and partially annealed Zircaloy 4 tubing, which is plugged and seal-welded at the ends to clad the fuel. Nominal dimensions include 9.29-mm (0.3659-in.) pellet diameter, 10.71-mm (0.422-in.) tube OD, and 0.62-mm (0.0243-in.) tube thickness.

Sufficient void volume and clearances are provided within the rod to accommodate fission gases released from the fuel, differential thermal expansion between the cladding and the fuel, and fuel swelling due to accumulated fission products without overstressing of the cladding or seal welds. Shifting of the fuel within the cladding is prevented during handling or shipping prior to core loading by a carbon steel helical compression spring that bears on the top of the fuel pellet column. The holddown force to prevent fuel shifting is obtained by compression of the spring between the top end plug and the top fuel pellet of the stack.

During assembly, the pellets are stacked in the cladding to the required fuel height. The compression spring is then inserted into the top end of the fuel, and the end plugs pressed into the ends of the tube and welded. During the welding process, the fuel rods are internally pressurized with helium to 28.3 bar (415 psia) for "T" assemblies and 26.2 bar (385 psia) for "V" assemblies.

The fuel rod void space is sized to ensure adherence to the pressure criteria. The end-of-life pressure is evaluated for the worst rod under expected conditions of fuel operation and at the peak steady-state power. The model used to predict the quantity of fission gas in the gap at end-of-life is based on an extensive comparison to published performance of fuel rods under a variety of conditions. The composition of the gas in the gap at the end of life is a maximum of approximately 50% fission gas.

The fuel pellets are right circular cylinders consisting of slightly enriched uranium dioxide powder, which is compacted by cold pressing and sintering to the required density. The ends of each pellet are dished slightly to allow the greater axial expansion at the center of the pellets to be taken up within the pellets themselves and not in the overall fuel length. The nominal design enrichment is 3.1 wt% and 2.9 wt% for the "T" and "V" assemblies, respectively. The nominal density is 95% of theoretical density for all of the fuel pellets.

Predicted Decay Heat Rates

The ORIGEN2 code (6) was used to predict decay heat generation rates of the Surry PWR spent fuel assemblies used in the CASTOR-V/21 cask performance test. A brief description of ORIGEN2, a summary of the input, and the predicted decay heat rates and average axial decay heat profile are provided.

ORIGEN2 Computer Code. The ORIGEN2 computer code is widely used in the nuclear industry to predict decay heat rates of spent fuel assemblies. It is a general

purpose burnup and decay code featuring extensive data libraries containing information on over 1200 nuclides. The code can be used to perform transmutation calculations in steps of constant power or constant neutron flux level. The resulting nuclide concentrations can be decayed with user-specified time intervals. Output options are available for decay heat rate as well as spent fuel compositions and radioactivity.

Input Specifications. The Surry spent fuel assembly design data were provided in a previous section for the assemblies used in the CASTOR-V/21 cask performance test. Additional input data used in the ORIGEN2 calculations for the assemblies included:

- reactor operating histories and decay times after final cycle of operation for each assembly
- monthly measured fuel assembly relative power density (RPD)
- measured end-of-cycle (EOC) fuel assembly burnups
- as-built fuel batch assembly average metric ton uranium (MTU) loadings and isotopics.

The Surry 2 reactor operating history for each cycle was based on the monthly core exposure log sheets obtained from the VP Nuclear Operations Department (NOD). The reactor operating histories for cycles 3 through 6 are given in Figure 3-12 and Appendix A. The monthly measured fuel assembly RPDs were extracted from the monthly INCORE (7) computer code maps produced by NOD. The measured EOC fuel assembly burnups were obtained from NEWTOTE (8) computer code results. A history of the assembly EOC average burnups is given in Table 3-1. The batch average assembly MTU loadings were obtained from Westinghouse as-built data. These data are provided in Appendix A.

The assembly-specific power for each irradiation step was calculated using three equations:

$$POWER(K) = (LOADF * RPDAVG * 2441) / 157 \quad (3\text{-}1)$$

$$BURNUP = (SUM(POWER(K) * DAYS)) / MTFUEL \quad (3\text{-}2)$$

$$IRP(K) = POWER(K) * AVGEOC / BURNUP \quad (3\text{-}3)$$

where POWER(K) = specific power for irradiation step K based on reactor operating history and measured RPDs

LOADF = reactor power level from reactor operation history for irradiation step K (fraction of 2441 MWth)

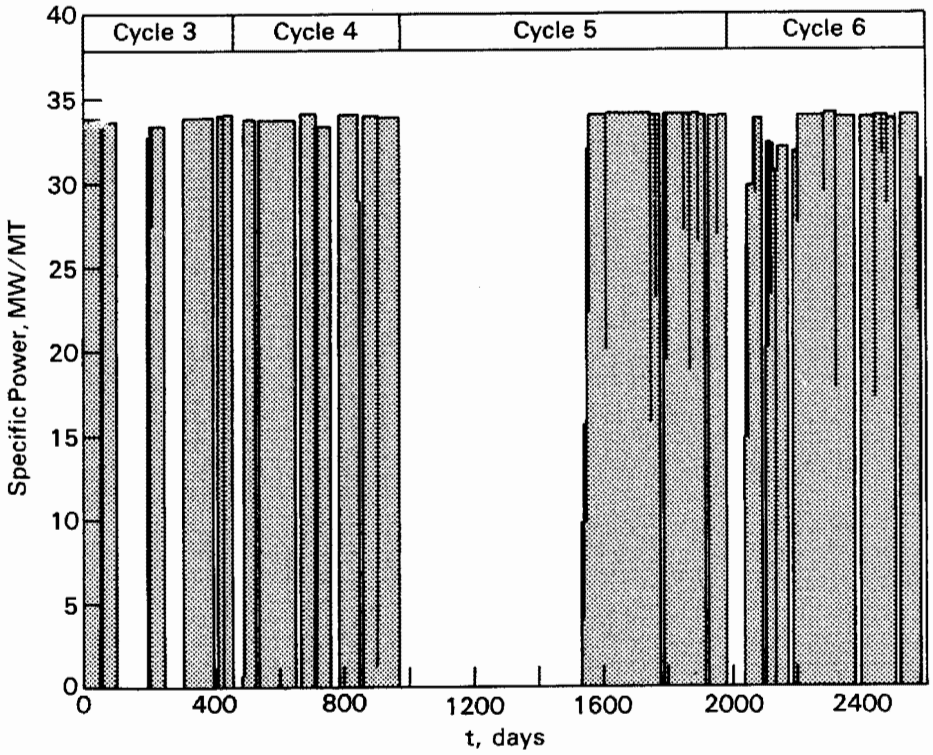

Figure 3-12. Surry2 Operating History

RPDAVG = average RPD for symmetric fuel assemblies for irradiation step K
2441 = full power core heat output (MWth)
157 = total number of assemblies in Surry core
BURNUP = average EOC assembly burnup based on reactor operating history
SUM = summation over all irradiation steps
DAYS = number of days operated for irradiation step K
MTFUEL = metric tons uranium (MTU) loading per assembly
IRP(K) = specific power input for irradiation step K
AVGEOC = average measured EOC burnup for symmetric assemblies.

The above data were compiled for each assembly, and calculations were performed for each similar set of fuel assemblies. A typical assembly power history is shown in Figure 3-13.

Decay Heat Predictions. Using the data and technique described above, predictions of decay heat rates were made with ORIGEN2. The results of these calculations are given in Table 3-2 for the 21 assemblies that were used in the CASTOR-V/21 cask during performance testing. Fuel assembly decay heat generation rates were predicted

Table 3-1

ASSEMBLY AVERAGE BURNUP HISTORIES (MWd/MTU)

Assemblies/Cycle	EOC S2C3	EOC S2C4	EOC S2C5	EOC S2C6
T16, T07, T11, T03, T08, T12, T09, T13	6,114	21,671	35,722	
V12, V24, V04, V08		15,698	31,146	
V05		15,751	31,511	
V15, V13, V14, V11		12,638		29,823
V27, V25, V09, V01		12,663		30,214
Cycle burnup, MWd/MTU	9,427	13,689	13,957	15,997
Cooling time between cycles, days	29	559	54	

to total 28.4 kW at the start of testing and 27.5 kW at the end of testing. A total decay heat load of 28 kW was required to produce fuel rod temperatures in vertical helium and nitrogen test runs near the 380°C allowable (9). Thirteen of the twenty-one fuel assemblies had decay heat rates near 1 kW, and the remaining eight assemblies had decay heat rates of 1.8 kW at the start of the month-long test.

The load pattern for the cask is shown in Figure 3-14. Assembly placements were selected to create quarter symmetry of heat generation within the basket and to produce a relatively flat temperature profile across the fuel assemblies. The HYDRA heat transfer computer code (Section 5) was used to optimize the load pattern.

Predicted Axial Decay Heat Profile

Measured axial decay heat profiles or gamma scans for the Surry spent fuel assemblies were not available as input data to the ORIGEN2 computer code to predict axial decay heat profiles. Axial gamma radiation scans previously obtained on Turkey Point reactor spent fuel assemblies were therefore used to develop a typical assembly axial burnup distribution (10). The Turkey Point and Surry PWR reactors and spent fuel assemblies are of the same designs, so axial decay heat profiles should be very similar.

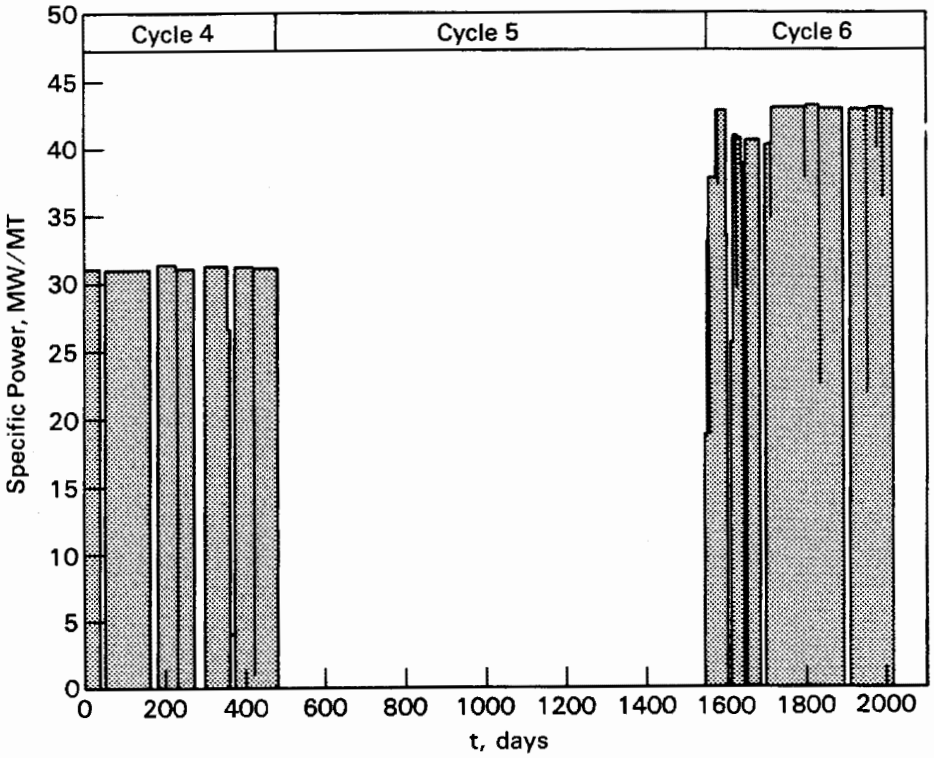

Figure 3-13. Assembly V27 Power History

Table 3-2

SURRY PWR SPENT FUEL CHARACTERISTICS

Assembly	Burnup, GWd/MTU	Cooling Time, months	Initial Enrichment, wt%	Sept. 1985 Pred. Decay Heat, kW Start	End
V04, V08, V12, V24	31.1	46	2.91	1.00	0.98
V05	31.5	46	2.91	1.02	0.99
T03, T07, T08, T09, T11, T12, T13, T16	35.7	46	3.11	1.11	1.09
V11, V13, V14, V15	29.8	26	2.91	1.79	1.72
V01, V09, V25, V27	30.2	26	2.91	1.83	1.75
			Total	28.4	27.5

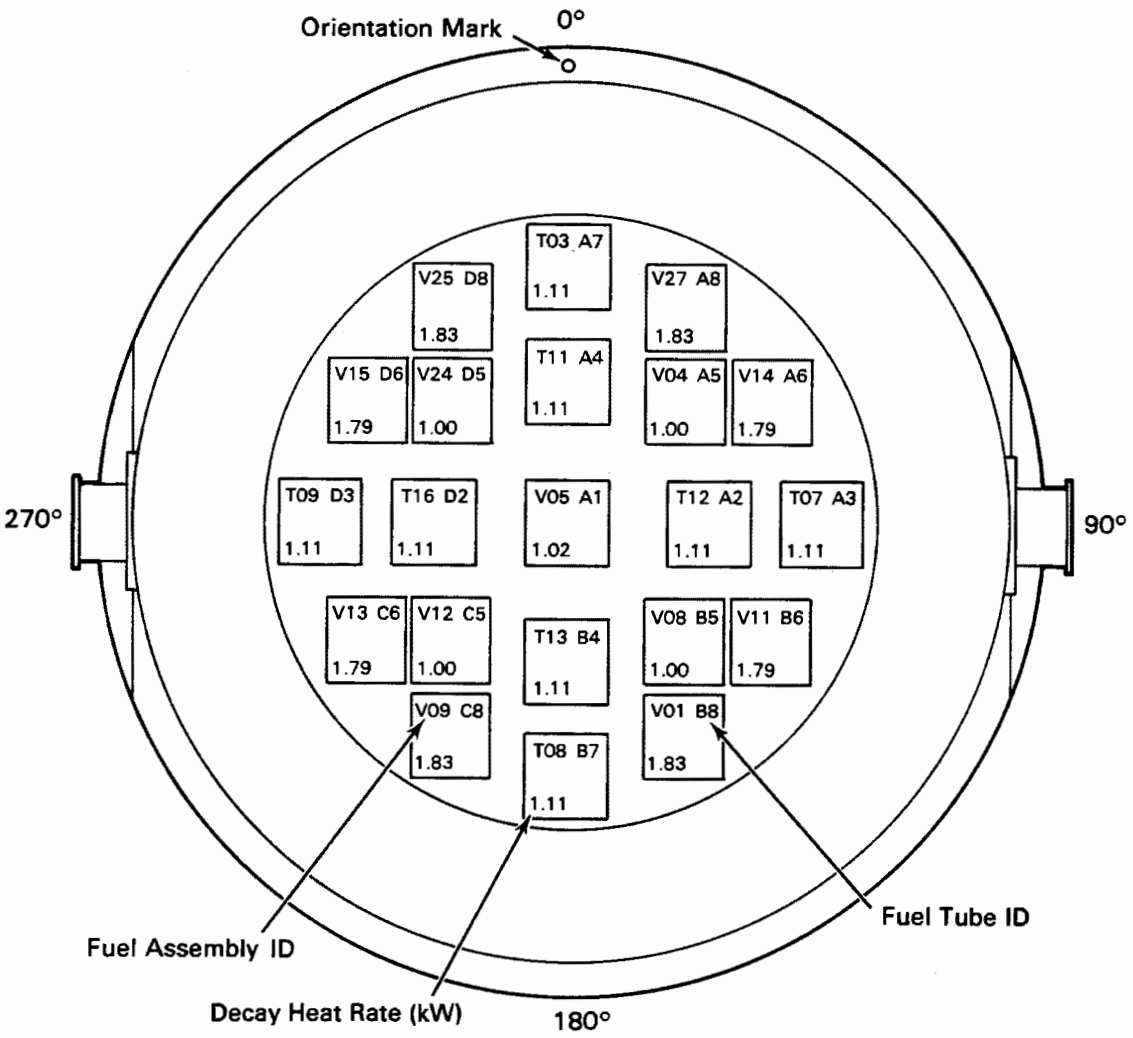

Figure 3-14. Spent Fuel Load Pattern

The axial burnup distribution required as input to ORIGEN2 consisted of an average from gamma scans of 25 rods from five Turkey Point assemblies. ORIGEN2, with the measured gamma distribution and the appropriate Surry operating history, was then used to predict the relationship between burnup values and decay heat rates in specific axial regions (nodes) along the length of a fuel assembly. The measured gamma activity from Turkey Point assemblies and predicted Surry assembly decay heat axial profiles are shown in Figure 3-15. Both profiles are typical of those for spent fuel assemblies from PWR reactors. The dips in the profiles are a result of grid spacers at those locations.

Axial decay heat profiles are important because they strongly influence the shape of axial temperature profiles in the fuel assemblies, especially in vacuum and in a

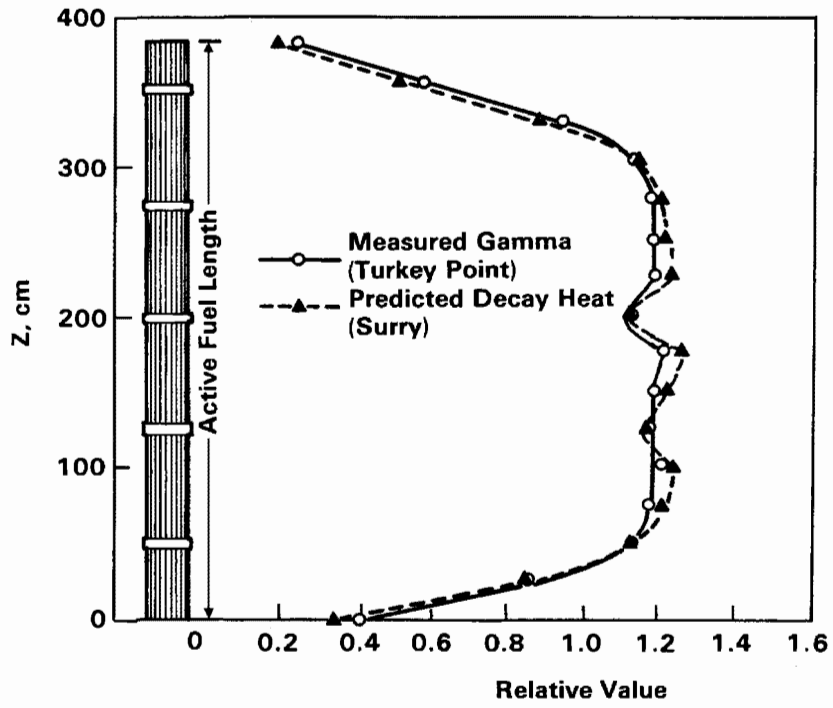

Figure 3-15. Predicted Axial Decay Heat Profile

horizontal orientation where convection heat transfer is minimized. A smoothed representation of the predicted axial decay heat profile (Figure 3-15) was used as input to the HYDRA heat transfer computer program to facilitate pre- and post-test temperature predictions (Section 5).

Fuel Assembly Instrumentation

Seven of the 21 Surry PWR spent fuel assemblies were instrumented with TC lances (tubes) shown in Figure 3-16. Each TC lance had six TCs installed in the 8-mm-diameter (0.315-in.) tube. Lances were inserted through instrumentation penetrations in the primary test lid (Figure 3-3) and into selected guide tubes of the seven assemblies (Figure 3-17). Standard elastomer O-rings in the TC lance flanges were used to establish seals between the cask inner cavity containing spent fuel and the outside environment.

Note that two additional TC lances were inserted through the lid, but not into assembly guide tubes. These two TC lances were used to measure gas temperatures near the center and edge of the fuel basket.

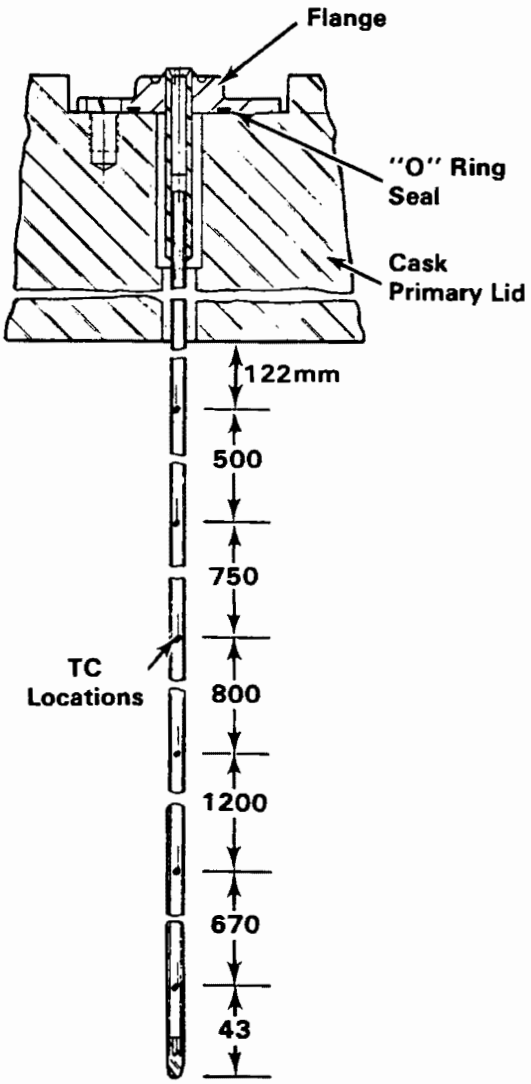

Figure 3-16. Thermocouple Lance

The axial spacing (Figure 3-16) of the TCs in the lances was determined from pre-test predictions obtained with the HYDRA heat transfer code discussed in Section 5. HYDRA pretest predictions were used to determine the cross-sectional locations of the TC lances shown in Figure 3-17. Note that two TC lances were inserted in guide tubes 1 and 3 of the center assembly to determine rod-to-rod temperature gradients. The selected axial and cross-sectional locations of the TC lance thermocouples facilitated redundancy, evaluations of temperature symmetry, and determinations of axial and radial temperature profiles in both vertical and horizontal orientations.

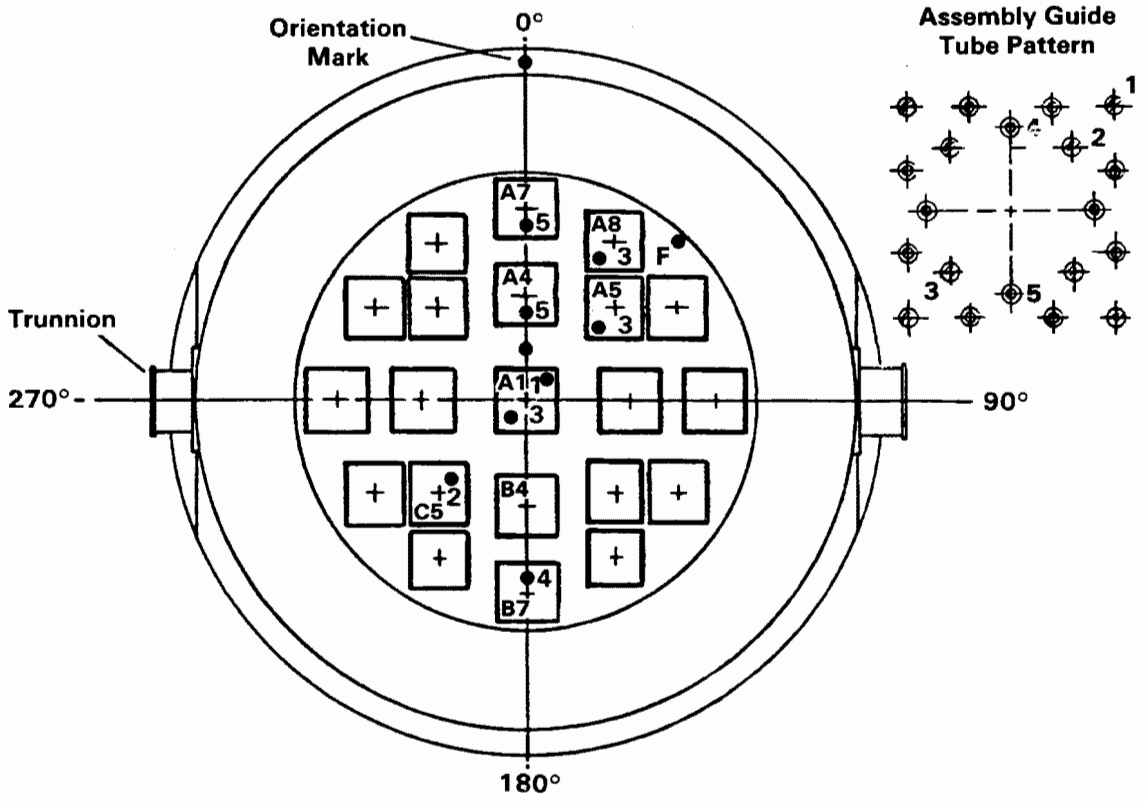

Figure 3-17. Thermocouple Lance Locations

Spent Fuel Integrity

Selected spent fuel assemblies used in the CASTOR-V/21 cask performance test were examined to determine the condition of the spent fuel prior to the test. Further examinations of the spent fuel assemblies upon completion of the long-term surveillance period will help determine whether long-term dry storage affected the spent fuel integrity or characteristics. Information on integrity is of interest in evaluating the impact of dry storage on the behavior of spent fuel rods during long-term dry storage and fuel-handling operations associated with dry storage. The main areas of interest for the spent fuel include the integrity of the fuel cladding, the condition of the spent fuel assembly hardware, and the character and condition of the crud. Specific information that was desired included the amount and type of damage, if any, to the cladding or fuel assembly hardware prior to fuel loading into the cask for performance testing and long-term dry storage; confirmation that no fission gas was being released from the spent fuel rods prior to the cask performance test; and characterization of the crud from both the fuel rods and the shipping cask prior to performance testing and long-term dry storage.

Four examination methods were used to assess the integrity of the Surry fuel assembly rods prior to the performance test. These included ultrasonic examinations at VP; visual observations, including full-length black and white videos at both VP and INEL, and color photographs at INEL; and analyses of the cover gas in the CASTOR-V/21 cask. Although crud behavior does not directly relate to fuel rod integrity, crud sampling was performed because crud spallation has been known to impact fuel-handling operations. Evidence that crud soaks loose during wet storage of some spent fuel rods has led to increased interest in crud behavior during rod consolidation and other dry operations.

Each fuel integrity examination is discussed in the following subsections. The results of the crud sample analyses for both the cask and fuel assemblies are also discussed.

Inpool Ultrasonic Inspections. The Babcock & Wilcox Failed Fuel Rod Detection System (FRDS) is a portable system designed to be used underwater in spent fuel pools as shown in Figure 3-18. The system consists of an underwater manipulator (Figure 3-19) an ultrasonic probe (Figure 3-20), electronic controls, recording equipment, and a support plate (Figure 3-18). The manipulator with its probe (Figure 3-19), is attached to the support plate before it is submerged into the pool. The support plate, which rests upon the spent fuel pool storage racks, positions and stabilizes the fuel assembly being examined. The manipulator is doubly enclosed in a sealed steel casing, which reduces the chances of leakage and facilitates decontamination.

The FRDS is based upon ultrasonic techniques and is able to differentiate between sound and leaking rods by detecting the presence of moisture in the latter. The system uses a dual probe as shown in Figure 3-20. The probe incorporates a miniature ultrasonic transmitter and receiver on opposite sides of the probe arms. The probe is inserted in the gap between fuel rods while an ultrasonic pulse is transmitted between the arms of the probe. Defective fuel rods contain moisture, and even small amounts of water diffuse and attenuate the signals, providing distinctive traces on the oscilloscope and X-Y plotter (Figure 3-21). The arms of the test probe are quite flexible and able to accommodate differences between rod diameter and guide tube diameters as well as to accommodate distortions that may have occurred in the fuel assembly. Contact between the probe arms and the fuel rods is minimal. In addition, the probing system incorporates a load-sensitive limit switch that stops the probe if resistance is encountered.

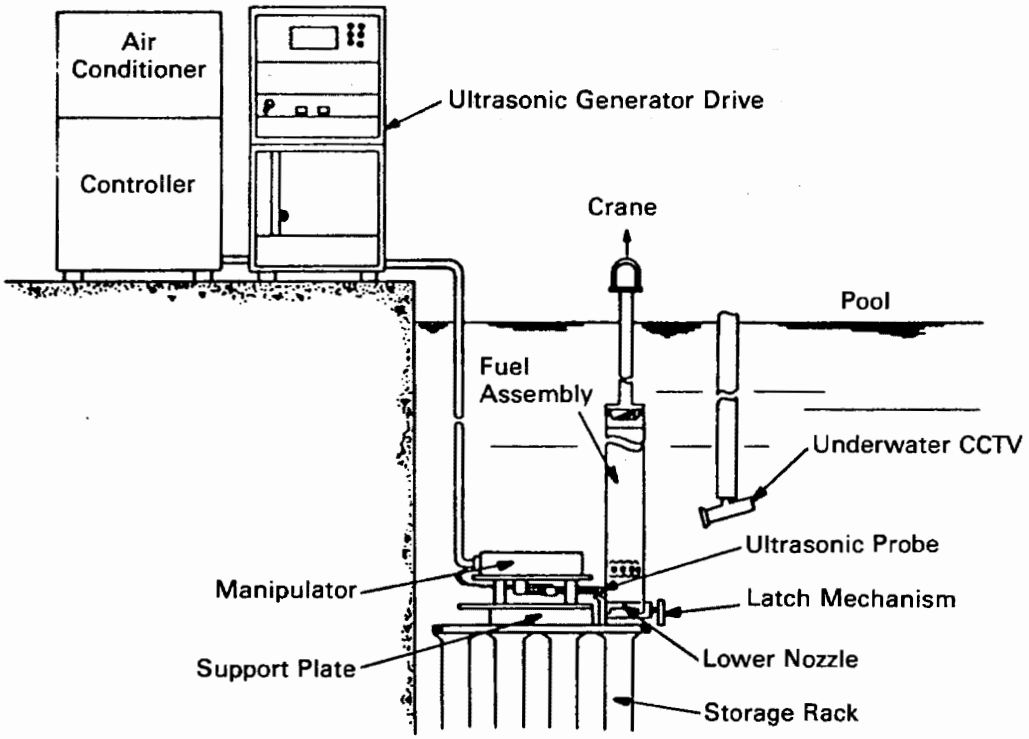

Figure 3-18. Failed Rod Detection System

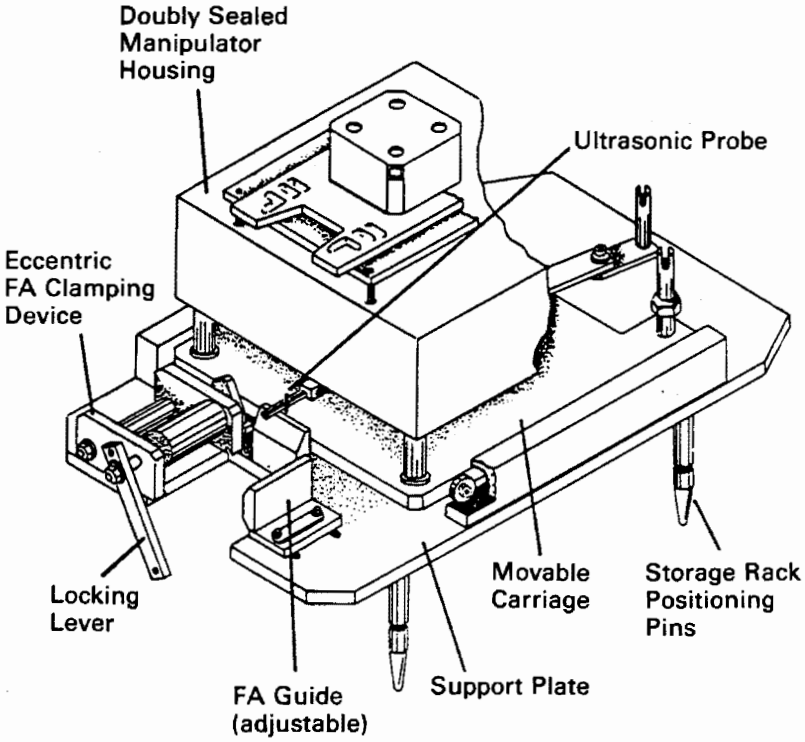

Figure 3-19. Failed Rod Detection System Manipulator and Support Plate

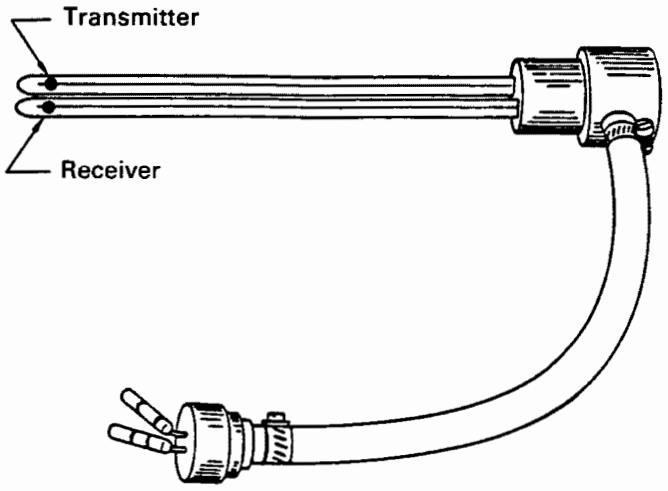

Figure 3-20. Failed Rod Detection System Ultrasonic Probe

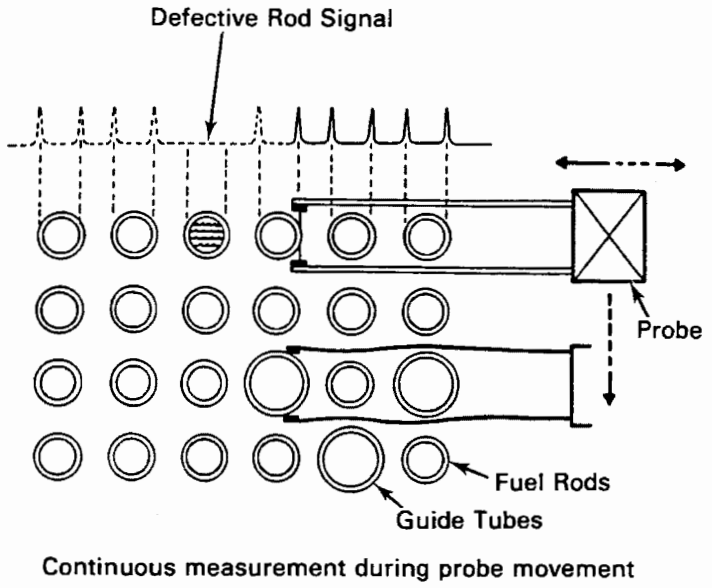

Figure 3-21. Typical Failed Rod Detection System Signal

During examinations, the fuel assembly is suspended from the overhead crane and positioned so that the lower region of the fuel rods is located in front of the manipulator and probe. After initial alignment and calibration, the probe is automatically aligned with the rods and inserted and withdrawn sequentially in each gap between fuel rods. The fuel rods can be examined during both the insertion and

withdrawal stroke; however, traces are normally taken during the withdrawal sequence only. After the entire side has been examined, the fuel assembly is rotated 90 degrees and each row of rods is reexamined providing a cross-check on the ultrasonic indications. All of the fuel was examined from two faces during the initial scans; however, those assemblies considered suspect were later examined on the other two faces.

Before the Surry fuel was inspected, a detailed inspection procedure was prepared and reviewed by all concerned parties, including the Surry Station Plant Review Committee. Only the salient points of that procedure are included here.

A. Equipment Pre-Test Checkout

- Before the FRDS equipment was moved into the spent fuel pool area, a radiation work permit was obtained and site health physical prepared the necessary area corresponding to the needs of the FRDS equipment.

- All components of the FRDS, including electronic components, cables, and manipulator, were removed from their shipping cartons and placed in the prepared area adjacent to the spent fuel pool. The support plate, which had been previously used and stored at the Surry Station, was mated with the manipulator, and a television camera was affixed to the manipulator with a pre-prepared bracket.

- Electronic cables were interconnected between the controller, air conditioner, UT electronics, X-Y plotter, and the UT probes attached to the manipulator.

- Each of the electrical components was individually adjusted to conform to manufacturer's calibration standards, and the entire system was checked for continuity to ensure that the system operated as expected.

- Each of the detailed steps of checkout and inspection procedure required signoff by the individual responsible for the respective action, and each signoff was dated.

- At this point, before the manipulator/support plate was lowered into the spent fuel pool, a "site hold point" was initiated to allow health physics and site quality control to confirm that all procedural steps had been completed, that no site procedures were being violated, and that potential hazards had been considered.

B. System Calibration

- The overhead crane was used to lower the manipulator/support plate into the spent fuel pool and to position it in its predetermined location on the fuel storage racks.

- Following confirmation that the manipulator/support plate was properly located and secured in place, a calibration fuel assembly was moved into position in the support plate. Functional

checkout of the FRDS system, consistent with the detailed inspection procedure, was then completed.

C. Fuel Examination

- The spent fuel assembly to be examined was moved from its position in the spent fuel storage rack to the manipulator/support plate using the spent fuel handling bridge. The fuel assembly was positioned in the support plate using the "Excenter", a device integral to the design of the support plate that accurately positions the fuel assembly in its proper position for inspection. Fuel rod inspections were performed at a level approximately 2 cm (0.8 in.) above the lower fuel assembly grid.

- The manipulator automatically moved the UT probe along the entire length of the first row of fuel rods in the assembly. It then automatically shifted its position to the second row of fuel rods and continued the inspection of the second row of rods in the same manner as the first. Subsequent rows of fuel rods were similarly examined until all 15 rows of rods had been examined.

- The fuel assembly was then removed from its position in the support plate, rotated 90 degrees, and repositioned in the support plate. The second face was then examined in the same manner as the first. Each fuel assembly was examined in 20 to 30 min in the exact same manner as the first. Most of this time was spent in transferring the fuel assembly to and from the FRDS. Hard copy printouts of each fuel rod examined were produced on the X-Y plotter. Each face of each fuel assembly was recorded by the plotter and retained for record purposes.

- A number of the suspect fuel assemblies were reinspected from the two alternate faces of the assembly. The UT probes for those reinspected assemblies were located approximately 25 mm (1 in.) above the bottom grid of the fuel assemblies.

D. Equipment Disassembly and Decontamination

- When the fuel examinations were completed, the manipulator/support plate was removed from its position on the fuel storage racks to the periphery of the spent fuel pool. The equipment was removed with the overhead crane under guidance of the surry station site health physics personnel. As the manipulator/support plate was removed from the water in the pool, it was thoroughly hosed down with clean station water to remove all loose radioactive contamination.

- After the manipulator/support plate was wiped dry, smear samples were taken by site health physics staff on all of the FRDS equipment including the electronics. The decontamination process resulted in no detectable radioactive contamination on the electronics and minor levels on the manipulator/support plate (approximately 1 to 3 mr.).

- All components were returned to their respective shipping containers for offsite shipment.

All of the fuel inspected assemblies were examined from two adjacent faces. During the examination, fuel rods within the assemblies were determined to be CLEAR, SUSPECT, or leaking as indicated by the term INDICATION. Those assemblies that were CLEAR were not reexamined; however, all SUSPECT assemblies were reexamined from the remaining two faces. Those assemblies that clearly had INDICATIONS were not reexamined; however, several SUSPECT assemblies were reexamined to verify the validity of the initial examination.

The amplitude of pulses is the chief indication of the status of each fuel pin examined. Other factors tend to invalidate the results and must be considered. Specifically, crud buildup on a fuel pin may well distort the UT signal, resulting in a faulty indication. Rod bow, which causes variation in proximity of the probe to the fuel rod, may also result in a faulty indication.

Table 3-3 presents a summary of the fuel examination findings. A sample trace is shown in Figure 3-22.

Table 3-3

SUMMARY OF FUEL INSPECTION RESULTS

Assembly ID	Date Inspected	Clear	Indication	Suspect	Faces
T03	8/20/84	X			1/4
T07	8/20/84	X			1/4
T08	8/19/84	X			1/4
T09	8/20/84	X			1/4
T11	8/20/84	X			1/4
T12	8/20/84	X			1/4
T13	8/18/84	X			1/4
T16	8/20/84	X			1/4
V01	8/19/84	X			1/4
V04	8/18/84	X			1/4
V05	8/19/84	X			1/4
V08	8/18/84	X			1/4
V09	8/19/84		X		1/4
V09	8/28/84	X			2/3
V11	8/18/84	X			1/4
V12	8/18/84	X			1/4
V13	8/18/84	X			1/4
V14	8/18/84		X		1/4
V14	8/26/84	X			2/3
V15	8/18/84	X			1/4
V24	8/19/84	X			1/4
V25	8/19/84	X			1/4
V27	8/18/84	X			1/4

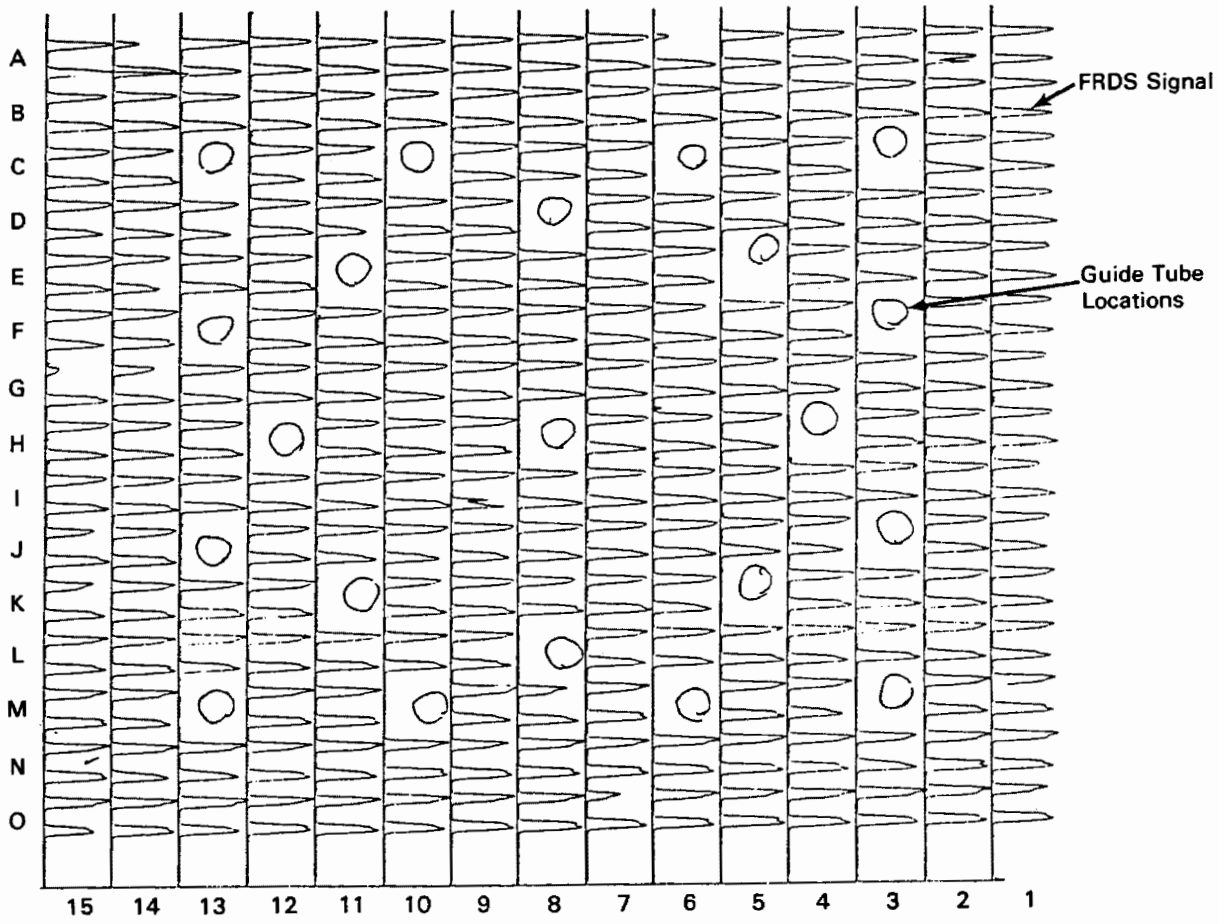

Figure 3-22. Sample FRDS Trace

Evaluation of data entailed the systematic interpretation of the output traces from the FRDS system. To ensure consistent and reliable interpretation of these traces, a calibration assembly was examined using the FRDS system at the beginning and completion of each work shift. During the latter stages of fuel examinations, the calibration assembly was evaluated only once per shift. This was deemed acceptable due to the continuity between calibration traces obtained during the initial days of fuel examinations.

As previously noted, numerous factors must be considered when interpreting the X-Y plots of each fuel assembly examined. These factors include pulse height, crud deposits on the fuel rods, fuel assembly, and fuel rod bowing. Because the proximity of the UT probe to the fuel rods may vary with fuel rod bowing, pulse amplitudes would also tend to vary in height. Fuel assemblies that produced such traces

were reexamined from all four faces. In each case, fuel rods that were SUSPECT during the initial examination were found to be either CLEAR or INDICATION (failed) during reexamination.

The following criteria delineate standards used to determine the integrity or failure of specific fuel rods:

1. Fuel Rods That Do Not Exhibit Failure

   For each fuel pin examined, two pulses appear as output to the X-Y plotter. The presence of these two pulses with peak amplitudes of 1.5 to 2.0 cm (0.6 to 0.8 in.). indicate a fuel rod that has not undergone failure.

2. Fuel Rods With Failure Indications

   Several types of indications may appear to denote fuel rod cladding degradation to the point that leaks have occurred. Such indications are as follows:

   - No peaks appear on the X-Y recorder trace at the location of the fuel rod undergoing examination.
   - One or both of the pulses appear indistinctly; the peak height in this case is less than one-fifth the normal pulse height.
   - While two peaks do appear, their heights are less than one-half the normal peak, and a discontinuity (crack) appears at the peak of one or both pulses.
   - Only one peak appears; the height is less than one-half the normal peak, and a discontinuity appears at the peak of the pulse.

3. Fuel Rods With "Suspect" or "Likely" Failures

   Two types of indications generally denote a suspected fuel pin failure:

   - Only one pulse appears and has no discontinuity at the peak of the pulse.
   - One or two peaks appears; however, the amplitude of each or both is approximately one-half the normal pulse amplitudes, and there are no discontinuities in the pulse peak.

   If either of these two conditions occurs, the procedure was to reexamine the fuel assembly from the remaining two fuel assembly faces. In the event uncertainty still existed regarding integrity of the fuel rod, the assembly was examined at a different vertical location. As a result of the inspections, all assemblies subsequently shipped from the Surry Station for CASTOR-V/21 cask performance testing were determined to be free of defects.

Cask Cover Gas Sampling. The cask cover gas was sampled several times during performance testing, to evaluate the integrity of the spent fuel rods. Cover gas samples were taken as indicated in Table 3-4. Each sample was collected in a separate 500-cc stainless steel cylinder equipped only with quick disconnect-fittings and no bellows-sealed valves as part of the closure. The cylinders were checked for leaks prior to sampling. Because only quick disconnect-fittings were used for the cylinder closure, the cover gas samples in the cylinders were diluted with ambient air from the vicinity of the sampling apparatus, air that leaked into the cylinder during shipment, and argon introduced at Lawrence Livermore National Laboratory (LLNL) when it was necessary for valves to be fitted to the cylinder quick-disconnects in an argon atmosphere to perform the sample analyses. In many cases, this dilution was made more severe by the collection of small amounts of cask cover gas, presumably due to short equilibration times between the cask and the sample bottle during the actual cask cover gas collection procedure. The end effect

Table 3-4

CASK GAS SAMPLES

LLNL Sample No.	Sample No.	Sample Collection Time/Date	Cover Gas	Cask Orientation	LLNL Calculated Sample Pressure, mbar
1	1A	1400/9-06-85	He	Vertical	513
2	1B	1400/9-06-85	He	Vertical	569
3	1C	1330/9-11-85	He	Vertical	386
4	1D	1300/9-11-85	He	Vertical	152
5	2A	1920/9-11-85	N2	Vertical	421
6	2B	1930/9-11-85	N2	Vertical	606
7	2C	1345/9-13-85	N2	Vertical	99
8	2D	1430/9-13-85	N2	Vertical	150
9	4A	1410/9-16-85	He	Vertical	391
10	4B	1419/9-16-85	He	Vertical	158
11	4C	1045/9-20-85	He	Horizontal	590
12	4D	1050/9-20-85	He	Horizontal	704
13	5A	NA/9-20-85	N2	Horizontal	121
14	5B	NA/9-20-85	N2	Horizontal	761
15	5C	1300/9-23-85	N2	Horizontal	164
16	5D	1300/9-23-85	N2	Horizontal	142

of small, diluted samples on the cask cover gas analyses is to increase detection limits, increase measurement uncertainties, and introduce questions of sample validity.

Three types of gas analyses were performed at LLNL: sample pressure, mass spectra, and radionuclide concentration. For the purpose of intercomparison of the gas analyses, it was necessary to renormalize the concentrations measured to the cover gas content of the samples (helium or nitrogen excess after subtraction of air based on oxygen). The sample pressures shown in Table 3-4 were determined by assuming that the sample bottle volume was 500 cc, expanding the gas into a calibrated volume, and measuring the pressure in the calibrated volume. The pressure values given in Table 3-4 have been reduced to the equivalent pressure at 0°C and may be corrected to the pressures at sampling time when corrected for cask and system temperatures and expansion volumes during sampling. The fact that the sample cylinder pressures are significantly different from the nominal 600 mbar in the cask indicates sampling difficulties and possible air leakage into the gas samples. The overall accuracy of the pressure measurement is about ±1%.

The results of the LLNL gas analyses are presented in Table 3-5. Mass spectra were analyzed for all common fixed gases with masses less than 100. Only N_2, O_2, He, Ar, and CO_2 concentrations above 0.01% are detected in any of the samples. Analyses of the other species reported are of marginal reliability. Water is reported as a lower limit due to absorption on vessel walls. The accuracy of the mass spectra measurements is noted in Table 3-5. It is obvious that significant amounts of air were introduced in each gas sample. The problem was traced to leaking quick-disconnects on each sample cylinder.

Table 3-6 presents measured concentrations and detection limits for ^{85}Kr, and ^{14}C from the cover gas samples. The radionuclide concentrations ^{85}Kr, $^{14}CO_2$, and ^{14}CO were determined in two stages. The first stage involved screening analyses which were done by thin window beta counting to find ^{85}Kr activity greater than 1 nCi/ml. Activity can be measured as low as 1 pCi/ml. At least one of each sample pair was processed for ^{85}Kr and at least one sample from each test run was processed for ^{14}C as both CO_2 and CO. The second stage involved elution chromatography to obtain the separated, pure gases for radioassay. In all cases, inactive carrier gases were added to the samples prior to processing and were recovered in good yield. The separated krypton gas was analyzed either by thin window beta counting for high levels or by internal proportional counting for low levels. Carbon-14 was measured as $^{14}CO_2$ by internal proportional counting for low levels. The CO was separated

Table 3-5

CASK GAS SAMPLE COMPOSITION

LLNL Sample No.	Sample Run No.	Volume Percent[a]								
		He	N_2	O_2	A	CO_2	CO	H_2O	N_2O	H_2
1	1C	89.05	6.021	1.350	3.496	0.050	<0.1	>0.01	<0.01	<0.01
2	1A	69.30	21.90	5.967	2.798	0.029	<0.01	>0.01	<0.01	<0.01
3	1B	62.51	25.57	6.692	5.148	0.033	<0.1	>0.01	<0.01	<0.01
4	1D	59.59	17.59	4.110	18.66	0.048	<0.01	>0.01	<0.01	<0.01
5	2A	<0.01	95.34	1.180	3.457	0.017	<0.01	>0.01	<0.01	<0.01
6	2B	<0.01	90.58	6.81	2.581	0.024	<0.01	>0.03	<0.01	<0.01
7	2C	0.031	68.79	3.134	27.95	0.059	<0.01	>0.02	0.019	<0.01
8	2D	0.042	70.08	8.43	21.29	0.153	<0.01	>0.01	<0.01	<0.01
9	4B	70.59	14.23	5.95	9.09	0.060	<0.1	>0.05	<0.01	0.018
10	4A	32.38	50.55	13.31	3.700	0.053	<0.01	>0.02	<0.01	<0.01
11	4C	65.69	1.560	0.156	32.58	<0.01	<0.01	>0.01	<0.01	<0.01
12	4D	<0.01	76.94	20.26	2.746	0.054	<0.01	>0.01	<0.01	<0.01
13	5A	0.050	74.92	11.441	13.43	0.120	<0.01	>0.02	0.015	0.016
14	5B	<0.01	73.95	18.77	7.217	0.060	<0.01	>0.02	<0.01	<0.01
15	5C	0.048	85.63	5.559	8.533	0.065	<0.01	>0.01	<0.01	0.159
16	5D	0.068	91.06	0.158	8.462	0.044	<0.01	>0.01	<0.01	0.207

[a]Species present in mass spectra at 0.01% or more. Accuracy of these measurements is ±0.2% of 1 unit in the least significant digit.

from the gas sample, converted to CO_2 over CuO at 500°C, and also analyzed by internal proportional counting. Typically, activities above 0.02 pCi/ml can be detected by this method. The amounts of ^{85}Kr and ^{14}C are relatively low and are what would be expected to result from crud, not a leaking fuel rod.

It was generally expected that the screening analysis would agree with the processed ^{85}Kr result. However, for these samples the screening counts were significantly greater than the processed krypton results. Tritium would not be detected by the screening analysis. Argon-79 and $^{14}CH_4$, the other long-lived beta emitters that might be present, were not detected during an exploratory analysis of Sample 4 in February 1986. Similarly, no ^{127}Xe was found in xenon separated from the sample. Because screening was done in November 1985 and processing in February 1986 (for Sample 4), the possibility of sample contamination with short-lived fission xenon or possibly other activities accompanying the air leakage cannot be ruled out. To

Table 3-6

CASK GAS RADIONUCLIDE CONCENTRATION

LLNL Sample No.	Sample Test Run No.	Radionuclide Concentration, pCi/ml[a]			
		Analysis	^{85}Kr	$^{14}CO_2$	^{14}CO
1	1C	28.7 ± 0.4	<0.02	3.18 ± 0.28	<0.06
2	1A	4.78 ± 0.39	0.09 ± 0.05[b]	--	--
3	1B	4.60 ± 0.57	--	--	--
4	1D	15.9 ± 3.5	0.37 ± 0.13[b]	--	--
5	2A	<0.13	<0.05	--	--
6	2B	0.22 ± 0.08[b]	--	--	--
7	2C	7.15 ± 0.69	0.26 ± 0.09[b]	1.36 ± 0.02	<0.14
8	2D	5.98 ± 0.36	--	--	--
9	4B	5.77 ± 0.58	--	--	--
10	4A	0.23 ± 0.16[b]	0.07 ± 0.04[b]	--	--
11	4C	1.92 ± 0.16	0.05 ± 0.01[b]	0.59 ± 0.01	<0.03
12	4D	<0.08	--	--	--
13	5A	1.38 ± 0.46	<0.17	1.38 ± 0.04	<0.12
14	5B	<0.08	--	--	--
15	5C	4.01 ± 0.41	0.18 ± 0.07[b]	--	--
16	5D	8.28 ± 0.75	0.19 ± 0.11[b]	7.38 ± 0.04	0.47 ± 0.02[b]

[a]Picocuries per milliliter of sample at 760 mbar, 0°C, decay corrected to 1/1/85. Indicated errors are one standard deviation of the mean of replicate measurements.

[b]Marginally detectable. Detection limit defined as sample count rate greater than 25% that of the detector background. For ^{85}Kr the detection limit is adjusted by 5% of the krypton carrier background.

recheck the screening analysis, this measurement was repeated in February. Unfortunately, the sample was severely diluted with air. The results at that time were below the detection limit as defined, but were above background and consistent with the previous measurement. The analysis indicated the presence of a long-lived beta-emitting gas, which is not Ar, Kr, Xe, ^{14}C, or T, in the cover gas. The test results are summarized in Table 3-7. The consistency between sample pairs is generally good and strongly suggests that the measured activity is associated with the cask gases. The disparity between screening and processed concentrations remains unexplained. However, the relatively low amounts of ^{85}Kr detected indicate that no leaking fuel rods were present in the cask during performance testing. This is particularly significant because the first few assemblies loaded in the cask were exposed to air for approximately 200 h during incremental loading of the cask and fuel assembly/basket inspections at a reduced temperature. In addition, after testing was completed and long-term surveillance started, all the fuel assemblies

Table 3-7

NORMALIZED RADIONUCLIDE CONCENTRATION (pCi/ml in He or N_2)

Sample Test Run No.	LLNL Sample No.	% He or N_2-O_2 Air		Date	Based on Analysis Screening		Based on Separated ^{85}Kr
1A	2	63.30	He	9/6	7.93	7.73	0.13
1B	3	62.51	He	9/6	7.53	7.73	--
1C	1	89.05	He	9/11	32.4	33.2[a]	(≤0.07)
1D	4	59.59	He	9/11	34.0	33.2[a]	0.62
2A	5	90.94	N_2	9/11	--	--	(≤0.05)
2B	6	65.20	N_2	9/11	--	--	--
2C	7	57.11	N_2	9/13	13.9	13.5	0.45
2D	8	38.66	N_2	9/13	13.2	13.5	--
4A	10	32.38	He	9/16	--	--	0.22
4B	9	70.59	He	9/16	--	--	--
4C	11	65.69	He	9/20	2.51	2.51	0.08
4D	12	≤0.01	He	9/20	--	2.51	--
5A	13	32.28	N_2	9/20	7.96	7.96	(≤0.5)
5B	14	3.99	N_2	9/20	--	7.96	--
5C	15	64.91	N_2	9/23	4.33	9.41	0.28
5D	16	90.47	N_2	9/23	9.41	9.41	0.21

[a]Sample test run 1D (LLNL #4) screening analysis was repeated, and results show 38.8 pCi/ml He.

were in a 70% He and 30% air environment for approximately four months because a quick disconnect fitting on the cask lid had not sealed shut.

Video and Photographic Examinations. The fuel assemblies were examined visually to establish their general condition after shipment from VP, after handling at the INEL hot shop, and after CASTOR-V/21 cask performance testing, but prior to the long-term surveillance. Two kinds of visual examinations were used: black and white videos

of eight fuel assemblies (V05, V12, V24, V27, T03, T08, T11, and T13), and color photography of two fuel assemblies (V05 and V27). The fuel examination test plan specified that any fuel assemblies with unusual characteristics also be scanned and that unusual areas be photographed.

The black and white videos taken at both VP and INEL did not provide sufficient detail to characterize the crud or very small features on the fuel rods. However, they did reveal no indications of significant variations in the fuel rods after shipment, handling, and performance testing. The videotapes alone, did not provide enough detailed information to adequately determine the integrity and condition of the fuel and fuel cladding. Examination of the video scans shows that all of the fuel assemblies and fuel rods look basically the same when viewed from the outside of the assemblies. There was some discoloration of the fuel rod cladding in the area of the grid spacers, which was expected.

Color photographs were taken at six levels on each of four sides of fuel assemblies V05 and V27. A typical orange/reddish crud (probably Fe_2O_3) was evenly deposited on all of the Zircaloy 2 cladding and fuel assembly hardware. A photograph showing typical fuel assembly conditions near the upper hardware and upper portions of the fuel assemblies is shown in Figure 3-23. There were no noticeable changes in the characteristics or adherence of the crud during handling operations involving the spent fuel assemblies at INEL. Figure 3-24 shows typical details of the fuel rods in the area of spacer grids. Some scratches and worn spots were apparent on the spacer grids and some fuel rods, but these features did not change as a result of examination or handling operations. In general, the fuel rods were in excellent condition, with a very adherent crud layer.

Crud and Smear Sampling. The crud from the fuel assemblies was sampled to establish its characteristics and determine if any crud spallation occurred during the fuel shipment and fuel-handling operations. If crud spallation had occurred during dry storage testing or in the basin after the long term testing, then the characteristics of the crud might prove useful in evaluating the performance and long-term dry storage data. Crud and smear samples were also collected from the bottom and side of a TN-8L shipping cask after the first fuel shipment and again after the final shipment to INEL.

The results of the analysis of seven smear and crud samples are given in Table 3-8. The values in brackets are from the final TN-8L shipment and values in parentheses are estimates of the precision of the measurements expressed as percentages. The

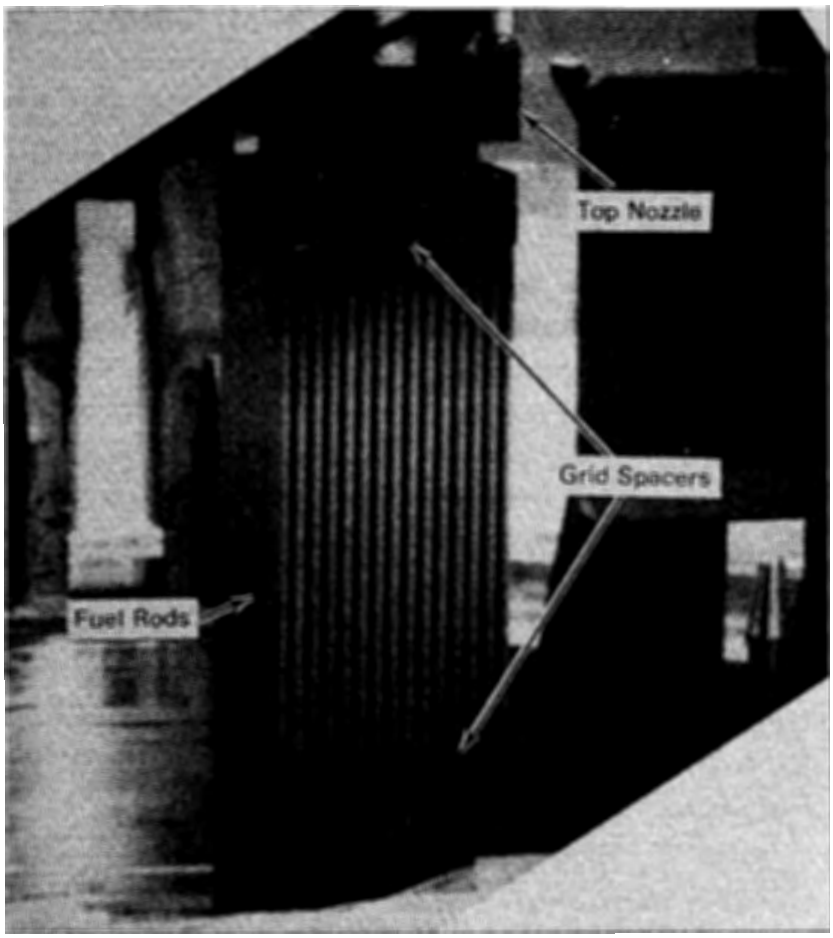

Figure 3-23. Typical Fuel Assembly Condition Near Upper Hardware

crud and smear data from the TN-8L shipping cask show that the cask was actually cleaner after the final shipment and indicates cleaning of the cask between shipments was effective. No fission product species were detected. Species such as ^{137}Ce would be detected at levels of more than a few thousand disintegrations per minute in these spectra. The samples were counted in the as-received condition at an ill-defined (nominally 5 cm) distance from the detectors. Because of this, the relative amounts of species detected in the swipes should be reliable, but absolute amounts are of questionable accuracy. Data were processed by the GAMANAL code (11) which finds peaks, calculates photons per minute., identifies radionuclides, and outputs disintegrations per minute for various species. The absence of a result for any given species means only that the code was unable to identify its characteristic gamma rays in the spectra. The detection of less abundant species was precluded or reduced by the presence of large quantities of ^{60}Co in the samples.

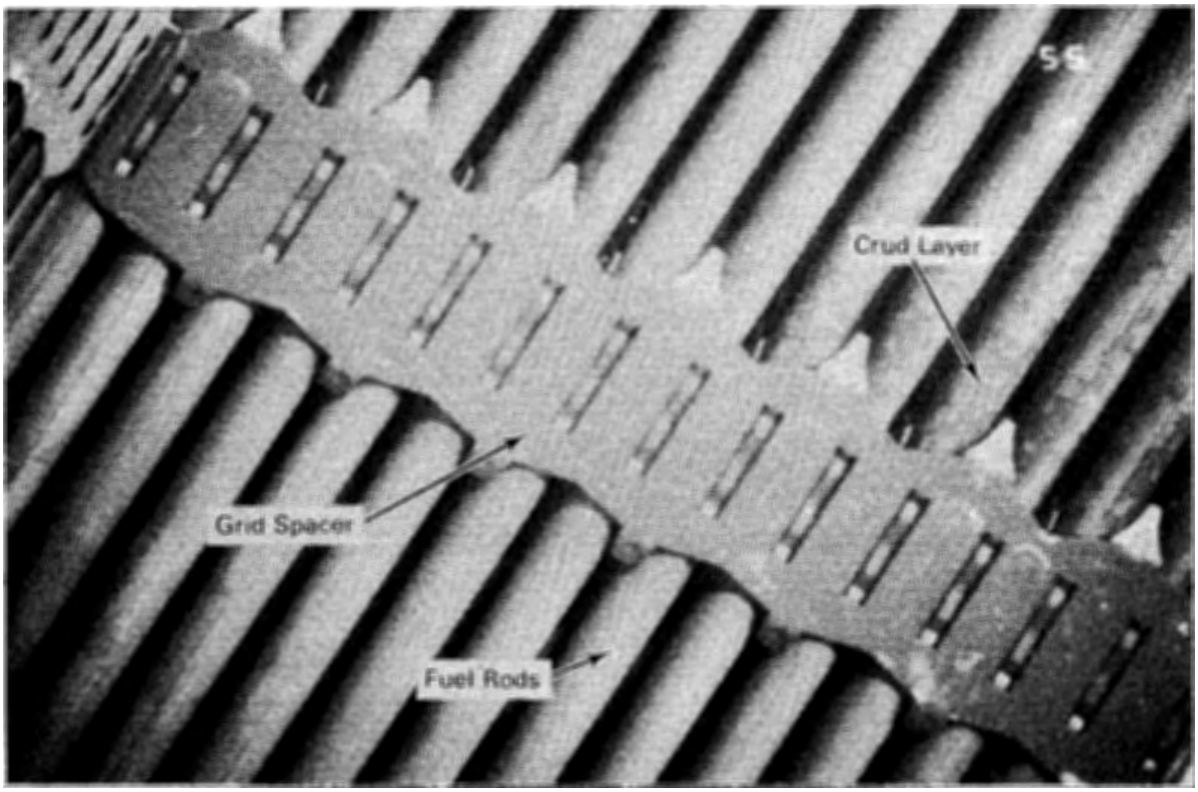

Figure 3-24. Fuel Assembly Condition Near Spacer Grids

Table 3-8

ANALYSIS OF CRUD AND SMEAR SAMPLES FROM A TN-8L SHIPPING CASK AND SURRY FUEL

Source:	TN-8L Shipping Cask		
Date Swiped:	8-16-85 [10-2-85]		
Description:	Side Smear TN8L-SS	Bottom Smear TN8L-BS	Bottom Crud TN8L-BC
LLNL ID No:	[9040199001 85-324T02]	9030599005 [9040299002 85-324C01]	9030699005 [9040399003 85-324C02]
	10^4 dpm at noon January 1, 1985 (±%)		
^{54}Mn	[2.2(7.4)]	37.4(4) [4.7 (5.8)]	160(2) [12.9 (3.3)]
^{60}Co	[245.0(1.1)]	2940.0(1) [832.0 (0.5)]	5790.0(1) [1040.0 (0.5)]
^{65}Zn	[0.7(68)]	-- [--]	272.0(29) [--]
^{125}Sb	[0.3(22)]	2.98(28) [0.7 (26)]	82.8(3) [1.4 (19)]

Table 3-8

(CONTD)

Source:	Surry Fuel	
Date Swiped:	10-2-85	
Description:	ANSI ID side of FA LND 425 VP + V05 Between 3rd and 4th grid spacer	180° from ANSI side of FA LMO 425 VP + V05
LLNL ID No:	9050199001 86-044T01	9050299002 86-044T02
	10^4 dpm at noon January 1, 1985 (±%)	
^{54}Mn	15.1(1.6)	7.8(1.7)
^{60}Co	519.0(0.5)	327.0(0.6)
^{65}Zn	2.6(66)	1.6(19)
^{125}Sb	18.7(0.7)	4.1(1.5)

DATA ACQUISITION SYSTEM

The data acquisition system (DAS) used to receive and process signals from the cask and fuel TCs and the cask pressure transducer is shown schematically in Figure 3-25. The system consisted of extension leads from the respective sensors to a junction box (JB#1). Additional extension leads were required from junction box 1 (JB#1) to junction box 2 (JB#2) located near the Keithly 500 DAS.

The Keithly 500 DAS is a general-purpose data acquisition and control device consisting of a Keithly 500 mainframe and a standard IBM PC with a CRT display, floppy disk drive, and printer (12). The Keithly 500 mainframe provides an interface between an IBM PC and the real world (instrumentation sensors). Therefore, any IBM PC can be used for direct data acquisition and intelligent process control.

The Keithly 500 mainframe is a modular system, centered around a low-noise chassis containing a precision power supply and baseboard with slots for 10 plug-in modules.

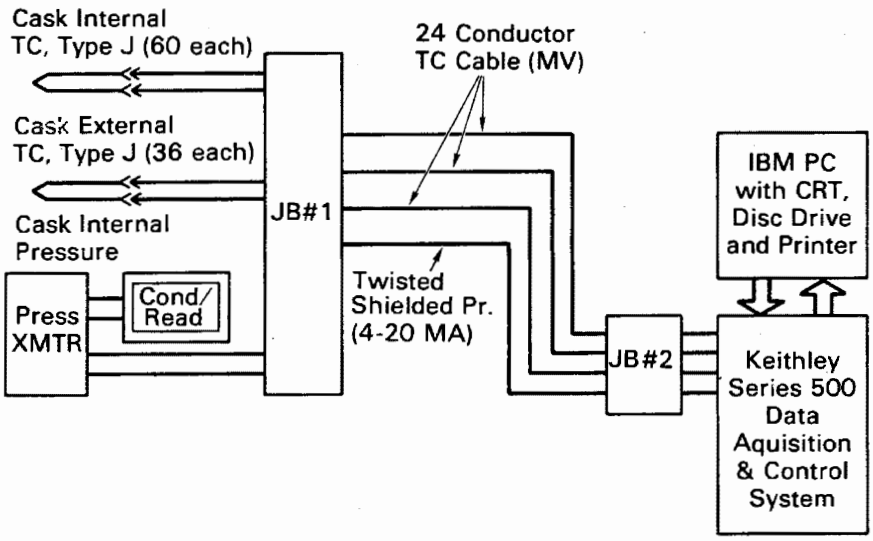

Figure 3-25. Data Acquisition System

The module family provides all of the conditioning, conversion, and control capabilities needed for laboratory and industrial automation. All four kinds of real-world signals--analog input, analog output, digital input,and digital output--are accepted by the Series 500.

Analog input from the cask instrumentation pressure and temperature sensors was processed in two stages. The initial conditioning and selection of all signals was provided by modules in the analog input (AIM) series. Different modules offer amplification, isolation, bridge detection, excitation, and cold junction reference. Programmable gain allowed the range of the signal to match that of the converter. Signals were then directed to a single analog-to-digital module (ADM) that accesses the level of the signal with an A/D converter, returning a digital value understood by the IBM computer.

Signals from the Keithly 500 were received, converted to engineering units, stored on floppy disks, and printed out on hard copy by the IBM PC. Further processing of the pressure and temperature data consisted of applying appropriate calibrations to the raw temperature data and plotting selected data presented in Section 4. The following calibration corrections were made to the raw temperature data.

DATA UNCERTAINTY ESTIMATES

Temperature uncertainties for the internal TC lance temperature measurements are within ±4°C, and external temperature measurements are within ±4.5°C, based on the

combined uncertainties of the thermocouples, extension wires, and data acquisition system. The internal measurements are more highly accurate because the TC lance thermocouples were calibrated independently, whereas the thermocouples attached to the casks surface were not. Where independent calibration data were not obtained, vendor certifications were used to estimate the TC contribution to temperature measurement uncertainty.

Pressure measurement uncertainties were within ±1.5 mbar for the low-pressure vacuum measurements and within ±2 mbar for the readings near 600 mbar. The pressure measurement uncertainty is a combination of the uncertainty in the pressure transducer's 4- to 20-milliampere output and the voltage drop across a precision resistor in the data acquisition system. Detailed uncertainty calculations for both pressure and temperature measurements are presented in Appendix B.

The passive dosimeters were used primarily to give more detailed dose rate profiles on the surface of the cask than are possible with the portable survey instruments, which average counts over relatively large areas. The TLDs are individually selected to have a dose response within 5% when exposed to 1 R of ^{137}Cs gamma rays, and should respond within 10% when exposed on the cask. The TEDs were used only for obtaining a relative profile of the cask, because they are not very sensitive to low and intermediate energy neutrons and require long exposures.

Survey instruments are field instruments and can have large overresponses depending on the energy spectrum of the calibration source and the energy spectrum being measured. The gamma survey instruments should be accurate to within 10% for room temperature measurements. For measurements not in the range of 15 to 27°F, an appropriate temperature correction should be applied. This was not necessary for the cask survey where the front of the instrument was 2.5 cm (1 in.) from the surface at about 25°F. The neutron survey instruments can overrespond by a factor of 1.5 to 2 for neutrons with energies in the hundreds of keVs (the average energy on the surface of the cask was between 150 to 200 keV). They overrespond by a factor of 3 to 4 for lower energy neutrons; for 14-MeV neutrons, they underrespond by a factor of about 3.

The TEPC directly measures absorbed neutron dose, and neutron dose equivalent can be determined using the pattern of energy deposition. The TEPC has demonstrated a response to monoenergetic neutrons between 0.1 and 17 MeV that, on the average, falls within 3% of the calculated or known dose. The multisphere spectrometer has low energy resolution but is responsive to neutrons over a very large range of

energies (thermal to 20 MeV). Neutron dose and dose equivalent rates can be determined from the measured spectra to within 20%. The ^{3}He spectrometer directly measures neutron energy spectra between 30 KeV and 1 MeV and is dependent only on the neutron capture cross section of ^{3}He over that range. For determining neutron energy spectra, the ^{3}He spectrometer is accurate to within 3% but, because of the neutrons that fall outside the range used, the total neutron fluence and dose equivalent determined are not always extremely accurate.

INEL CASK TESTING FACILITY

The primary INEL facilities are shown in Figure 3-26. The spent fuel storage cask performance tests are being performed at the Test Area North (TAN) facilities. The Test Area North is a large, multi-purpose testing and support area near the northern boundaries of INEL. Storage casks arrive at the INEL Central Facilities Area (CFA) by rail and are transported by heavy haul transporter to the TAN facility where all fuel-handling and testing activities are performed.

TAN-607 Facility

The primary cask testing facility is Building TAN-607 (Figure 3-27). This building includes several large shops: a high-bay hot shop area with unique capabilities for remote handling of highly radioactive materials involving either delicate and precise work or massive, industrial-sized operations; a water pit for interim storage of radioactive materials and components; a hot cell for observation and analysis of small radioactive objects, as well as for disassembly and examination of fuel rods; and a high-bay warm shop for receipt, assembly, and decontamination of low contaminated items, and testing. The two shops used for cask testing are the hot shop and warm shop at the north end of TAN-607 (Figure 3-28). In addition, a pad was constructed west of TAN-607 for long-term surveillance of the cask.

TAN-607 Hot Shop. The TAN-607 hot shop shown in Figure 3-29 is a shielded cell designed for the remote handling of large radioactive components. The shop is 15.5 m (51 ft) wide by 48.8 m (160 ft) long by 16.8 m (55 ft) high and constructed with 2 m (7 ft) thick concrete walls. Shielded viewing is provided by nine 1.8-m-thick (6-ft) glass windows. The main door to the hot shop is 8.5 m (28 ft) wide by 9.8 m (32 ft) high, allowing the entry of large vehicles including rail cars. The hot shop is serviced by a four-rail railroad system. The TAN hot shop is designed to a Uniform Building Code (UBC) Seismic Zone 2. The floor loading for the shop is 1222 kg/m^2 (250 lb/ft^2), but heavily concentrated loads can be located within the hot shop by positioning them over specific support areas. The ventilation system exhausts the hot shop air through prefilters, HEPA filters, and silver zeolite

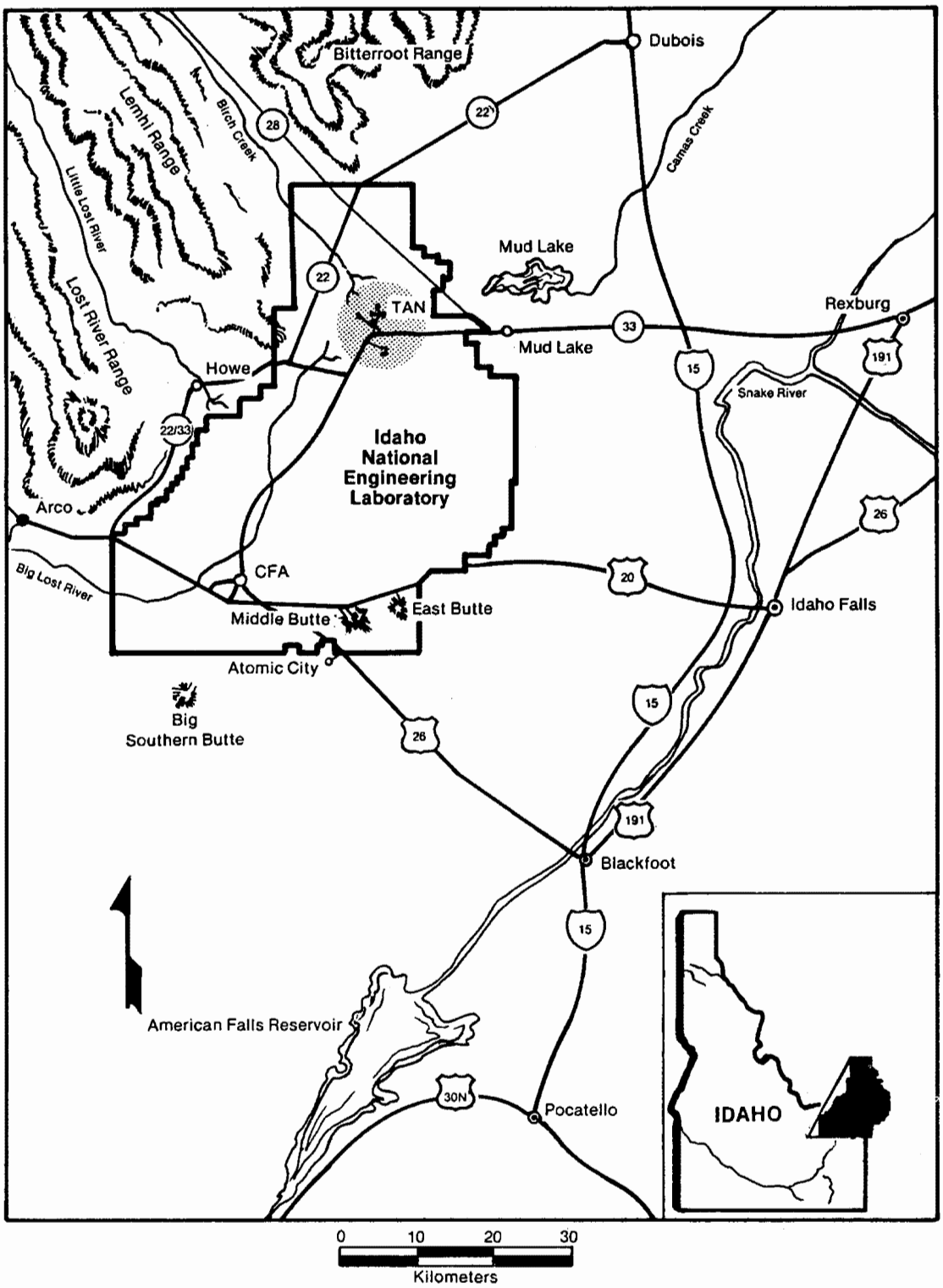

Figure 3-26. INEL Facility

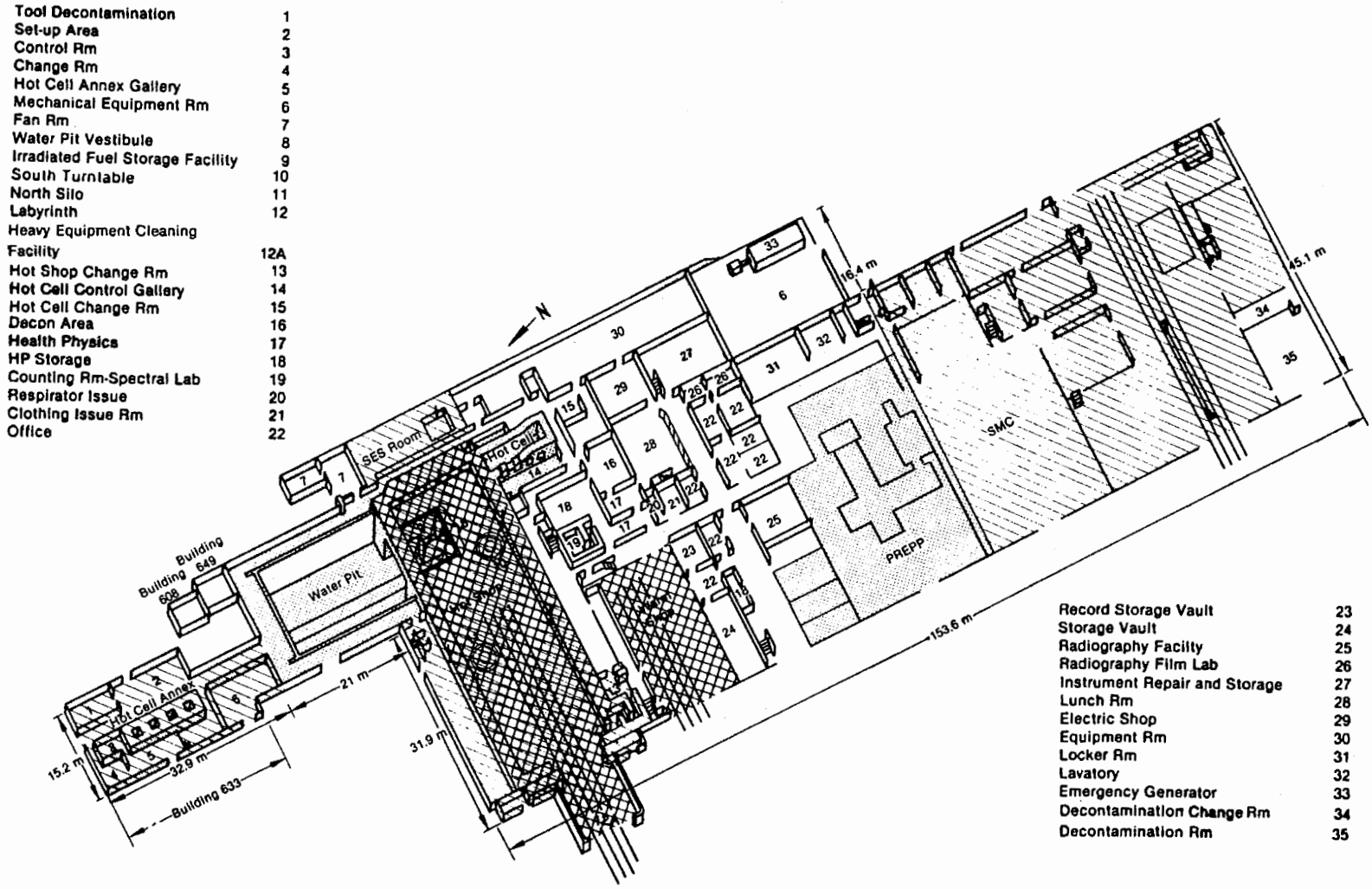

Tool Decontamination	1
Set-up Area	2
Control Rm	3
Change Rm	4
Hot Cell Annex Gallery	5
Mechanical Equipment Rm	6
Fan Rm	7
Water Pit Vestibule	8
Irradiated Fuel Storage Facility	9
South Turntable	10
North Silo	11
Labyrinth	12
Heavy Equipment Cleaning Facility	12A
Hot Shop Change Rm	13
Hot Cell Control Gallery	14
Hot Cell Change Rm	15
Decon Area	16
Health Physics	17
HP Storage	18
Counting Rm-Spectral Lab	19
Respirator Issue	20
Clothing Issue Rm	21
Office	22

Record Storage Vault	23
Storage Vault	24
Radiography Facilty	25
Radiography Film Lab	26
Instrument Repair and Storage	27
Lunch Rm	28
Electric Shop	29
Equipment Rm	30
Locker Rm	31
Lavatory	32
Emergency Generator	33
Decontamination Change Rm	34
Decontamination Rm	35

Figure 3-27. TAN-607 Facility

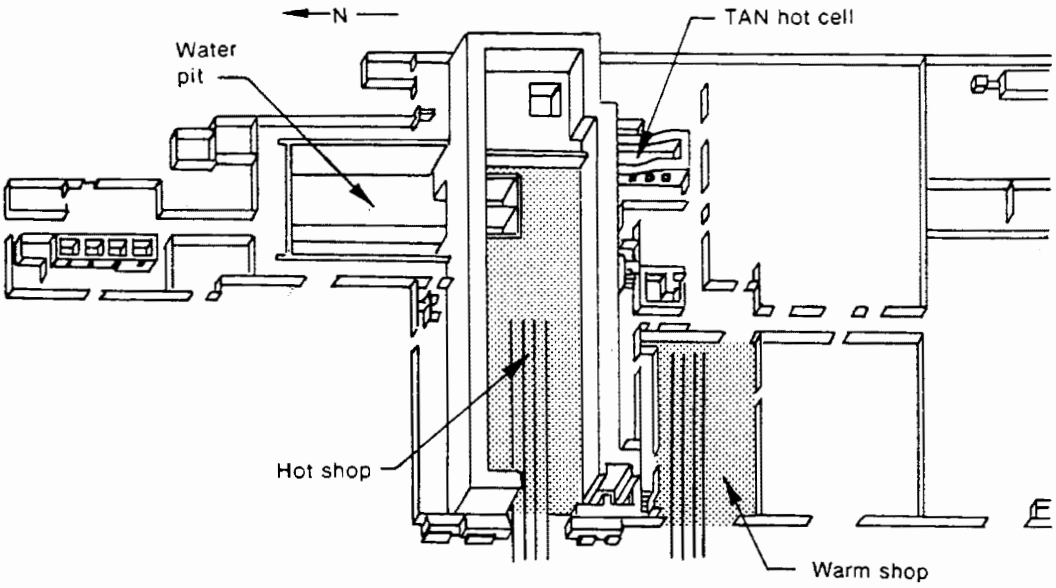

Figure 3-28. North End of TAN-607

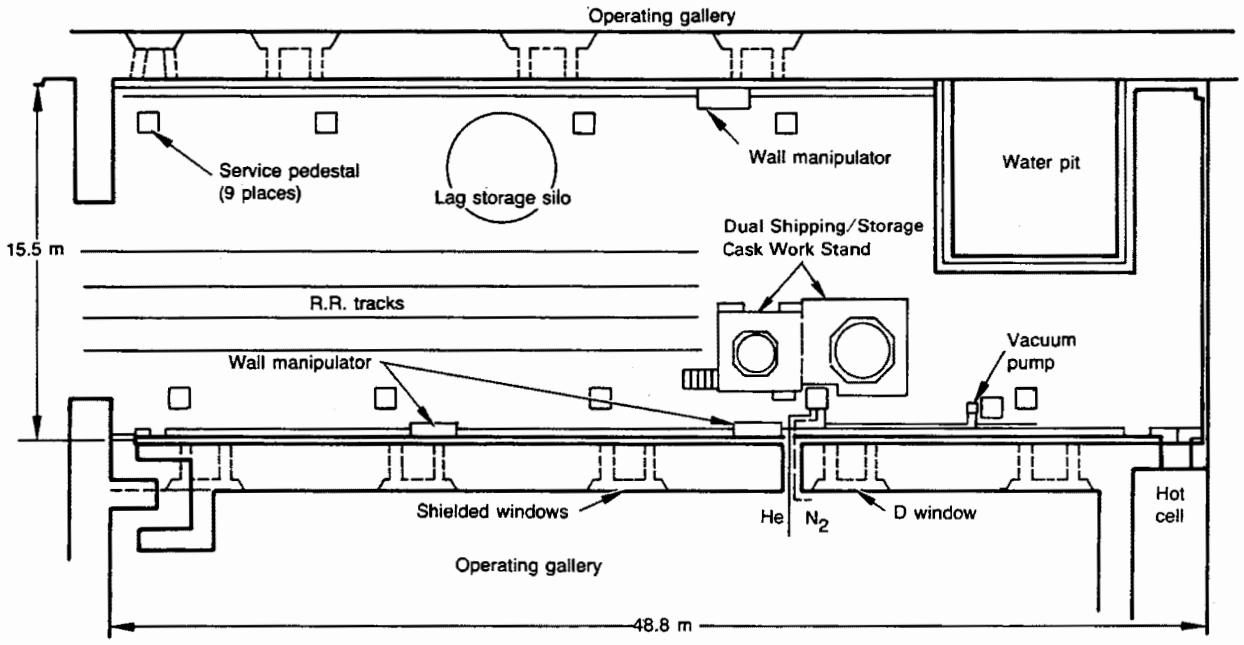

Figure 3-29. TAN-607 Hot Shop

absorbers to a 45.7-m (150-ft) stack. A negative pressure is maintained in the hot shop to ensure constant air flow into the shop. The hot shop is not a sealed alpha-containment facility. Appropriate hot and warm waste systems are provided in the facility.

The hot shop is served by a variety of remotely operated handling equipment as shown in Figure 3-30. The largest piece of equipment is the 100/10-ton bridge crane, which is currently upgraded for 125-ton lifts. The crane services the entire shop and has a maximum lift height of approximately 15.5 m (51 ft). A bridge-mounted overhead electro-mechanical manipulator can also cover the entire shop. The manipulator can lift a 272-kg (600-lb) load with its hand, and has a shoulder hook capable of lifting 2270 kg (5000 lb) to a height of 9.1 m (30 ft). Three wall-mounted manipulators are installed for lighter-duty work. These manipulators can travel both horizontally and vertically (up to about 9.1 m, 30 ft) along the hot shop

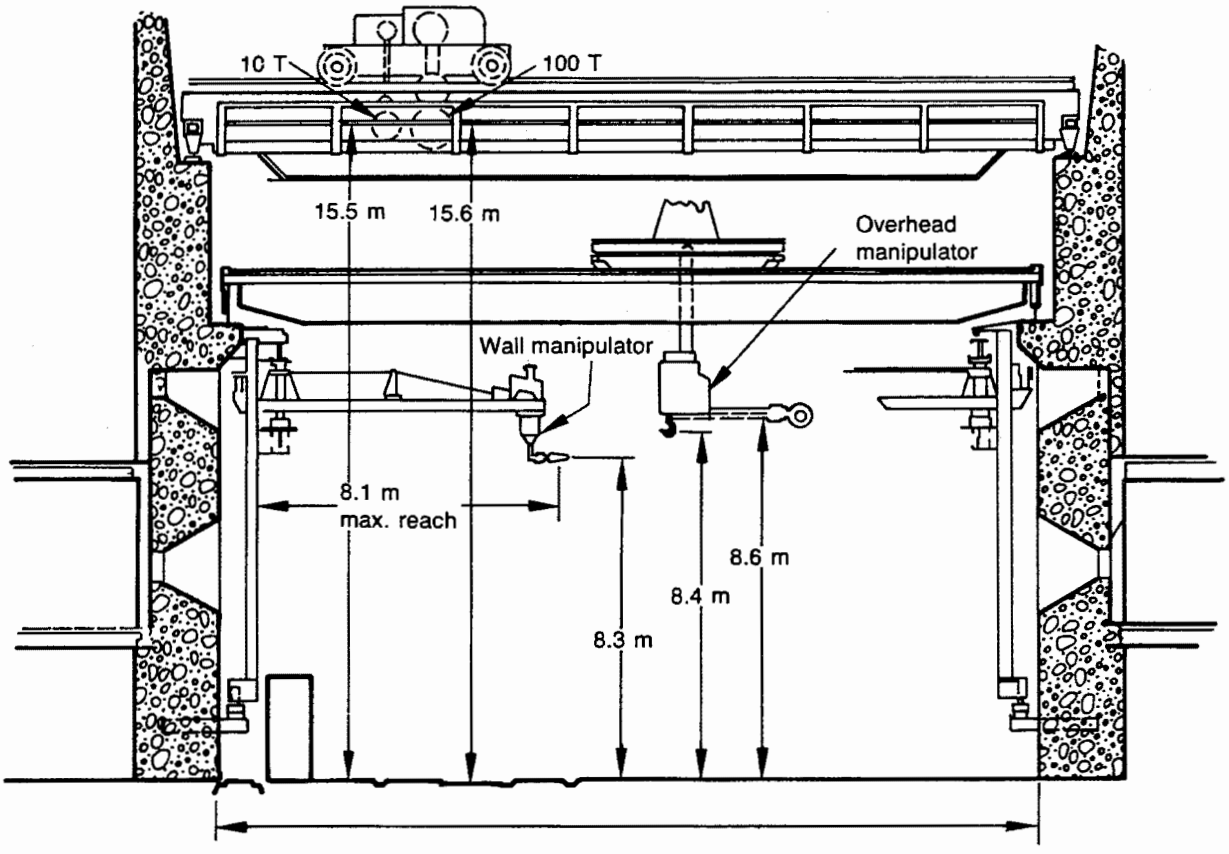

Figure 3-30. Elevation View of Hot Shop and Handling Equipment

walls, and have jib booms that can be swung from the wall to the center of the shop. The shielded window in the northwest corner of the hot shop contains heavy duty master-slave manipulators.

Service pedestals are located on the hot shop floor to provide all of the utilities normally used in the hot shop operations, including compressed air, oxygen, acetylene, demineralized water, raw water, electricity, telephone, and intercom. All are conveniently accessible via quick-disconnect couplings designed for remote manipulation. Remotely operated power tools are plugged into these service pedestals by the manipulators when needed. Pedestal "D" has been expanded to include helium and nitrogen gas supplies, a vacuum system to evacuate the casks, instrument hookups to a data acquisition system (DAS), and electrical hookups for the video camera pan-tilt controls and light system.

Visual access to the hot shop is gained through a series of 1.8-m-thick (6-ft) windows arranged and installed on either side of the shop and in two rows corresponding roughly to second and third story heights. Binoculars, mirrors, periscopes, remote microscopes, and closed circuit television are all used to enhance the visual observation and control of the remote functions within the hot shop. At each window is located a control pedestal for controlling the functioning of the crane and the pertinent manipulators. All of the stations on a given side and level are housed in a common "operating gallery."

A vestibule has been extended from the main doorway of the hot shop to provide an enclosed area for equipment preparation and truck-trailer deicing before they enter the hot shop (Figure 3-31). A work platform was fabricated and installed below control window "D" in the hot shop to contain a shipping and storage cask during fuel transfer between the two (Figure 3-32). The work platform is divided into two sections; one section services the shipping cask, while the other services the storage cask. The two sections are joined to permit personnel travel between the two halves.

The working level of the platform is 4 m (13 ft) above the hot shop floor. The top of the cask is approximately 1 m (3 ft) above the platform's working level, thus allowing operators easy access to the cask lid bolts and gas connections.

The casks are placed into the work platforms by using a lifting yoke attached to the 100-ton hot shop crane (Figure 3-33). Each half of the work platform has a removable section of grating that permits side access, thus precluding lifting the cask

Figure 3-31. TN-8L Shipping Cask and Trailer in Hot Shop Vestibule

above the platform's working level (Figure 3-34). The grating is removed and replaced by using the 10-ton hot shop crane and lifting slings attached to lifting lugs on the removable sections.

TAN-607 Warm Shop. The TAN-607 warm shop is located south of the hot shop as shown in Figure 3-28. The warm shop is designed as a service area for handling test assemblies with low to medium radiation or contamination. It is currently used as an area for familiarization and training on casks upon receipt, instrumenting casks, and testing casks in a controlled environment. The warm shop is 15.5 m (51 ft) wide by 24 m (80 ft) long by 15 m (50 ft) high. It has a main door 8.5 m (28 ft) wide by 10 m (33 ft) high as shown in Figure 3-35. The warm shop is served by a 30/5-ton overhead bridge crane. The warm shop is designed to UBC Seismic Zone 2 requirements. The floor drains for the facility are connected to a hot waste holding tank.

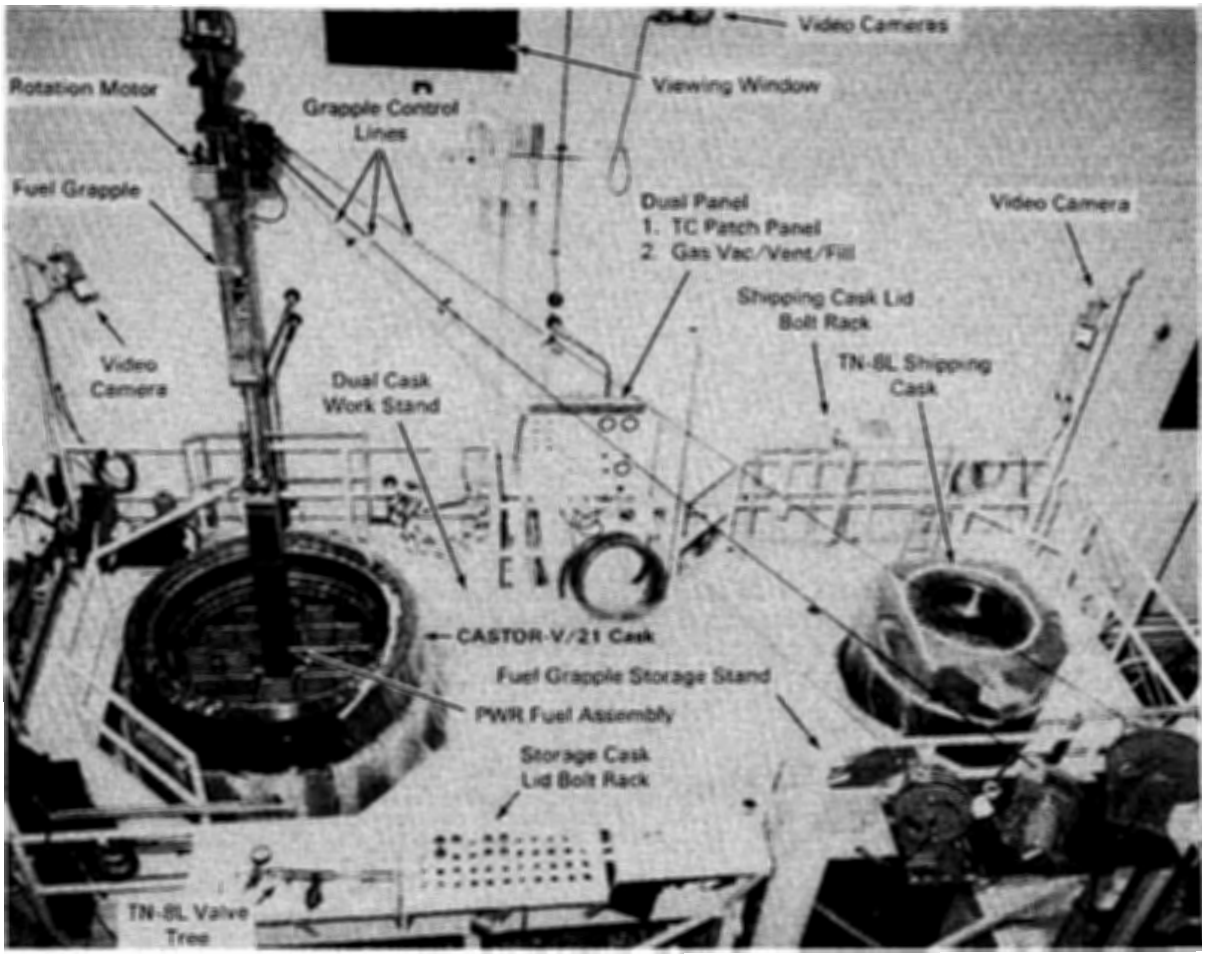

Figure 3-32. Dual Work Stand for Spent Fuel Transfers

The warm shop was modified to include helium and nitrogen gas supply systems and a vacuum system for use in cask performance testing. These systems interface with corresponding hot shop systems. Two gas cylinder banks, one helium and one nitrogen, were installed against the north wall of the TAN warm shop. These banks supply gas to either the hot shop control panel at the work platform or the warm shop control panel that is also mounted on the north wall (Figure 3-36).

The warm shop control panel provides connection to a vacuum system. The vacuum suction line and a pressure relief line are routed from the control panel, out of the warm shop and into the hot shop where they join the hot shop systems. The control panel also provides a connection between an instrumented cask in the warm shop and the DAS located in the hot shop control room at "D" window.

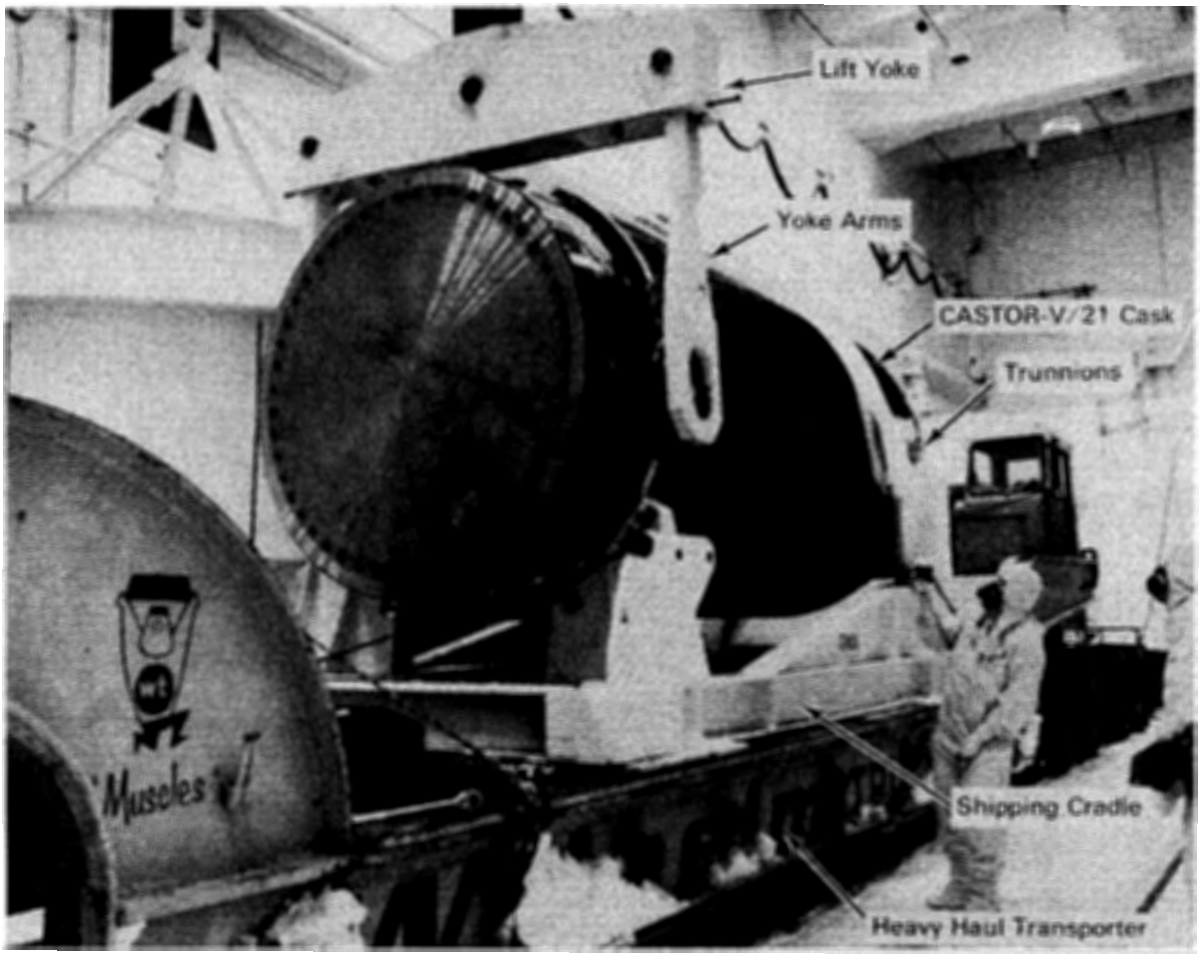

Figure 3-33. Cask with Lift Yoke Being Attached

A radiation shielding wall was added to the warm shop to protect personnel in adjoining hallways and change rooms from exposure when a loaded cask is being tested.

TAN Railroad System

Movement of casks between the TAN hot shop, warm shop, and pad is accomplished by means of a special shielded locomotive and railcar dolly over a four-track standard gauge railroad system (Figure 3-37). A 27-m-diameter (90-ft) turntable is located just west of the hot shop and pad in the four-track railroad system. Indicators for showing the position of the turntable, turntable alignment, controls for positioning the turntable, and turntable locking controls are located in the Turntable Control Building adjacent to the turntable.

Figure 3-34. Installing Loaded TN-8L Shipping Cask in Work Stand

The double-wide railcar dolly used to move the casks was modified with a heavier underframe to support the weight of the storage casks (Figure 3-38).

Long-Term Surveillance

Facilities for conducting long-term surveillance of the casks have been constructed west of TAN-607 (Figure 3-39). These consist of a concrete long-term surveillance

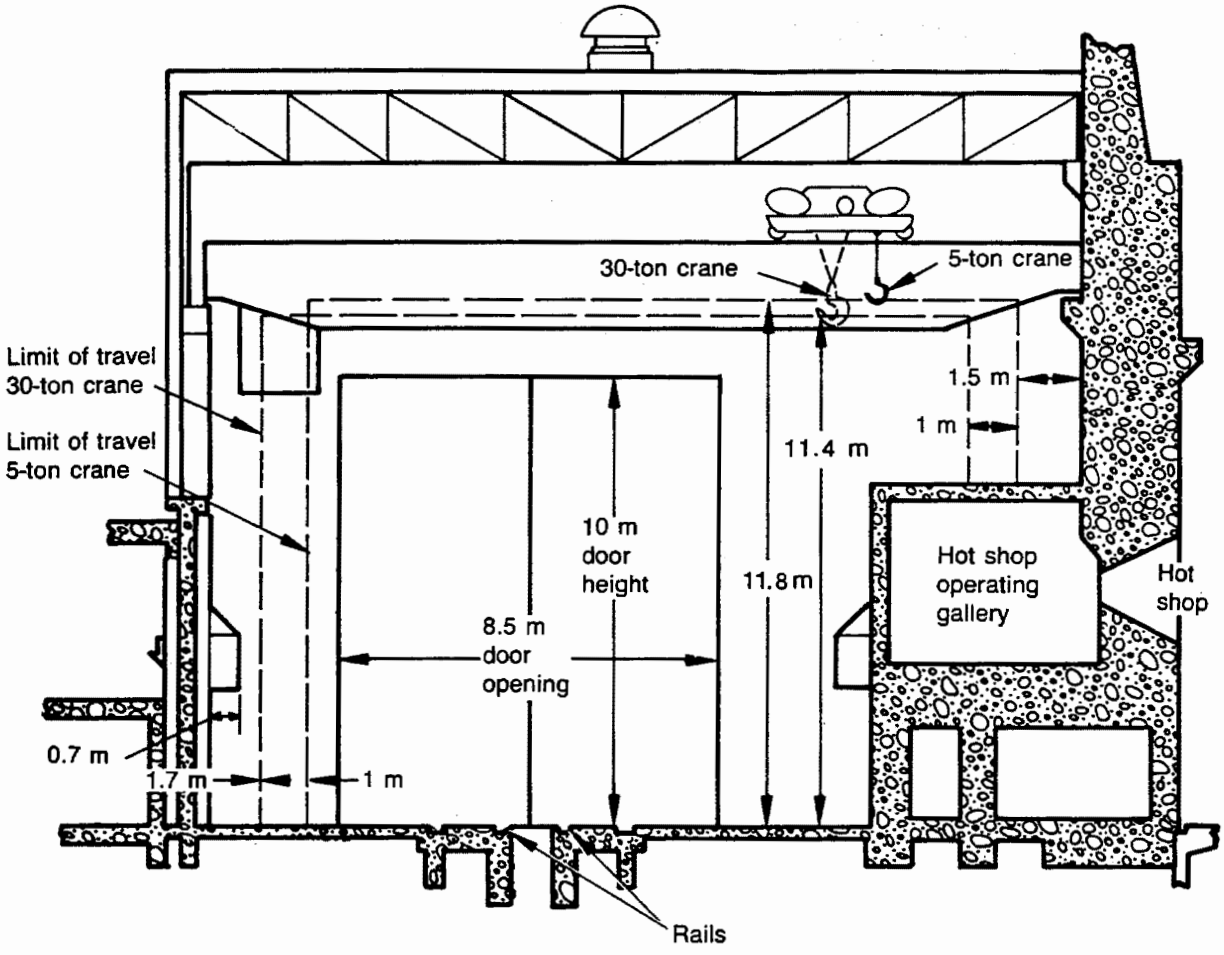

Figure 3-35. Elevation View of TAN Warm Shop

pad, data acquisition building, and weather station. A photograph of the pad with the data acquisition shack in the background is shown in Figure 3-40.

The long-term surveillance pad is located adjacent to the rail track that exits the TAN hot shop. It is sized to hold six spent fuel storage casks, four from the VP project and two from the Nuclear Fuel Services (NFS) project. The pad is 0.6 m (2 ft) thick reinforced concrete, 28.7 m (94 ft) long by 12 m (40 ft) wide. Its elevation is the same as the railroad bed to facilitate crane transfers from railcars to the pad. An asphalt paved apron surrounds the pad to permit vehicle access. A fence will be constructed to limit access and provide radiation area exclusion after the casks are placed on the pad.

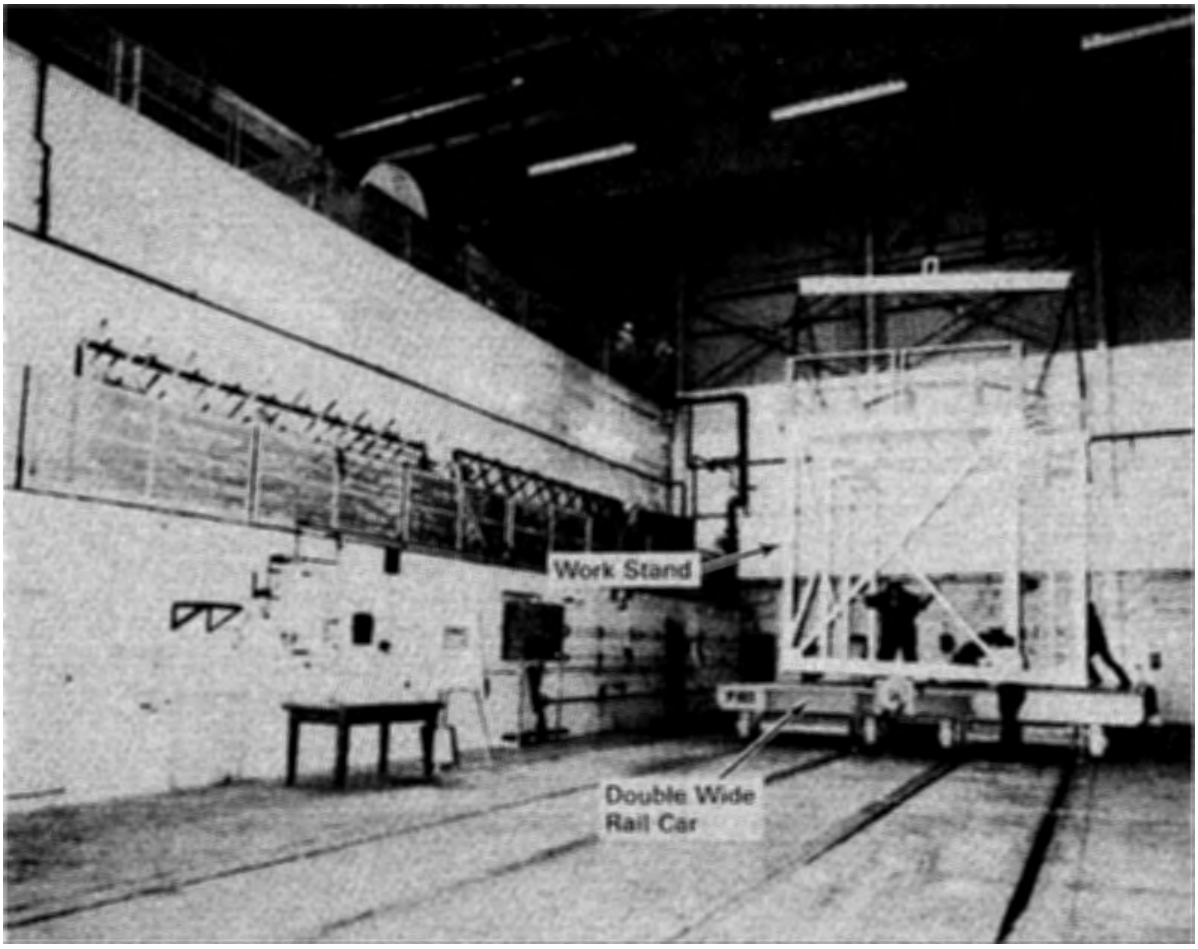

Figure 3-36. Warm Shop Test Area

The data acquisition shack rests on a small concrete pad near the test pad. The shack, constructed of metal framework and siding, is 3.35 m (11 ft) square by 2.75 m (9 ft) tall. Instrumentation leads pass through underground conduit from the pad to the shack. Inside the shack are a Keithly DAS with an IBM XT personal computer. The PC will be used for storing and reporting monitored data. The shack is heated during winter to protect the electronic equipment.

The weather station is located adjacent to the data acquisition shack. The small, self-contained unit measures wind speed and direction, atmospheric pressure, air temperature, precipitation, relative humidity, and solar insolation (4). Instrument cables connect the weather station to the DAS.

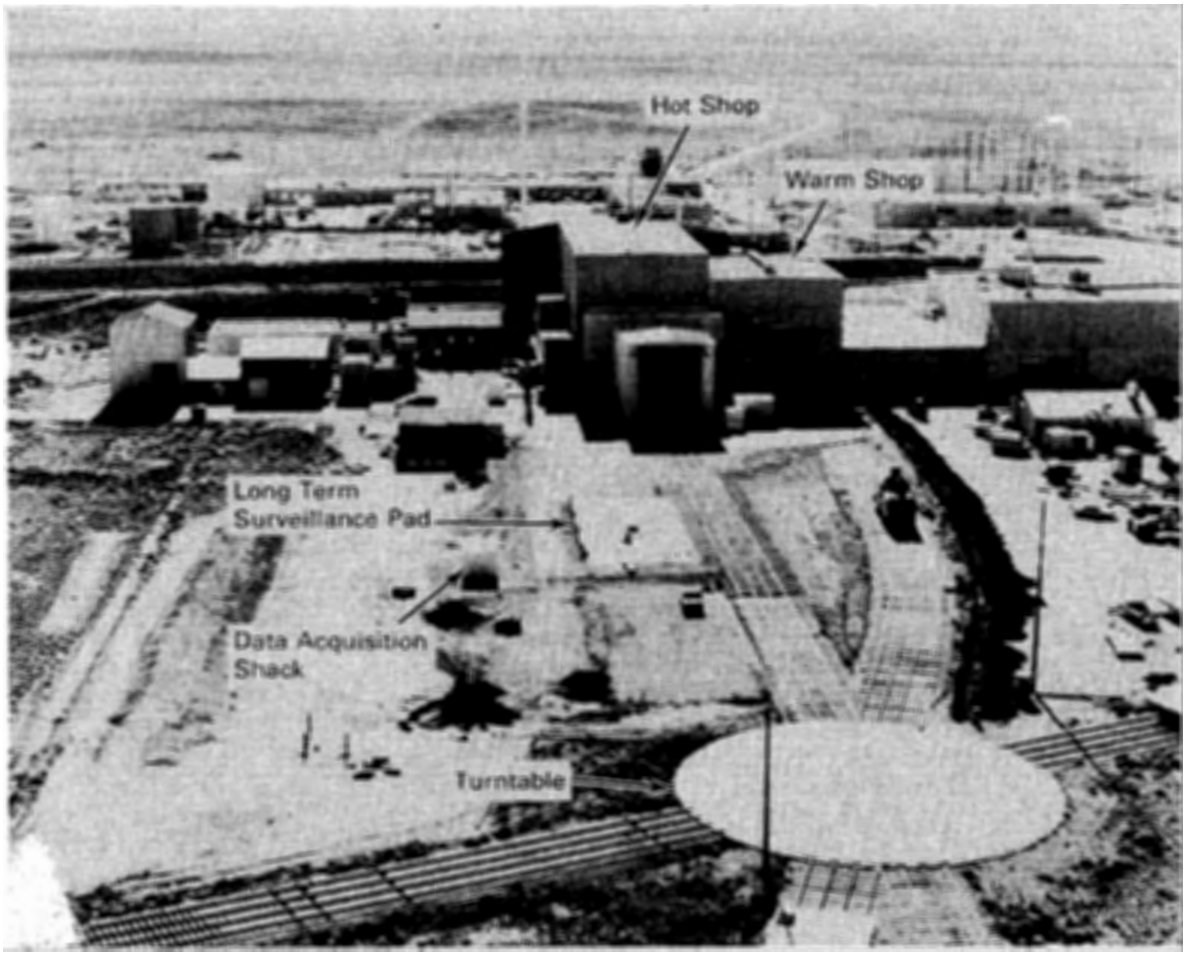

Figure 3-37. Hot Shop Complex and Four-Track Rail System

TEST PLAN

The CASTOR-V/21 cask performance test consisted of the five runs indicated in Table 3-9. The test runs involved a fully loaded cask (21 spent fuel assemblies), three backfill media (vacuum, nitrogen, and helium), and two cask orientations (vertical and horizontal). A test plan specified the order of the runs, the fuel assembly load pattern (see Figure 3-14 in Fuel Assembly Section), instrumentation/measurement locations, calibration requirements, and gas and crud sampling intervals. The test plan also addressed cask handling and fuel assembly characterization activities that were required prior to, during, and after performance testing.

Before loading the cask with fuel at INEL, VP inspected each fuel assembly using ultrasonic scanning and video (see Fuel Integrity Section). The assemblies were then shipped from Surry to TAN, three at a time, in Transnuclear TN-8L shipping

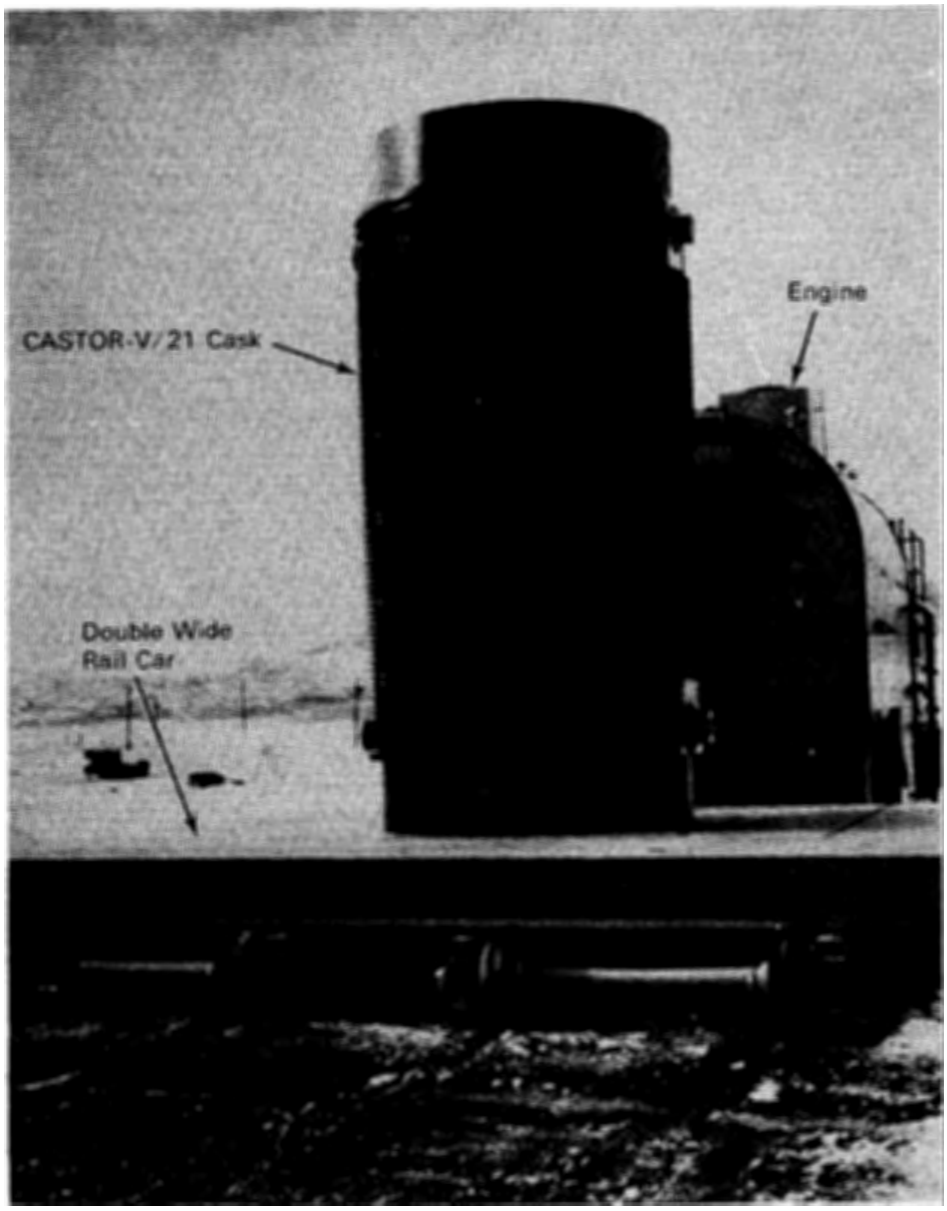

Figure 3-38. Moving CASTOR-V/21 Cask Between Hot Shop and Warm Shop on Modified Railcar Dolly

casks. Upon receipt at TAN, the three assemblies were unloaded from a TN-8L cask and transferred directly into the CASTOR-V/21 cask in the TAN hot shop without first being temporarily stored in lag storage (see section on INEL cask testing facility). After the twelth assembly was loaded in the CASTOR-V/21 cask, a TC lance was installed in the center assembly and temperatures were intermittently monitored to assure safe fuel rod operating temperatures. This procedure was followed until the storage cask was fully loaded. Once the CASTOR-V/21 storage cask was fully loaded,

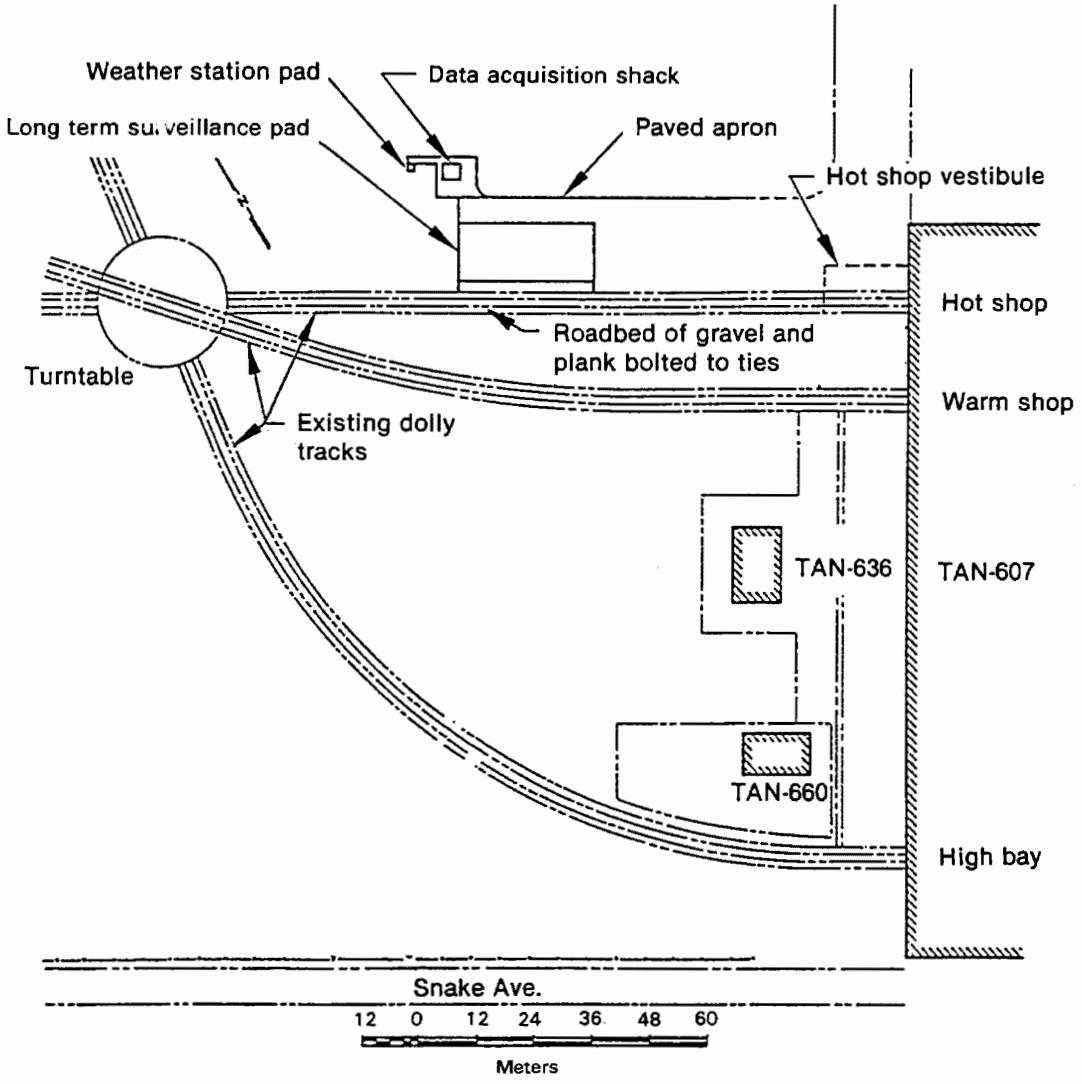

Figure 3-39. Long-Term Surveillance Pad and Data Acquisition System Shack Location

the remaining nine TC lances were inserted through the primary test lid into guide tubes of selected fuel assemblies. The cask was then moved from the hot shop to the warm shop on a double-wide railcar. Instrumentation leads were connected to appropriate sensors and the test matrix shown in Table 3-9 was completed.

The fuel assembly load pattern used during testing was previously shown in Figure 3-14. Fuel assembly locations were selected based on a pretest thermal analysis performed using the HYDRA heat transfer computer program (Section 5). The load pattern maintained 1/8 symmetry in the cask to evaluate temperature and dose rate symmetry, and to ease the analytical modeling effort. In addition, loading the high

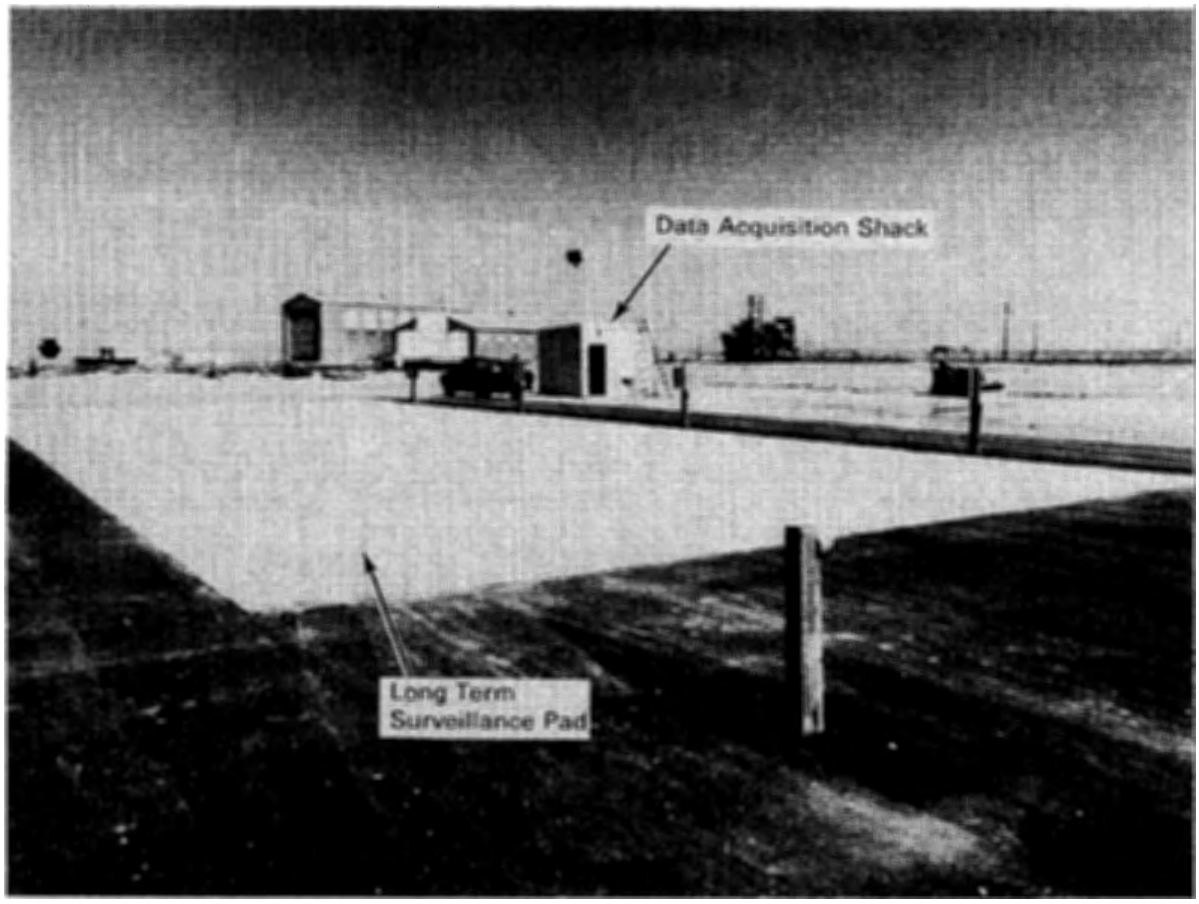

Figure 3-40. Long-Term Surveillance Pad and Data Acquisition System Shack

Table 3-9

CASK PERFORMANCE TEST MATRIX

Run Number[a]	Cask Orientation	Backfill Medium
1	Vertical	Helium[b]
2	Vertical	Nitrogen[b]
3	Vertical	Vacuum
4	Horizontal	Helium[b]
5	Horizontal	Nitrogen[b]

[a]All runs were performed with a fully loaded cask (21 assemblies) and the total predicted cask heat load was 28.4 kW at the beginning of the month long test and 27.5 kW and the end of the test.

[b]Gas samples were taken at the beginning and end of each of these test runs.

decay heat (1.8-kW) assemblies in the outer region of the cask created a relatively uniform temperature across the cask basket (Section 4).

The test plan required that gas samples be taken shortly after the cask was filled with a different gas, and immediately prior to evacuating a gas from the cask. The gas samples obtained during the test are indicated in Table 3-9. Each time the cask backfill medium was changed, the cask was pumped down, backfilled with the desired medium, pumped down again, and finally backfilled. This ensured purity of all backfill media to >99%. Nitrogen was used immediately prior to vacuum test runs to obtain a low pressure (1 to 3 mbar), low conductivity, vacuum/ nitrogen environment.

The test plan formed the basis for developing a set of detailed operating procedures by INEL that outlined the steps required to perform the cask performance test. The procedures resulted in the test data presented in Section 4; they basically consisted of:

- Storage Cask Transfer from Transporter to Railroad Dolly
- CASTOR-V/21 Storage Cask Setup, Checkout, and Training in Warm shop
- Move Unloaded CASTOR-V/21 Cask from Warm Shop to Hot Shop Work Platform
- Dry Run Fuel Receipt Using TN-8L Shipping Cask and GNS CASTOR-V/21 Storage Cask
- Dummy Fuel Assembly Handling and Storage
- CASTOR-V/21 Storage Cask Bottom Grid Marking and Thermocouple Installation
- Installation and Operational Check of Data Acquisition System (DAS) and Transducers
- Checkout of Thermocouple Lances for CASTOR-V/21 Storage Cask
- Termination, Labeling, and Continuity Check of CASTOR-V/21 Storage Cask Test Cables
- Fuel Receipts and Transfers from TN-8L Shipping Cask to CASTOR-V/21 Storage Cask
- Move Loaded CASTOR-V/21 Storage Cask from Hot Shop to Warm Shop
- CASTOR-V/21 Storage Cask T/C Lance Installation and Leak Test
- CASTOR-V/21 Test Matrix Run No. 1, 2, and 3 (Vertical Position)
- Rotate CASTOR-V/21 Storage Cask from Vertical to Horizontal Orientation

- CASTOR-V/21 Test Matrix Run No. 4 and 5 (Horizontal Position)
- Dosimetry Installation and Removal for CASTOR-V/21 Storage Cask
- Move Loaded CASTOR-V/21 Cask (Horizontal Position) from Warm Shop to Hot Shop Storage Cask Work Platform (Vertical Position) and Remove T/C Lances
- Fuel Assembly Integrity Examinations
- CASTOR-V/21 Preparation for Interim Surveillance in Warm Shop (Gas Sampling)
- Move V/21 Storage Cask to Warm Shop for Interim Gas Sampling
- CASTOR-V/21 Secondary Lid Replacement and Gas Preparation for Long-Term Surveillance
- Move CASTOR-V/21 to Test Pad and Set Up for Long-Term Surveillance Testing
- CASTOR-V/21 Cask Long Term Surveillance.

These procedures are discussed in the next section. The experience gained during their performance is also described.

INEL CASK HANDLING AND OPERATING EXPERIENCE

This section describes the cask handling and operating experience gained during cask performance testing. The tasks required to conduct cask performance testing included performing storage and shipping cask handling studies, assessing utilization of existing facilities and equipment, installing cask ancillary and research equipment at the INEL TAN cask testing facility, operation preparations, storage cask receipt and preparations, operational dry runs, a facility readiness review, fuel transfers and loading, cask performance testing, fuel assembly inspections, and long-term surveillance. INEL personnel performed a dry run to train personnel and check out equipment. After the dry run was evaluated, necessary equipment and procedure changes were made. The cask performance test was then conducted.

When the fuel assemblies arrived from the Surry reactor at the INEL TAN 607 Hot Shop in TN-8L shipping casks, the fuel assemblies were transferred in air to the CASTOR-V/21 cask. Operations personnel monitored the cask during this time. Preliminary testing began when the cask was partially loaded with 12 fuel assemblies. When the cask was fully loaded with fuel, the cask was transferred to the Warm Shop test bay where formal testing began.

Upon completion of the cask performance test, the cask was moved to the TAN Hot Shop. There, crud and smear samples were collected from selected assemblies. A fuel assembly integrity video characterization was also performed. During the fuel characterization, apparent cracks in corners of some basket fuel tubes were observed (see Figure 4-8 of Section 4). When the fuel integrity examination was complete, the cask was prepared for temporary storage and monthly gas sampling. It was then placed in the Warm Shop while test data were verified and the basket cracks were evaluated.

Later, a gas sample analysis indicated the cover gas sample cylinders used during the test had a high oxygen content. Evaluating the possible problems revealed the cask and sample cylinder quick-disconnect couplings were leaking. The backfill gas was replaced in the cask and resampled to verify purity.

Storage and shipping cask handling studies, facilities and equipment, operational preparations, storage cask receipt and preparations, operational dry runs, the facility readiness review, fuel transfers and loading, cask performance testing, fuel assembly inspections, and long-term surveillance activities are presented and discussed in the following sections.

Storage and Shipping Cask Handling Studies

Two detailed cask handling studies were performed. One study developed the handling logic for the CASTOR-V/21 storage cask, and the other defined handling of the Transnuclear TN-8L shipping cask and fuel. The handling studies identified how the shipping and storage casks would be received at INEL and how fuel could be handled. They compared test requirements of the approved test plan with INEL site capabilities. The studies identified the existing base facility equipment and specified required modifications or upgrades to the base facility equipment. The specific equipment and systems required to accomplish the cask performance test were defined. The two handling studies became the bases for identifying the equipment and operational preparation subtasks required to accomplish the cask performance test.

Facilities and Equipment

Existing INEL equipment and facilities were used as much as possible. Those at CFA and TAN were the most extensively used. Facility equipment capability, modification requirements, and maintenance requirements were evaluated. Equipment at CFA--the rail system, gantry crane, and heavy haul trailers, roads, and bridges--were identified. Equipment located at the TAN 607 Hot Shop was also evaluated. Equipment and

systems evaluated included the Hot Shop crane; manipulators; direct viewing shielding windows; floor loading; hot cell transporter; in-shop utility pedestals; operating galleries and shielding; in-shop rail track; shield doors; Hot Shop lighting; cask gas venting system; and facility safety support systems. Equipment and systems evaluated outside the Hot Shop were the local in-plant rail track; turntable; locomotive; and the Warm Shop capability for cask testing. Areas along and adjacent to the Hot Shop were evaluated as a site for the long-term surveillance pad. These base facility systems and equipment were previously discussed in the section on the INEL cask testing facility.

Two types of project-specific equipment were identified: cask-test-support and cask-handling/operation equipment. Cask test support equipment was that required to gather test data. It consisted of the gas/vacuum/vent system and the data acquisition system. Cask handling/operation equipment was that required to handle the cask, such as lift yokes, cask lid lifting fixtures, cask surface seal protectors, thermocouple lance template, and the cask gas/vacuum/vent valve tree.

The base facility equipment modifications and project-specific equipment systems were designed, procured, and installed concurrent with performance of the tasks to prepare the facility for operation. The CASTOR-V/21 cask manual and drawings were reviewed. The specialized handling fixtures and tools were developed for hands-on and remote cask operation. Thermocouple lance insertion was closely reviewed. Special semi-remote insertion tools were developed to reduce personnel radiation exposure and contamination spread while installing and removing the lances.

Both base and project-specific equipment were operationally tested before they were actually used for remote operation. The equipment was tested either during a dry run training task or by an independent, formal system-operation test. When problems were encountered, they were resolved, and the equipment or system was retested.

Operational Preparations

Numerous tasks were required to prepare the facilities for the cask testing project. Operating documentation was developed, personnel were trained, the CASTOR-V/21 storage cask was received and moved to the TAN test facility, and a dry run was performed to check out the equipment and operating procedures. A facility readiness review was held, and the facilities approved for operation.

Documentation Development. Reviews compared the base facility safety and standard operating documentation with the cask testing work scope. A fuel criticality analysis was performed. Operational sequences were verified, and revised addendums to the facility Safety Analysis Report (SAR) and Operational Safety Requirements Document (OSRD) were prepared and approved. Facility Standard Operating Practices were also reviewed and revised as required to meet the cask-testing requirements.

Site Work Releases (SWRs) or Hot Cell Work packages controlled all operating tasks performed at the facilities. The SWR work, general work using craft labor, does not require rigorous control and review. It usually involves equipment installation or maintenance. Hot Cell Work packages identify the tasks or subtasks required to accomplish a specific scope of work, and delineate a specific sequence for facility operating tasks. These work packages usually contain one or more detailed operating procedures (DOPs), step-by-step instructions for performing a specific task. The SWRs, work packages, and DOPs are controlled documents. As such, they must be revised and approved, should a work step need changing. Work stops while the package is being revised, and work does not resume until the revision is approved.

The overall project statement of work and the CASTOR-V/21 test plan were used to develop this operating documentation. Information for preparing the procedures came from the cask vendor, safety analysis, equipment drawings, and operating and maintenance manuals. Safety, quality, project, independent safety, and operations personnel rigorously reviewed these work packages and DOPs.

Three Hot Cell Work packages were prepared to provide operating instructions for the operating personnel. The first was a training procedure to familiarize personnel with the cask, check out and perform the cask operating equipment fit-up, and check the operating procedure. The second work package provided instructions for actual fuel receipt and cask loading. The third package instructed personnel in cask testing and long-term surveillance at the pad.

The Detailed Operating Procedures used for handling, operating, and testing the CASTOR-V/21 dry fuel storage cask are listed in Table 3-10.

A document control office managed the release and change control of the cask operating and safety procedures and documents. The document control office maintained the facility operating project, research data, research photographs, project equipment, and operating cost and schedules files.

Table 3-10

DETAILED OPERATING PROCEDURES FOR CASTOR-V/21 CASK

DOP Number	Title
1.13.1	TAN SFSC Program First (GNS) Storage Cask Transfer from Transport to P103 Railroad Dolly
1.13.2	TAN SFSC Program (Dry Run) Fuel Receipt Using TN-8L and GNS CASTOR-V/21
1.13.3	TAN SFSC Program Fuel Receipt and Transfer from TN-8L Shipping Cask to CASTOR-V/21 Storage Cask
1.13.4	TAN SFSC Program Rotate CASTOR-V/21 Storage Cask from Vertical to Horizontal for Test Plan
1.13.5	TAN SFSC Program Dummy Fuel Assembly Handling and Storage (use for dry run)
1.13.6	TAN SFSC Program CASTOR-V/21 Storage Cask Setup, Checkout, and Training in Warm Shop
1.13.7	TAN SFSC Program Move Loaded CASTOR-V/21 Cask (Horizontal Position) from Warm Shop to Hot Shop Storage Cask Work Platform (Vertical Position)
1.13.8	TAN SFSC Program Fuel Assembly Integrity Examinations
1.13.9	TAN SFSC Program CASTOR-V/21 Test Matrix Run No. 1, 2, and 3 (Vertical Position)
1.13.10	TAN SFSC Program CASTOR-V/21 Test Matrix Run No. 4 and 5 (Horizontal Position)
1.13.11	TAN SFSC Program CASTOR-V/21 Preparation for Interim Surveillance Testing in Warm Shop (Gas Sampling)
1.13.12	TAN SFSC Program CASTOR-V/21 Secondary Lid Replacement and Gas Preparation for Long-Term Surveillance
1.13.13	TAN SFSC Program Move CASTOR-V/21 to Test Pad and Set Up for Long-Term Surveillance Testing
1.13.14	TAN SFSC Program CASTOR-V/21 Cask Long-Term Surveillance Test
1.13.15	TAN SFSC Move V/21 Storage Cask to Warm Shop for Interim Gas Sampling
1.13.16	TAN SFSC Program Move Unload CASTOR-V/21 Cask from Warm Shop to Hot Shop Work Platform
1.13.17	TAN SFSC Program Move Loaded CASTOR-V/21 Storage Cask from Hot Shop to Warm Shop
1.13.18	TAN SFSC Program CASTOR-V/21 Storage Cask TC Lance Installation and Leak Test
1.13.19	TAN SFSC Program CASTOR-V/21 Storage Cask Bottom Grid Marking and Thermocouple Installation
1.13.20	TAN SFSC Program Checkout of Thermocouple Lances for CASTOR-V/21 Storage Cask
1.13.21	TAN SFSC Program Installation and Operational Check of Data Acquisition System (DAS) and Transducers
1.13.22	TAN SFSC Program Termination, Labeling, and Continuity Check of CASTOR-V/21 Storage Cask Test Cables
1.13.23	TAN SFSC Program Dosimetry Installation and Removal for CASTOR-V/21 Storage Cask

Operational Training. Personnel training requirements were developed for the CASTOR-V/21 cask and the Transnuclear (TN)-8L shipping cask. This training consisted of both classroom and hands-on training. Operation technicians and supervisory personnel received personal training packages before beginning classroom training sessions. These packages contained cask manuals, operating DOPs, and safety document addenda. Thus, personnel could study the material before the discussions. The training session discussions included base facility equipment, documentation changes, and all new project-specific equipment drawings, operating manuals, and procedures. The project test engineer described any new equipment and answered questions.

When the equipment was installed and tested, the operating technicians assisted with its startup testing. Thus, each technician obtained hands-on experience with the equipment.

Storage Cask Receipt and Preparation. The CASTOR-V/21 storage cask was received at the CFA Scoville rail siding on a cold day in mid-December 1984 (Figure 3-41). It had traveled across country from the east coast to the INEL on a special heavy depressed center rail car. The site locomotive then moved the cask to the CFA gantry crane siding (Figure 3-42). The cask, attached to a horizontal shipping and storage cradle, was offloaded from the rail car (Figure 3-43). The 200-ton gantry crane was used for this operation in spite of the -26°C (-15°F) temperature. Before hoisting, special note was taken of the lowest service temperature of all lifting equipment. Wooden cribbing was placed on the ground near one end of the gantry crane travel to support and elevate the cask above the snow cover (Figure 3-44). The cask remained at CFA while the TAN area was being prepared.

A heavy-haul transport plan was prepared to coordinate moving the cask from CFA to TAN. An over-the-road 150-ton heavy-haul trailer was leased to transport the cask in late February. It was first loaded with test weights to simulate the center of gravity and weight of the cask. Then the loaded trailer traveled the route between CFA and TAN (Figure 3-45). After making the uneventful test run, the weights were offloaded and the cask prepared for transfer to TAN. The cask was transported to TAN in March and moved to the TAN 607 Hot Shop preparation area before the spring thaw to minimize road damage (Figure 3-46).

Operations technicians uncrated the cask from its special hardwood container and prepared to offload it at TAN (Figure 3-47). While the cask was being prepared, the

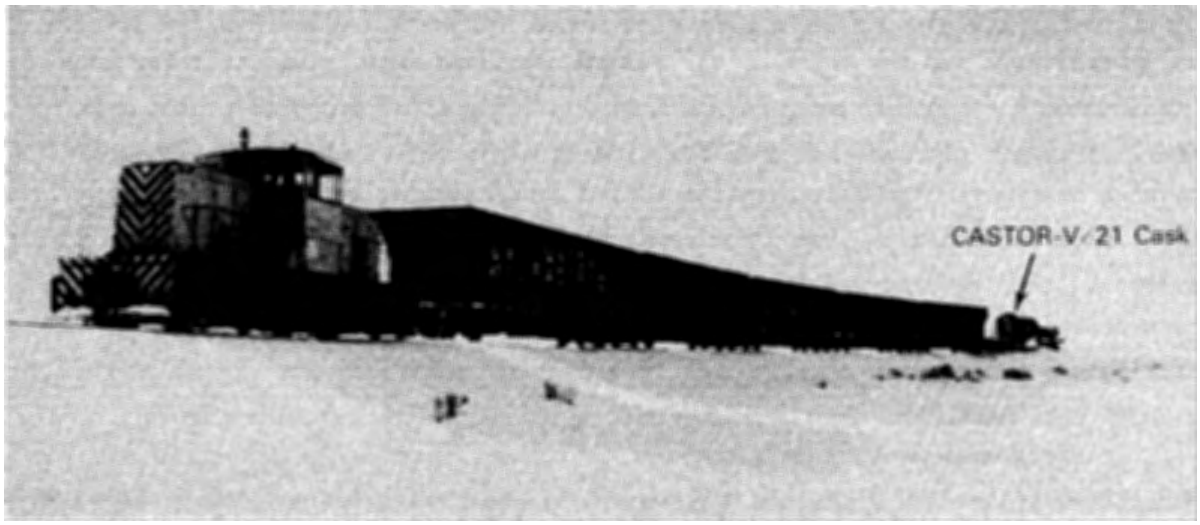

Figure 3-41. Receiving the CASTOR-V/21 Storage Cask at Central Facilities Area at the Idaho National Engineering Laboratory

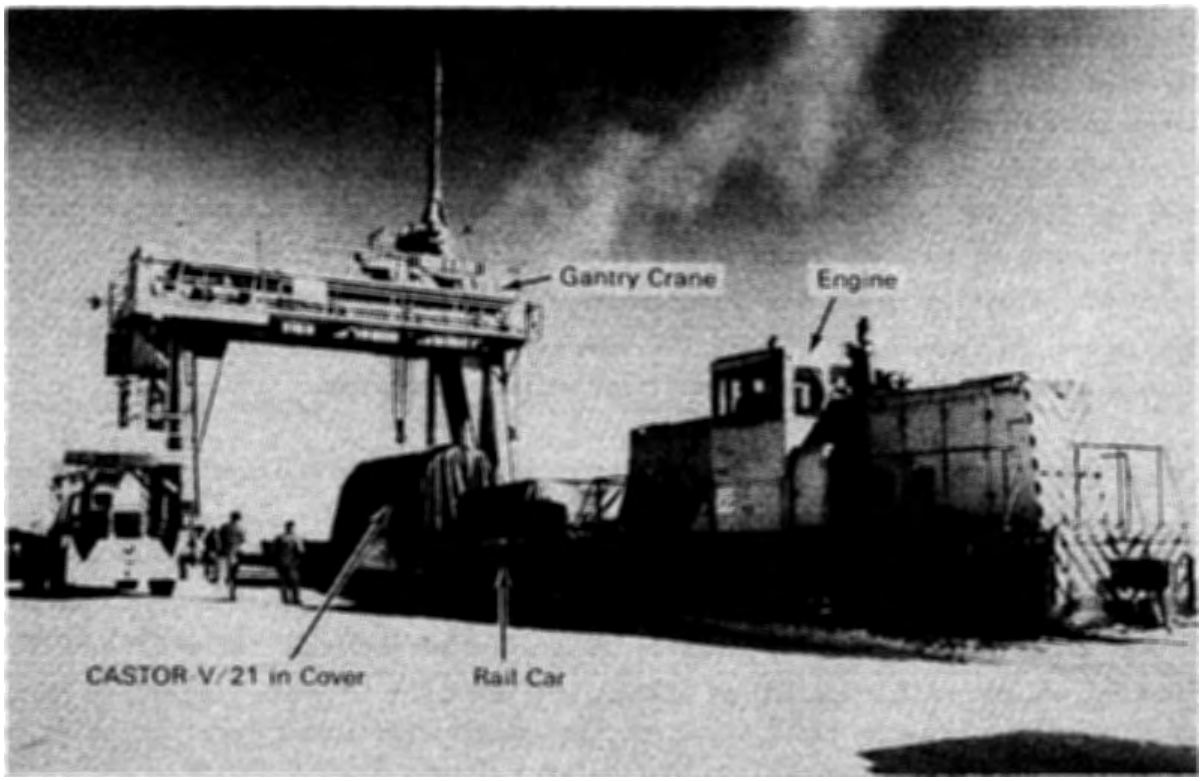

Figure 3-42. Positioning the CASTOR-V/21 Storage Cask Under the Central Facilities Area Gantry Crane

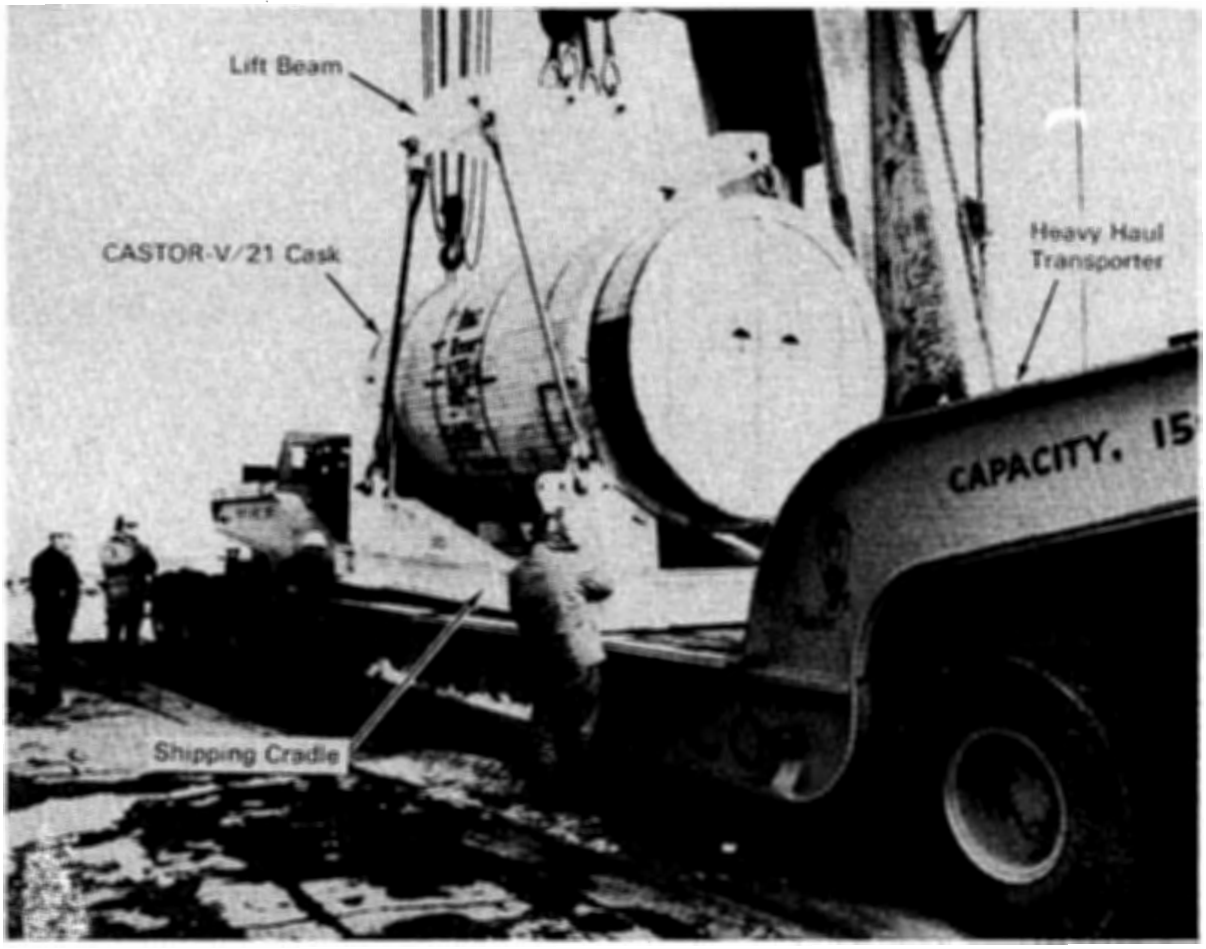

Figure 3-43. Offloading the CASTOR-V/21 Storage Cask from the Rail Car at the Central Facilities Area Gantry Crane

Hot Shop was readied for lifting the cask. A contamination-free zone was established inside the Hot Shop. The heavy-haul trailer containing the cask was moved into the Hot Shop and located parallel to the bridge crane (Figure 3-48). The cask-lifting yoke was attached to the crane hook and connected to the top trunnions of the cask. Operations technicians used the crane bridge travel and hoist motion to rotate the cask to a vertical orientation (Figure 3-49). The rigging and crane hook were kept vertical throughout cask rotation. Then, the cask was suspended from the crane off to the side of the depressed center heavy-haul trailer and the trailer was removed from the Hot Shop. The horizontal cask storage cradle was removed and placed into temporary storage. The TAN area locomotive moved a 150 ton-capacity double-wide rail car into the Hot Shop and positioned the car for cask loading. The cask was placed onto the rail car (Figure 3-50) and moved to a temporary storage

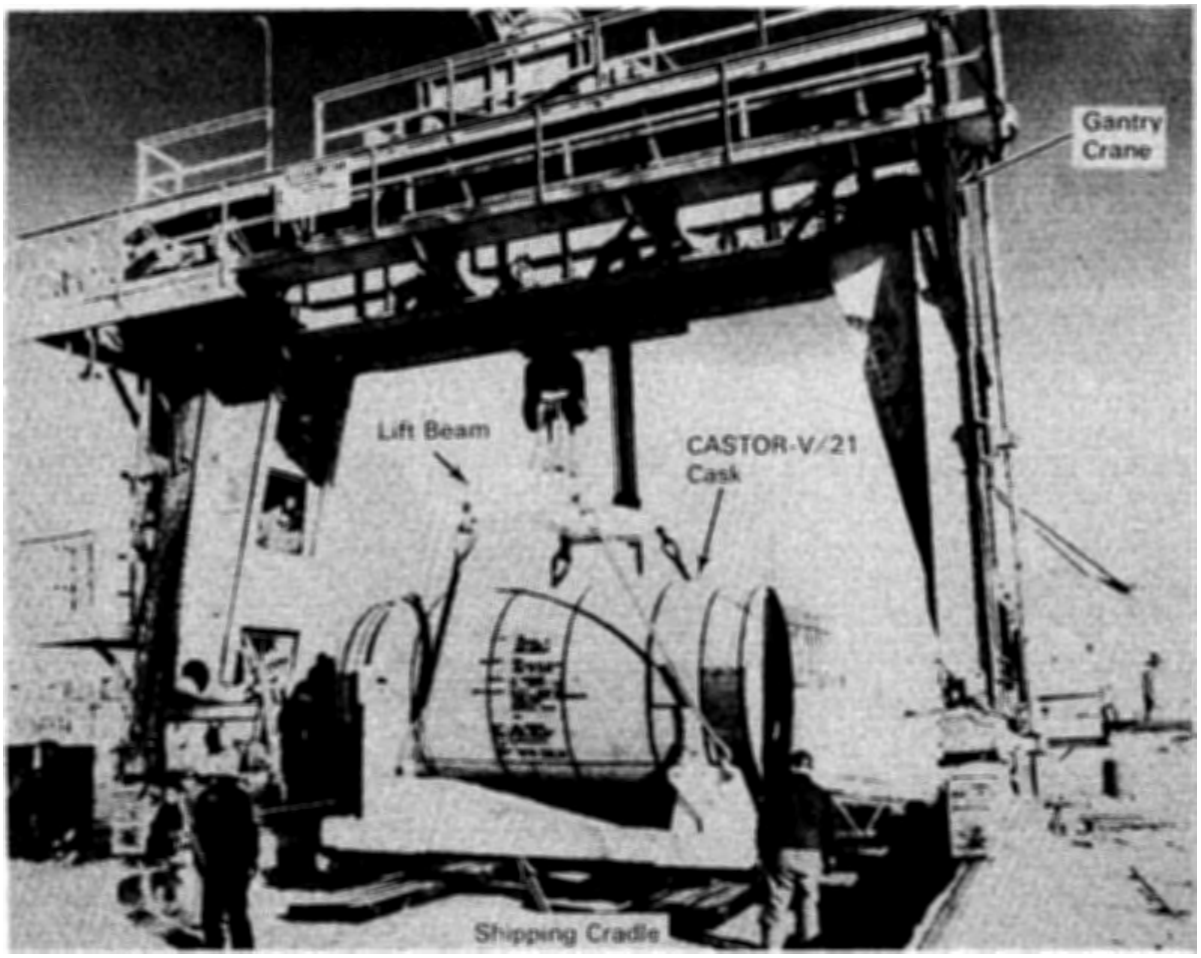

Figure 3-44. Positioning the CASTOR-V/21 Storage Cask on the Wooden Cribbing for Temporary Storage at the Central Facilities Area

area just outside the TAN Warm Shop where it remained until late April (Figure 3-51). The cask ancillary operating equipment and spare parts were uncrated and placed in controlled storage.

The Warm Shop was prepared for cask testing. In early May, the cask was moved into the Warm Shop and a personnel work platform placed around it (Figure 3-52). Cask familiarization, training, and ancillary equipment/tool checkout were performed. Using the personnel work platform for access and the Warm Shop crane for hoisting, operations technicians vented the cavity between the primary lid and secondary lid, removed the secondary lid, and placed the lid in temporary storage. Seals and seal surfaces were inspected, and the secondary lid surface seal protector installed.

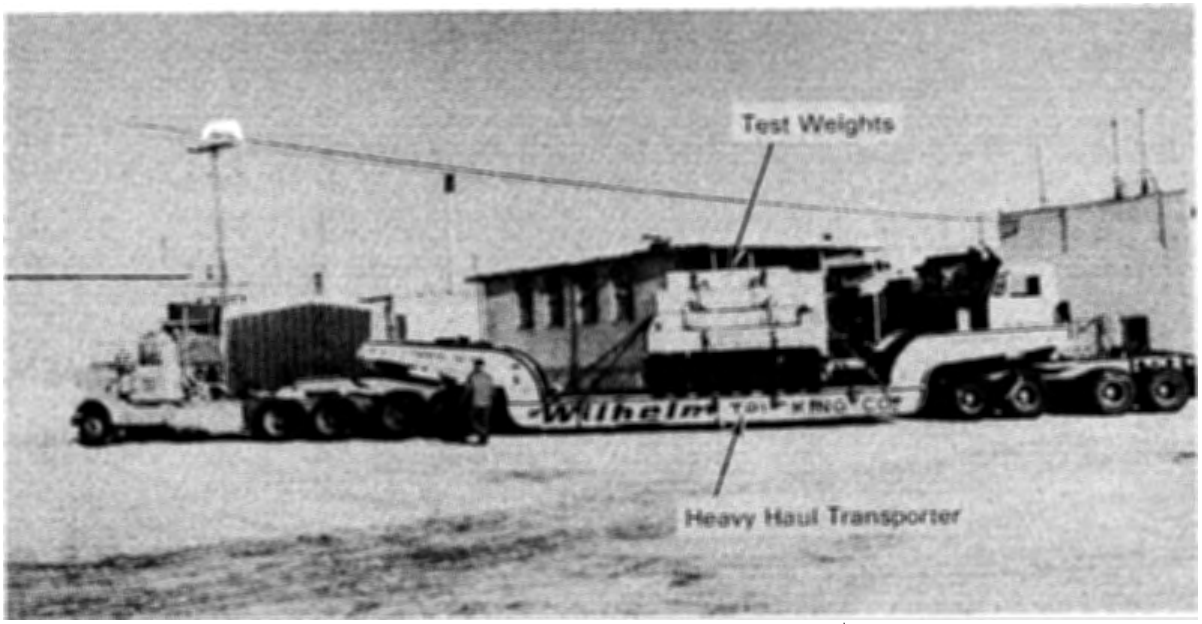

Figure 3-45. Route, Bridge, and Transporter Testing of the 150-Ton Depressed Center Heavy-Haul Cask Transport Vehicle Using Test Weights

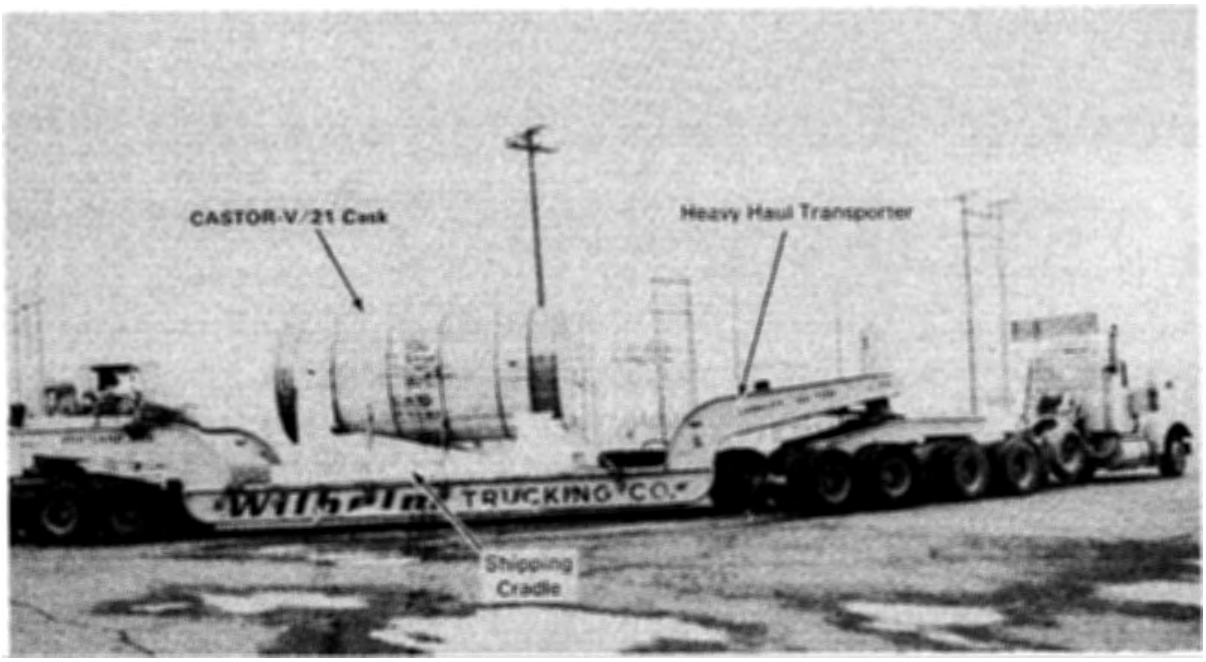

Figure 3-46. Moving the CASTOR-V/21 Storage Cask from CFA to TAN on the Heavy-Haul Transporter

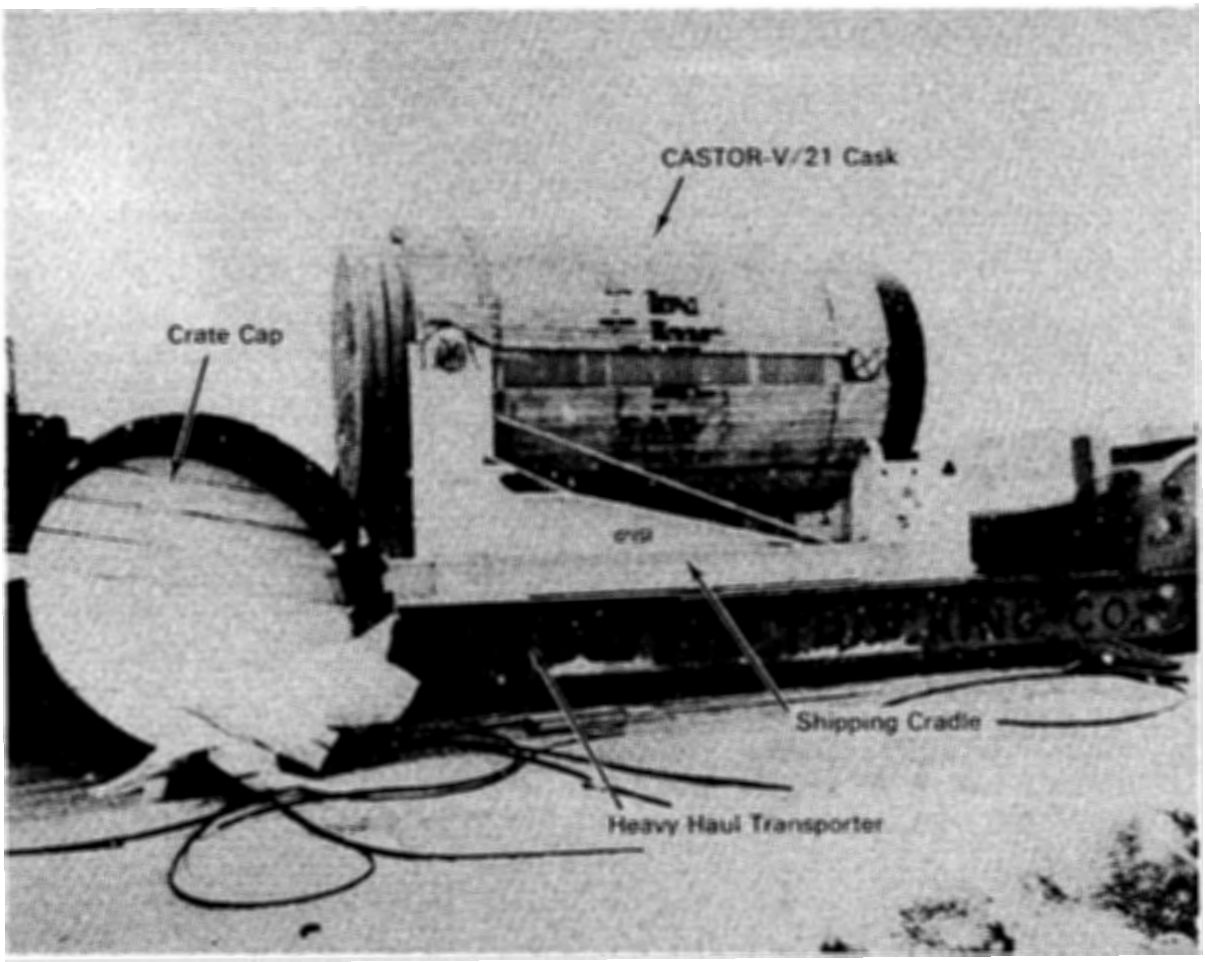

Figure 3-47. Uncrating and Preparing the CASTOR-V/21 Storage Cask for Offloading at the TAN 607 Hot Shop

Operations technicians then vented the cask cavity and removed the primary shield lid. The seals were inspected, and the primary lid surface seal protector was installed. A shipping basket restraint was removed, and the cask internals were viewed. Clearances were checked to ensure they would allow a thermocouple lance position template to be installed on top of the fuel basket. The template would verify the test lid lance penetration locations and assist in lance insertion training. The test lid was then reinstalled. Thermocouple (TC) lance blind flanges covering the test lid penetrations were removed. These were removed one at a time with a semi-remote reach tool. A mockup TC lance was inserted through each lid penetration and template location hole. A rope block and tackle and remote reach tools for positioning the tip of the lance were used for installing the lances. When the TC lance installation training was completed, the blind flanges were

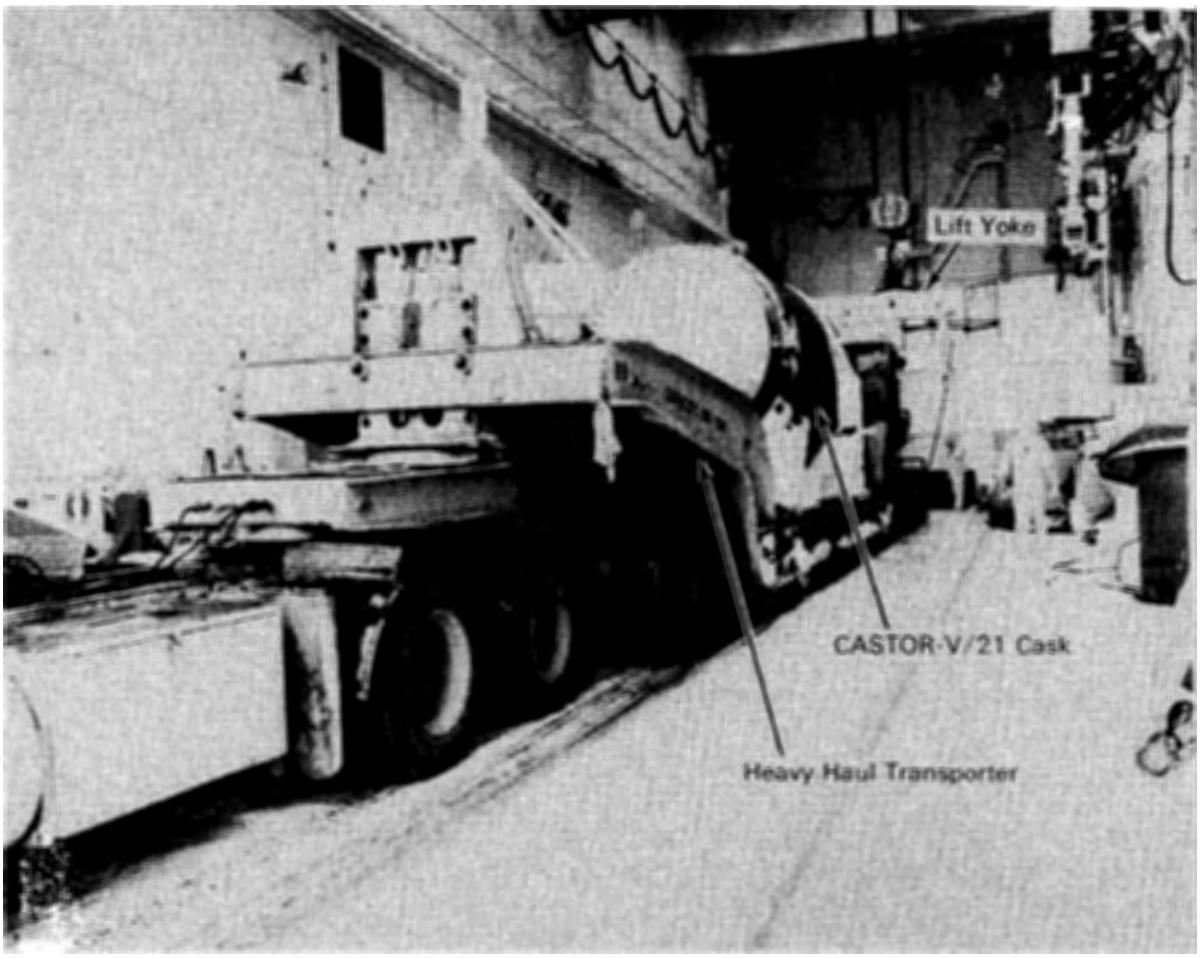

Figure 3-48. The CASTOR-V/21 Storage Cask Inside the TAN 607 Hot Shop Ready for Offloading

replaced and the test lid and the TC lance template were removed. The test lid was then reinstalled, and the cask was moved to the Hop Shop preparatory to the dry run.

After the Warm Shop familiarization, the remote lid removal and replacement rigging and technique were evaluated. The evaluators recommended that a ridged lid-lifting fixture replace the shackles and turnbuckles furnished with the cask. This fixture was the only equipment needed to remotely connect the crane hook to the fixture. Further, it provided a cylinder-into-cylinder effect rather than a disk-intocylinder effect. This helped prevent the lid from binding when it was placed into the cask lid cavity.

The rail car was then used to move the cask from the Warm Shop to the Hot Shop. Technicians used the Hot Shop crane to offload it into the Hot Shop work platform.

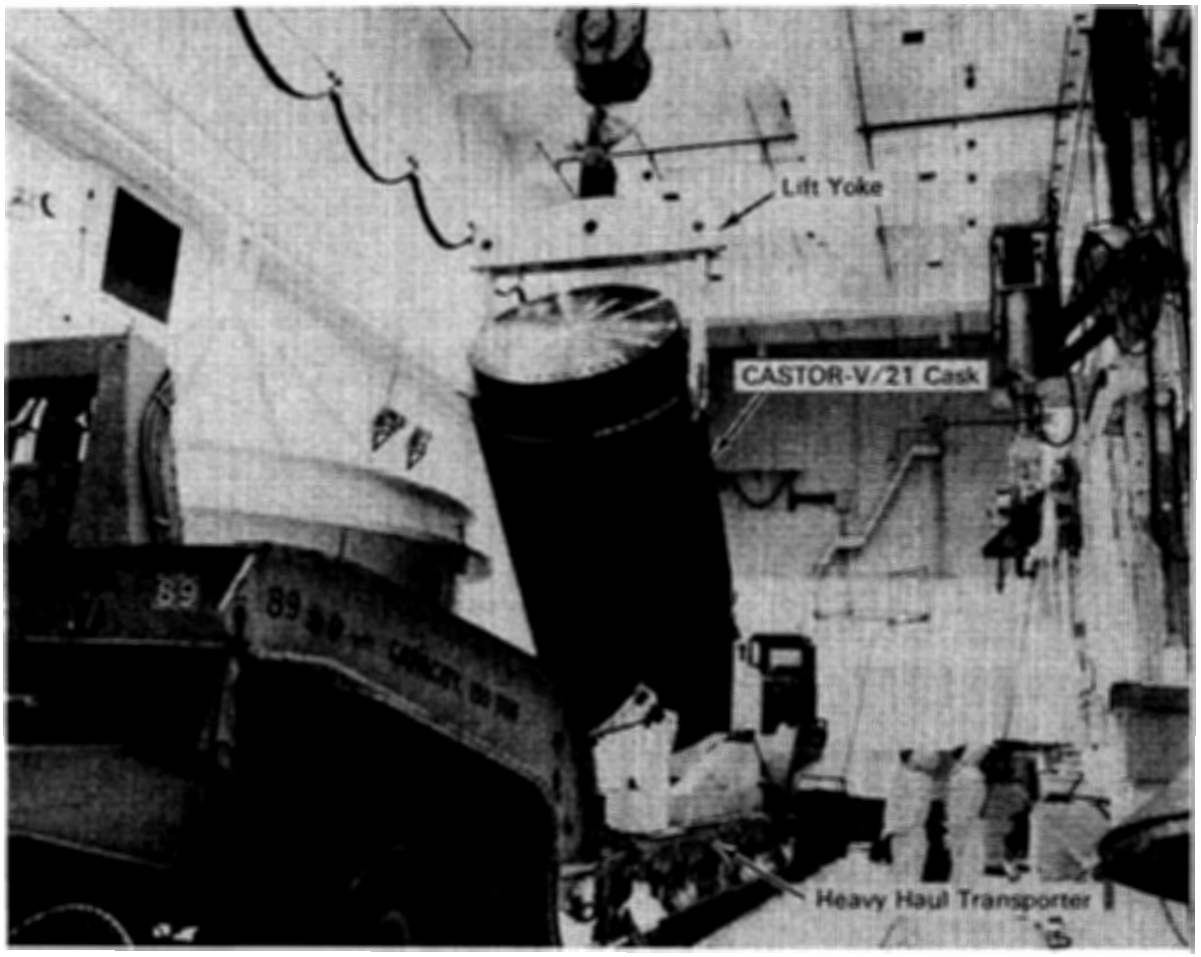

Figure 3-49. Offloading the CASTOR-V/21 Storage Cask in the TAN 607 Hot Shop

Shims were used to level the cask so the lid surfaces would be as level as possible. Level lid surfaces facilitate remote lid removal and fuel assembly loading. Because the fuel assemblies were transferred in air, a contamination barrier was required to reduce the possibility of contaminating the outer cask surfaces. Teflon® was used for this because of its high melting point. Teflon sheets were attached to the cask with Teflon tape.

Operational Dry Run. An operational dry run was performed in the Hot Shop. Personnel used the TN-8L Shipping cask and CASTOR-V/21 storage cask to perform the actual tasks required to receive, transfer, and place spent fuel in the storage cask.

®Registered tradename of the E. I. duPont de Numours Company.

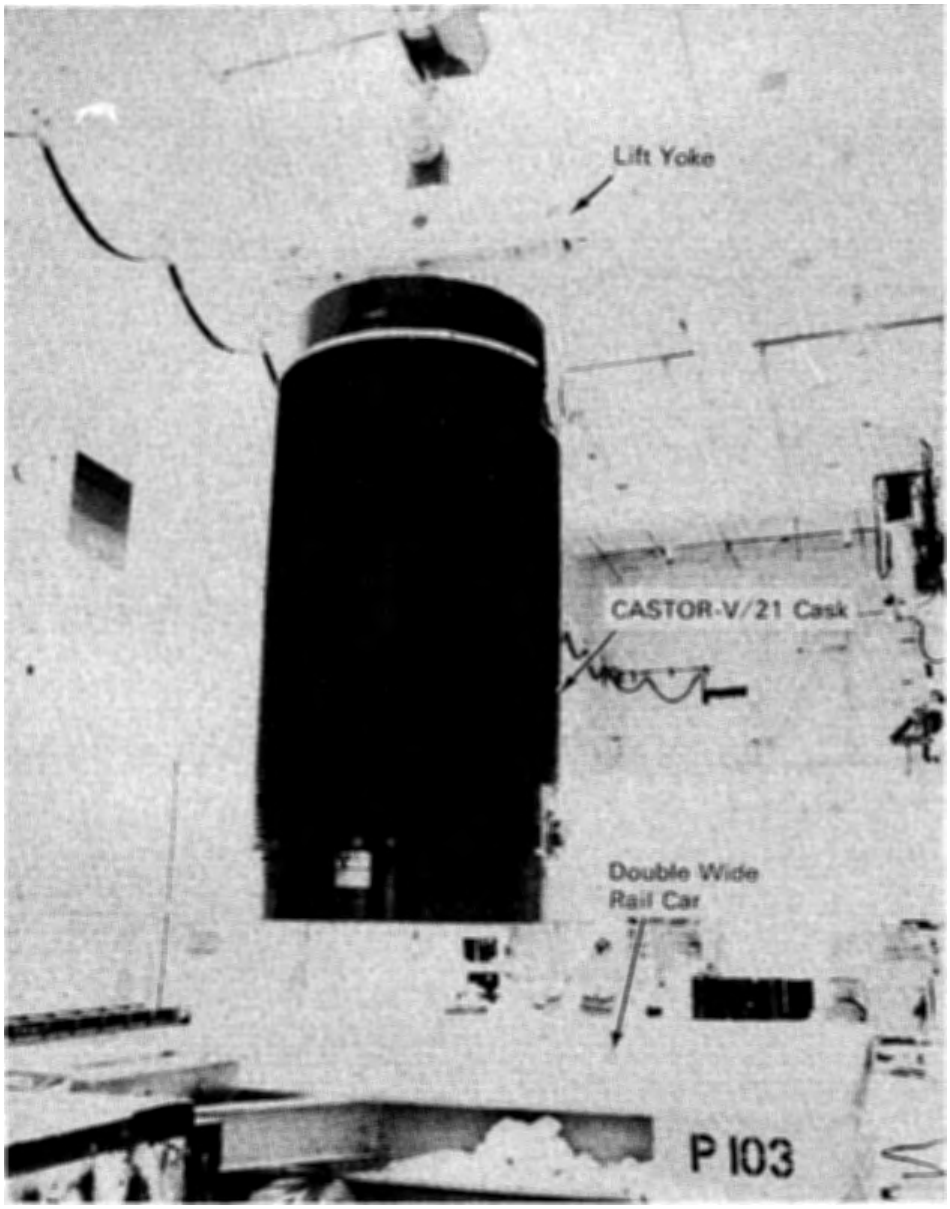

Figure 3-50. Offloading the CASTOR-V/21 Storage Cask in the TAN 607 Hot Shop Onto a Double-Wide Rail Car

The dry run trained personnel and checked out the final operating facility, project-specific equipment, and procedures.

The dry run began with the CASTOR-V/21 already on the Hot Shop work platform. Then, the TN-8L shipping cask was received at the Warm Shop and prepared to enter the Hot Shop (Figure 3-53). The shipping cask rain/dust cover was slid back so a radiological contamination and radiation survey could be performed.

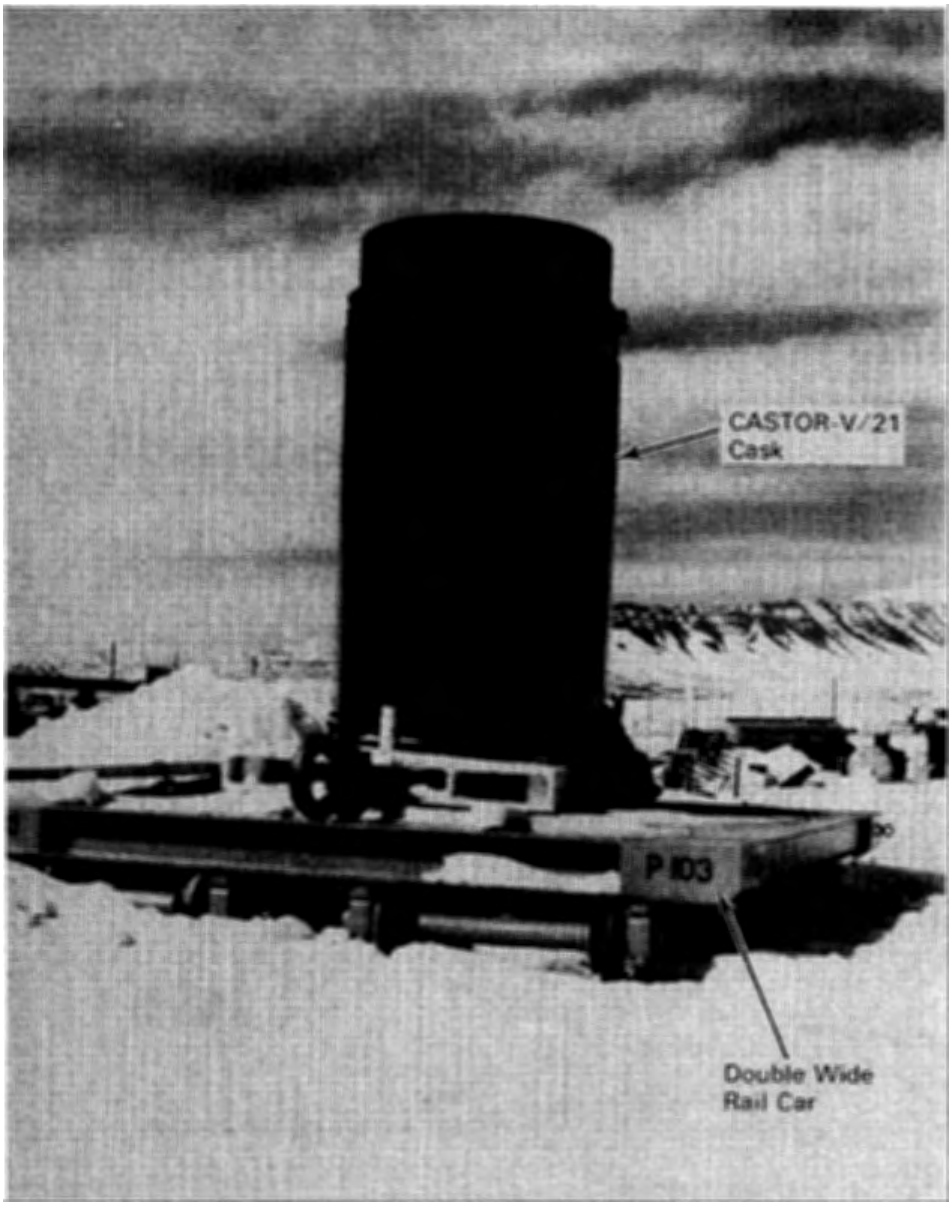

Figure 3-51. Temporary Storage of the CASTOR-V/21 Storage Cask Outside the TAN 607 Warm Shop Prior to Cask Training and Familiarization Activities

Operations technicians removed the top and bottom shock absorbers from the cask. The rigging furnished by TN, a load cell, and the Warm Shop Crane were used (Figure 3-54). The trunnion impact limiters were unbolted and manually lifted off the four trunnions. The cask was moved on the trailer to the Hot Shop where the trunnion tie-downs were disconnected. The crane was connected to the TN-8L lift yoke,

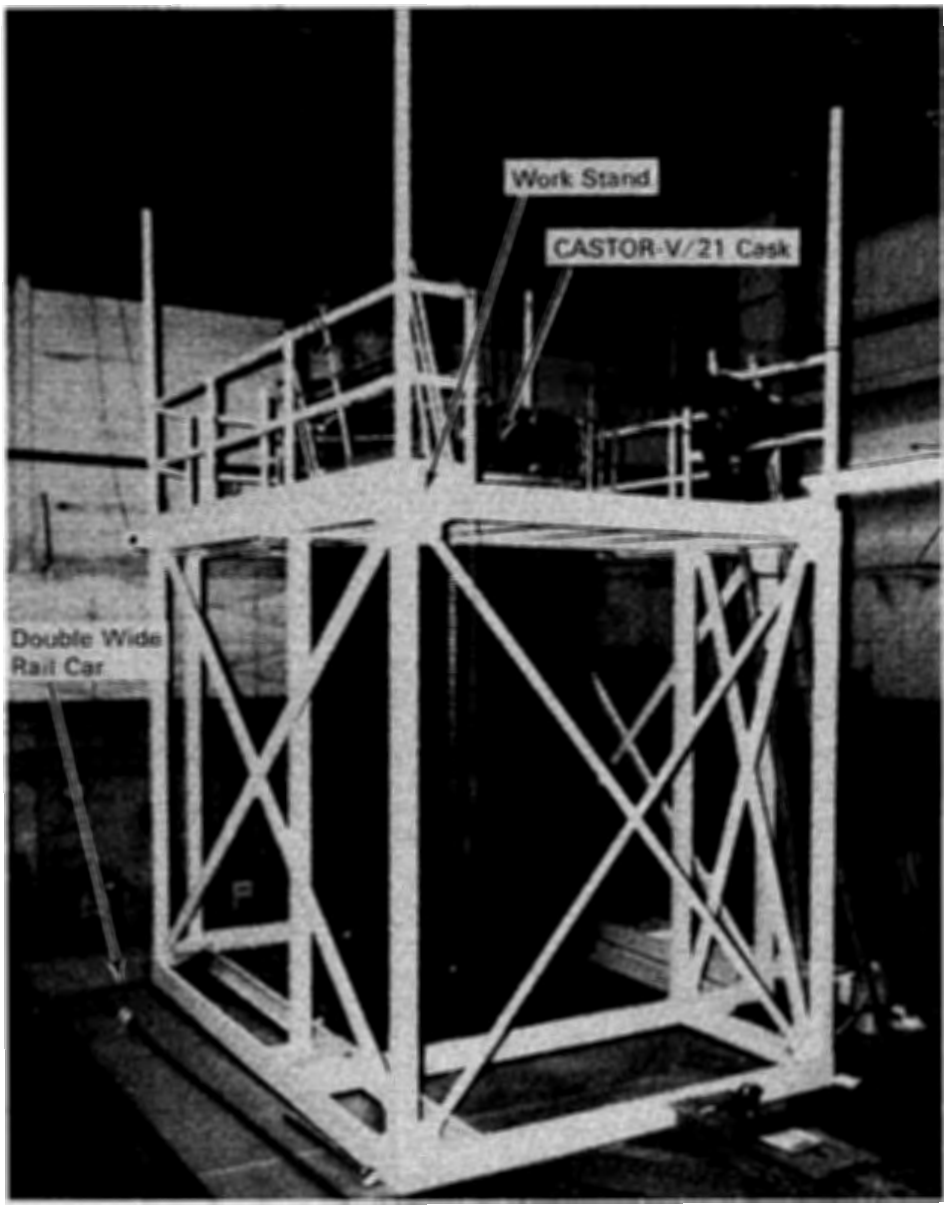

Figure 3-52. Preparing and Training on the CASTOR-V/21 Storage Cask in the TAN 607 Warm Shop Prior to Fuel Loading

and the yoke was connected to the top trunnions of the shipping cask (Figure 3-55). The cask was rotated to a vertical position and moved laterally to the shipping cask work platform adjacent to the storage cask work platform (Figure 3-56). At this point, a gas sample was taken from the shipping cask. The gas was analyzed, and both casks were vented through a controlled gas/vacuum/vent system. Then, technicians removed the lid bolts and installed the lid-lifting fixtures on both cask

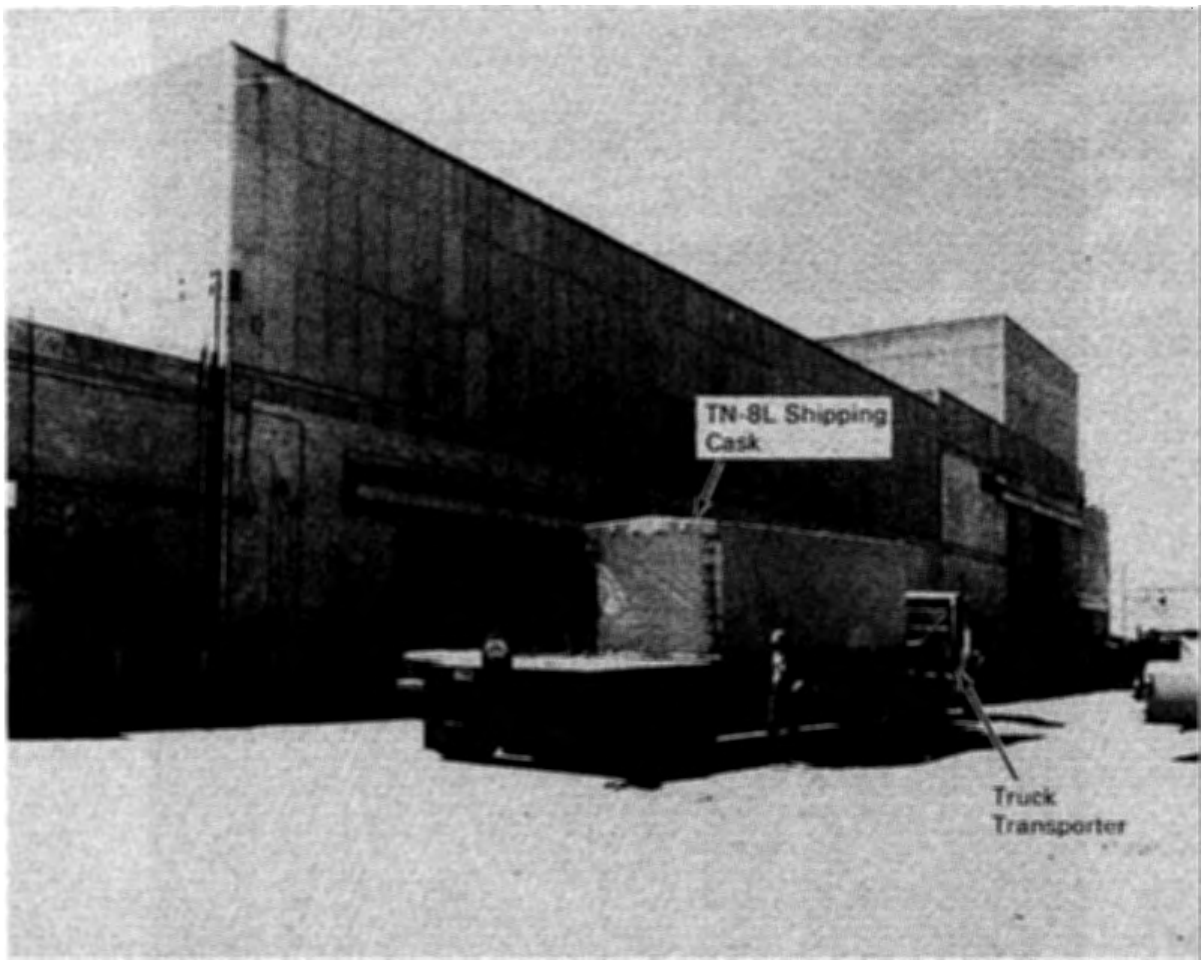

Figure 3-53. Receiving the Transnuclear TN-8L Spent Fuel Shipping Cask at the TAN Facility

lids (Figures 3-57 and 3-58). Numerous pre-remote equipment checkout procedures were performed to verify that all cask handling equipment and facility safety systems were ready for remote operation.

Although the actual procedure would ensure that all personnel were evacuated from the Hot Shop, certain personnel remained in the Hot Shop for the dry run to observe the operation. However, they did not assist any of the remote operations. During the dry run, different operating technicians repeated the following handling sequences several times:

- removing the TN-8L shipping cask and CASTOR-V/21 storage cask lids and placing them on lid support stands on the Hot Shop floor

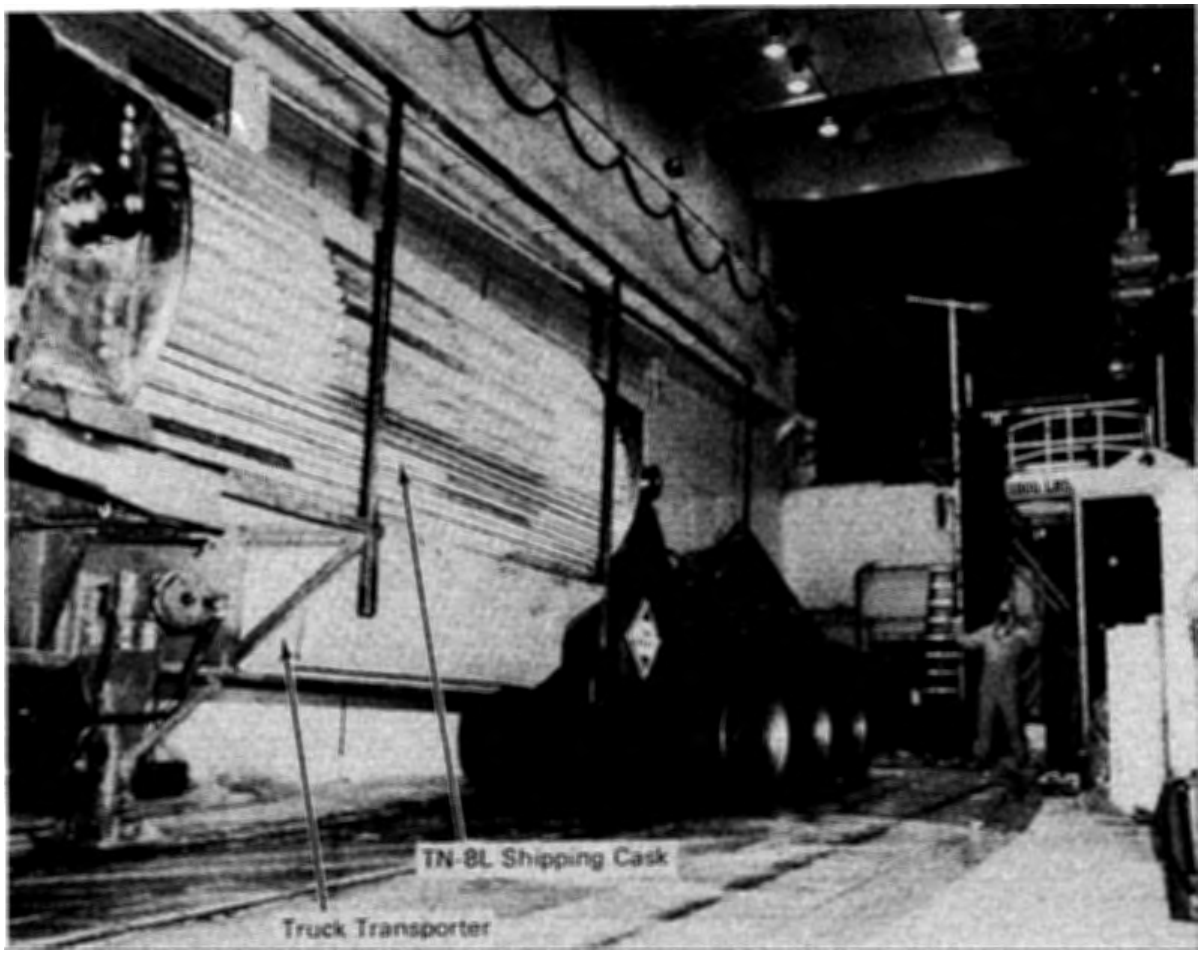

Figure 3-54. The Transnuclear TN-8L Spent Fuel Shipping Cask in the TAN 607 Hot Shop Ready for Offloading to the Shipping Cask Work Stand

- installing the lid seal surface protectors on the storage and shipping casks (Figure 3-59)
- connecting the crane to the fuel grapple and attaching the grapple to the mockup fuel assembly
- placing the fuel assembly into one of the shipping cask baskets and disconnecting the assembly
- repositioning the grapple above the mockup fuel assembly and connecting the assembly to the grapple.
- removing the fuel assembly from the shipping cask and placing it above a storage cask basket
- using the power rotate on the grapple to align the fuel assembly vertically and rotationally
- lowering the fuel assembly into the storage basket (Figure 3-60).

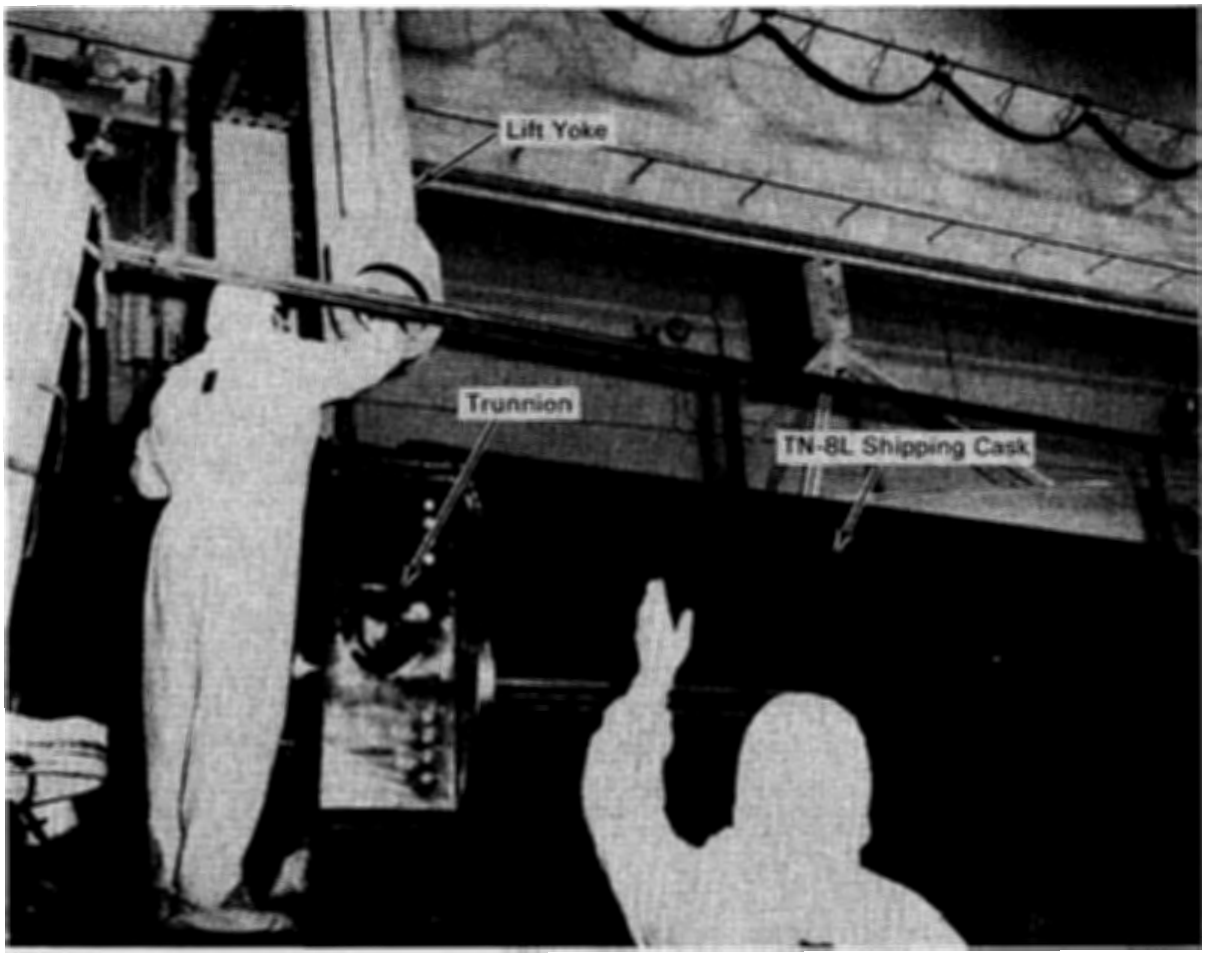

Figure 3-55. Connecting the Transnuclear TN-8L Cask Lift Yoke to the TN-8L Spent Fuel Shipping Cask

During these operations, the fuel grapple load cell had to be closely observed to prevent the possibility of hanging up the fuel assembly, which could cause the grapple system to fail. When the mockup fuel assembly had been inserted into each fuel tube of the storage and shipping cask baskets, the assembly and grapple were returned to their storage racks.

The operations technicians then remotely removed the cask seal surface protector from the storage cask. Using a tool held in the overhead manipulator, the seal surfaces were wiped down to remove any foreign material from the mating surface. The primary shield lid was then reinstalled on the storage and shipping casks (Figure 3-61).

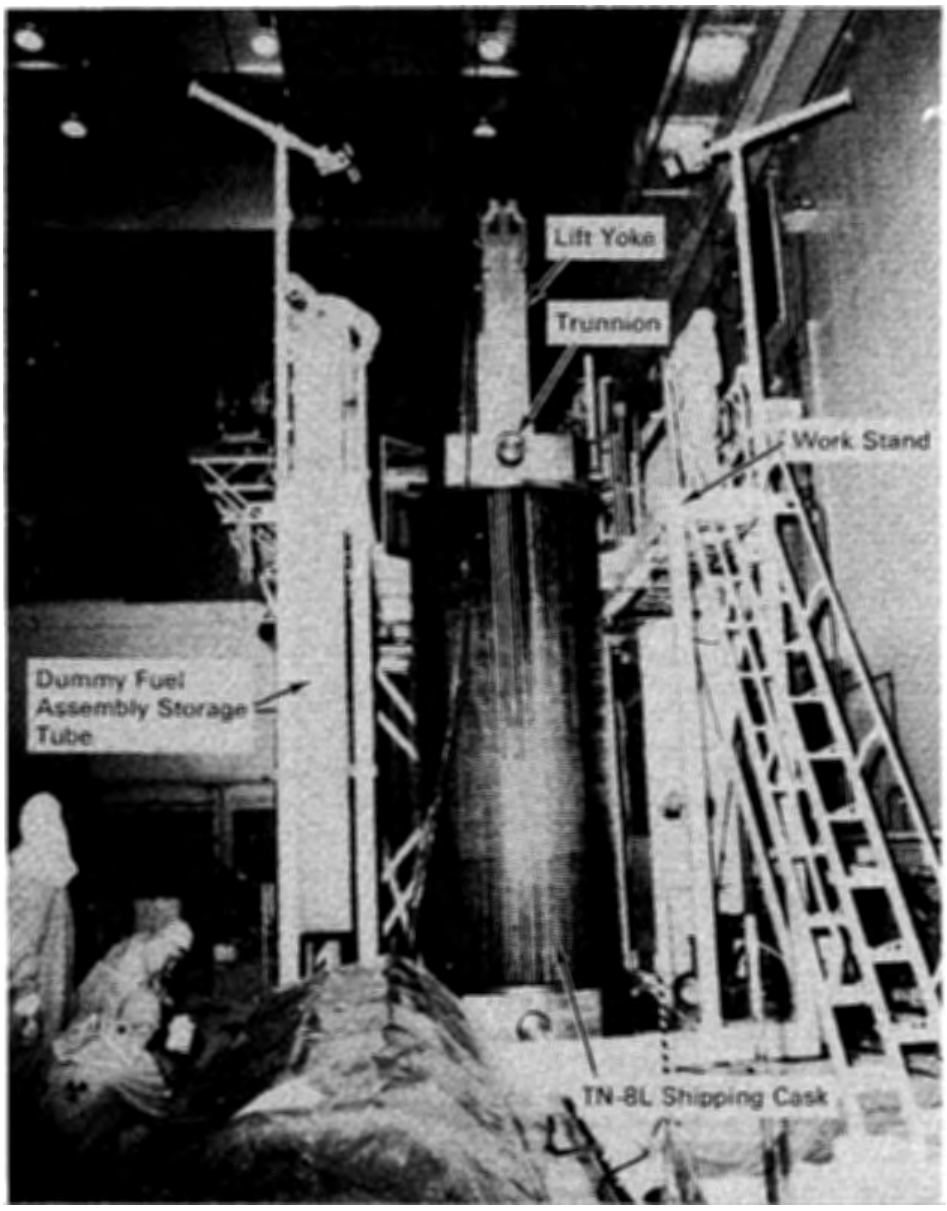

Figure 3-56. Placing the Transnuclear TN-8L Spent Fuel Shipping Cask Into the TAN 607 Hot Shop Work Stand

At this point in the handling sequence, hands-on work was performed in the Hot Shop. Operations technicians installed and torqued the cask lid bolts. The casks were evacuated and backfilled with nitrogen.

The shipping cask trailer was moved to the Hot Shop and the cask was loaded onto the trailer. The cask was moved to the Warm Shop to reinstall the trunnion impact limiters and replace the shock absorber in preparation for shipment to the Surry reactor.

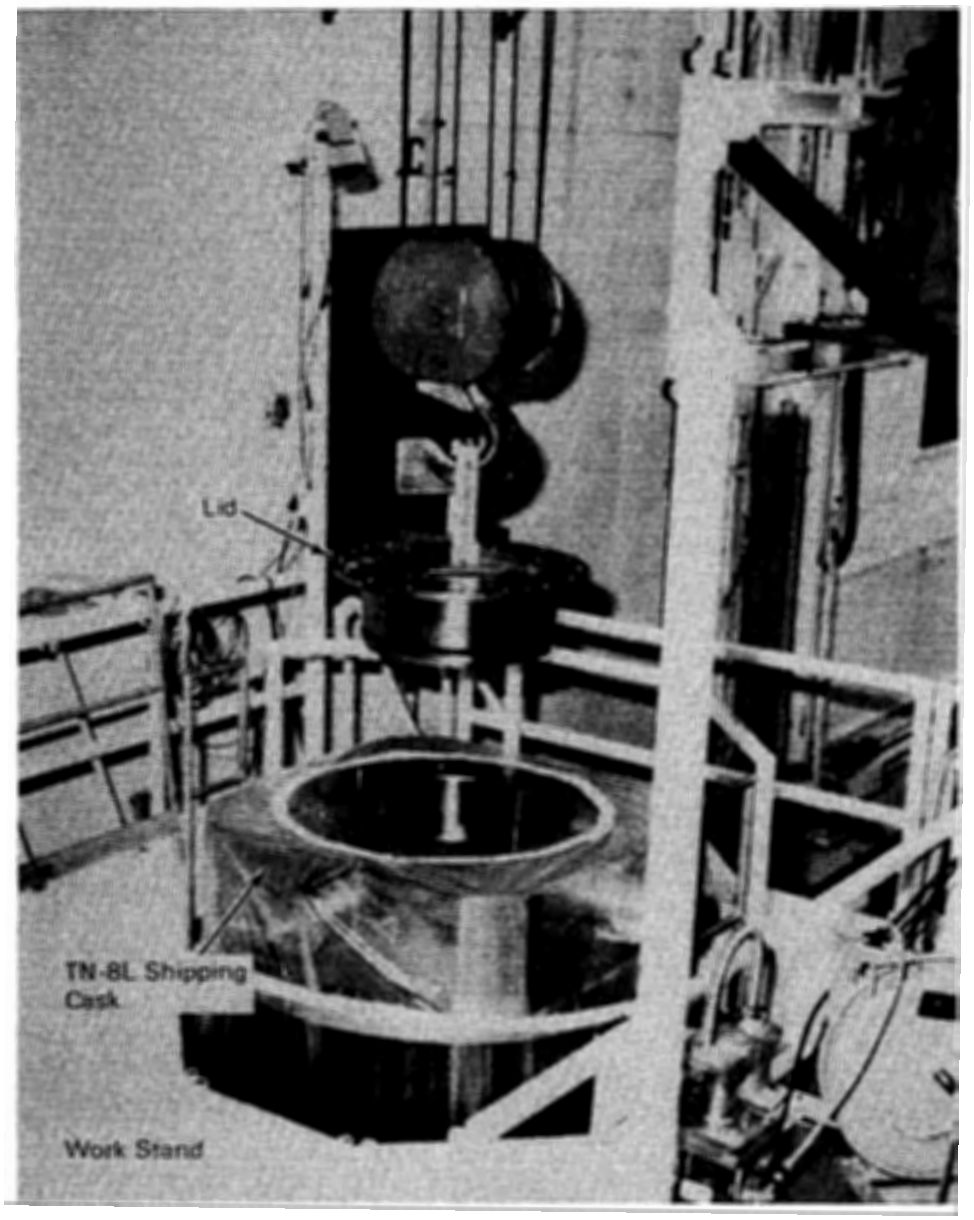

Figure 3-57. Attaching the Transnuclear TN-8L Spent Fuel Shipping Cask Remote Lid Lift Fixture to the TN-8L Shield Lid and Removing the Lid

Facility Readiness Review. When the dry run was completed, a facility readiness review was held. An independent committee reviewed the status of the facility, equipment, personnel training, procedures, safety documentation, operation, quality, and safety. An operational checklist was prepared, and each item was signed off. Quality, Safety, and Management issued readiness approval certificate letters to the facility operations management before the first fuel receipt.

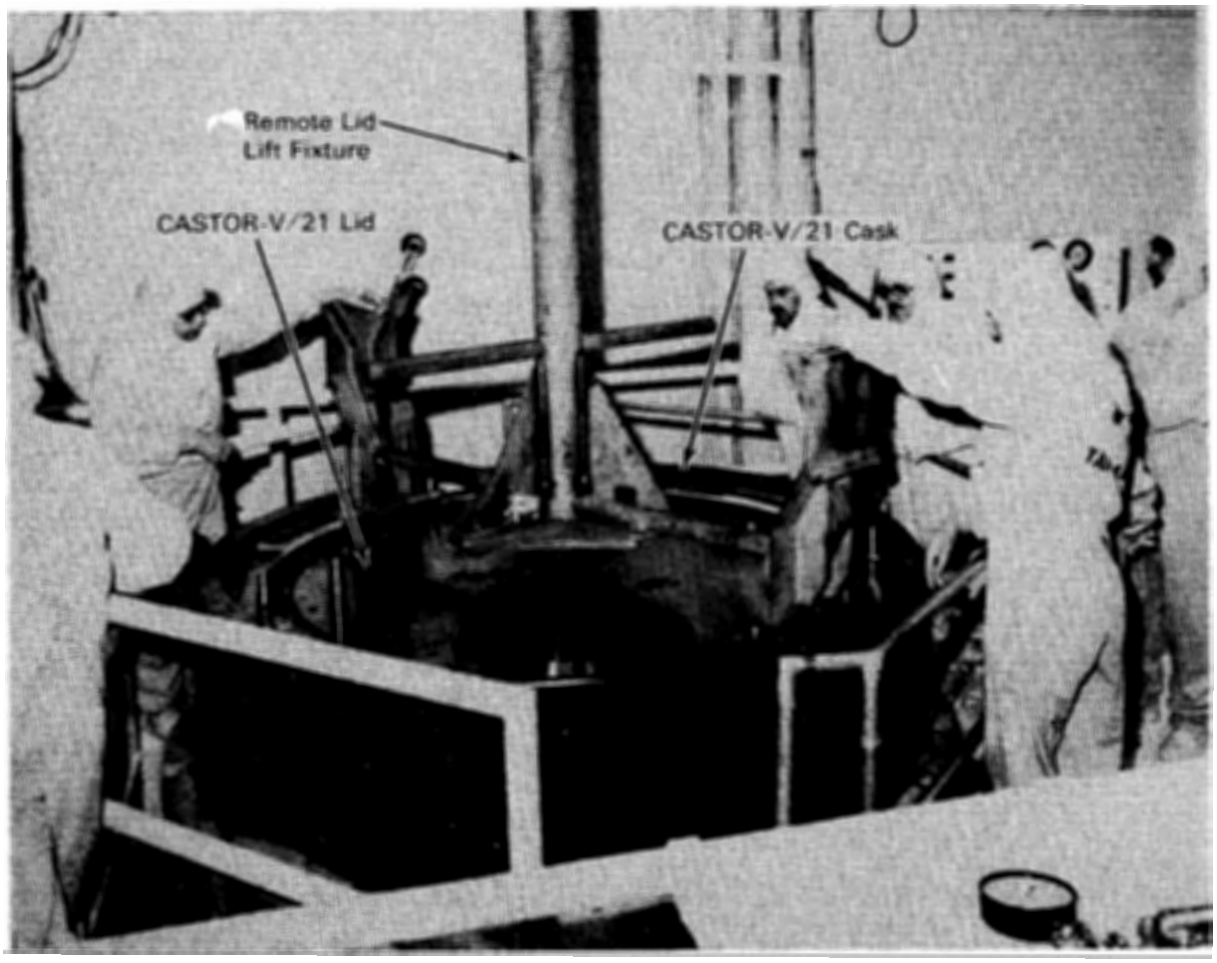

Figure 3-58. Attaching the CASTOR-V/21 Storage Cask Remote Lid Lift Fixture to the Cask Primary Lid

Fuel Transfers and Loading

The CASTOR-V/21 storage cask was loaded with fuel during July and August 1985. Loading fuel into the CASTOR-V/21 cask was routine, and only minor problems were encountered. The fuel transfers and loading followed the procedures verified during the dry run. The loading, vacuum pumpdown, and decontamination operations and experience are discussed in this section. Personnel radiation exposure levels estimated to have occurred during fuel transfers, loading, and testing are also presented.

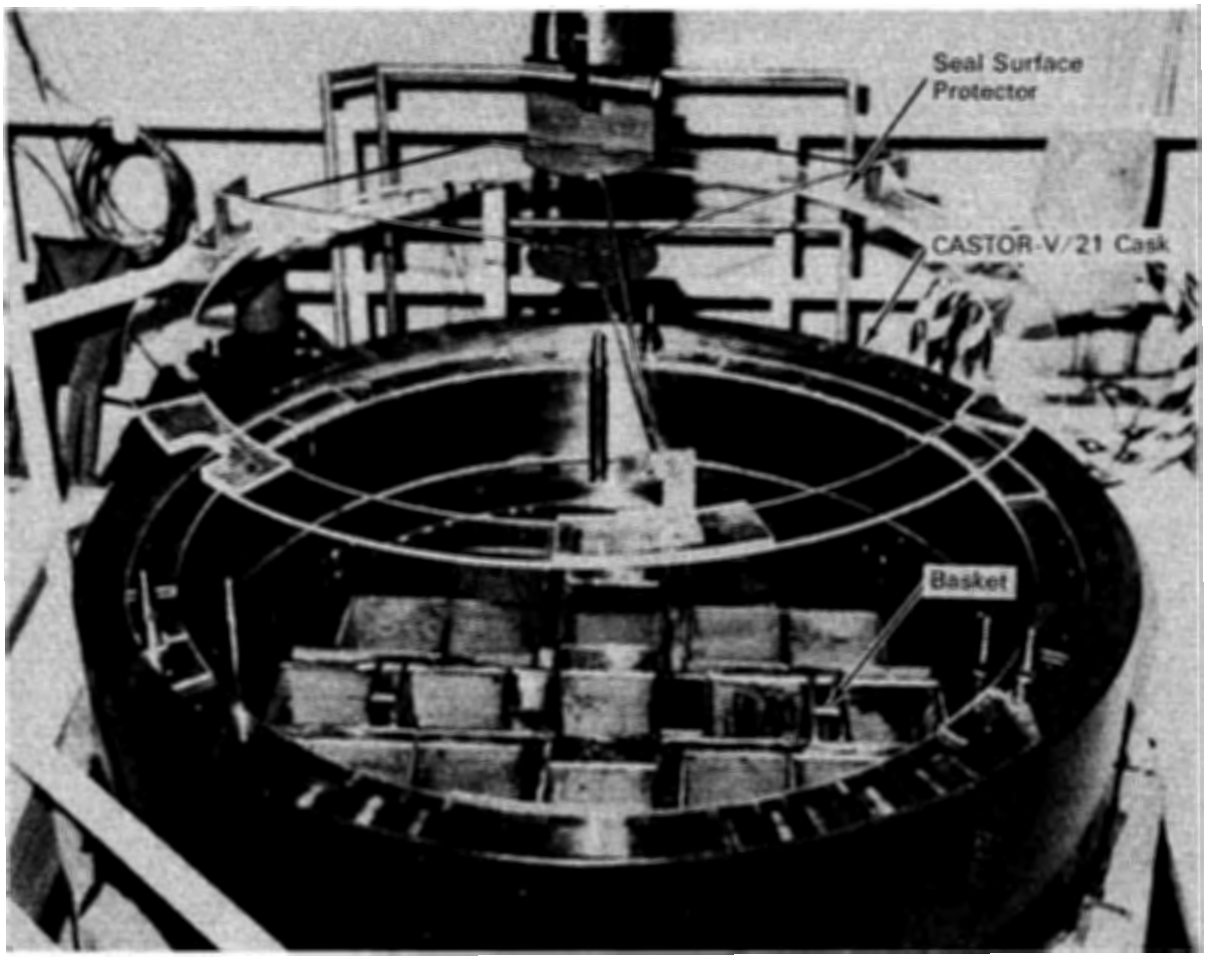

Figure 3-59. Remote Installation of the CASTOR-V/21 Storage Cask Primary Lid Surface Seal Protector Using the Hot Shop Overhead Manipulator

Cask Loading. The seven TN-8L shipping casks arrived at the TAN facility any hour of the day or night. Because each cask shipment was tracked along the shipping route, facility operations personnel received the estimated time of arrival. They then could schedule the unloading with other facility project work. Generally, if the cask arrived on the weekend or late at night, it remained at the TAN guard gate. Sometimes, the area health physicist (HP) would escort the shipment to the TAN Warm Shop, where it was parked inside. The cask would be unloaded at the next regular work shift. The cask unloading turnaround time usually required two and one-half shifts or about 20 hours. Planned overtime and weekend work supported a shorter cask shipping schedule.

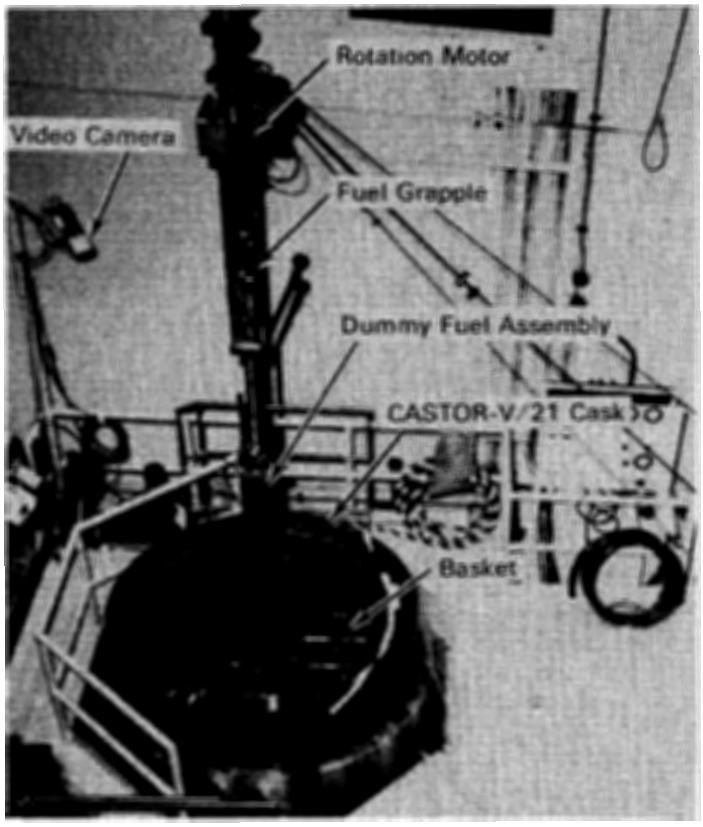

Figure 3-60. Insertion of a Mockup Fuel Assembly Into the CASTOR-V/21 Storage Cask During a Training Exercise Using the Westinghouse Fuel Grapple

Seven shipments, with three fuel assemblies each, were received to fully load the CASTOR-V/21 storage cask. No handling problems were encountered, and the cask-handling equipment and operating ancillary equipment performed well.

Gas samples were taken from each shipping cask and analyzed before the cask was vented. No fission product gases were detected. The shipping cask radiological surveys were below legal shipping limits. INEL shipping requirements made minor decontamination necessary before casks could be shipped from INEL.

The first and seventh shipments arrived in the same cask. The cask internals were radiologically smeared after the first and seventh shipment to determine if contamination had increased. Standard smears with 4.25 cm (1.67 in.) diameter tabs over areas of 100 cm^2 (15.5 $in.^2$) with an applied force of 35 kPa (5 psi) were taken from the fuel basket bottom and near the bottom on the side wall. Crud collection

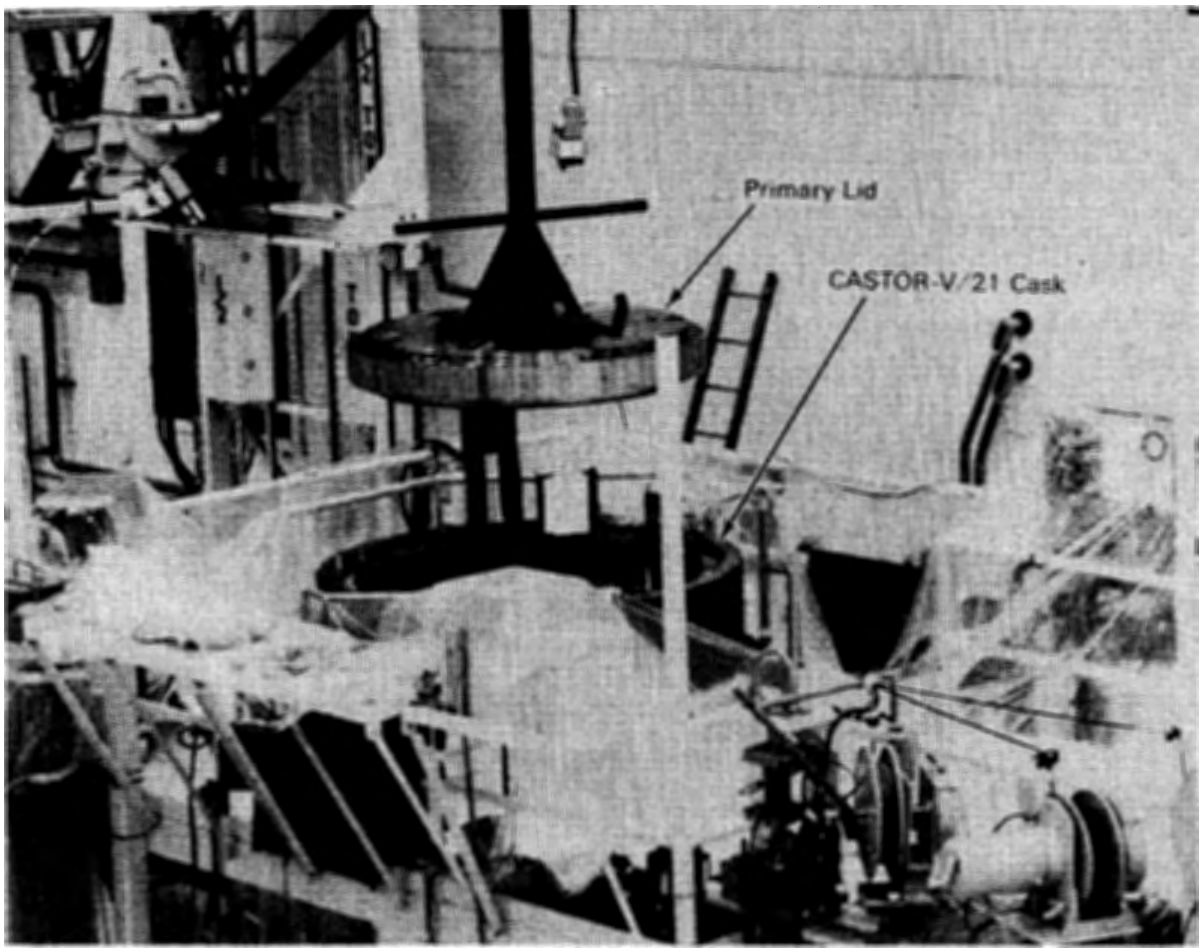

Figure 3-61. Remote Installation of the CASTOR-V/21 Storage Cask Primary Lid Using the Lid Lift Fixture

samples were also taken from the bottom surface of the cask fuel basket. The samples were sent to LLNL to compare the samples from the seventh shipment with those from the first (see Table 3-8).

The CASTOR-V/21 storage cask surface temperatures were relatively high (~80°C). Therefore, Teflon sheeting replaced the standard polyethylene sheeting. The sheeting served as a barrier to prevent storage cask contamination. Teflon sheeting in the temperature range required was available only in rolls 0.9 m (34 in.) wide. Thus, the sheeting, attached to the side of the cask with Teflon tape, hung vertically in strips down the cask. The loosely taped seams overlapped.

To prevent other top surfaces of the work platform near the cask from being contaminated, the following arrangement was used. Teflon sheeting was attached to

areas contacting the cask. Polyethylene sheeting was taped to the Teflon at a safe distance from the cask. This contamination barrier also acted as a thermal barrier, preventing some heat transfer from the cask. However, the contamination barrier was used only while the cask was being loaded. It was removed during formal thermal cask testing.

When the cask surface temperatures increased, the Teflon tape lost its adhesiveness, and new tape had to be applied at the cask surfaces. The Teflon sheets tended to curl and roll from the edges when attached to hot cask surfaces. This made it harder to apply and required more sheeting to cover the cask. External thermocouples monitored the cask surface under the Teflon sheeting to warn personnel in the event cask maximum temperatures were approached. Had these temperatures been reached, the Teflon sheeting would have been removed to allow increased cooling.

When replacing the primary shield lid during the dry run, personnel observed a remote handling problem. During remote operations, it was difficult to determine when the cask lid was fully seated on the cask. A mark was scribed on the inside wall of the cask barrel above the lid. This mark indicated when the lid was properly seated and provided a visual verification to the operating technicians.

The CASTOR-V/21 storage cask operations were very satisfactory. Cask handling and loading operations were easy. Vendor service and information response were good.

Vacuum Pumpdown. A valve tree connected to the cask lid was used to accomplish vacuum pumpdown and gas backfill operations. The valve tree was connected to a quick disconnect in the cask primary test lid and in the gas/vacuum/vent system. Quick disconnects were provided for the vacuum hose and gas supply hoses. A pressure transducer, teed into the valve tree, monitored cask cavity pressure.

The cask vacuum pumpdown system required approximately 3/4 to 1 h to pump the cask from 850 mbar atmosphere pressure (12.25 psi) at 1463 m (4800 ft) elevation down to less than 1 mbar (0.01 psi). Backfilling with cover gas required about 15 min.

The following problems were encountered with the vacuum hoses during pumpdown and backfill operations:

1. When the cask cavity was pumped down, hot gases removed from the cask tended to soften the vacuum hose near the cask valve tree. Occasionally, the hose would collapse. Personnel had to stop the pumpdown and reform the collapsed section of the hose before they could resume pumpdown.

2. When the cask was backfilled through the valve tree after the pump-down, the gas supply hose collapsed. The vacuum in the cask removed gas from the hose faster than the gas supply system could provide it at the system set pressure. A vacuum rated supply hose should be installed on future systems.

3. When the cask was backfilled, the pressure transducer indicated the gas supply pressure rather than the cask cavity pressure. The transducer was mounted on the valve tree just above the cask lid disconnect. The lid quick-disconnect acted as an orifice and restricted flow. To obtain the cask cavity pressure, operating technicians shut the gas flow off and allowed the system pressure to equalize. If the cavity pressure was not at the desired level, the flow was started and stopped as required to get the desired final pressure.

Decontamination. Contamination spread was not a major problem during the fuel assembly air transfers between the shipping and storage casks. However, minor contamination did occur in three of the seven shipments. The contamination was localized to the personnel work platform between the casks. About 4 h of decontamination were required before personnel could continue hands-on work for cask shipping and interim storage activities.

The fuel assembly grapple lower assembly and tool fingers were highly contaminated after each fuel unloading. They had to be decontaminated before storage and bagged while in the storage rack. The grapple had to be decontaminated. Otherwise, it would have spread contamination when it was operated during preoperational checkout before each cask/fuel transfer.

Estimated Personnel Radiation Exposures. During the 3 months personnel were loading and testing the CASTOR-V/21 cask, operational radiation and temperature monitoring were performed. The monitoring provided current actual data for personnel safety. Temperatures and radiation increased with each fuel loading, and more personnel safety equipment was used. A combination of materials was used on top of the cask to remove bolts, install TC lances, and take gas samples. Thermal blankets were placed on the top and down the sides of the cask to reduce the effect of the high temperature hazards. Blankets for thermal insulation were 0.61 m x 1.2 m x 2.5 cm (2 ft x 4 ft x 1 in.) thick. Two-and-one-half-centimeter-thick (1-in.) borated poly sheets were used for neutron shielding, and 1.27-cm-thick (1/2-in.) lead wool blankets provided gamma shielding. This looselaid protective material was repositioned as required for access to different cask penetrations and for lid bolt installation. When it was not practical to use shielding, every effort was taken to reduce personnel exposures. Time in the radiation field was minimized. Special tools and efficient handling procedures maximized personnel distance from the source.

Personnel radiation exposures during the handling, loading, and testing of the CASTOR-V/21 storage cask were:

- Fuel receipt and loading — 0.5 man-rem
- Thermocouple lance installation and removal — 0.5 man-rem
- Cask handling — 0.5 man-rem
- Testing (instrumentation) — 0.3 man-rem

Loading and testing the cask required extensive hands-on operation. For example, thermal testing, radiation dose rate monitoring, multiple gas backfilling, and sampling were hands-on operations. These operations were performed to support the cask performance test. They would not be required for commercial power plant underwater fuel loading; hence, radiation exposures under actual storage scenarios would be much lower than those encountered during this cask performance testing effort.

Cask Performance Testing

Preliminary thermal testing was started when the CASTOR-V/21 storage cask was loaded with 12 fuel assemblies. This was done to ensure that fuel would not exceed maximum allowable temperatures during the cask loading and to obtain early cask heat transfer data. The preliminary data ensured that fully loaded cask surface temperatures and fuel temperatures would not exceed allowable values.

Personnel collected the temperature data using TC lances inserted through a penetration in the test lid and into the guide tube of a selected fuel assembly (Figure 3-16 and 3-62). The TC lances were connected to the data acquisition system. The DAS collected temperature and pressure data during cask pumpdown and interim storage between fuel loadings.

When personnel tried to install the first TC lance, they found the TC lances were too long for the cask and fuel length. Cylindrical spacers (8.9 cm, 3.5 in. long) were placed between TC lance flanges and the cask primary test lid to permit proper installation.

A TC lance was installed after each subsequent fuel loading until the cask was fully loaded. Data were collected weekly and transmitted to PNL.

When the CASTOR-V/21 storage cask was fully loaded, it was tested according to the approved test plan. The primary shield/test lid was bolted on. Operations personnel installed all the remaining nine TC lances through the test lid into eight

Figure 3-62. Thermocouple Lance Installation Through the CASTOR-V/21 Storage Cask Test Lid Into Selected Fuel Assembly Guide Tubes

fuel assembly guide tubes and two basket locations (see Figure 3-17). The cask was double-pumped and backfilled with helium cover gas to ensure gas purity. Then, the cask was moved into the Warm Shop Test Bay (Figure 3-63). There, it was externally instrumented with TCs at predetermined locations (Figures 3-6 and 3-7). All TCs and the pressure monitor were connected to the DAS.

The cask was already near the equilibrium temperature because of the relatively long interim storage period. It required only a short period to reach the peak equilibrium temperature. Monitoring continued for at least 24 h after steady-state temperatures had been reached, to verify that the peak temperature had been obtained. Cask cavity gas samples were taken just after the vertical helium test run was initiated and just prior to completion of the run.

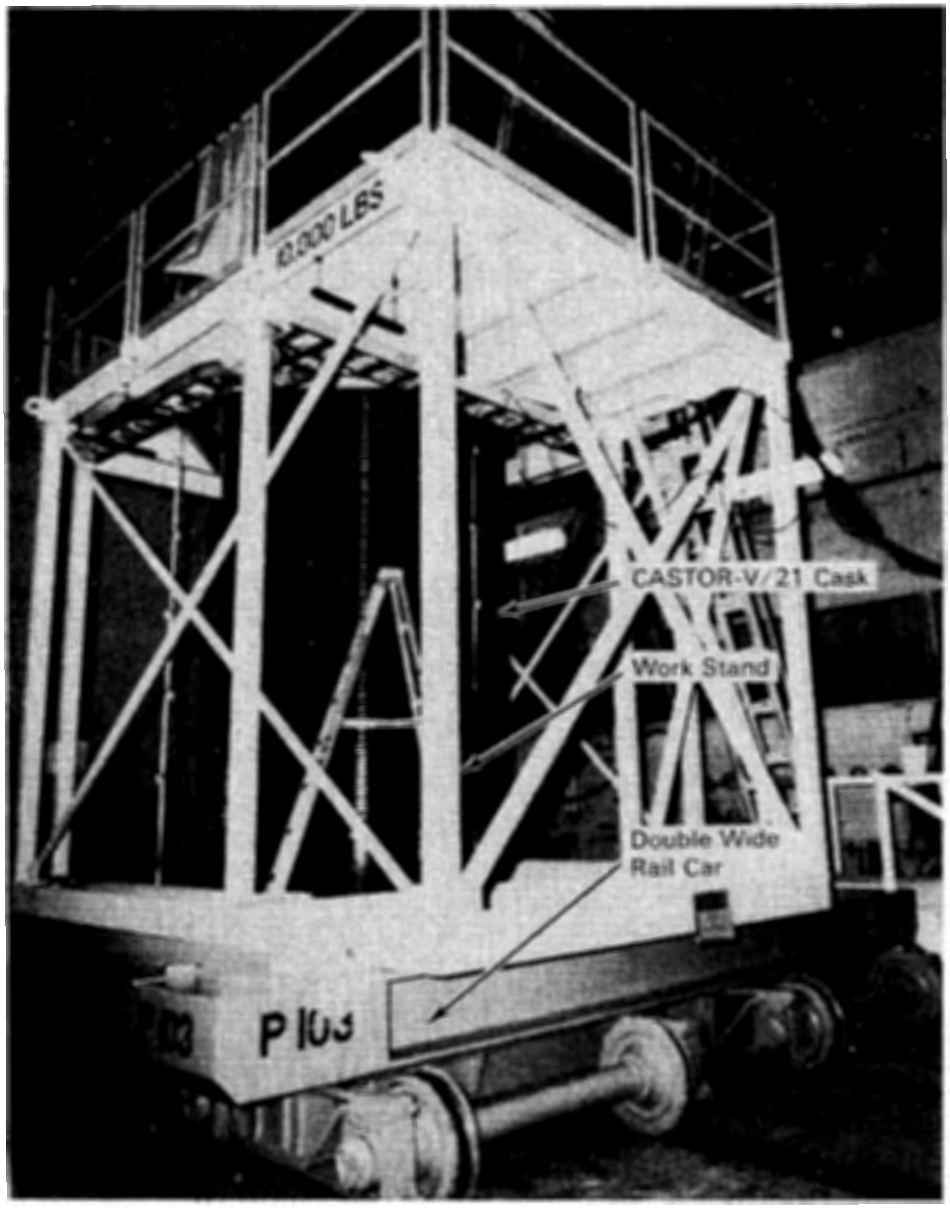

Figure 3-63. CASTOR-V/21 Storage Cask Vertical Performance Testing in the TAN 607 Warm Shop

Once the vertical helium test run data had been verified, the cask cover gas was changed to nitrogen. Gas samples were taken at the beginning and end of the vertical nitrogen test run. Temperature and pressure monitoring continued throughout the vertical nitrogen test run. A vertical vacuum test run was conducted in a similar manner.

Two to three days of monitoring were required to verify that the cask had reached a steady-state temperature after a position or cavity backfill gas change. Therefore, backfill gas and position changes were timed to use the weekends to allow the cask to reach steady-state temperatures.

To move the cask to the horizontal position for the horizontal test runs, the following procedure was used. The cask TCs were disconnected from the DAS. The cask was moved to the Hot Shop where the crane was used to rotate it to a horizontal position. This move required one 8-h shift. When the cask was back in the Warm Shop Test Bay, the TCs were reconnected, and the test run monitoring began (Figure 3-64).

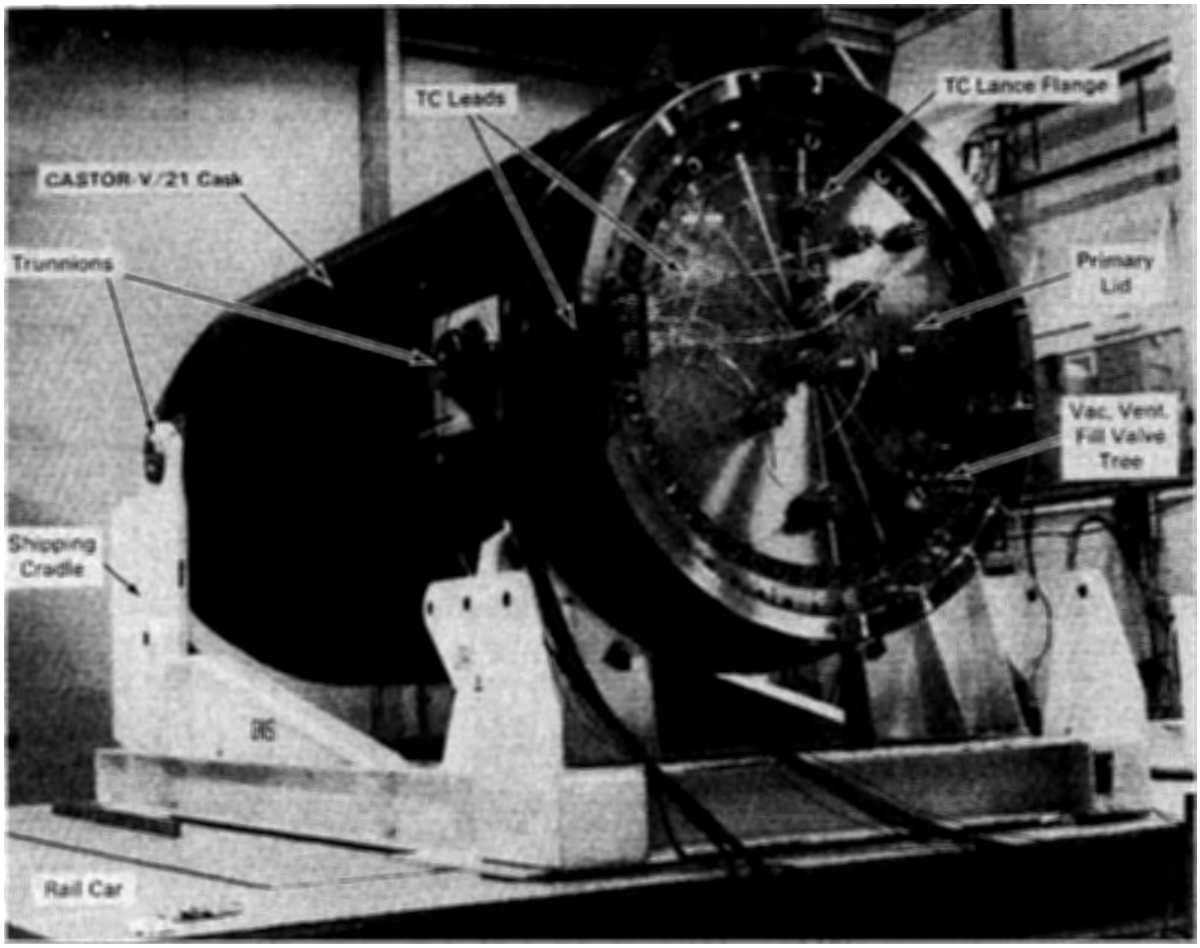

Figure 3-64. CASTOR-V/21 Storage Cask Horizontal Performance Testing in the TAN 607 Warm Shop

During the vertical and horizontal test runs, neutron/gamma radiation dose rate measurements were taken on all cask surfaces using both portable survey instruments and dosimeters (Figures 3-8 and 3-9). EG&G Idaho Inc. health physics technicians conducted the portable surveys, and PNL technicians conducted the dosimetry.

Fuel Assembly Inspections

After the cask performance test was completed, the cask was prepared for fuel integrity inspections. It was moved to the Hot Shop and placed in the storage cask work platform. The TC lances and the test lid were removed. Eight fuel assemblies were removed from the cask, one at a time.

A color TV camera system performed a four-surface video characterization examination while the fuel assemblies were being removed from the cask. Two of the eight assemblies were color photographed using a periscope for high resolution confirmation of the condition of the fuel rods and crud (Figures 3-64, 3-22, and 3-23). Note the misalignment of the upper ends of the fuel rods in Figure 3-65. These misalignments may affect rod consolidation activities and should be considered in future rod consolidation efforts.

Crud and smear samples were collected from these two fuel assemblies. A 2.54-cm-diameter (1-in.) rubber bottle stopper with a 2.54-cm-diameter (1-in.) smear filter attached to one side was used to take the smear samples. The rubber stopper was held in the overhead manipulator hand and remotely pressed against a fuel rod. It was then moved vertically about 20 to 26 cm (8 to 10 in.). The rubber stopper was remotely placed in an open plastic bag. When hands-on operations began inside the Hot Shop, the smear filters were manually removed from the stopper and placed in small shielded pigs ready to send to LLNL for analyses.

Crud collection samples were taken in a similar manner. A large-diameter rubber stopper with double-sided sticky tape was remotely pressed against a fuel rod and then retracted. The sample was then placed in a plastic bag, and the bag was manually placed into a shielded shipping pig.

During fuel integrity inspections, operating technicians using the color video cameras to characterize the fuel assemblies observed what appeared to be cracks in the top surface of the cask fuel basket near weld areas. Further investigation found eight such areas located in the basket configuration (see Section 4 for details). Using the four-color TV cameras, the crack areas were videotaped from two

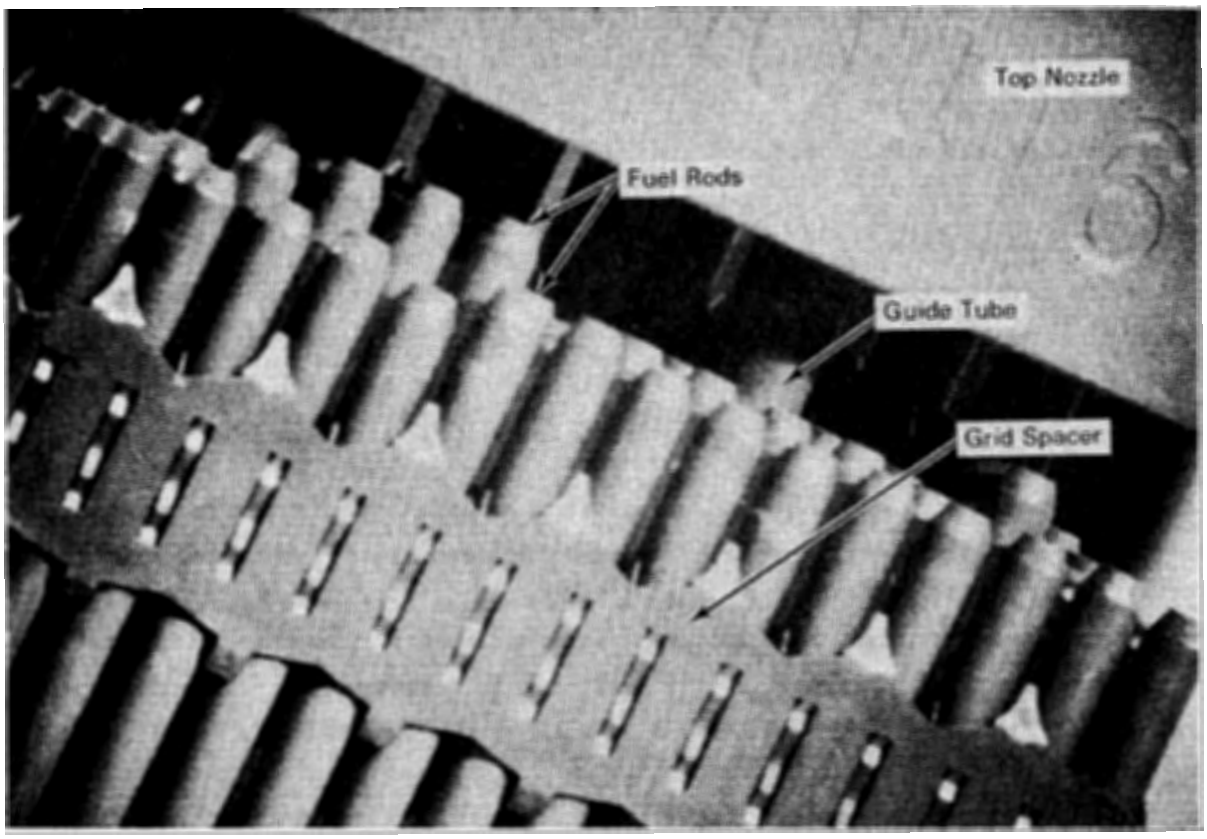

Figure 3-65. Top Nozzle of a Surry PWR Fuel Assembly Placed Into the CASTOR-V/21 Storage Cask

different angles. Both closeup and extended views were taken. No still photographs were taken of the apparent crack areas because the periscope could not view far enough down into the cask cavity. However, still color photographs were taken from still images on the TV monitors (Figure 3-66). Subsequent evaluations of the basket cracking indicated no adverse safety implications. There was no observable effect on the capability to remove or reinsert fuel assemblies during the fuel examinations (see Section 4 for discussions of the basket cracks).

Long-Term Surveillance

Long-term surveillance of the CASTOR-V/21 storage cask at the pad area has not started. The cask was kept on the rail car to facilitate cask handling. Long-term gas sampling and temperature monitoring are being performed in the ensuing time period using the Warm and Hot Shop monitoring systems. These gas samples indicated a high oxygen content of helium cover gas. Subsequent leak testing revealed the

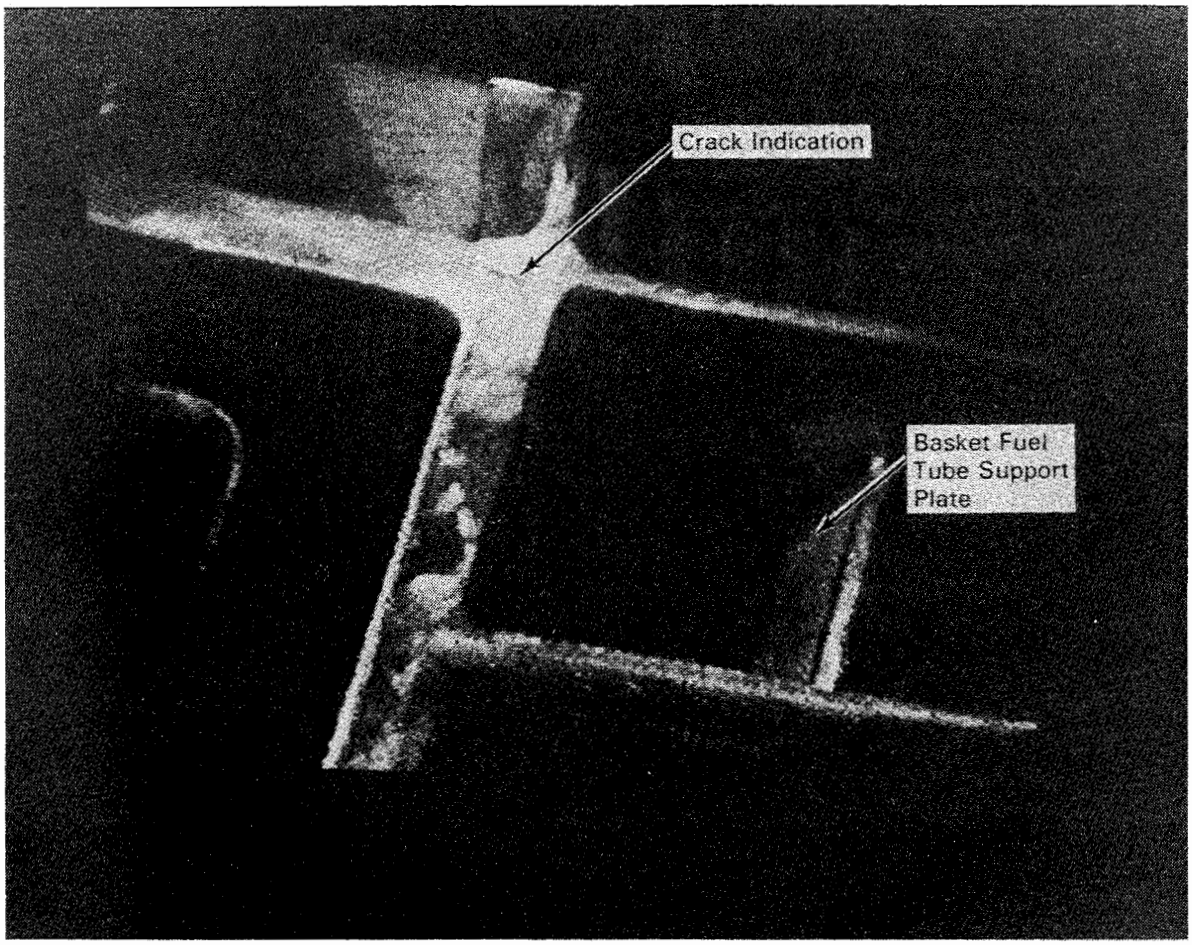

Figure 3-66. Typical Basket Crack

test lid gas sample quick-disconnect was leaking, allowing air into the negative pressure cask cavity. The disconnect was replaced, gas samples retaken, and cask cavity gas purity restored. The cask is currently waiting movement to the long-term surveillance pad.

Section 4

CASK HEAT TRANSFER AND SHIELDING PERFORMANCE

Heat transfer and shielding performance data obtained for the CASTOR-V/21 PWR spent fuel storage cask are presented and discussed in this section. Both cask and fuel assembly peak temperatures and associated temperature profiles are presented to assess heat transfer performance. Cask exterior surface peak dose rates and corresponding dose rate profiles are provided to evaluate shielding performance. Spent fuel integrity results were previously presented and discussed in Section 3.

HEAT TRANSFER

The cask heat transfer performance test consisted of the five runs previously discussed in detail in Section 3. Test runs were performed inside the TAN Warm Shop, in both vertical and horizontal orientations, and with vacuum, nitrogen, and helium backfills. The predicted total decay heat generation of the spent fuel was approximately 28 kW during the month-long performance test. A vacuum environment was used to determine the maximum temperature that could be encountered in the cask and to assess the radiation heat transfer performance of the cask. Nitrogen runs were performed to determine the effects of convection heat transfer in the CASTOR-V/21 basket. In addition, studies are underway to provide the technical basis for using nitrogen as a long-term storage medium (13). The use of helium as a backfill gas permitted determination of the minimum expected operating temperature of the cask because of the relatively high thermal conductivity (four times higher than nitrogen) of helium. Both vertical and horizontal orientations were incorporated in the test to determine differences in performance. Heat transfer data in the three backfills and both orientations are presented in the following sections, along with discussions of cask performance.

Heat Transfer Performance Overview

The cask performance test matrix was developed to determine the effects of cask orientations and backfills. Table 4-1 presents the peak measured guide tube temperatures for all five test runs. Peak cladding temperatures were estimated by using predicted guide tube-to-peak fuel rod temperature differences from the HYDRA

Table 4-1

CASTOR-V/21 CASK TEST MATRIX AND PEAK TEMPERATURES

Run No.	Loading	Orientation	Backfill	Cask Heat Load, kW	Ambient Temp, °C	Side Surface Temp, °C	Measured Guide Tube Temp, °C	Estimated Peak Clad Temp, °C
1	Full	Vertical	Helium	28	27	93	347	352
2	Full	Vertical	Nitrogen	28	24	78	358	368
3	Full	Vertical	Vacuum	28	25	88	414	424
4	Full	Horizontal	Helium	28	24	81	360	365
5	Full	Horizontal	Nitrogen	28	24	77	395	405

computer code (see Section 5). Peak ambient and cask surface temperatures are also shown in Table 4-1; all temperature data are contained in Appendix C.

For the vertical orientation, measured peak temperatures in helium (347°C) and nitrogen (358°C) were less than the 380°C allowable (1). This was also the case for the horizontal helium run (360°C). The vertical vacuum (414°C) and horizontal nitrogen (395°C) runs resulted in measured peak temperatures higher than 380°C, but the peak cladding temperatures were not estimated to be excessively high (<425°C). The high thermal conductivity of the helium resulted in the lowest measured peak temperature (347°C), and the low conductivity vacuum run produced the highest measured temperature (414°C), as would be expected. It is interesting to note that the measured peak temperature in the vertical nitrogen run was not much higher (<15°C) than in the vertical helium run. This indicates that the added convection heat transfer in nitrogen nearly compensated for the higher thermal conductivity of helium.

A comparison of measured peak temperatures in vertical (347°C) and horizontal (360°C) helium runs indicates that the enhanced conduction heat transfer resulting from fuel assemblies contacting basket fuel tubes in a horizontal orientation did not quite compensate for the convection in helium. This is opposite the results of another cask test (4) and surprising because density changes resulting from temperature changes in helium do not usually result in significant convection heat transfer when compared to gases like nitrogen or argon. A comparison of vertical and horizontal nitrogen runs shows a similar but magnified effect to be true, i.e.,

the additional conduction in a horizontal orientation due to assemblies contacting fuel tubes (peak equal 395°C) is not nearly as significant as convection in vertical nitrogen (peak equal 358°C).

In general, the cask heat transfer based on peak temperatures can be concluded to be exceptionally good and exceeded design expectations because peak temperatures in helium, when the cask was dissipating 28 kW, were less than that specified for the cask operating limit of 21 kW (2). It appears that the relatively open design of the fuel basket (see Figure 3-2 of Section 3) permits significant convection heat transfer in a vertical orientation. More discussions on contributions of the different modes of heat transfer are presented in the following sections.

Vacuum Runs

The single vertical vacuum run (run 3) resulted in selected axial and radial temperature profiles presented in Figures 4-1 and 4-2 and additional data contained in Appendix C. Curves are used to connect data points in Figures 4-1, 4-2 and all subsequent figures in Section 4 for clarity only, and do no represent actual temperature profiles. Axial temperature profiles shown in Figure 4-1 for three fuel assembly

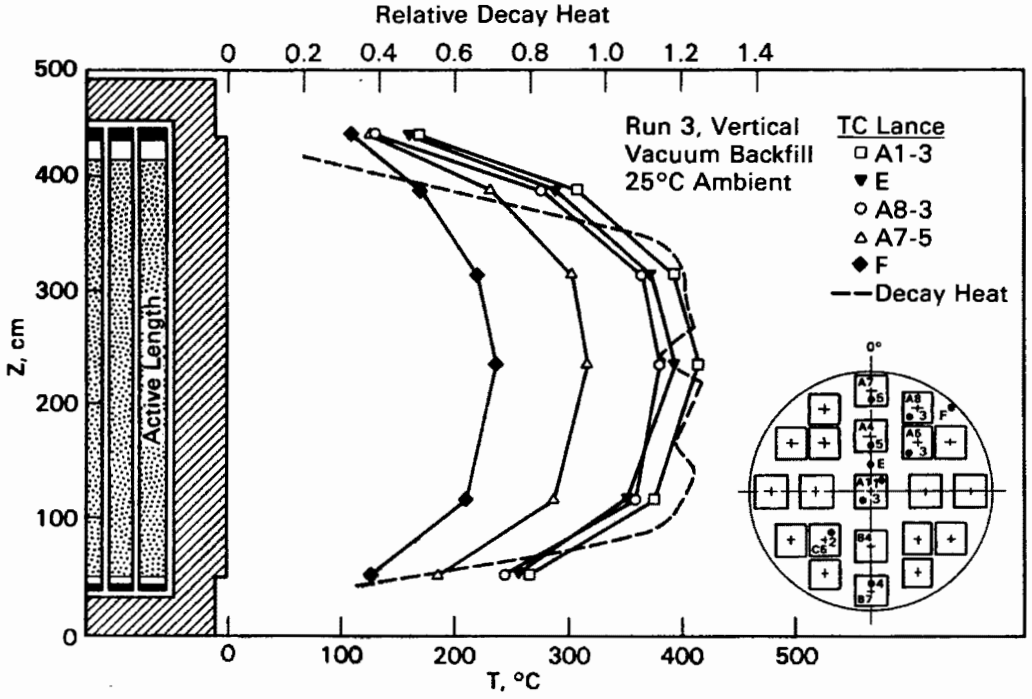

Figure 4-1. Axial Temperature Profiles for Vertical, Vacuum Test Run 3

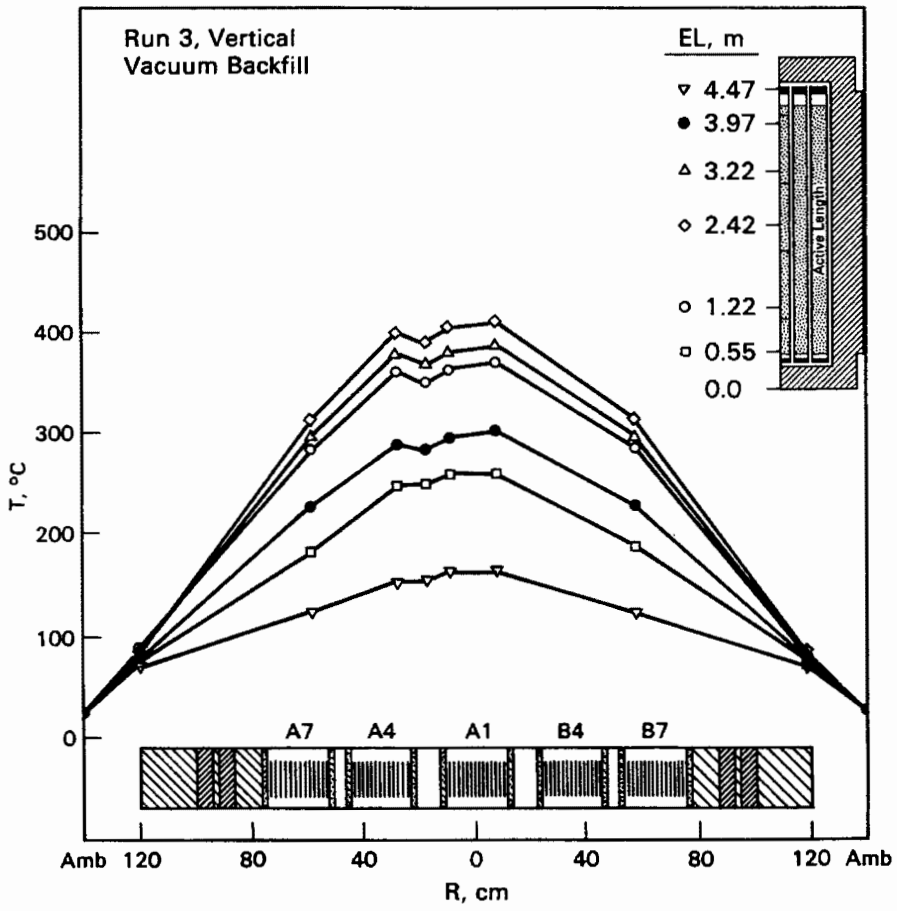

Figure 4-2. Radial Temperature Profiles for Vertical, Vacuum Test Run 3

guide tubes and two TC lances measuring vacuum temperatures peak near the axial centerline of the fuel assembly active length (242 cm) and are symmetrical relative to the active length. The predicted relative axial decay heat profile (Figure 3-15 of Section 3) is included above the temperature profiles to show similarities between temperature and decay heat profiles. It can be concluded that convection was negligible in the vacuum run, as would be expected, because the temperature profiles are similar in shape to the decay heat profile and the temperature profiles are not skewed toward the top of the assemblies.

A comparison of the axial temperature profile of outer assembly A8 (1.8 kW) with center assembly A1 (1 kW) indicates the center assembly was hotter than the higher decay heat outer assembly. This indicates that the additional effective thermal resistance and heat generated by other assemblies between the center and outer assemblies were enough to more than compensate for the higher heat generation rate

in the outer assembly; i.e., even though the center assembly generated less heat, the higher resistance to ambient and additional heat generated by other assemblies between it and the outer high decay heat assembly resulted in higher temperatures. It is interesting to note that temperatures measured with the inner gas TC lance E are very near (20°C) those in adjacent assembly A1. The radial temperature profile in the center of the basket appears to be reasonably uniform. Temperature profiles in Figure 4-2 provide a better perspective on radial temperature gradients in the cask.

Radial temperature profiles from assembly A7 to B7 are presented in Figure 4-2 for each axial location were data were obtained. The profiles indicate that reasonably uniform temperatures existed in the cask between assemblies A4 and A1 and significant gradients occurred from assemblies A1 and A4 to outer assemblies A7 and B7. In addition, severe gradients were measured from outer assemblies A7 and B7 to the cask surface. It is shown via HYDRA temperature predictions (Section 5) that a significant part of this temperature drop occurred from the outer assemblies to the inner cask wall. These steep temperature gradients indicate the basket-to-inner wall gap may be important to the heat transfer performance of the cask.

Maximum temperature differences shown in Figure 4-2 between assemblies A1 and A4 and gas TC lance E are 21°C and 11°C, respectively. These relatively small temperature differences indicate a lack of convection in the vacuum backfill and that a reasonable value of vacuum thermal conductivity existed in the cask. Convection or extremely low conductivity would result in relatively large temperature gradients near the assemblies. Effects of convection on temperature gradients near the assemblies are shown in the nitrogen data presented in the next section. The conductivity of the vacuum, which was essentially low pressure (2.5-mbar) nitrogen, was probably not much different than the conductivity of higher pressure nitrogen. This is because most gaps in the basket are wider than the mean free path of nitrogen molecules at test temperatures and 2.5 mbar and, until gaps become less than the mean free path of a gas molecule, no significant affect on thermal conductivity results. The vacuum thermal conductivity value selected for the HYDRA heat transfer analysis is indicated in Section 5. The use of a nonzero conductivity for vacuum is probably not a standard practice, but is necessary to accurately predict cask performance with a vacuum environment.

The temperature difference within a fuel assembly can be examined by comparing axial temperature profiles from TC lances placed in guide tubes 1 and 3 in assembly A1, i.e., lances A1-1 and A1-3 of Figure 3-17. Figure 4-3 indicates that temperatures

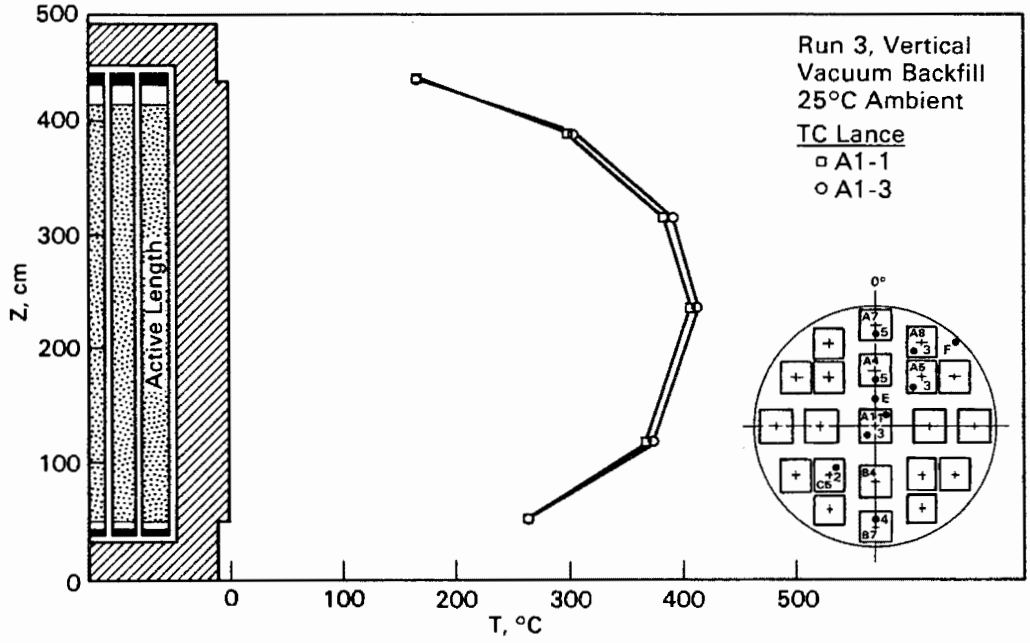

Figure 4-3. Temperature Differences Within Center Assembly A1 for Vertical, Vacuum Test Run 3

near the ends of the guide tube were approximately equal and differences of 6°C to 8°C existed at the other axial locations. Because there is one fuel rod between guide tubes 1 and 3 (actually between their relative symmetrical locations within the assembly as shown in Figure 3-11 of Section 3), it appears there may be a 3°C to 4°C temperature difference between rods in the assembly. Therefore, peak cladding temperatures of the centermost fuel rods can be roughly estimated by adding 9°C to 12°C to measured temperatures of centermost guide tubes; i.e., there are three rod-to-rod spaces between measured centermost guide tube temperatures and centermost fuel rods, and a 3°C to 4°C temperature difference across each space results in an estimated total temperature difference of 9°C to 12°C. A more precise estimate of the centermost fuel rod temperature could be obtained by considering the predicted assembly temperature profile from HYDRA (Section 5) because the above estimate assumes a linear profile.

Symmetry of temperatures measured in the vertical cask can be determined from Figure 4-4. Temperatures in assembly guide tubes A5-3 and C5-2 and in A7-5 and B7-4 should, from symmetry, be equal. As shown in Figure 4-4, the temperature profiles in these pairs of assemblies are essentially the same. This indicates that the cask thermal resistance and the assembly decay heat generation rates were very symmetrical within the cask.

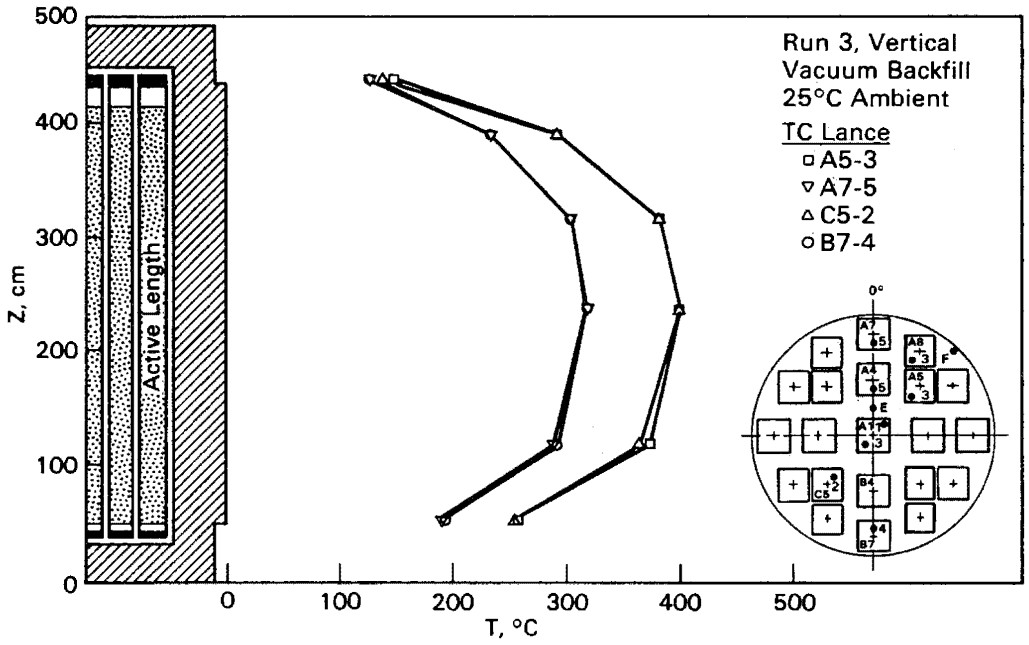

Figure 4-4. Axial Temperature Profiles With Vacuum Showing Symmetry in Basket/Fuel Assemblies

The vacuum data demonstrated that fuel rod temperature would not be excessive (<425°C) in a low conductivity, low convecting backfill. The axial vacuum temperature profiles established a symmetrical, nonconvecting shape about the fuel rod active length; this shape can be used as a reference for the profiles in convecting nitrogen and helium that are presented in the following sections. In addition, comparisons of symmetric axial temperature profiles verified that basket thermal resistances and fuel assembly decay heat generation rates were very symmetrical. Radial temperature profiles in vacuum indicated that a steep gradient existed from the outer assemblies to the cask surface. HYDRA predictions in Section 5 show that a significant part of the gradient could occur across the basket-to-inner wall gap. Therefore, this gap may be important to the heat transfer performance of the cask.

Nitrogen Runs

Axial temperature profiles for the vertical nitrogen run are presented in Figure 4-5 for selected TC lances. As shown, the axial temperature profiles are vividly skewed toward the upper ends of the assemblies, indicating the presence of significant convection heat transfer. Peak temperatures occurred at an elevation of 322 cm in each TC lance, and the highest peak temperature (358°C) occurred in center assembly A1. The peak temperature in the outer 1.8-kW assembly (A8-3) was 353°C.

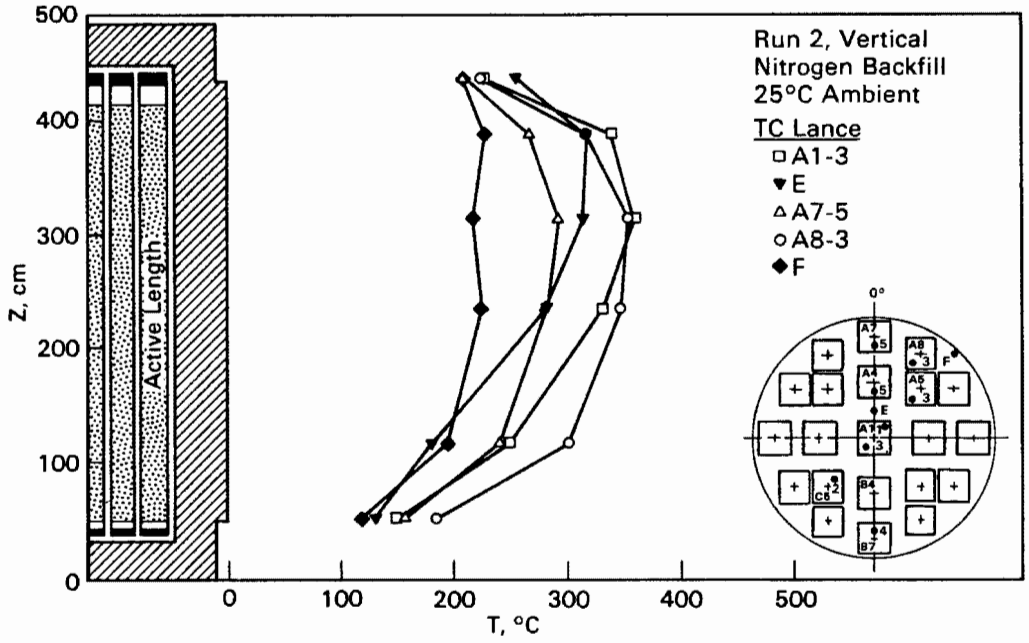

Figure 4-5. Axial Temperature Profiles for Vertical, Nitrogen Test Run 2

Temperatures measured in center assembly A1-3 indicate the most convection of the assembly TC lance temperatures. This is based on the fact that temperatures in the lower region of the assembly are among the coolest, but temperatures in the upper region of the assembly are among the hottest. Temperature profiles for outer assemblies A8-3 (1.8 kW) and A7-5 (1 kW) indicate much less convection heat transfer. Gas TC lance temperatures in the center of the cask (E) verify that significant convection occurred in the interior regions of the cask by the vivid upward skew to the axial profile. In contrast, temperatures of the gas TC lance near the inner wall of the cask (F) show little signs that significant convection was occurring in outer regions of the basket. Near the cask wall, conduction and radiation heat transfer apparently became substantial compared to convection heat transfer and tended to cause uniform heat transfer along the length of the outer fuel assemblies. In contrast, in the center region of the basket the conduction and radiation resistances are higher, and convection heat transfer is significant.

A better appreciation for the degree of convection in the vertical cask with nitrogen backfill can be attained by comparing axial temperature profiles for a horizontal orientation with vertical profiles shown in Figure 4-5. Such comparisons are shown in Figures 4-6 and 4-7, in which axial temperature profiles for inner assembly A1, and outer assembly A8 (Figure 4-6) and inner gas TC lance E and outer TC lance F

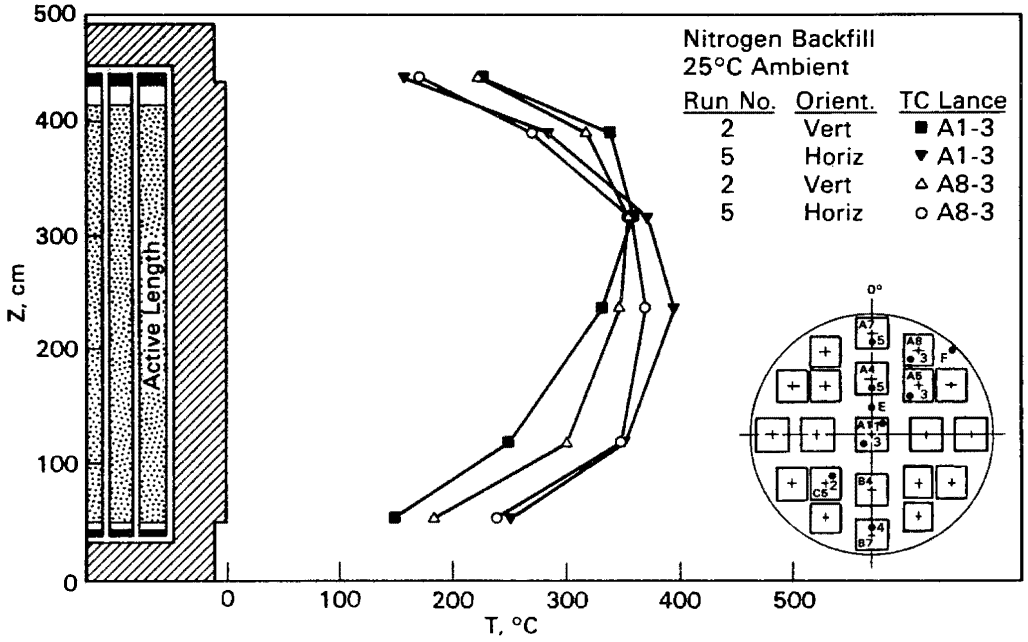

Figure 4-6. Assembly Axial Temperature Profiles for Horizontal and Vertical Nitrogen Test Runs 2 and 5

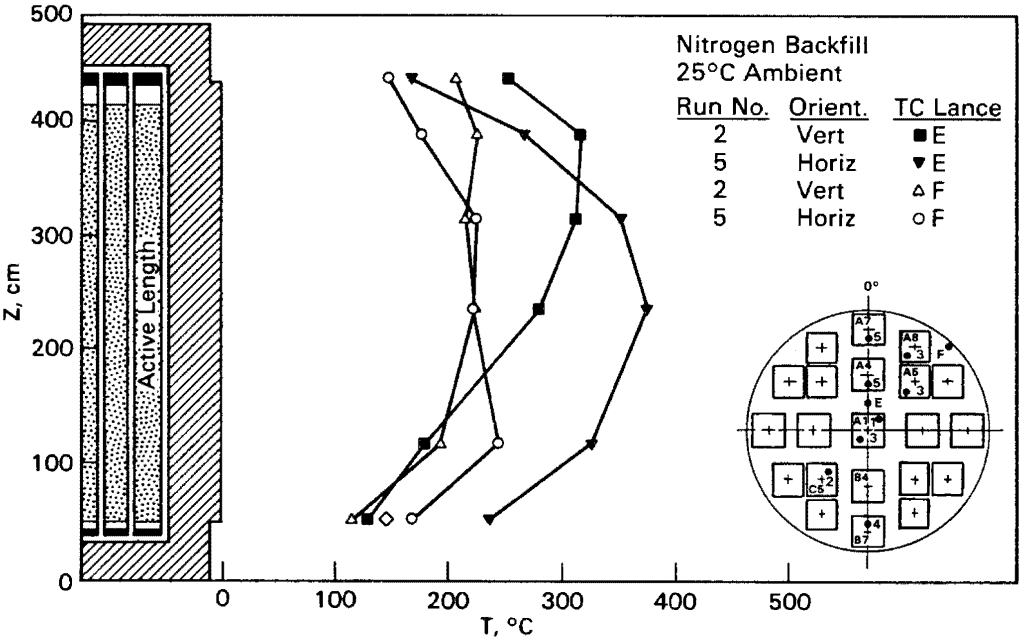

Figure 4-7. Backfill Gas Axial Temperature Profiles for Horizontal and Vertical Nitrogen Test Runs 2 and 5

(Figure 4-7) are presented. Comparisons of corresponding axial profiles in the interior of the cask (A1-3 and E) all vividly indicate the effects of convection in a vertical orientation. In contrast, profiles in the outer regions of the basket (A8-3 and F) indicate only minor differences in the two orientations. Note that the temperature profiles obtained in a horizontal orientation peak near the centerline of the fuel (242 cm) and are similar to those of vacuum and the predicted axial decay heat profile (Figure 4-1), indicating the lack of convection.

The lack of axial convection in vacuum or horizontal runs is reasonable because significant density gradients cannot develop in a vacuum or in an orientation with low axial gravitational forces. It can be concluded that the relatively open design of the CASTOR-V/21 basket (Figure 3-2 of Section 3) led to significant free convection in the cask.

The peak temperature measured in a horizontal orientation was 37°C higher (395°C versus 358°C) than that measured in a vertical orientation. This indicates that enhanced conduction heat transfer created in a horizontal orientation as a result of additional contact between fuel assemblies and basket fuel tubes was not enough to compensate for significant convection heat transfer indicated in Figures 4-5, 4-6, and 4-7.

Radial temperature profiles at the six axial locations obtained in a vertical orientation are presented in Figure 4-8. The profiles indicate that temperatures increased with elevation, peaked at Z = 322 cm, and decreased in the upper regions of the assemblies, which is consistent with axial profiles of Figures 4-5, 4-6, and 4-7. Temperatures in inner assemblies A1 and A4 were very uniform at all axial locations, and temperatures in all assemblies were relatively uniform at the two lower elevations (Z = 55 cm and 122 cm) and the upper elevation (Z = 447 cm). Slight gradients existed from inner assemblies (A1 and A4) to outer assemblies (A7 and B7) at the center three elevations (Z = 242 cm, 322 cm, and 397 cm). Steeper gradients existed from outer assemblies A7 and B7 to the cask surface. HYDRA temperature predictions presented in Section 5 indicate that most of the temperature drop from assemblies A7 and B7 to the surface occurred between the assemblies and the inner cask wall. Steep gradients may indicate that the basket-to-inner wall gap is important to the heat transfer performance of the cask. A detailed discussion of the effects of gap size is presented in Section 5.

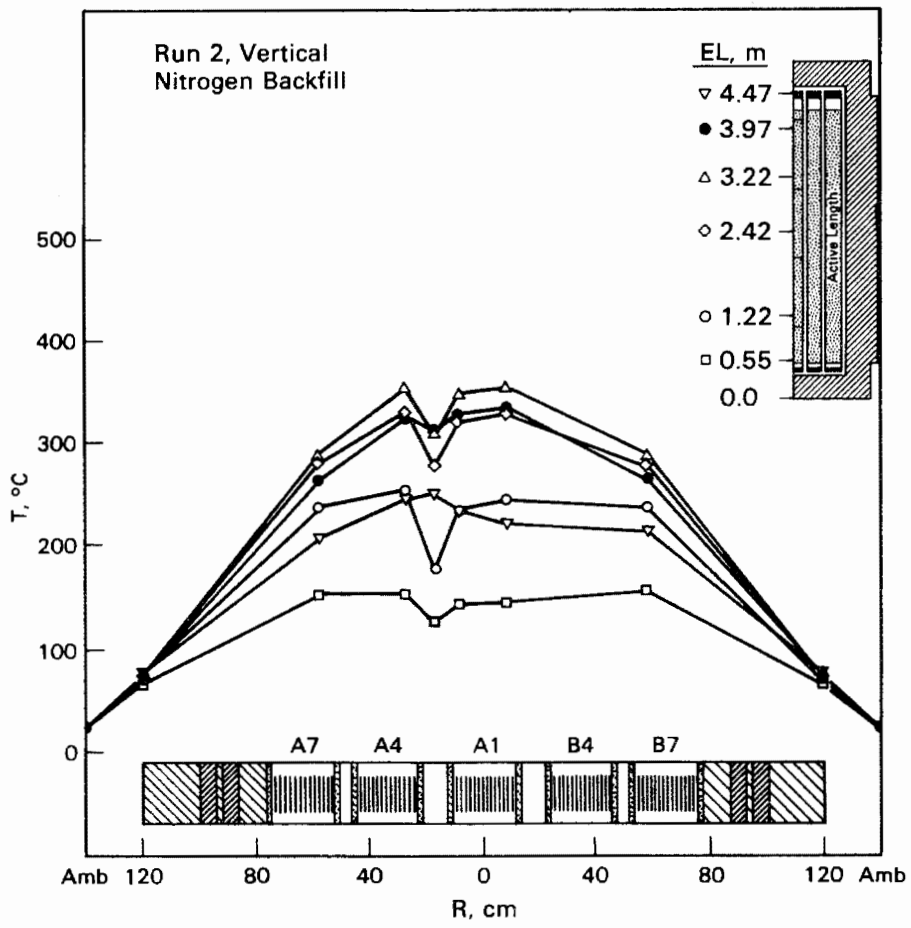

Figure 4-8. Radial Temperature Profiles for Vertical, Nitrogen Test Run 2

Temperature differences between gas TC lance E and guide tube temperatures of assemblies A1 and A4 are significant and as high as 79°C (Figure 4-8 at Z = 122 cm). Differences in temperatures are greater in the axial central region of the assemblies (Z = 122 cm, 242 cm and 322 cm) than in the lower or upper regions. Note that the gas temperature at an elevation of Z = 447 cm near the upper end of the assemblies was slightly hotter (14°C) than measured guide tube temperatures. The uppermost TC was actually above the active length at an elevation corresponding to the upper end fitting of the fuel assemblies, and the absence of heat generation resulted in the gas being hotter than the upper ends of the fuel assemblies. In addition, the uppermost TC was only 3.3 cm (1.3 in.) from the bottom of the primary lid, and heat conduction upward through the TC lances themselves may have been the cause of lower guide tube temperatures.

Radial temperature profiles for horizontal and vertical orientations at axial locations of peak temperatures in horizontal and vertical orientations (242 cm and 322 cm, respectively) are compared in Figure 4-9. The profiles are similar, but temperature differences between gas TC lance E and assemblies A1 and A4 were greater in a vertical orientation than a horizontal orientation. This, of course, was caused by significant convection of nitrogen in a vertical orientations and the lack of axial convection in a horizontal orientation. Temperature differences from inner assembly A4 to outer assembly A7, inner assembly A1 to outer assembly B7, and from outer assemblies A7 and B7 to the cask surface are less in a vertical orientation. Convection in a vertical orientation increases the effective conductance of the basket/fuel assembly conglomerate and, therefore, a lower temperature gradient is

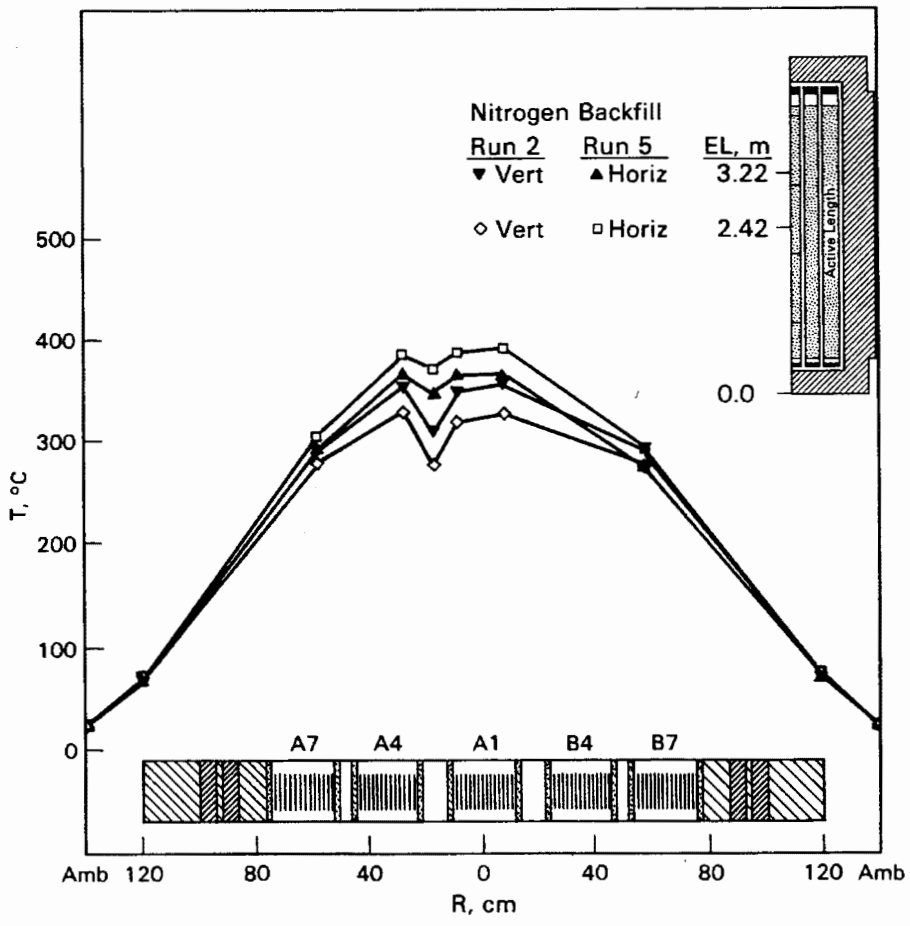

Figure 4-9. Radial Temperature Profiles for Horizontal and Vertical Nitrogen Test Runs 2 and 5

required to transfer the same amount of heat; i.e., $q \alpha U \Delta T$, where q is heat transfer, U is effective conductance, and ΔT is temperature difference, and if U is increased, ΔT must decrease for q to remain the same (energy to be conserved).

Radial temperature differences that existed within a fuel assembly can be visualized by comparing axial temperature profiles in guide tubes 1 and 3 in assembly A1 shown in Figure 4-10. The center regions of the profiles for both vertical and horizontal orientations indicate temperature differences on the order of 6°C to 13°C and 3°C, respectively. The difference between guide tube-to-guide tube temperature differences in vertical and horizontal orientations may be nonuniform contact between TC lances and their guide tubes. Because there is one fuel rod between the respective symmetrical location of guide tubes 1 and 3, it appears there may be a 3°C to 6°C temperature difference between rods in vertical nitrogen and 2°C in horizontal nitrogen. Therefore, peak cladding temperatures in vertical nitrogen runs can be roughly estimated by adding approximately 12°C to measured centermost guide tube temperatures in vertical nitrogen runs and adding 5°C in horizontal nitrogen runs; i.e., there are three rod-to-rod spaces between centermost guide tubes and centermost fuel rods, and a 4°C (vertical) or 2°C (horizontal) temperature difference across each space results in estimated temperature differences of 12°C (vertical)

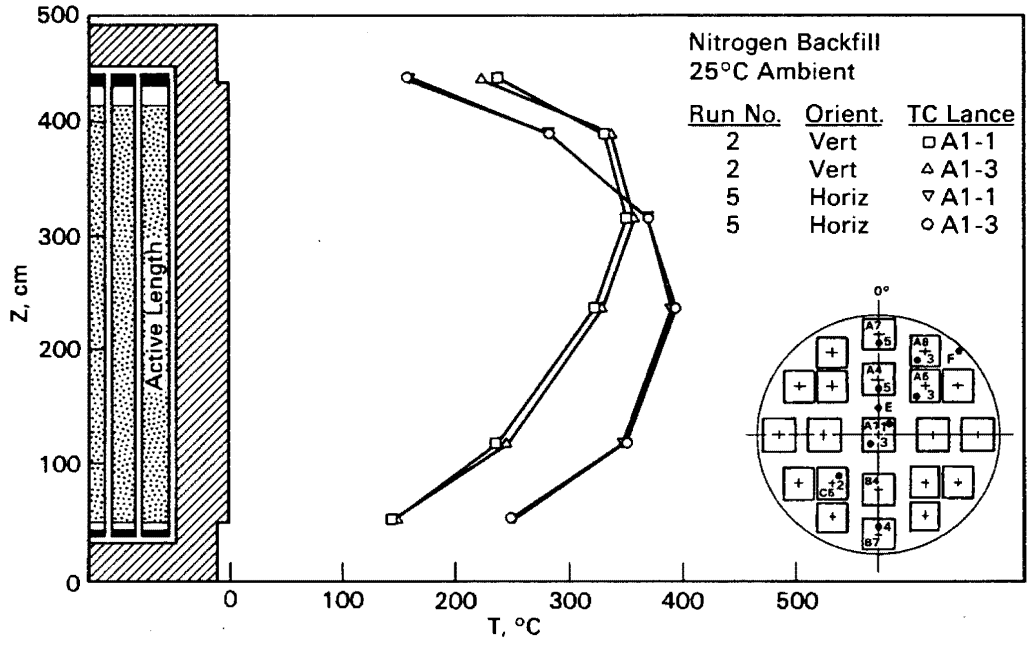

Figure 4-10. Temperature Differences Within Center Assembly A1 for Horizontal and Vertical Nitrogen Test Runs 2 and 5

and 6°C (horizontal). A more precise estimate of the centermost fuel rod temperature could be obtained by considering the predicted assembly temperature profile from HYDRA (Section 5) because the above estimate assumes a linear profile.

Temperature symmetry or nonsymmetry in vertical and horizontal cask orientations with nitrogen can be determined from Figure 4-11. The two axial temperature profiles for vertical symmetrical assemblies A7 and B7 are essentially the same.

Temperature profiles in vertical assemblies A5 and C5 agree closely, with differences being on the order of only 7°C. Small temperature differences indicate that cask radial thermal resistances and fuel assembly decay heat generation rates were essentially the same. The 7°C difference in symmetric vertical assemblies may have been caused by different assembly-to-fuel tube contact. Comparisons of vertical temperature profiles with horizontal profiles again indicate the degree of nitrogen convection present in the cask in a vertical orientation.

Asymmetry caused by rotating the cask to a horizontal orientation is also shown in Figure 4-11. Differences in the axial temperature profiles for assemblies A5 and C5

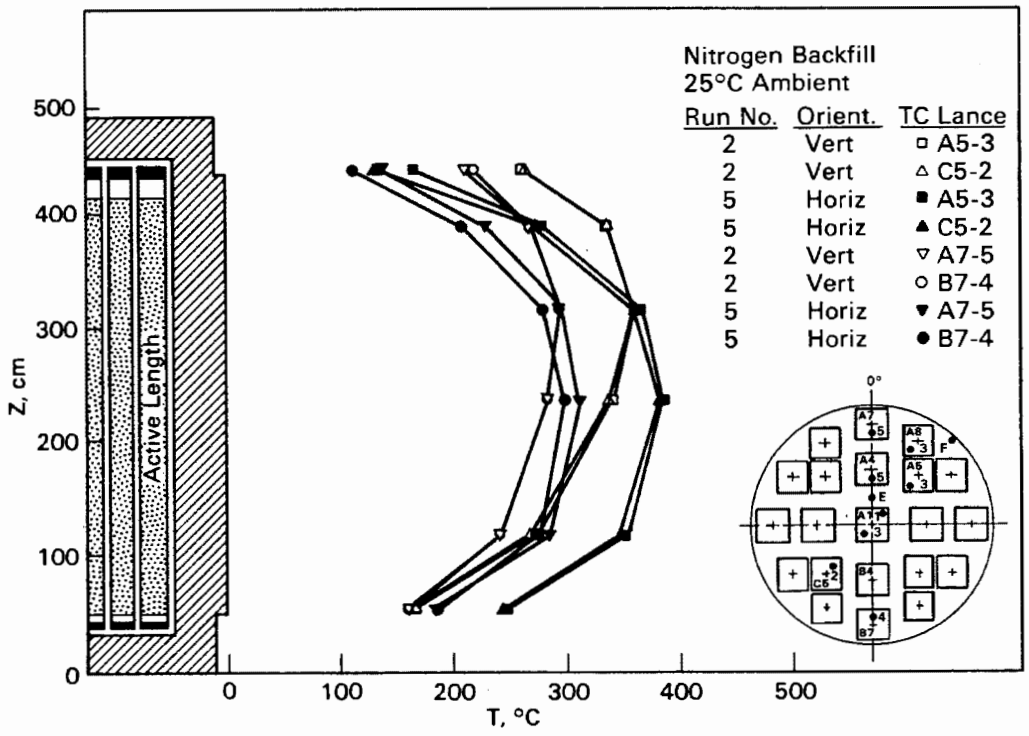

Figure 4-11. Axial Temperature Profiles in Symmetrical Assemblies for Horizontal and Vertical Nitrogen Test Runs 2 and 5

are approximately 7°C in the center region and as high as 34°C in the upper region. It is surprising that symmetry in the center region was not grossly affected when fuel assemblies A5 and C5 come in better contact with their basket fuel tubes as a result of the horizontal orientation. A comparison of temperature profiles for assemblies A7 and B7 indicates temperature differences in the center region as high as 20°C for a horizontal orientation compared to essentially 0°C in a vertical orientation. It is hypothesized that the relatively large asymmetry in a horizontal orientation results from basket eccentricity within the cask cavity. The basis for this hypothesis is that temperatures in the lower B7 assembly, which is adjacent to the basket-to-inner cask wall contact region, are lower than temperatures in the upper A7 assembly, which is adjacent to the basket-to-inner wall gap that was widened as a result of the horizontal orientation. It is anticipated that radial convection within the assemblies and basket enclosures did not noticeably contribute to the asymmetry shown in Figure 4-11; however, an analysis of the existing experimental data cannot confirm this hypothesis.

Temperature data obtained in a nitrogen backfill demonstrated that nitrogen was a more effective backfill than vacuum. Peak guide tube temperatures in vertical nitrogen were 58°C less than in vacuum (358°C versus 414°C). Significant axial convection occurred in the CASTOR-V/21 cask as indicated by much hotter temperatures in the upper one-third of the cask cavity than in the lower one-third in a vertical orientation. Axial temperature profiles in the outer assemblies did not show as much convection as did the inner assembly profiles. Peak temperatures in a horizontal orientation were significantly higher (37°C) than in a vertical orientation, and the location of peak temperatures in the horizontal was 1 m (3 ft) below that in the vertical. Therefore, the added conduction resulting from contact between assemblies and basket fuel tubes did not compensate for significant convection in a nitrogen backfill. Radial temperature profiles again indicated relatively uniform temperatures in the center of the basket and steep gradients from the outer assemblies to the cask surface. The steep gradients may indicate the importance of the basket-to-inner wall gap on cask heat transfer performance. The radial temperature profiles also showed that the flowing nitrogen gas actually became slightly hotter than adjacent guide tubes near the upper end of the assemblies.

Helium Runs

Axial temperature profiles for the vertical helium run are presented in Figure 4-12. The axial profiles for center assembly A1-3 and center gas TC lance E are skewed toward the top of the assemblies in essentially the same way as they were in nitrogen (Figure 4-5). Peak temperatures occurred in the upper one-half of the

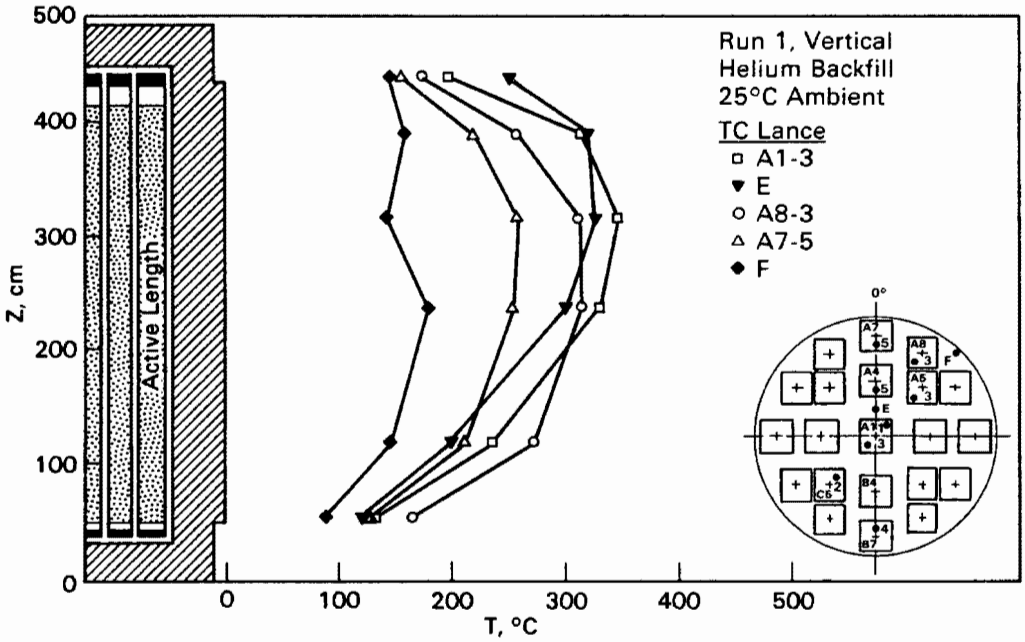

Figure 4-12. Axial Temperature Profiles for Vertical, Helium Test Run 1

assemblies at an elevation of 322 cm, the same elevation as those in nitrogen. The highest peak temperature (347°C) was measured in the center A1 assembly, and the outer 1.8-kW assembly peaked much lower at 313°C.

The axial temperature profile for center assembly A1-3 indicates the presence of the most convection. Gas TC lance temperatures in the center of the cask (E) confirm that significant convection heat transfer was present in the cask interior during the helium test run. The high decay heat assembly, A8 (1.8 kW), and the outermost assembly, A7 (1 kW), have axial profiles showing much less convection. In addition, the axial profile measured with the outer gas TC lance (F) indicates less convection than that measured with the inner gas TC lance. The "waviness" of the profile measured at F is thought to be caused by contact of the unsupported TC lance with the cask inner wall. This again indicates, as did the nitrogen data, that convection was less dominant in the outer fuel assemblies, and conduction and radiation were more significant, possibly due to their proximity (lower heat transfer resistances) to the cask inner wall.

The center assembly (A1-3) axial profile (Figure 4-12) shows much more helium convection than has been indicated in other cask performance test data (4, 14, 15). The vivid skewing of the axial profile toward the top of the assembly in helium may

indicate that the CASTOR-V/21 basket, with its relatively open design (Figure 3-2 of Section 3), is very close to being optimally designed for convection heat transfer. An extensive parametric heat transfer analysis with the HYDRA heat transfer computer program (Section 5) would have to be undertaken to verify this hypothesis.

Further appreciation of the degree of convection that was present in the vertical helium test run can be gained by comparing vertical axial profiles with those measured in a horizontal orientation. Axial profiles for assemblies A1 and A8 and the two gas TC lances are compared in Figures 4-13 and 4-14. Each of the horizontal profiles is very symmetrical about the active length of the fuel, similar to the axial decay heat curve (Figures 3-15 and 4-1), and shows the absence of convection in a horizontal orientation. The significant convection that was present in the inner basket region during the vertical helium run is obvious. The axial temperature profiles during the vertical run for the 1.8-kW outer assembly, A8 (Figure 4-13), and the outer gas TC lance, F (Figure 4-14), are similar to the horizontal profiles, again indicating less dominant convection in the outer region of the basket.

It is interesting to note that, even though the locations of the peak temperatures in the assemblies in the two orientations are significantly different, with the

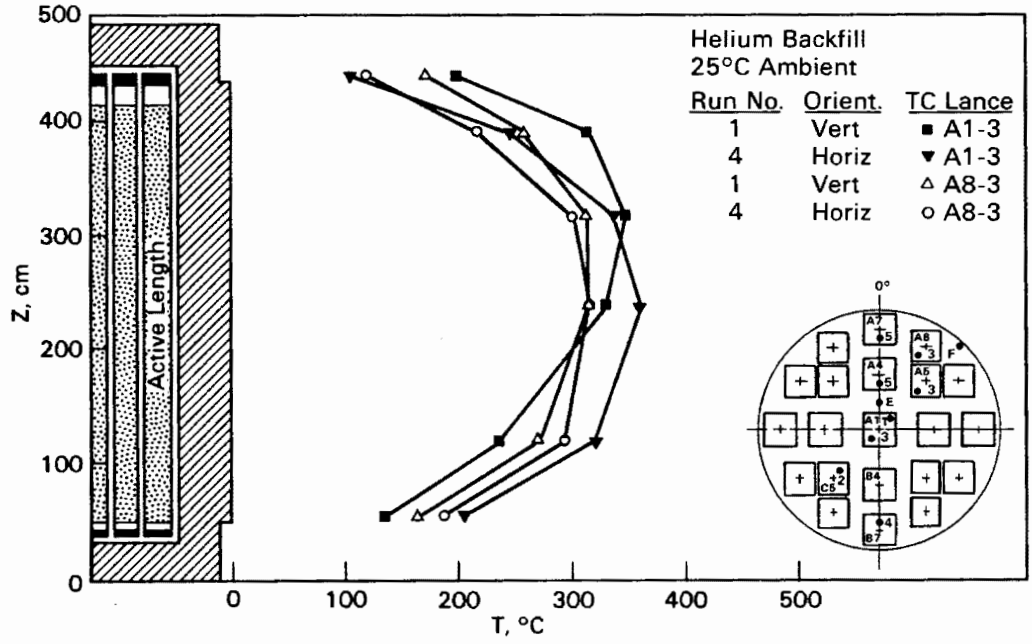

Figure 4-13. Assembly Axial Temperature Profiles for Horizontal and Vertical Test Runs 1 and 4

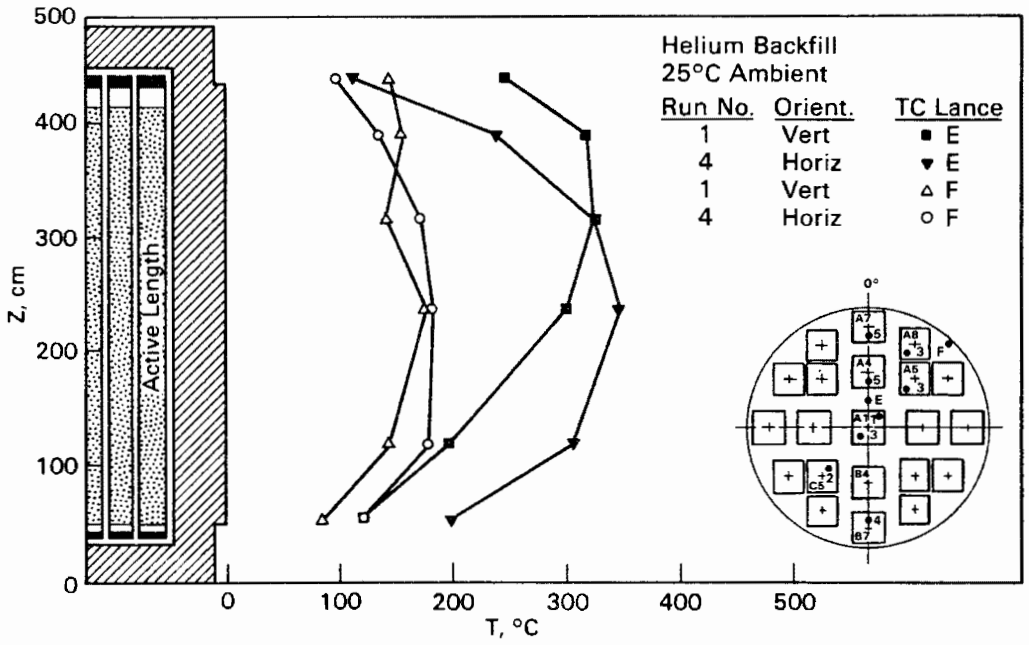

Figure 4-14. Backfill Gas Axial Temperature Profiles for Horizontal and Vertical Test Runs 1 and 4

horizontal being at 242 cm (near the axial centerline of the fuel) and the vertical being at 322 cm, the peak temperature magnitudes are not significantly different. The measured peak guide tube temperature in a vertical orientation was 347°C, and in the horizontal it was 360°C, only 13°C higher (Figure 4-13). The additional conduction heat transfer gained by the assemblies contacting their basket fuel tubes in the horizontal was noticeable, but not enough to compensate for the significant degree of convection heat transfer that existed in the vertical helium run. This is opposite the results of other cask testing efforts (4).

Radial temperature profiles obtained in a vertical orientation at six axial locations are shown in Figure 4-15. Temperature profiles indicate that temperatures increased with elevation, peaked at Z = 322 cm, and decreased in the upper regions of the assemblies, which is consistent with axial profiles of Figure 4-12, 4-13, and 4-14. Temperatures from inner assemblies A1 to A4 are relatively uniform, indicating the effects of the high thermal conductivity of helium; i.e., the higher the thermal conductivity, the lower the temperature difference. Likewise, temperatures in all assemblies at lower elevations (Z = 55 cm and Z = 122 cm) and the upper elevation (447 cm) are relatively uniform. Temperature differences exist between inner assemblies A1 and A4 and outer assemblies A7 and B7 at the central elevations (Z = 242 cm, 322 cm, and 397 cm) and between the two outer assemblies (A7 and B7) to the

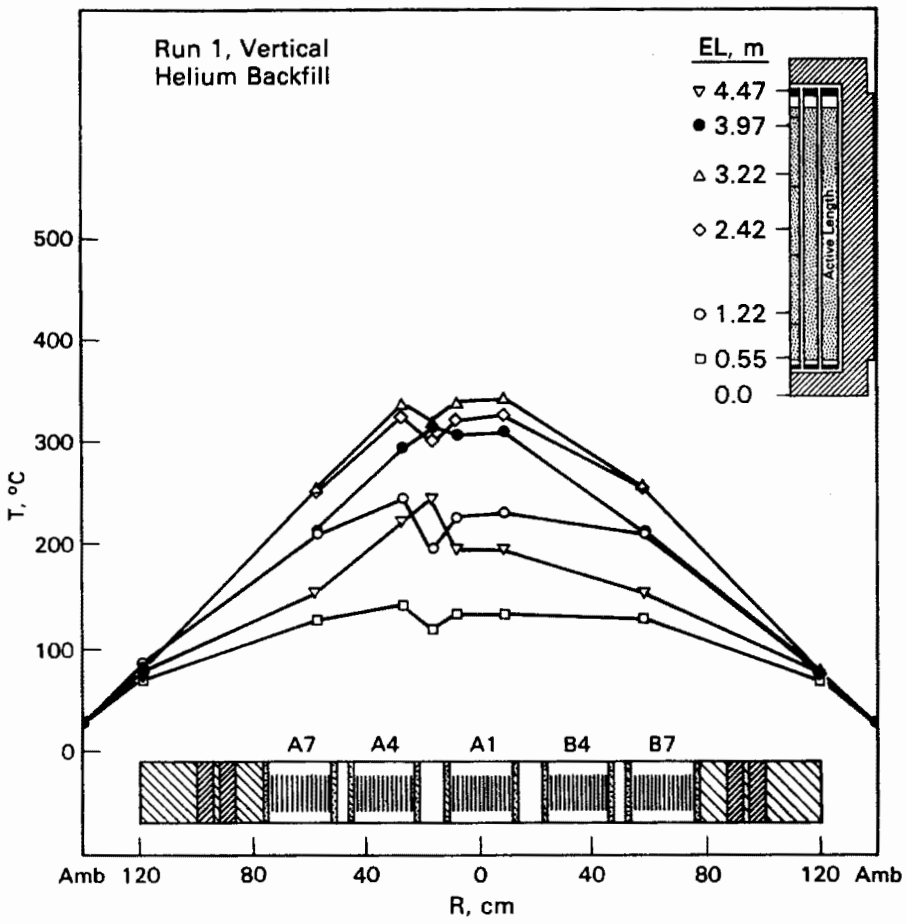

Figure 4-15. Radial Temperature Profiles for Vertical, Helium Test Run 1

cask surface at all elevations. HYDRA predictions presented in Section 5 indicate that most of the temperature drop occurs between the outer assemblies and the inner cask wall. Steep gradients indicate that the basket-to-inner wall gap may be important to the heat transfer performance of the cask. A detailed discussion of the effects of gap size is presented in Section 5.

Temperature differences between inner gas TC lance E and assemblies A1 and A4 are as high as 51°C near the upper end (Z = 447 cm) and 28°C near the axial center (Z = 242 cm) of the cask. Note that gas temperatures at the two upper axial locations (Z = 397 cm and 447 cm) were much higher (50°C) than were the adjacent measured A1 and A4 assembly guide tube temperatures.

Radial temperature profiles for both horizontal and vertical test runs using helium are compared at two central axial elevations in Figure 4-16. The profiles are similar, but horizontal profiles do not indicate as much difference between inner gas TC lance E temperatures and temperatures of adjacent assemblies A1 and A4 as is present in vertical profiles. Convection in a vertical orientation is responsible for the higher gradients because the helium is not stagnant, and is approximately isothermal. Temperature gradients from inner assemblies A1 and A4 to outer assemblies A7 and B7 and from the outer assemblies to the cask surface are less for a vertical orientation than for a horizontal orientation. Convection in a vertical orientation increases the effective conductance of the basket/fuel conglomerate and, therefore, a lower temperature gradient is required to transfer the same amount of heat. That is, $q \alpha U \Delta T$ where q is heat transfer, U is effective conductance, and ΔT is temperature difference, and if U is increased, ΔT must decrease for q to remain the same (energy to be conserved).

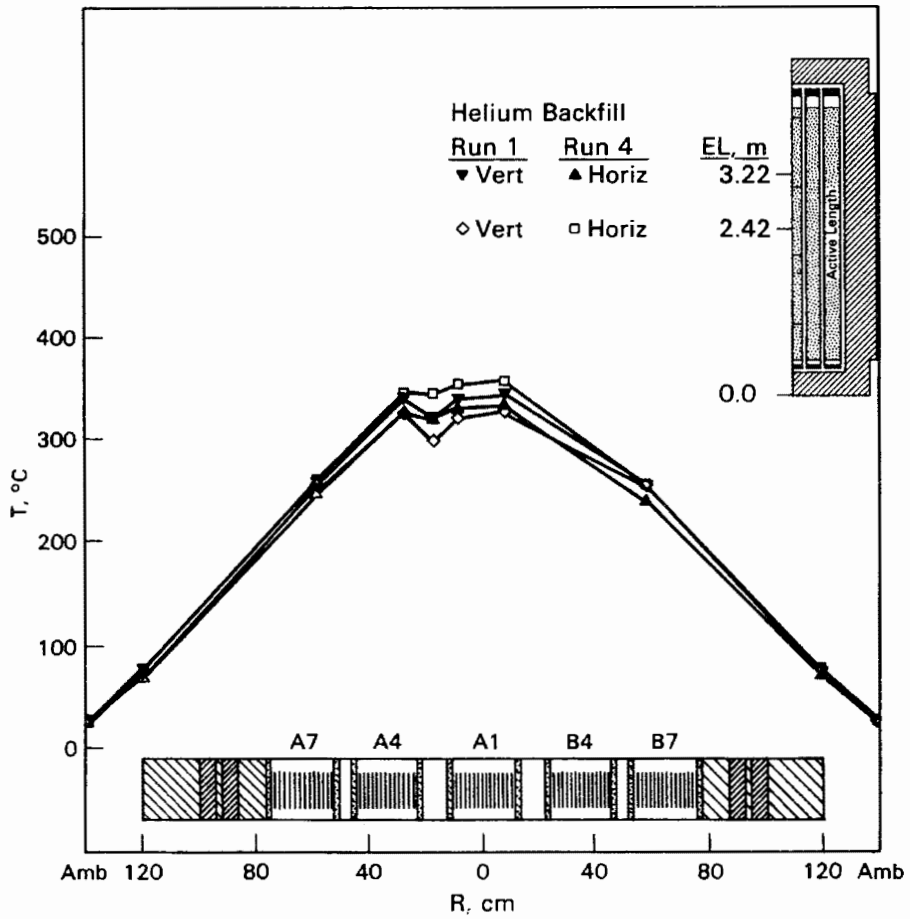

Figure 4-16. Radial Temperature Profiles for Horizontal and Vertical Helium Test Runs 1 and 4

Radial temperature differences within a fuel assembly during helium testing can be investigated better by comparing axial temperature profiles in guide tubes 1 and 3 in center assembly A1 shown in Figure 4-17. The center region of the profiles for both vertical and horizontal orientations indicates temperature differences on the order of 6°C and 4°C, respectively. Because there is one fuel rod (two rod-to-rod spaces) between the respective symmetrical location of guide tubes 1 and 3, it appears there may be a 3°C temperature difference between rods in vertical helium and 2°C in horizontal helium. Therefore, peak cladding temperatures in vertical helium runs can be roughly estimated by adding approximately 9°C to measured centermost guide tube temperatures in vertical helium runs and adding 6°C in horizontal helium runs. That is, there are three rod-to-rod spaces between centermost guide tubes and centermost fuel rods, and a 3°C (vertical) or 2°C (horizontal) temperature difference across each space results in estimated temperature differences of 9°C (vertical) and 6°C (horizontal). A more precise estimate of the centermost fuel rod temperature could be obtained by considering the predicted assembly temperature profile from HYDRA (Section 5) because the above estimate assumes a linear profile.

Temperature symmetry or asymmetry in vertical and horizontal cask orientations can be investigated by examining Figure 4-18. Axial temperature profiles from symmetrical vertical assemblies A5, C5, A7, and B7 are within 6°C. Small temperature

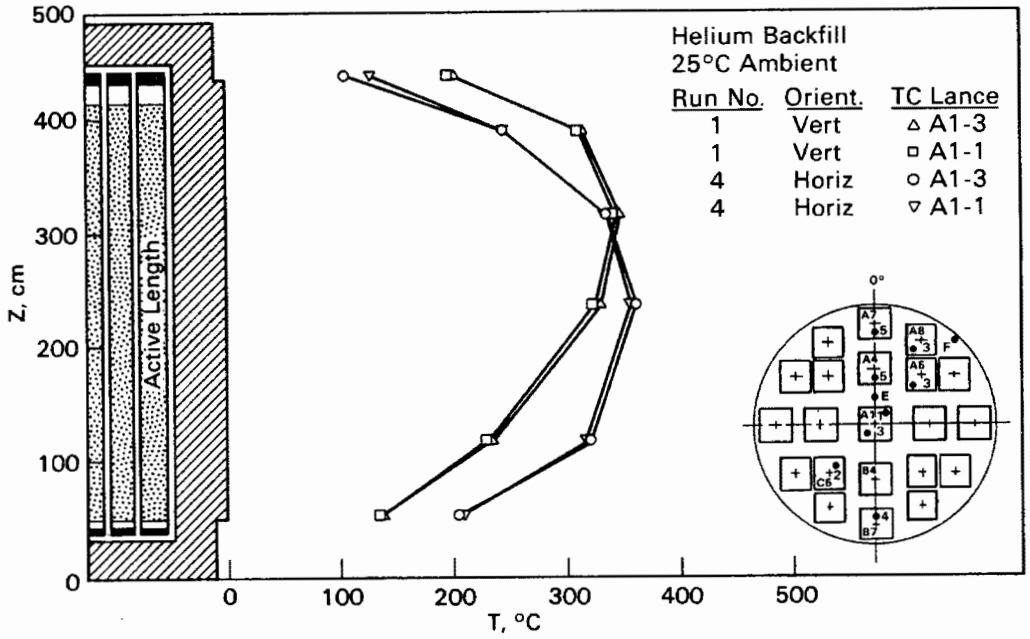

Figure 4-17. Temperature Differences Within Center Assembly A1 for Horizontal and Vertical Helium Test Runs 1 and 4

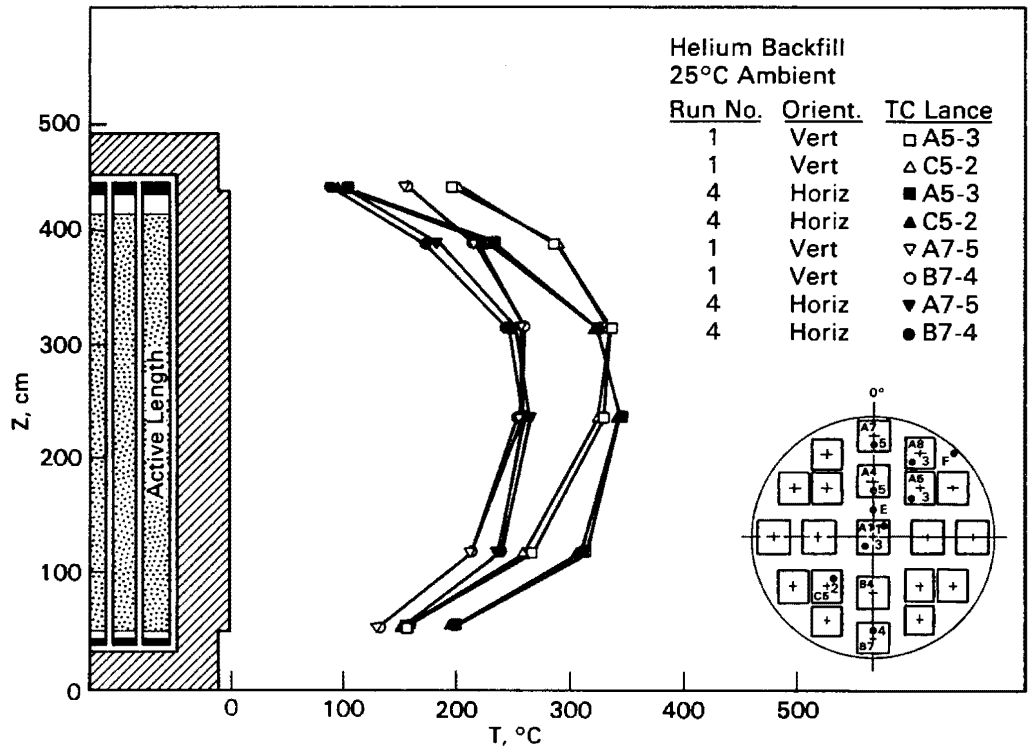

Figure 4-18. Axial Temperature Profiles in Symmetrical Assemblies for Horizontal and Vertical Helium Test Runs 1 and 4

differences indicate that cask radial resistances and fuel assembly decay heat rates were essentially the same. The 6°C difference in temperatures of symmetric vertical assemblies may have been caused by different assembly-to-fuel tube contact. Comparisons of vertical temperature profiles with horizontal profiles again indicate the degree of helium convection present in the cask in a vertical orientation.

Asymmetry caused by rotating the cask to the horizonal is also shown in Figure 4-18. Differences in temperature of assemblies A7 and B7 were as high as 14°C, with B7 temperatures being the lowest. As previously discussed for nitrogen runs, most of this temperature nonsymmetry in a horizontal orientation is thought to be due to basket contact with the inner cask wall near assembly B7, i.e., basket eccentricity within the cask cavity. The basis for this hypothesis is that temperatures of assembly B7 are lower than those for A7 because B7 is adjacent to the lower, basket-to-inner wall contact area, and A7 is adjacent to the upper, widened basket-to-inner wall gap.

Temperature data obtained in helium indicated helium to be the most effective backfill. Peak guide tube temperatures were significantly less (67°C) than temperatures in vertical vacuum and less (11°C in vertical and 35°C in horizontal) than temperatures in nitrogen. A surprising amount of convection was indicated in the vertical helium run. Axial temperature profiles were skewed toward the top of the fuel assemblies almost as much as those for nitrogen. Helium data emphasized the lower amount of convection heat transfer observed with nitrogen in the outer assemblies, however. Peak fuel temperatures in a horizontal orientation occurred significantly below (1 m) those in a vertical orientation, but the peak guide tube temperature was only 13°C higher in a horizontal orientation (360°C versus 347°C). Therefore, the added conduction heat transfer resulting from assemblies contacting their basket fuel tubes was not quite enough to compensate for the axial convection that occurred in a vertical orientation.

Effects of Backfill Environment

Effects of backfill environment on guide tube temperatures are discussed in this section. Axial and radial temperature profiles in both vertical and horizontal orientation are presented and discussed.

Effects of backfill environment on axial temperature profiles of vertical center assembly A1 and center gas TC lance E are shown in Figure 4-19. The vacuum profiles for both center guide tube A1-3 and center gas TC lance E show no skewing toward the top of the basket and, therefore, indicate a lack of convection heat transfer. The temperature profiles for guide tube A1-3 and gas TC lance E in nitrogen and helium are skewed toward the top of the basket and indicate that significant convection occurred. The temperature in A1-3 was slightly higher (<25°C) in nitrogen than in helium, but the helium temperature profile indicates that almost as much convection was occurring as in the nitrogen profile. The gas TC lance E indicates slightly lower temperature (up to 21°C) in nitrogen than in helium, but the two profiles have essentially the same shape. The lower nitrogen gas temperatures again indicate the significance of convection in a supporting gas, i.e., gases with densities and viscosities that support convection. In addition, the similarity of the helium profile to the nitrogen profile indicates that significant helium convection was allowed by the relatively open basket design.

Radial temperature profiles for vertical vacuum, nitrogen, and helium runs are shown in Figure 4-20. Profiles at these different elevations (lower, center, and upper) are presented. In the lower region at Z = 55 cm, the vacuum profile is relatively

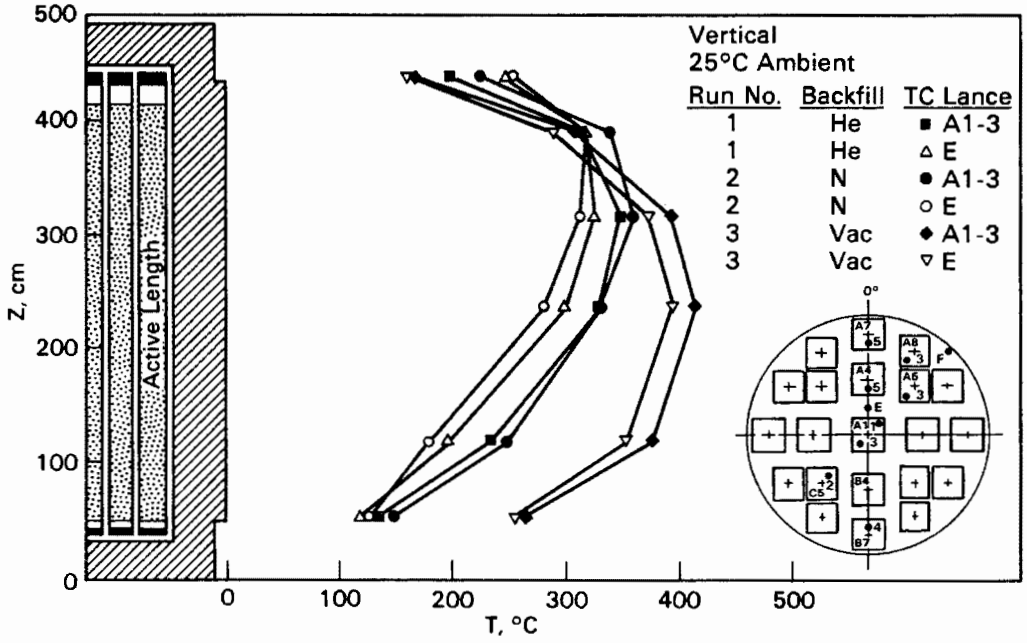

Figure 4-19. Axial Temperature Profiles in Assemblies and Backfill Gas for Vertical, Helium, Nitrogen, and Vacuum Test Runs 1, 2, and 3

flat between assembly A1 and A4. Temperatures drop off sharply and uniformly from A4 to the ambient. HYDRA predictions presented in Section 5 indicate that most of the temperature drop from A7 and B7 to the cask surface occurred from the assemblies to the inner cask wall. The temperature profiles with nitrogen and helium from center assembly A1 to outer assemblies A7 and B7 are flat, and a sharp gradient exists from the outer assemblies to the cask surface. The relatively flat profiles are a result of high effective conductances of the high conductivity helium and convecting nitrogen backfills. Profiles in nitrogen and helium indicate that the gas between assemblies A1 and A4 is cooler (up to 28°C) than the guide tube temperatures.

At an elevation of 322 cm where temperatures peaked in nitrogen and helium, the profiles are similar to those at 55 cm, but temperatures are higher and outer gradients are steeper. Peak measured guide tube temperatures in nitrogen in center assembly A1 are only slightly higher (<15°C) than temperatures in helium. The nitrogen gas temperature between assemblies A1 and A4 was actually cooler than the helium temperature, indicating that significant convection occurred in the vertical nitrogen run.

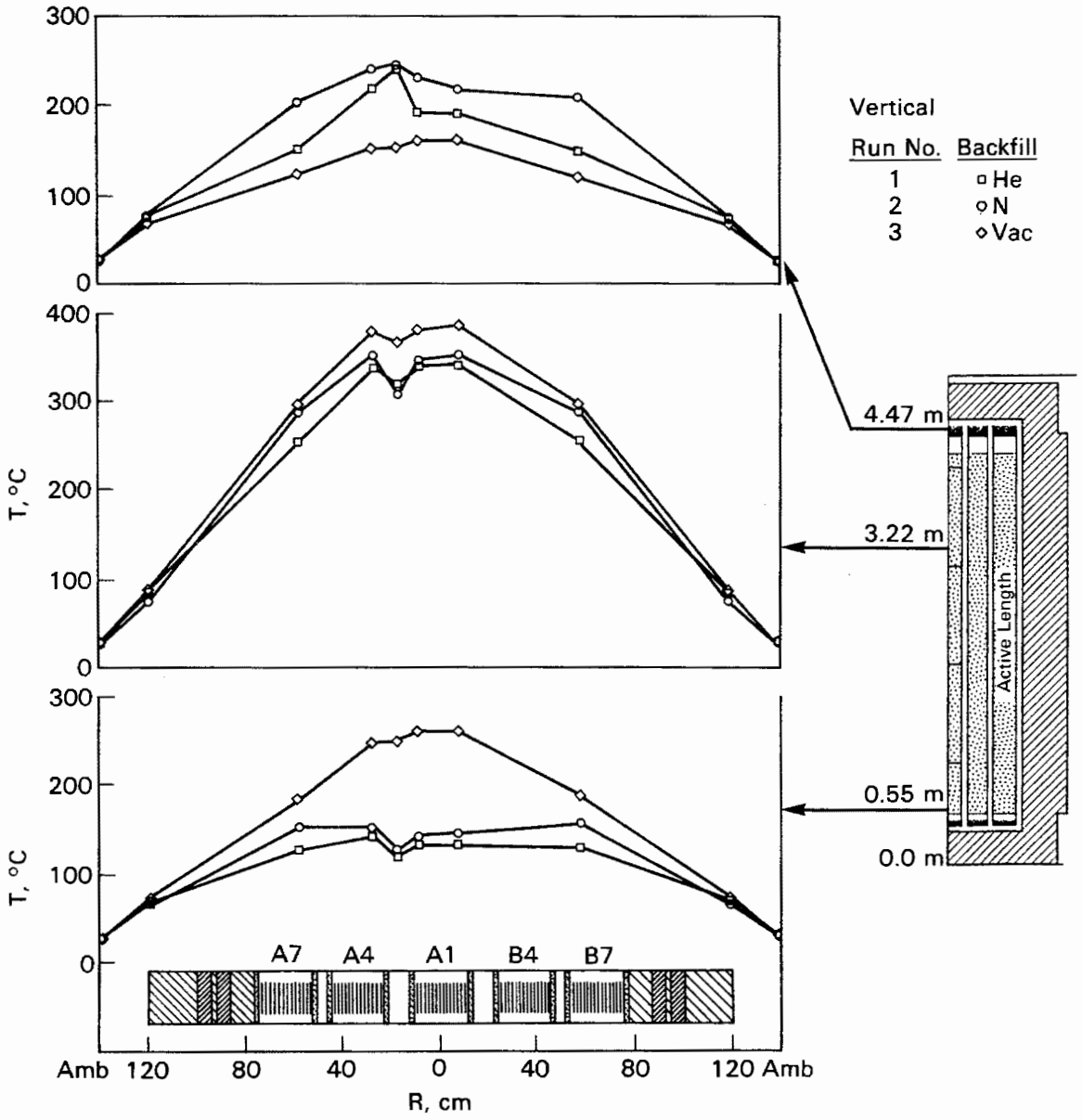

Figure 4-20. Radial Temperature Profiles at Three Axial Locations for Vertical, Helium, Nitrogen, and Vacuum Test Runs 1, 2, and 3

Near the top of the fuel assemblies at an elevation of 447 cm, the vacuum radial profile is similar to that at the two lower elevations, but the nitrogen and helium profiles are grossly different. The nitrogen gas between assemblies A1 and A4 is slightly hotter (15°C) than the A1 and A4 guide tube temperatures. In helium, this temperature differences is substantial (50°C). Note that temperatures in vacuum are less than either nitrogen or helium temperatures. Hotter gases near the top of the assemblies may indicate that accumulation of hot gases with relatively low axial

mass flow rates, i.e., flow resistances, are high enough to create a low flow plenum near the top of the basket. The limiting flow resistance could be across the top of the basket, in basket downflow channels, across the cask cavity bottom, or in the assemblies themselves. Further discussions on flow magnitudes and flow patterns are provided in Section 5.

Axial temperature profiles in center assembly A1-3 and center gas TC lance E for horizontal nitrogen and helium runs are presented in Figure 4-21. The profiles are symmetrical with the active lengths of the fuel assemblies, indicating lack of axial convection. Differences between gas and assembly temperatures are less near the ends of the fuel assemblies than in the center regions. Near the top, gas temperatures were actually slightly higher (<15°C). This may indicate the presence of convection between the ends of the basket and the bottom and lid of the cask cavity. Predicted mass fluxes in these regions are presented and discussed in Section 5.

Radial temperature profiles at these axial locations for a horizontal orientation are presented in Figure 4-22. All profiles are very uniform from assembly A1 to A4, and gradients exist from center assemblies to outer assemblies A7 and B7. Only slight temperature differences exist between the gas adjacent to assemblies A1 and

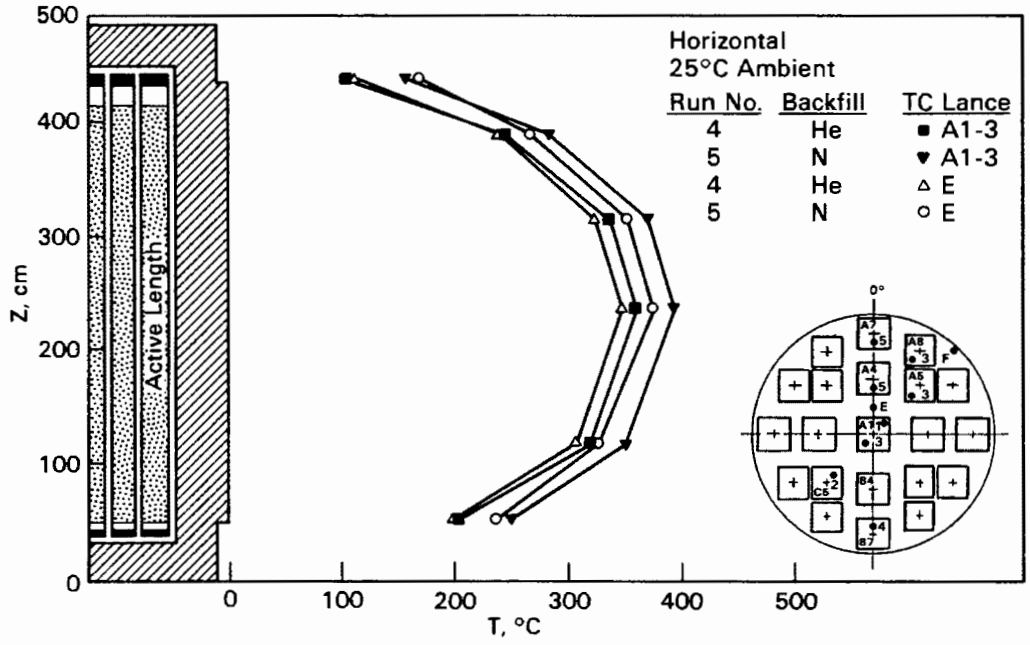

Figure 4-21. Axial Temperature Profiles in Assemblies and Backfill Gas for Horizontal, Helium and Nitrogen Test Runs 4 and 5

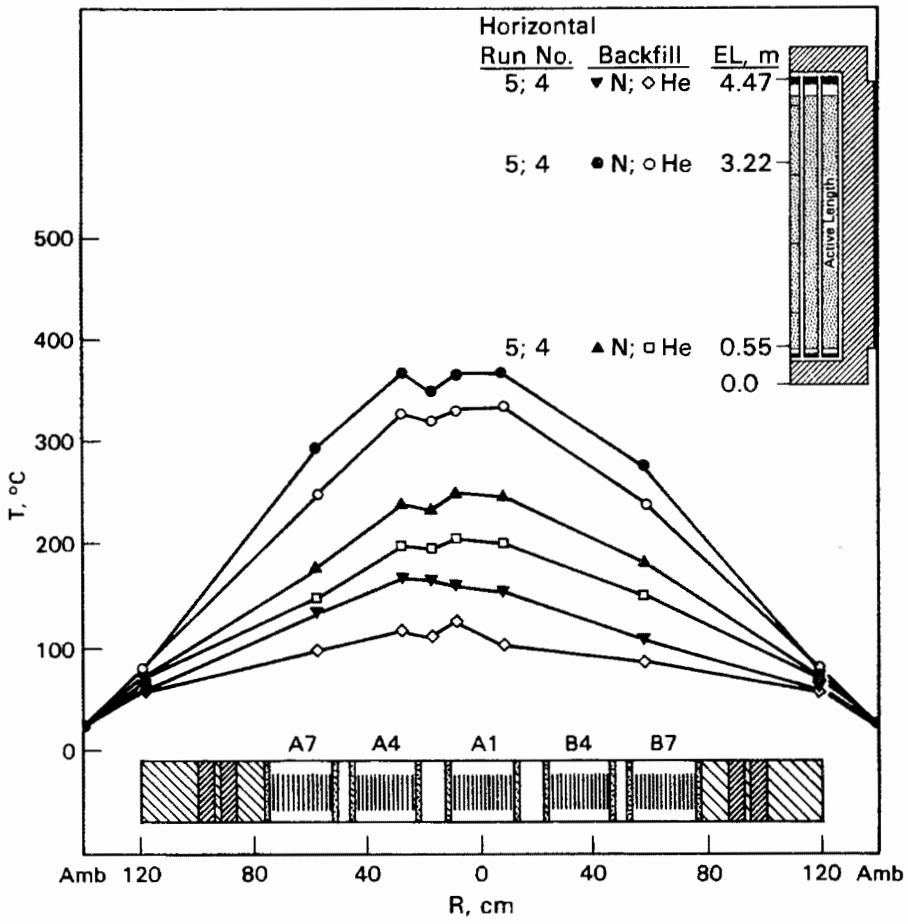

Figure 4-22. Radial Temperature Profiles at Three Axial Locations for Horizontal, Helium and Nitrogen Test Runs 4 and 5

A4 and the assembly guide tubes. The slight differences indicate the lack of axial convection, which is reasonable because insignificant axial density gradients can be set up in a horizontal orientation.

Attention is automatically focused on the outer eight high decay heat (1.8-kW) assemblies because their decay heats are 80% greater than the other thirteen 1-kW assemblies. Figure 4-23 presents axial temperature profiles for the 1.8-kW assembly A8 for all test runs. As indicated in Figure 4-23, the temperatures in assembly A8 were not excessive (<380°C). The vertical vacuum and horizontal helium and nitrogen profiles do not indicate that convection heat transfer was present. This is because the profiles are symmetrical with respect to the assembly active fuel length and are not skewed toward the top of the assemblies. The vertical helium profile indicates

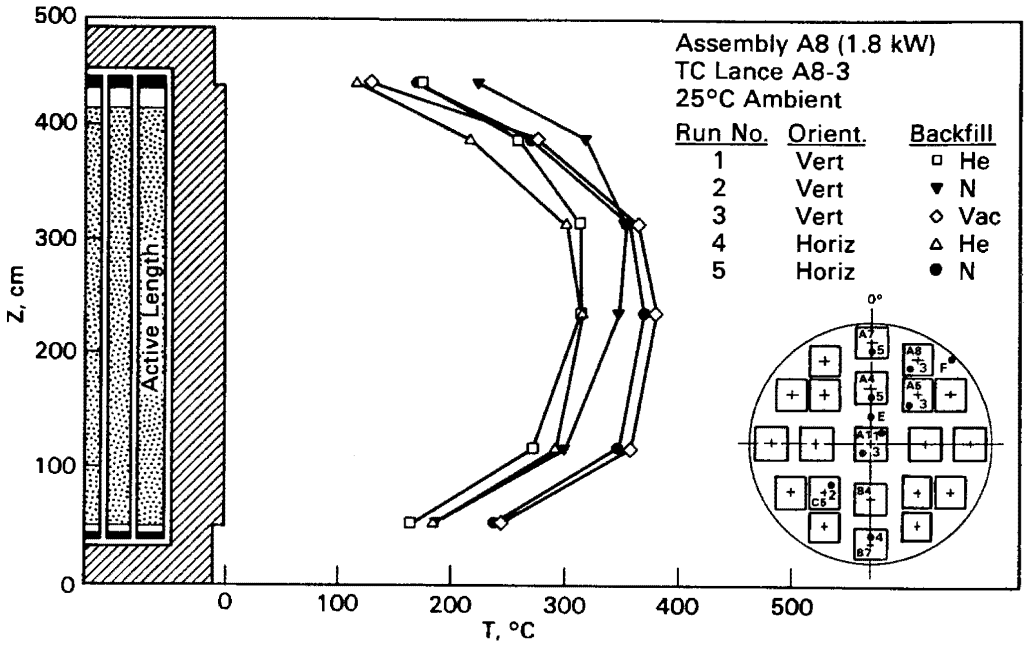

Figure 4-23. Axial Temperature Profiles in Outer, High Decay Heat (1.8 kW) Assembly A8 for All Test Runs

that a small amount of convection existed because temperatures in the upper one-third of the guide tube are slightly higher than other temperatures. The vertical nitrogen profile shows the greatest amount of convection, but not nearly that of the inner assemblies (Figure 4-6, 4-13, and 4-19). As previously indicated, conduction and radiation near the cask wall become more significant because of shorter heat transfer paths to the cask inner wall, and convection becomes less dominant.

The higher decay heat 1.8-kW outer assemblies had three effects on cask temperatures. First, they acted as guard heaters around the inner assemblies and raised overall temperatures in the fuel assemblies to those reported in the GNS Topical Safety Analysis Report (2). Second, they produced flatter, more uniform radial temperature profiles across the fuel assemblies in the basket than would have existed with 1-kW assemblies. Third, they resulted in higher temperature gradients from the outer assemblies to the ambient.

In summary, a vacuum backfill and a horizontal orientation provide the poorest cask heat transfer performance. High conductivity helium and axially convecting nitrogen and helium (vertical orientation) provide good heat transfer performance, with helium being the best. Significant axial convection currents were set up in the

helium even though its density and viscosity do not generally support convection. The relatively open basket design is probably the reason why significant convection occurred in a vertical orientation.

Surface Temperatures

Cask surface temperatures are important from an operation and maintenance standpoint. Selected axial temperature profiles measured on the cask surface are shown in Figure 4-24, and the remaining surface temperature data are provided in Appendix C. The peak surface temperature was measured during the vertical vacuum run and was 88°C. The vertical vacuum and horizontal nitrogen profiles do not indicate the presence of significant convection on the cask outer surface. Surface temperatures during the vertical helium run are hotter near the top of the cask. Skewing of the axial surface temperature profile toward the top of the cask was probably due to convection inside the cask rather than on the outer surface, because of the lack of skewing of the temperature profile for the vertical vacuum run. In general, the cask surface temperatures are thought to be satisfactory because they range between 57°C and 88°C and are less than 100°C.

Corresponding circumferential temperature profiles at an elevation of 235 cm are presented in Figure 4-25. Surface temperatures varied by up to 28°C from one run to

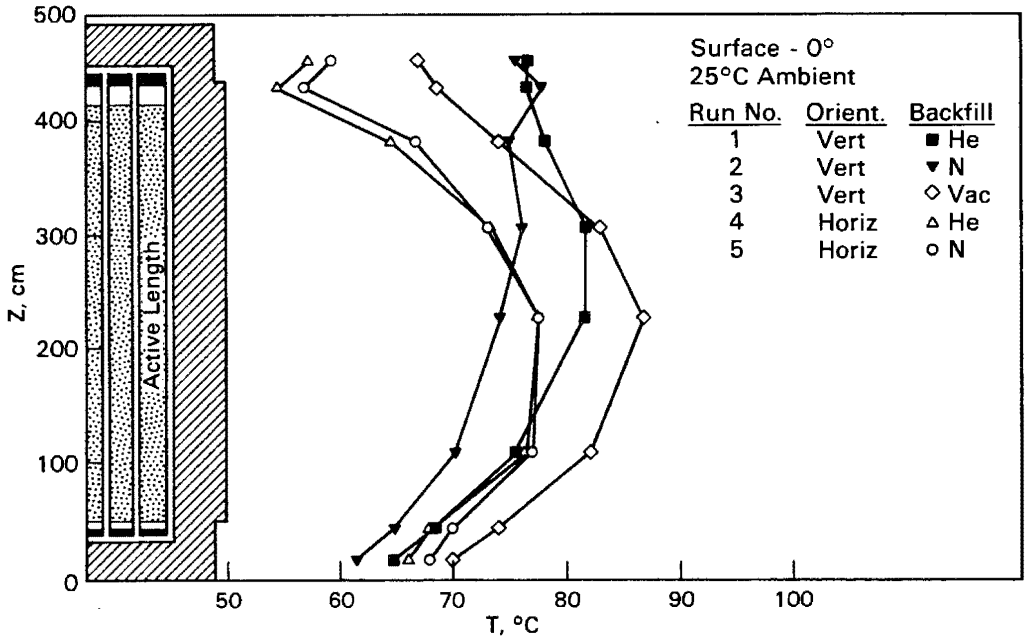

Figure 4-24. Cask Surface Axial Temperature Profiles at 0 Degrees for All Test Runs

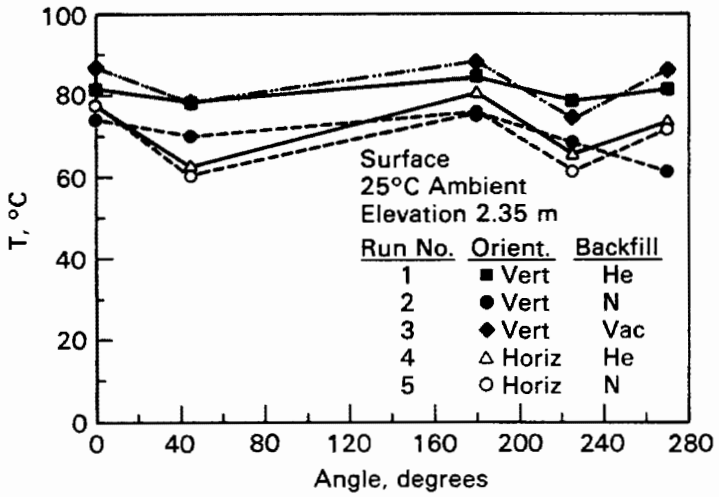

Figure 4-25. Cask Surface Circumferential Temperature Profiles at Elevation 235 cm for All Test Runs

another. However, temperatures within an individual circumferential profile varied by up to only 17°C, indicating that the circumferential heat transfer area and thermal conductivity of the cask wall were adequate to smooth the profiles on quadrant boundaries (0°, 180°, 270°) where assemblies are closest to the cask inner wall. Minimum temperatures occurred adjacent to quadrant diagonals (45°C, 225°C) where fuel assemblies were farther from the inner wall even though the higher decay heat assemblies (1.8 kW) were nearest these locations. "Valleys" in circumferential temperature profiles adjacent to the high decay heat assemblies again indicate that circumferential heat transfer in the cask wall was enough to smooth the temperature profiles. Orientation did not appear to noticeably affect the circumferential temperature profiles, i.e.; significantly higher peaks were not measured at possible stagnation points at 0°C and 180°C when in a horizontal orientation.

Effects on heat transfer of the circumferential fins in the cask surface are indicated in Figure 4-26. For the axial temperature profile at 0° during the vertical vacuum run, temperatures of fin tips were as much as 8°C lower than temperatures at fin bases. This relatively small temperature difference may indicate that the fin efficiency is not substantial.

Temperature Transients

Temperature transients occurred during testing as a result of changes in backfill environments and rotation of the cask from a vertical to a horizontal orientation.

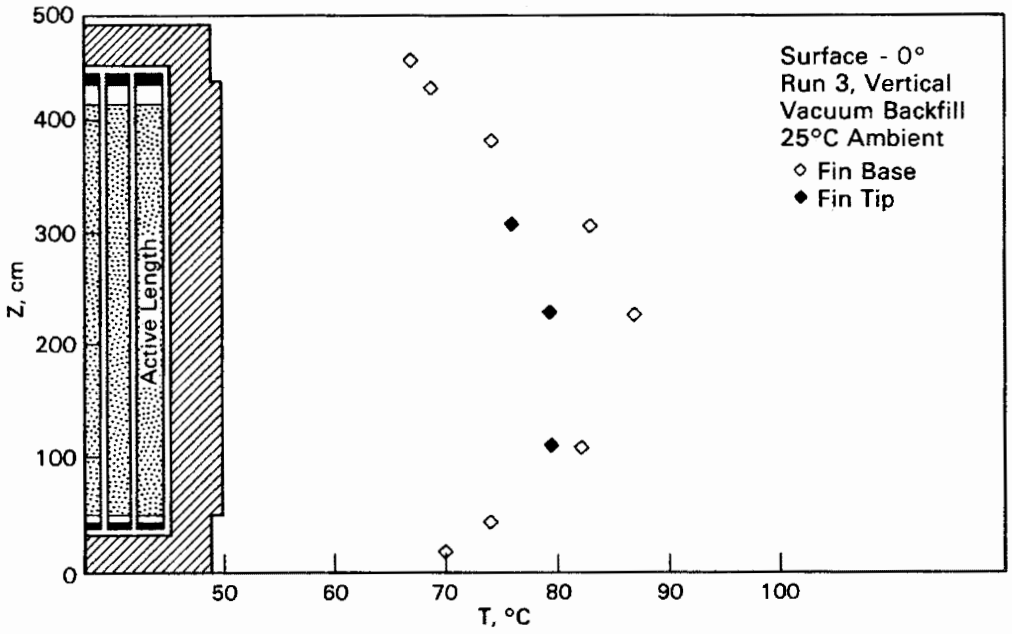

Figure 4-26. Fin Tip and Fin Base Axial Temperature Profiles for Vertical, Vacuum Test Run 3

As much transient temperature data as practical were collected but, because the TC lances were disconnected when the cask was being rotated, continuous data scanning was not possible.

Temperature histories for two TCs in the center A1 assembly, one center gas TC, and one exterior surface TC are presented in Figure 4-27. The internal cavity pressure is also shown in Figure 4-27. The data indicate that temperature transients were very mild. The steepest transient occurred at a time near 96 hours in the gas TC after pumping down from a nitrogen to a vacuum backfill. The transient was on the order of 85°C in 14 hr or 16°C/hr. The corresponding transient measured by the TC at an elevation of 242 cm in the hottest guide tube in center assembly A1 was 4°C/hr (50°C in 14 hr). Note that a similar, yet opposite and less severe, transient occurred in the top (elevation 447 cm) TC in assembly A1. Transients resulting from replacing high conductivity helium with low conductivity nitrogen in either a vertical (48 hr) or a horizontal (264 hr) orientation were very minor.

It can be concluded that abrupt changes in backfills from/to environments of significantly different thermal conductivities or convection characteristics did not result in significant temperature transients in the spent fuel rods. Transients that result from replacing a gas backfill with a vacuum can be reduced in severity

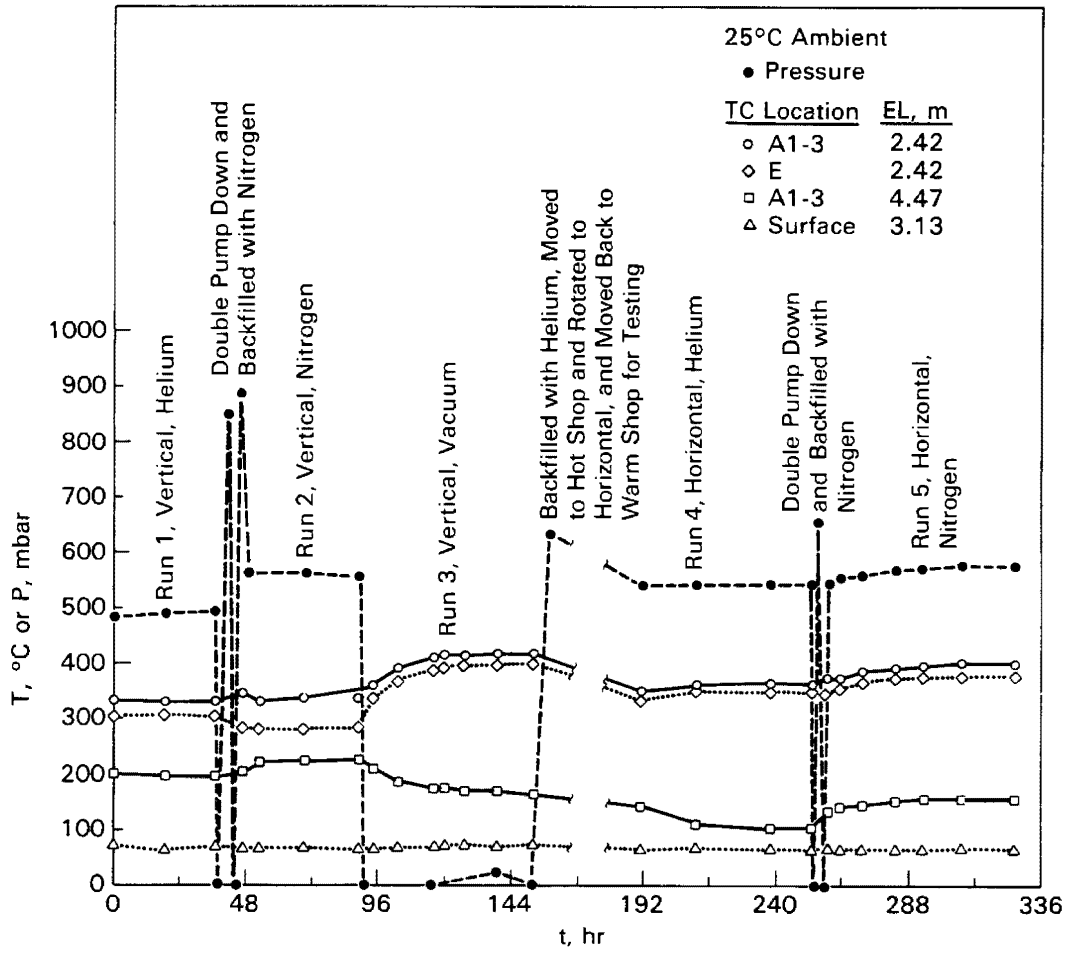

Figure 4-27. Internal Cask Pressure Transient and Selected Temperature Transients During Cask Performance Testing

by having a vacuum/helium environment instead of a vacuum nitrogen environment, i.e., by backfilling the cask with high conductivity helium prior to attaining a vacuum drying environment. Of course, this was not done in this cask performance test because one testing objective was to measure maximum temperatures that can be expected to exist in the CASTOR-V/21 cask.

Basket Weld Cracking Indications

After heat transfer performance testing was completed, and during post-test fuel assembly inspections discussed in Section 3, indications of cracking in welds near the top of the CASTOR-V/21 cask fuel basket were observed. These indications were observed at the eight locations shown in Figure 4-28. The basket plates are

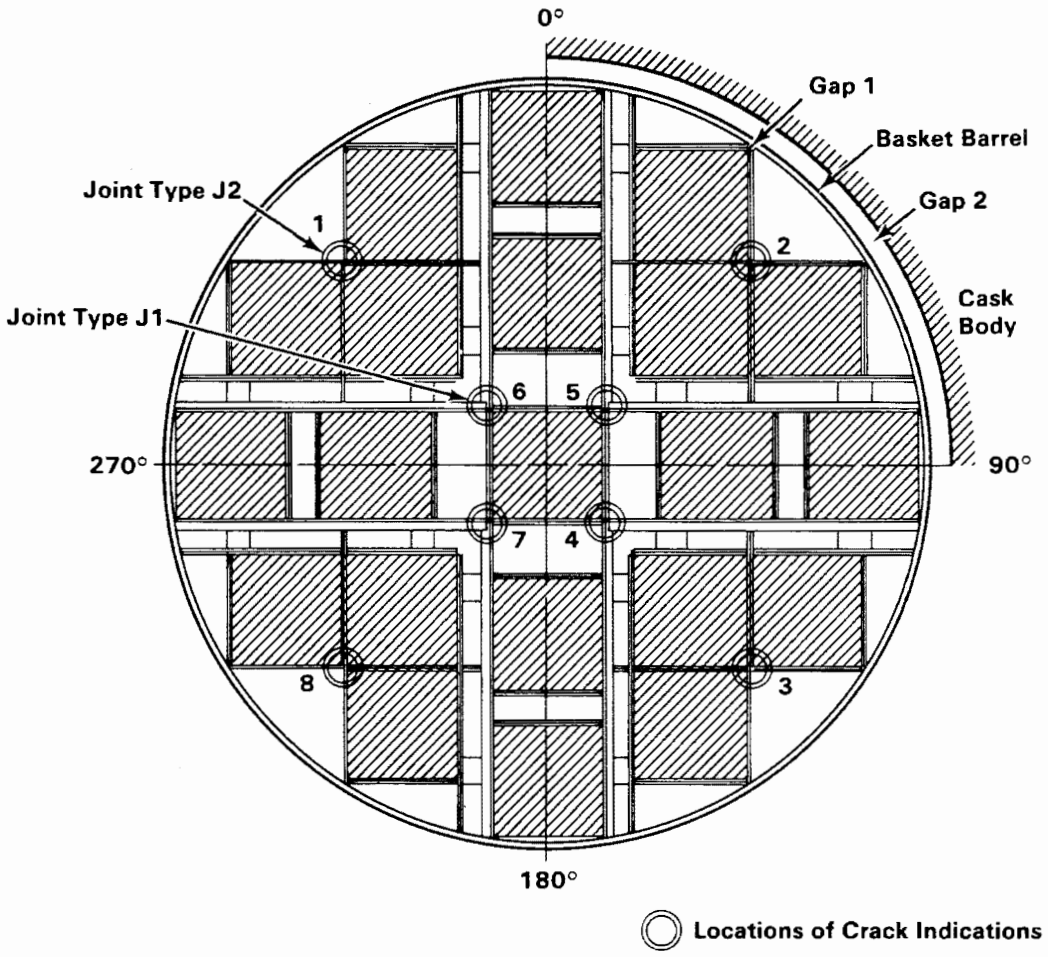

Figure 4-28. Locations of Basket Crack Indications

generally stitch-welded [100 mm (4 in.) weld every 250 mm (10 in.)]. The cracking indications were in the top stitch-welds at the eight locations. A typical crack in joint type J2 is shown in Figure 4-29.

The special basket used for cask performance testing was designed to have an unusually tight fit [basket-to-inner wall cold gap of 0.8 mm (0.032 in.) to 1.5 mm (0.059 in.)] in the cask inner cavity. The purpose of the tight basket-to-wall fit was to permit TC lances to pass through the primary lid and into fuel assembly guide tubes (Figure 3-16 Section 3). GNS performed a two-dimensional thermal stress analysis of the basket (16) and concluded that the basket had expanded and come in contact with the inner wall of the cask (Gap 2, Figure 4-28). It was also concluded that the outer fuel tubes adjacent to the basket diagonals came in contact with the basket barrel (Gap 1, Figure 4-28). Results of the GNS thermal analysis indicate

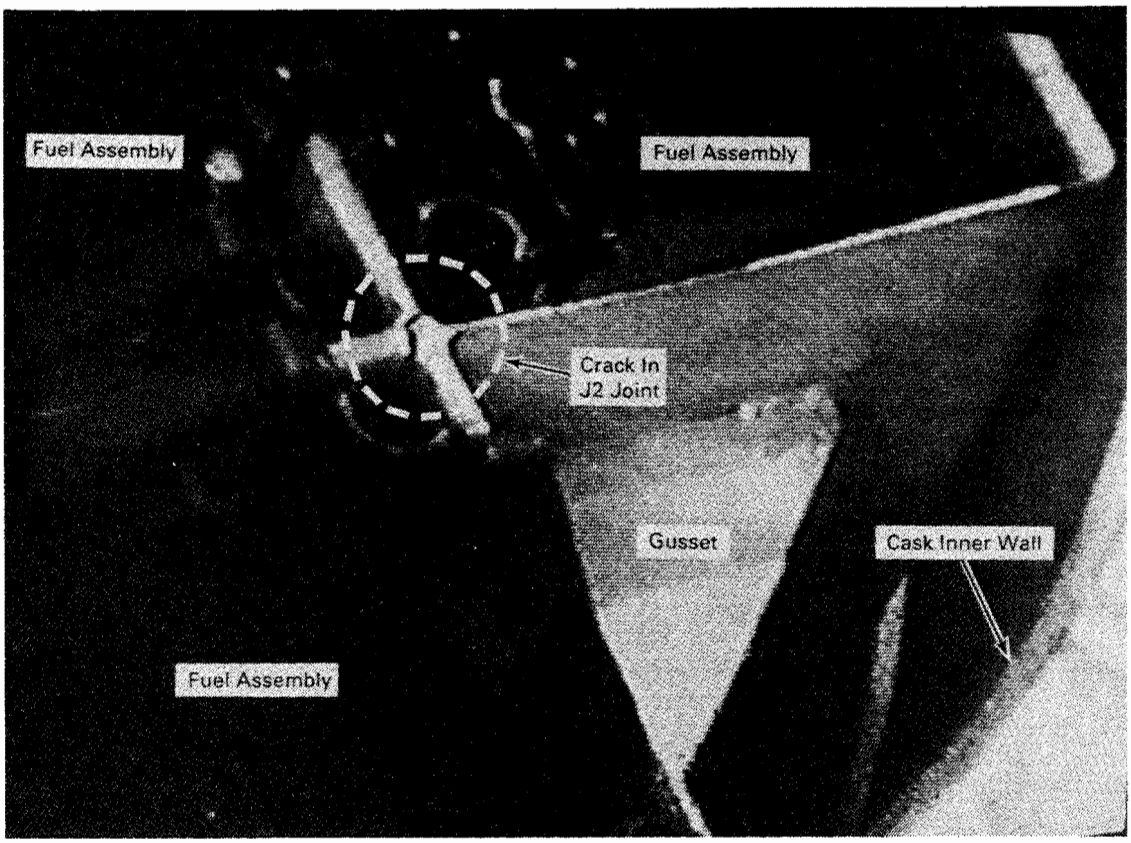

Figure 4-29. Typical Crack in Basket Joint Type J2

that thermal stresses between 114 ksi and 154 ksi existed in the joints at the eight locations of cracking indications. These stresses are well above the 50- to 55-ksi yield stresses measured during tensile testing of weld samples. Therefore, the most plausible reason for weld cracking was excessive inelastic strain buildup at the eight locations. Two main reasons for strain buildup were given to be 1) elastic follow-up at the locations occurred during basket cooldown each time the lid was removed during incremental (three at a time) fuel loading, and 2) possible buckling of basket plates resulted from containment when thermal growth created plate-to-basket barrel or basket barrel-to-inner cask wall contact (16).

An examination of the measured temperatures, the HYDRA temperature predictions presented in Section 5, and associated differential thermal expansion between the basket and cask body substantiates the GNS thermal stress analysis results. In addition, the substantial axial temperature gradients measured during testing (Figures 4-1, 4-6, and 4-13) could potentially impart relatively high stresses in the

ends of the basket. This is because the ends of the basket are relatively cold at some operating conditions, e.g., vertical and horizontal helium runs (Figure 4-13) while the axial central region of the basket is relatively hot, and differential radial thermal expansion could result in relatively high tensile stresses in the stitch-welds near the ends of the basket.

Enlarging gaps 1 and 2 in the basket, eliminating unnecessary, nonstructural welds near the ends of the basket, and welding basket plates only where structural support is absolutely necessary should alleviate basket weld cracking. Enlarging the basket-to-inner wall gap may result in the cask operating at higher temperatures, but the heat transfer performance of the cask is exceptionally good, so this will not adversely affect performance as verified in Section 5.

The observed cracking indications in the CASTOR-V/21 cask basket welds did not result in adverse safety implications because the cracked welds had minimal structural requirements. The cracks had no effect on the ability to remove or reinsert fuel assemblies from/into the basket.

SHIELDING PERFORMANCE

Dose rates (gamma and neutron) were measured at selected locations (see Figures 3-8 and 3-9 of Section 3) on the cask surface. Energy spectrum instruments identified and discussed in Section 3 were used to obtain reference dose rates and energy spectra at a few selected locations. The spectral measurement locations were: 1) the primary lid of the cask at a 90 degree angle and a radius of 34 cm (13.4 in.), 2) the center of the bottom of the cask, and 3) the side of the cask at a 90 degree angle and an elevation of 270 cm (105 in.) from the bottom of the cask. These reference energy measurements were used to determine accurate gamma and neutron fluences from thermoluminescent dosimeters (TLDs) and track etch dosimeters (TEDs), i.e., used to calibrate TLDs and TEDs.

Measurements were obtained with TLDs and TEDs at 17 points on the lid, 40 points along the cask side, and 12 points on the cask bottom. In addition, INEL obtained gamma and neutron portable survey instrument readings at each of the TLD/TED locations, and PNL obtained portable survey instrument readings at selected TLD/TED and spectrometer locations. The following sections present selected data obtained during dose rate measurements and associated discussions; the remainder of the data are presented in Appendix D.

Reference Energy Spectra and Dose Rates

The neutron dose equivalent rate data obtained from the spectrometer measurements are presented in Table 4-2. Survey instrument measurements have also been included for comparison. It should be noted that the measurements were made as close to the cask surface as practical, but because of the size of the detectors, the actual measurement location was several centimeters away from the surface and averaged over a large volume. The ^{3}He spectrometer, tissue equivalent proportional counter (TEPC), multisphere spectrometer (m/s), track etch dosimeter (TED), and Snoopy survey instrument measurements are in relatively good agreement. The ^{3}He measurement at the top of the cask was made with a smaller tube that is not as responsive to high neutron energies; this may explain the lower value shown in Table 4-2. The multisphere results are consistently about a factor of 2 below the other values. This result is unexpected and did not occur in previous measurements on the REA cask (4)

Table 4-2

REFERENCE NEUTRON DOSE EQUIVALENT RATE MEASUREMENTS

	Dose Equivalent Rate, mrem/hr					
	Spectrum-Based			Survey Instruments		
				PNL		INEL
Location	^{3}He[a]	TEPC[b]	M/S[c]	TED[d]	SNOOPY	PNR-4[e]
Top of Cask - 90°, 34 cm						
at contact	19.5	39.33	16.62	36	40	50
at 1 m	--[f]	--	--	--	11	--
Bottom of Cask - Centerline						
at contact	38.9	36.34	16.26	41	50	70
at 1 m	--	6.40	--	--	12	--
Side of Cask - 90°, 270 cm						
at contact	10.9	8.78	4.40	16	8.5	15
at 1 m		2.88			4	

[a] Helium-3 neutron spectrometer.

[b] Tissue equivalent proportional counter.

[c] Multisphere neutron spectrometer.

[d] Track etch dosimeter.

[e] Eberline PNR-4.

[f] Not measured.

or in laboratory measurements made just prior to CASTOR-V/21 measurements. Therefore, the multisphere data were not used for evaluating cask surface dose rates.

The neutron energy spectra measured by the ^{3}He spectrometer at the top, bottom, and side of the cask are given in Figure 4-30. The neutron flux distribution is given in 20-keV energy bins for energies between 40 keV and 1 MeV. The minima in the spectra on the side and bottom correspond to absorption resonances in the neutron cross sections for iron and oxygen. The fluctuations at the high energy end of the spectrum for the top are due to poor counting statistics; however, the spectrum should look like that of the bottom. The ^{3}He tube used for the top measurement was a small-diameter tube that has a low efficiency for high-energy neutrons and requires very long run times to obtain good data at high energies.

The average neutron energies at the top, bottom, and side were estimated to be 169, 145, and 174 keV, respectively, from the ^{3}He data. The Multisphere spectrometer determined the average energies to be 111, 67, and 146 keV at the top, bottom, and side, respectively. An average neutron energy of 150 to 200 keV was used to obtain a factor to convert the TED data from tracks per square centimeter to neutrons per square centimeter. Because the sources used to calibrate neutron survey instruments

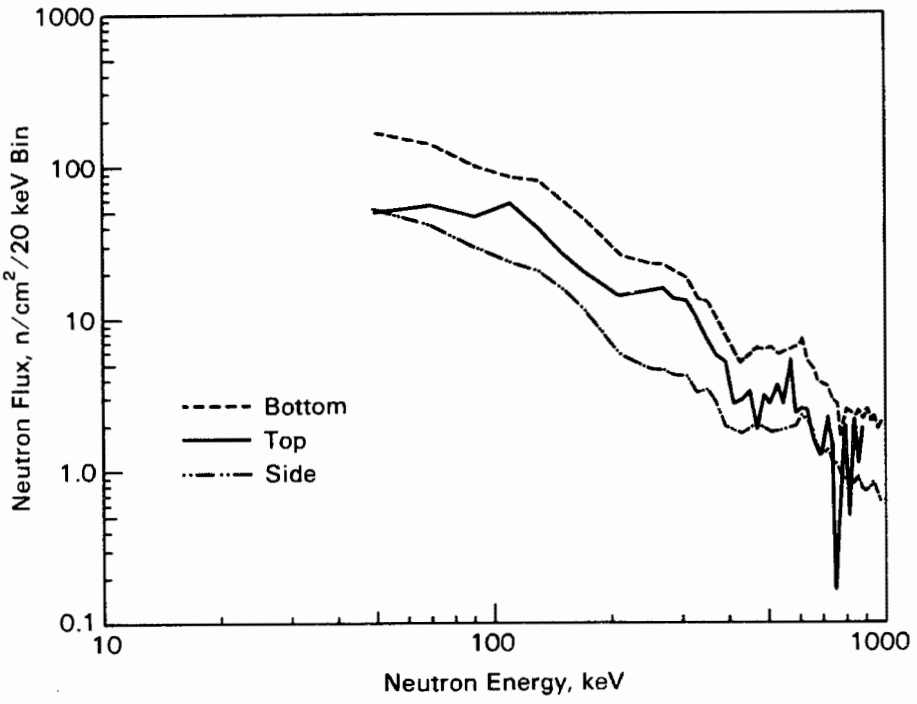

Figure 4-30. Neutron Energy Spectra Measured With a ^{3}He Spectrometer

usually have average neutron energies above 1 MeV, it is easy to see why the survey readings are consistently higher than the TEPC or TED results.

A comparison of gamma dose rate measurements can be made from the data presented in Table 4-3. The gamma dose rate measurements were made with TLDs and ion chamber survey instruments, which are both somewhat energy-dependent. Good agreement exists between all gamma dose rate data.

An intrinsic germanium spectrometer was used to determine the gamma energy spectrum and confirm the appropriate calibration for the TLDs and gamma survey instruments. The gamma energy spectra measurements were made at the top, bottom, and side of the cask as well, but they were made at some distance back from the surface to prevent pulse pile-up in the detector. The germanium spectrometer was used only to look at the energies of the source gammas. A representative gamma energy spectrum with the gamma energy peaks identified for the source radionuclides is shown in Figure 4-31. The major radionuclides identified were ^{60}Co and $^{144}Ce/Pr$ at the top and bottom of the cask, and $^{144}Ce/Pr$, ^{134}Cs, and ^{154}Eu on the side. The dominance of ^{60}Co at the top and bottom is due to the activation of the stainless steel on the ends of the fuel assemblies. The primary contributor at the side is $^{144}Ce/Pr$, a fission product present in the spent fuel.

Table 4-3

REFERENCE GAMMA EXPOSURE RATE MEASUREMENTS

Location	Exposure Rate, mr/hr		
	TLD[a]	RO-3B[b]	RO-3A[c]
Top of Cask - 90°, 34 cm at contact	36	35	40
Bottom of Cask - Centerline at contact	22	21	26
Side of Cask - 90°, 270 cm at contact	24	22	28

[a]Thermoluminescent dosimeter.

[b]Eberline RO-3B (Cutie Pie) used by PNL.

[c]Eberline RO-3A used by INEL.

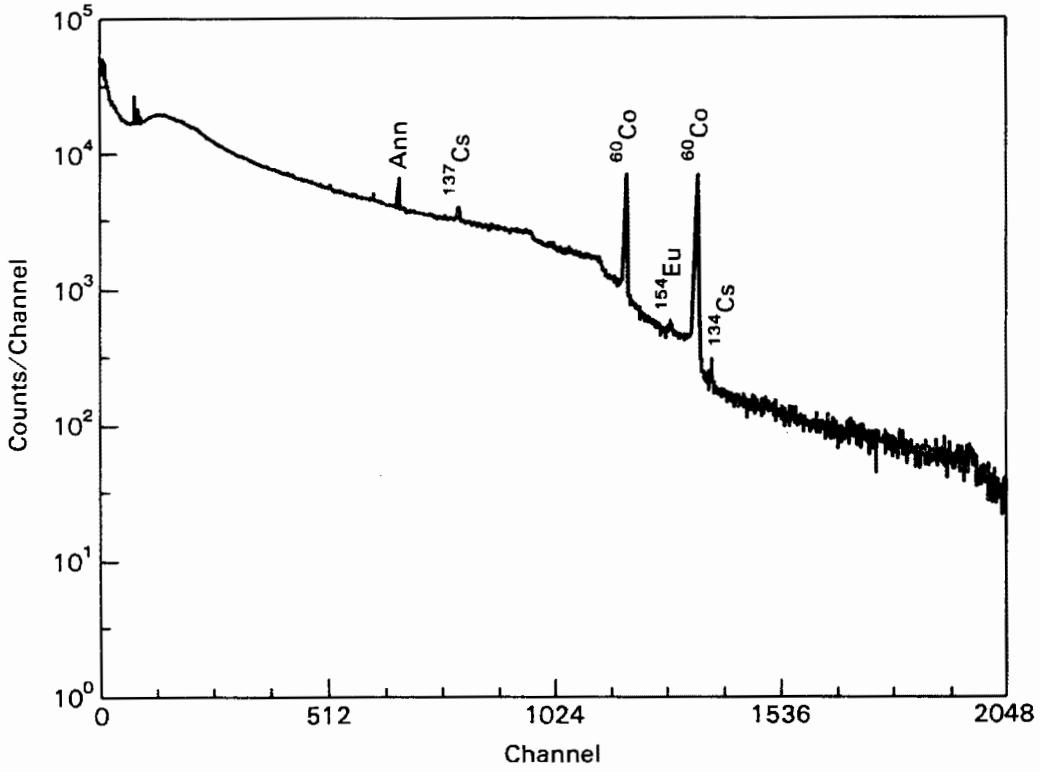

Figure 4-31. Gamma Energy Spectrum Measured With An Intrinsic Germanium Spectrometer

Based on the measured gamma energy spectra, the TLD measurements did not require a modified calibration factor to account for differences in the energy spectra between the cask and laboratory calibration sources. Measurements with the survey instruments are quite close to the TLD results.

Dose Rate Profiles

Gamma and neutron dose rate profiles measured on the primary lid (the outer secondary lid was not used during testing) at an angle of 45 degrees are presented in Figure 4-32; additional data are included in Appendix D. Data from TLDs (gamma), TEDs (neutron), INEL portable survey instruments, and selected PNL portable survey instruments are shown. The TLD and TED data are summed to show total dose rates.

Gamma and neutron dose rates are very close in magnitude (40 to 45 mrem/hr) directly above the fuel assemblies, with the exception of the portable neutron survey instrument data point at zero radius (70 mrem/hr versus 45 mrem/hr). The total peak [TLD (gamma) and TED (neutron)] measured dose rate at the lid centerpoint was 84 mrem/hr.

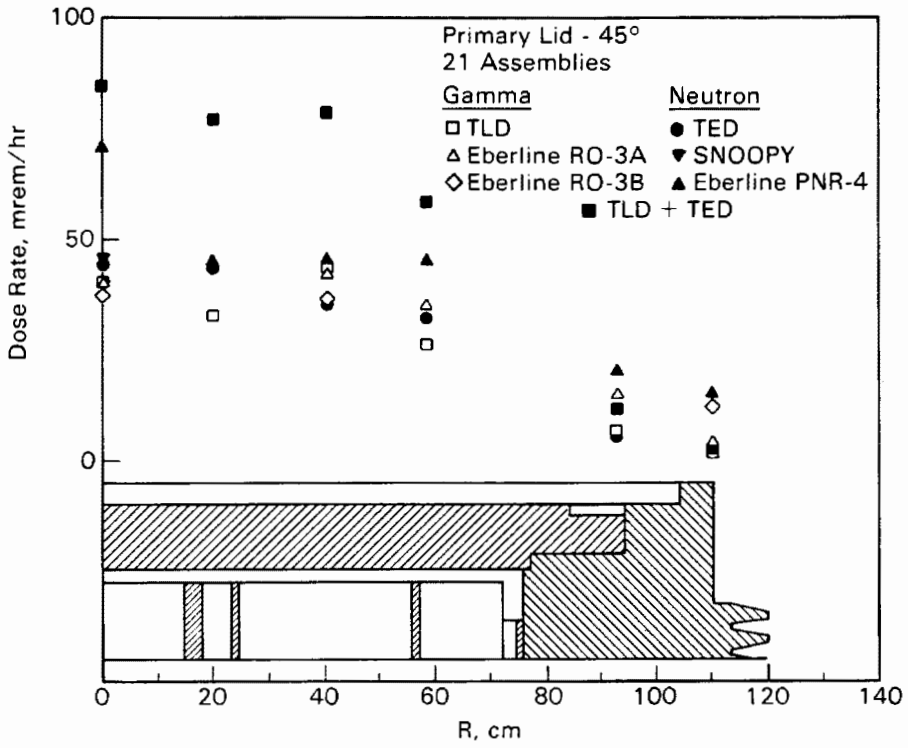

Figure 4-32. Gamma and Neutron Radial Dose Rate Profiles on the Primary Cask Lid

Radial profiles are reasonably flat from R = 0 cm to R = 58.5 cm. Sharp decreases in dose rates (<5 mrem/hr) occur from R = 58.5 cm to the edge of the top of the cask body. Sharp decreases in dose rates correspond to the absence of fuel assemblies directly below measurement locations along the 45 degree diagonal near the radius of the cask inner cavity. Profiles obtained with TLDs and TEDs generally have lower magnitudes than those obtained with portable survey instruments, but agreement between measurement techniques is exceptionally good. The profiles indicate that portable survey instruments, if properly calibrated and operated, can be used to obtain accurate gamma and neutron dose rates. It does not appear that the additional time and expense associated with TLD and TED measurements can be justified.

Additional dose rate measurements on the primary lid (Appendix D) resulted in a gamma dose rate peak of 196 mrem/hr measured near the drain/fill connection flange (Figure 3-3 of Section 3). However, during normal operation the outer secondary lid [90-mm (3.5-in.) thick] will be in place and gamma dose rates should be substantially reduced (<20 mrem/hr).

Dose rates measured on the exterior surface (fin tips) of the side of the cask are presented in Figure 4-33; additional data are included in Appendix D. Measurements from portable survey instruments agree exceptionally well with TLD and TED dose rate measurements. Gamma dose rate profiles near the ends of the cask have significant peaks (140 mrem/hr). The peaks correspond to the upper and lower end fittings of the Surry PWR spent fuel assemblies. If it is desirable to reduce these peaks, a minor refinement involving adding gamma shielding is required. Neutron dose rates near the cask ends show only slight peaks (<21 mrem/hr) and should not be of concern. Dose rate measurements obtained near lifting trunnions indicated peaks in total dose rates of less than 70 mrem/hr, which is good (see Appendix D for these data). Total gamma and neutron dose rates on the remainder of the side of the cask are relatively low, less than 50 mrem/hr.

Circumferential dose rate profiles obtained at Z = 270 cm are shown in Figure 4-34. Both the gamma and neutron dose rate profiles measured with TLDs and TEDs are reasonably uniform (24 mrem/hr to 37 mrem/hr for gammas and 9 mrem/hr to 16 mrem/hr for neutrons). Peaks in gamma dose rates occurred adjacent to the higher decay heat assemblies (1.8 kW) located near 45 degrees and 135 degrees. Additional TLDs and TEDs were placed continuously along the circumference of the cask at an elevation of 215 cm and angles from 74° through 76° as shown in Figure 4-35. The purpose of

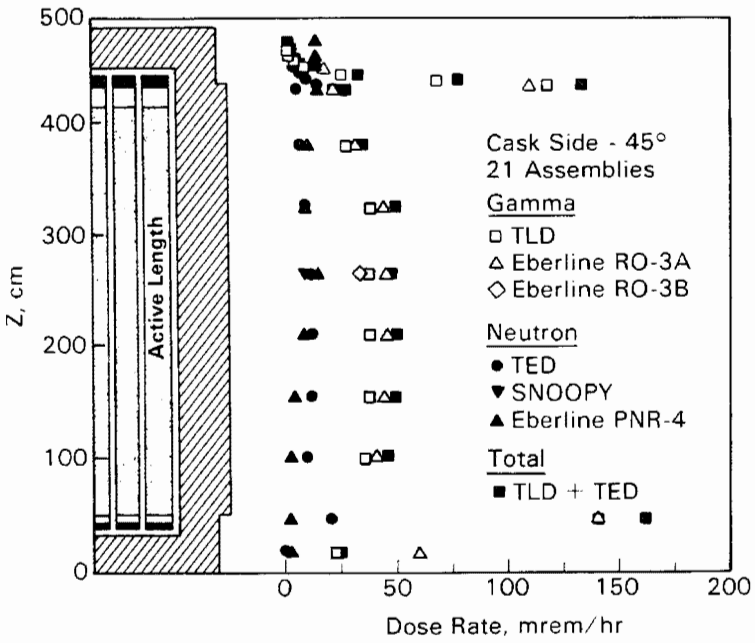

Figure 4-33. Gamma and Neutron Axial Dose Rate Profiles on the Cask Side

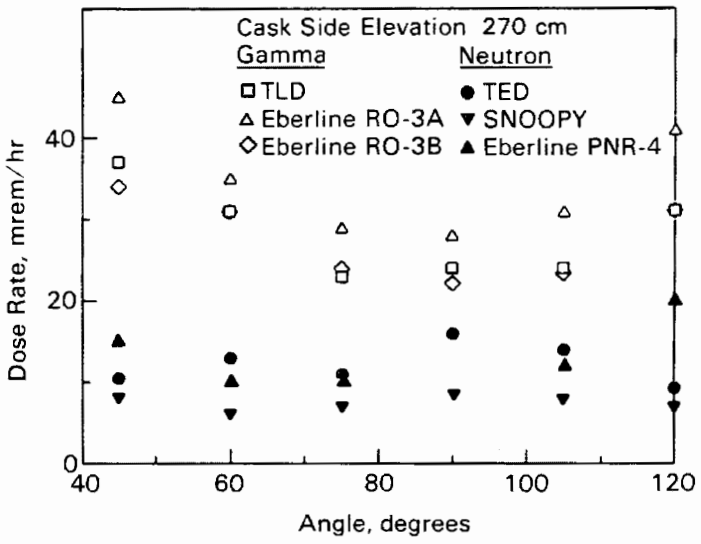

Figure 4-34. Gamma and Neutron Circumferential Dose Rate Profiles on the Cask Side

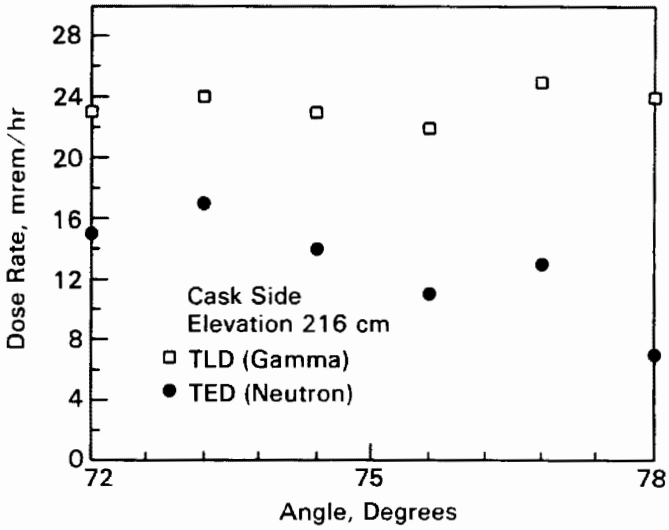

Figure 4-35. Gamma and Neutron Circumferential Dose Rate Profiles (close spaced measurements) on the Cask Side

these dose rate measurements was to determine if local peaks in neutron dose rates resulted from the circumferential spacing of the polyethylene neutron shielding cylinders in the body of the cask. As shown in the dose rate profiles of Figure 4-35, no significant peaks were measured. It was initially thought that minor neutron dose rate peaks and gamma dose rate valleys may be detected if the spacing was slightly wide.

Dose rate profiles measured on the bottom of the cask are shown in Figure 4-36; additional data are included in Appendix D. Measurements from portable survey instruments are slightly higher than TLD and TED measurements, but not enough to justify the added time and expense required to obtain good TLD and TED data. The gamma dose rate profile obtained with TLDs is reasonably uniform (18 to 25 mrem/hr) from the centerline of the bottom to a radius of approximately 93 cm, but drops off to less than 5 mrem/hr near the edge of the bottom. The neutron dose rate profile peaks at the centerpoint of the bottom (41 mrem/hr) and uniformly decreases to less than 5 mrem/hr at the edge of the bottom. The total (gamma and neutron) dose rate peaks (63 mrem/hr) at the centerpoint of the bottom and uniformly decreases to <5 mrem/hr at the edge of the bottom.

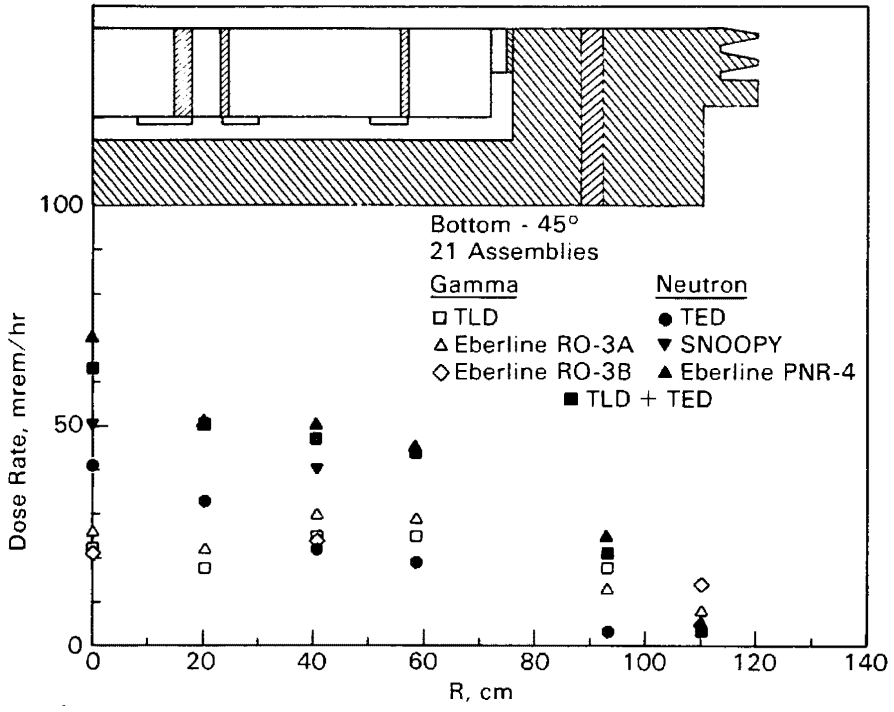

Figure 4-36. Gamma and Neutron Radial Dose Rate Profiles on the Cask Bottom

Approximately 6 months after initial dose rate measurements were obtained, dose rates at selected locations on the cask surface and in the air 1 m (3 ft) and 2 m (6 ft) adjacent to the cask were measured. Figure 4-37 indicates the attenuation that was measured from the cask surface to 2 m (6 ft) away from the cask.

Near the top of the cask, neutron surface dose rates adjacent to the centerline were attenuated from 290 mrem/hr (peak caused by single blind flange over vacant TC lance hole in lid) to 60 mrem/hr at a distance of 2 m (6 ft) away. Gamma surface dose rates were attenuated from 40 mrem/hr to 7 mrem/hr at 2 m. At R/2 and R distances from the lid centerline, neutron dose rates actually increased with distance from the cask because of contributions from several fuel assemblies instead of just the one immediately below the surface measurement point. That is, dose rates may peak some distance from the cask because the incidence angle to a point includes radiation from several assemblies instead of just the assembly directly adjacent to the point. The profile adjacent to R/2 did not peak between the surface and 2 m (6 ft), indicating that the peak may be a greater distance from the cask. However, the profile adjacent to the edge of the top (R) peaked between the surface and 2 m (6 ft) because the value (7 mrem/hr) at 2 m is less than that (8 mrem/hr) at 1 m. Gamma profiles at R/2 and R peaked within 2 m (6 ft) of the cask top because gamma dose rates are less at 2 m (6 ft) than at 1 m (3 ft). Note that the secondary lid was not on the cask during these dose rate measurements; when it is in place, its presence will significantly reduce dose rates near the cask top.

Near the side of the cask at an elevation of L/2 (halfway up the cask) and peripheral angles of 0, 45, 90, 180, 225, and 270 degrees, neutron dose rates were attenuated from 20 to 34 mrem/hr at the surface to 6 to 9 mrem at a distance 2 m (6 ft) away. Likewise, gamma dose rates were attenuated from 4 to 15 mrem/hr at the surface to 1 to 5 mrem/hr at 2 m (6 ft). On the side, all peaks occurred within 2 m (6 ft) of the cask because all valves at 2 m (6 ft) were less than those at 1 m (3 ft) adjacent to their respective peripheral locations.

It is apparent the shielding performance of the cask met the design goal of less than 200 mrem/hr (2). Total dose rates on the top of the cask were as high as 226 mrem/hr near the drain/fill flange, but should be less than 75 mrem/hr when the cask outer secondary lid is used during long-term storage. Total dose rates on the side of the cask were generally less than 50 mrem/hr, but peaks as high as 163 mrem/hr were measured. These peaks could easily be reduced to less than 75 mrem/hr with a minor refinement involving adding gamma shielding adjacent to the

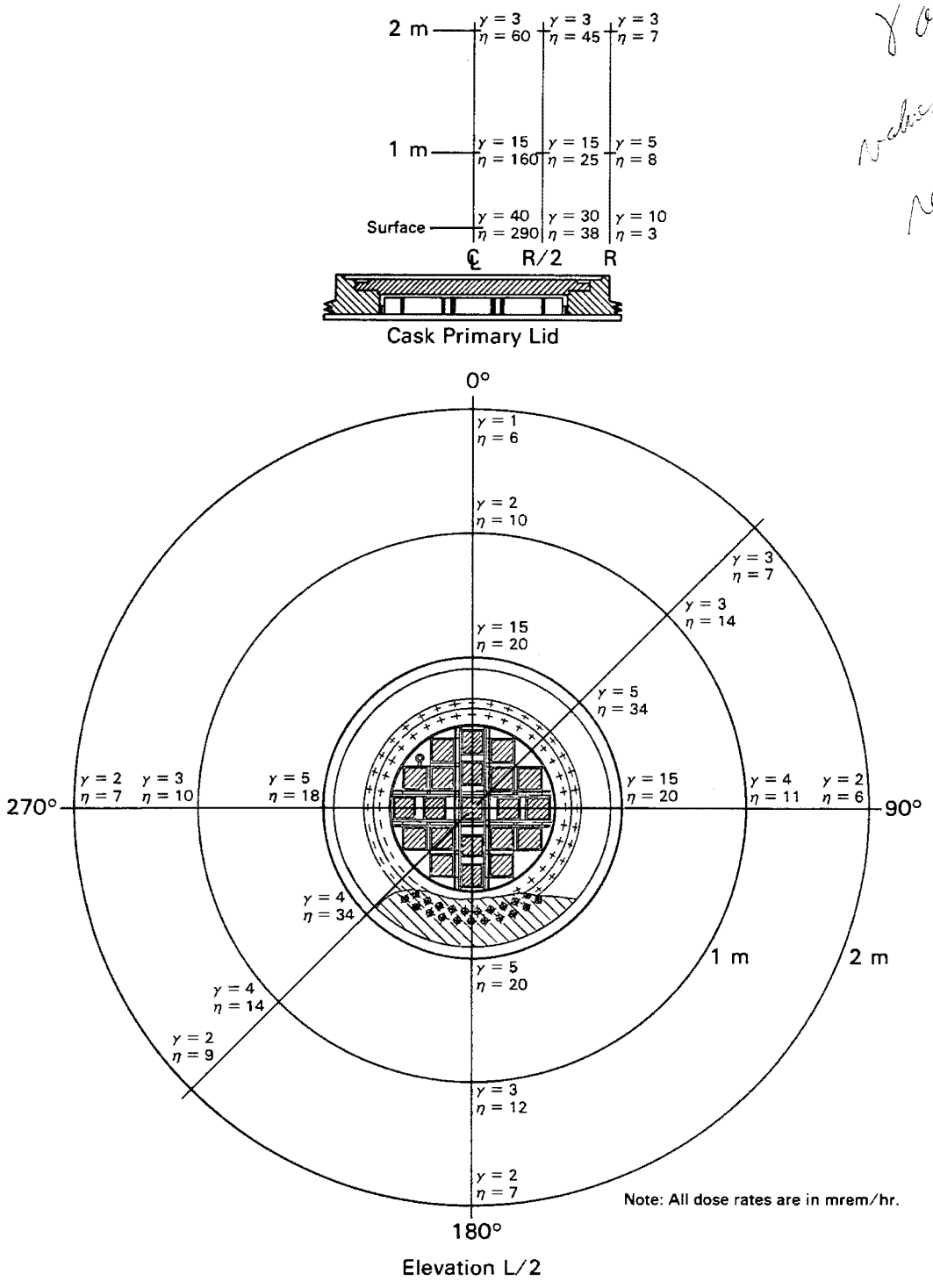

Figure 4-37. Gamma and Neutron Dose Rates on the Cask Surface and 1 m and 2 m from the Cask

top and bottom end fittings of the PWR spent fuel assemblies. Total dose rates on the bottom of the cask were less than 65 mrem/hr and should not be a problem during either vertical or horizontal storage.

Section 5

HYDRA HEAT TRANSFER ANALYSES

The pre- and post-test heat transfer analyses using the HYDRA thermal hydraulics computer code are discussed in this section. Pretest HYDRA temperature predictions were performed to 1) select the spent fuel to be used during testing, 2) determine the fuel loading pattern, and 3) identify optimal TC locations. After the HYDRA pretest predictions were evaluated and compared with test data, post-test predictions were performed with a more exact geometry model to improve predictions.

HYDRA is a fully three-dimensional thermal hydraulics computer code that solves equations of continuity, momentum, and energy by finite difference techniques. The code is currently under evaluation using applications ranging from problems with known analytic solutions to full-scale spent fuel storage system tests (14, 15, 17, 18). The use of HYDRA for predicting the operating characteristics of the CASTOR-V/21 spent fuel storage cask is one in a series of applications being performed to evaluate and qualify the program for design and safety analyses.

The numerical basis and features of HYDRA are briefly discussed, along with the geometry model, material properties, and important heat transfer and thermal hydraulic correlations. HYDRA predictions, both pre- and post-test, are presented and compared to CASTOR-V/21 test data. Best-estimate predictions of the cask heat dissipation capability with uniform fuel assembly heat generation rates are presented for a vertical cask with both nitrogen and helium backfill gases.

HYDRA COMPUTER CODE

HYDRA is a fully three-dimensional thermal hydraulics computer code. The time-dependent conservation equations of momentum and mass for compressible fluids are used as the basis for calculating single-phase flow fields. The time-dependent conservation equation of energy with convection and heat sources is the basis for calculating the temperature field. These conservation equations are as follows:

Momentum

$$\frac{\delta}{\delta t}(m) = \rho\vec{g} - \nabla\rho - D\vec{m} + \nabla\cdot(\mu\nabla\vec{v}) - \nabla\cdot(\vec{v}\vec{m}) \qquad (5\text{-}1)$$

where t = time
$\vec{m}$ = mass flux
ρ = density
$\vec{g}$ = gravitational vector
p = pressure
D = Darcy and orifice drag
μ = viscosity
$\vec{v}$ = superficial velocity (that velocity which would exist if the fluid occupied the volume alone).

Mass

$$\frac{\delta}{\delta t}(\rho) = -\nabla\cdot(\vec{m}) \qquad (5\text{-}2)$$

Energy

$$\frac{\delta}{\delta t}(\rho C_p T) = \nabla\cdot(\lambda\nabla T) - \nabla\cdot(C_p\vec{m}T) + \overline{q} \qquad (5\text{-}3)$$

where C_p = specific heat
T = temperature
λ = thermal conductivity.

The source term, $\overline{q}$, in the energy equation represents heat generation and thermal radiation heat transfer. The latter is given by an expression of the form

$$\overline{q}_{rad}\ i\to j = H_{ij}\,(T_i^4 - T_j^4) \qquad (5\text{-}4)$$

where H_{ij} is an exchange factor based on geometry and emittances.

A thermodynamic state relationship of the form

$$\rho = f(p,T) \qquad (5\text{-}5)$$

is required as well as other relationships needed for definition of temperature-dependent materials properties.

The conservation equations are converted to finite-difference equations using the locally one-dimensional philosophy embodied in Spaulding's hybrid scheme (19). Both the energy equation and the three linear momentum equations are solved using an alternating-direction algorithm described by Douglas and Gunn (20). The linking of the momentum equations with the conservation of mass equation is accomplished in a manner consistent with the spirit of the CTS SIMPLE algorithm described by Raithby and Schneider (21, 22).

HYDRA uses a Cartesian coordinate system for the computational mesh in the inner cask cavity (fuel basket region). A cylindrical coordinate system is available for convenience in calculating temperatures in the surrounding cask body. When both coordinate systems are invoked to model a cask, the code will automatically align the two systems and enforce conservation of energy at their interface.

HYDRA has been designed to provide a user-oriented input interface, which eliminates the need for internal code changes. Any application for which the code is an appropriate choice can be completely described through the construction of an input file. The user may optionally request a formatted echo of the input file to confirm that the intended parameters are actually those used by the code. A selectable commentary monitoring the progress of the code toward a steady-state solution is available, as well as a summary of energy balances. Finally, a tape may be written at the conclusion of a run if the user wishes to restart the solution from its most recent point.

HYDRA MODELS AND INPUT

The complete description for a given simulation is contained on an input file. The input file is read by HYDRA, and the information contained is stored and used to guide subsequent execution of the code. This section describes some of the information on the input file: the computational mesh, material properties, and correlations. Modeling uncertainties associated with the CASTOR-V/21 cask are also discussed.

Computational Mesh

A radial cross section of the cask has been illustrated previously in Figure 3-2 of Section 3. This cross section shows a cylindrical cavity inside the cask whose outside surface is approximately cylindrical. Figure 5-1 shows the corresponding

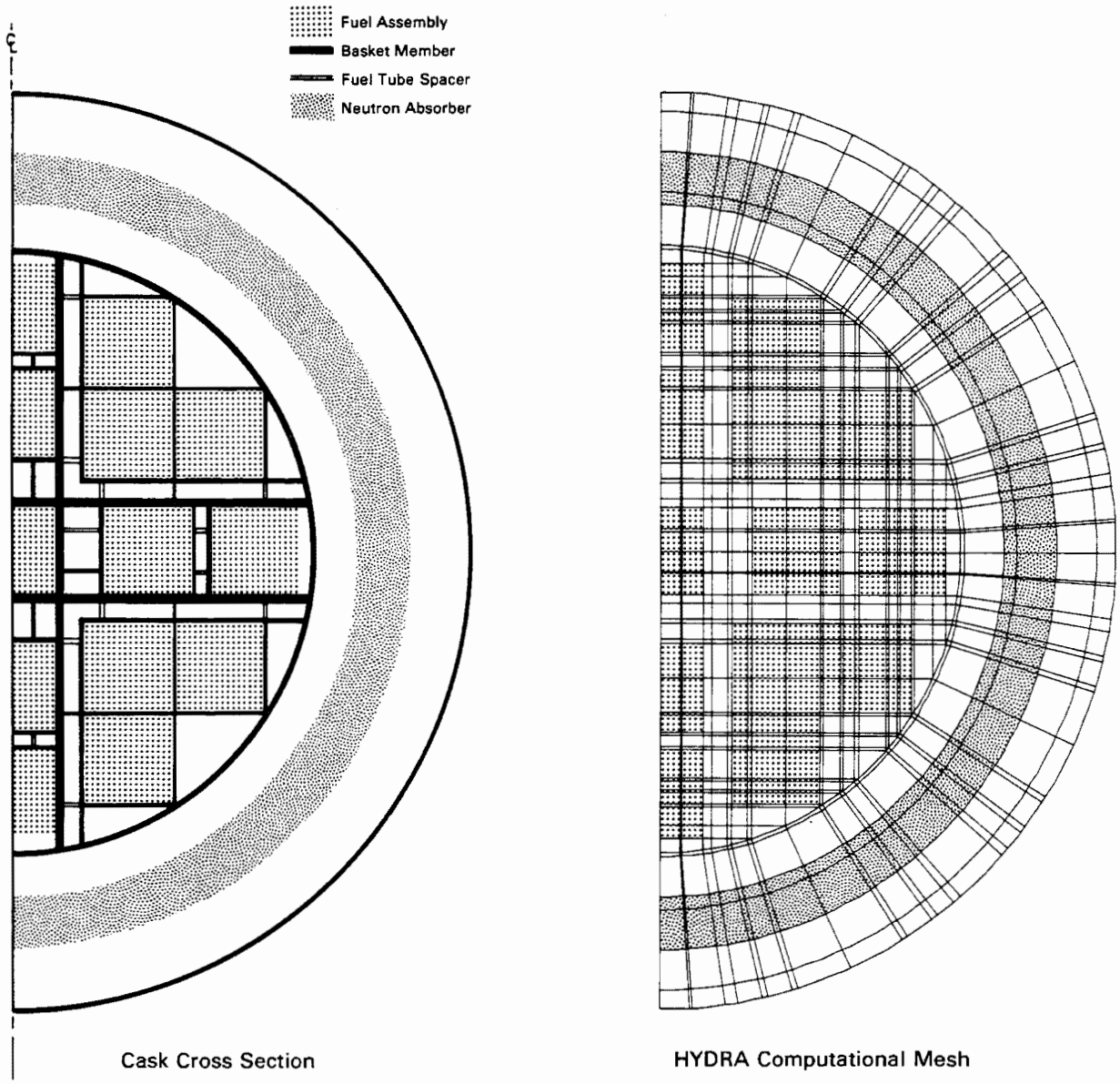

Figure 5-1. Transverse Computational Mesh and Alignment of Mesh with Physical Cask Features

radial computational mesh employed and indicates the alignment of the mesh with various physical features of the cask. Cartesian coordinates are used in the cask cavity, and a cylindrical coordinate system is used to represent the cask body.

An elevation view of the cask is seen in Figure 3-1 of Section 3. A corresponding cross section of the axial computational mesh is shown in Figure 5-2 and indicates the location of physical cask features relative to the computational mesh.

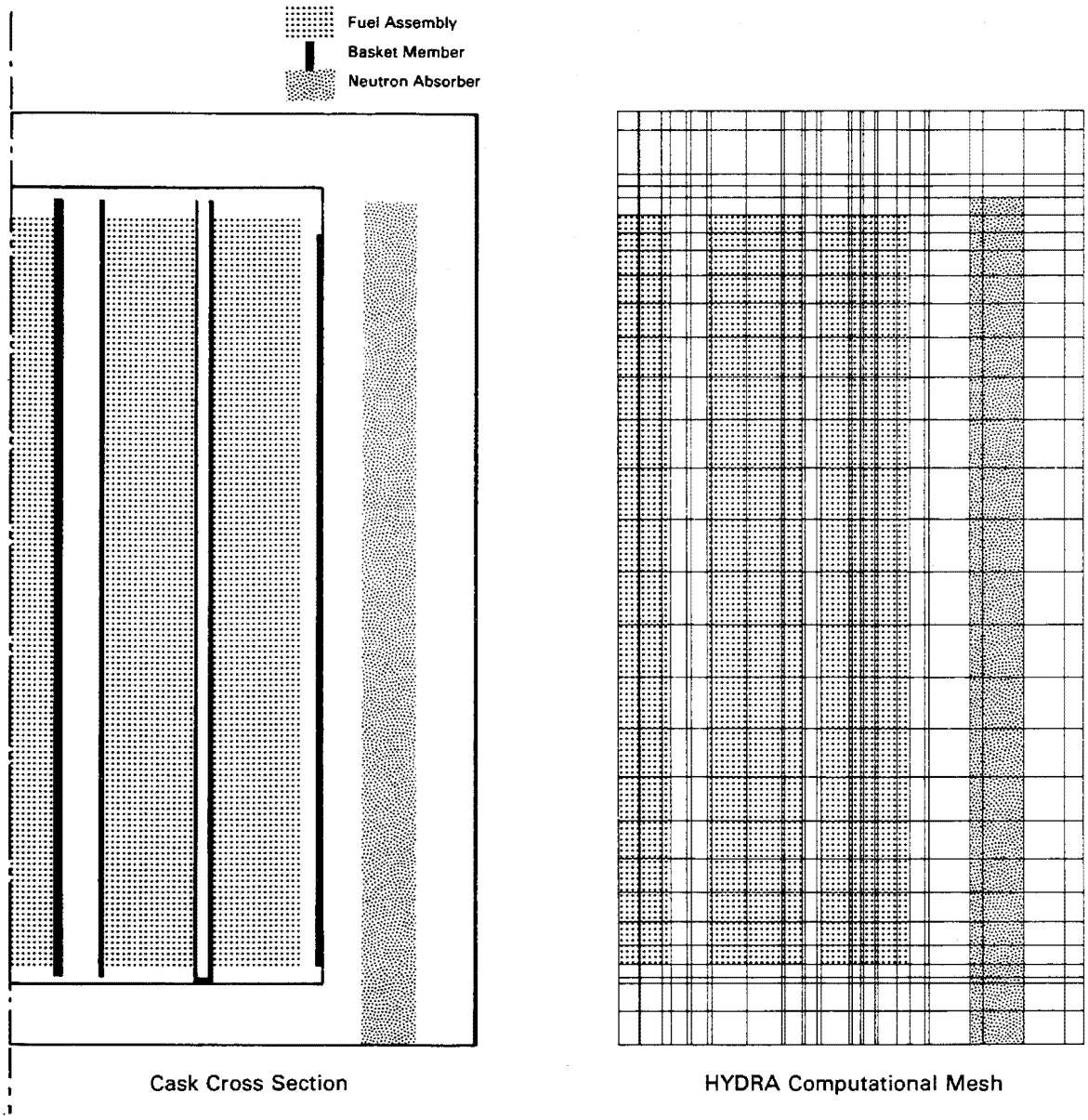

Figure 5-2. Axial Computational Mesh and Alignment of Mesh with Physical Cask Features

The code computes a temperature and three mass fluxes (if a fluid is present) corresponding to each computational cell. The shape and location of each cell is selected, insofar as practical, to coincide with physical structures or boundaries of the cask and its contents. The accuracy of predicted temperatures and mass fluxes is influenced significantly by how well the computational mesh is aligned with the physical structure.

Material Properties and Correlations

Material properties were obtained from the GNS cask topical safety analysis report (2) and from Touloukian and Ho (23). Table 5-1 lists the material properties used for all simulations. Effective thermal conductivities were estimated for those computational cells containing more than one material. For those simulations where the backfill is denoted as vacuum, it is to be understood that the actual backfill is nitrogen gas at low pressure. The pressure is, however, high enough so that the

Table 5-1

MATERIAL PROPERTIES

Thermal Conductivity ($W/cm^2°K$)	
Stainless steel	0.09215+(0.1465E-3)T
Boron steel (Radionox)	0.079+(0.21E-3)T
Nodular cast iron	0.5162-(0.3205E-3)T
Air	0.688E-4+(0.634E-6)T
Helium	0.52E-3+(0.32E-5)T
Nitrogen[a]	0.75E-4+(0.6167E-6)T
Specific Heat (W sec/g°K)	
Helium	5.234
Nitrogen	1.053
Viscosity (g/cm sec)	
Helium	0.700E-4+(0.400E-6)T
Nitrogen	0.794E-4+(0.355E-6)T
Emittance	
Fuel cladding	0.8
Fuel basket	0.4
Cast iron (nickel plated)	0.25
Cast iron (smooth)	0.3
Cast iron (painted fins)	0.92
Stainless steel	0.2

[a]Vacuum properties were the same as those for nitrogen because the vacuum was actually low pressure nitrogen.

mean free path of the gas is less than any significant lengths (gaps). The properties used for the vacuum simulations are, therefore, those of nitrogen.

The total heat transfer from the external surface of the cask to ambient was computed by the code for both convection and radiation modes acting in parallel. Heat transfer correlations were used to predict convection heat transfer from the external surface of the cask to ambient. The correlations used for all external surfaces relate the Nusselt number, Nu, to the Rayleigh number, Ra, and are of the form

$$Nu = C[Ra(L)]n \qquad (5\text{-}6)$$

The values of C, n, and the significant length, L are listed in Table 5-2. Correlations for smooth surfaces were taken from Sissom and Pitts (24) and the correlations for finned surfaces were estimated from Chaddock (25).

Table 5-2

CONVECTION HEAT TRANSFER CORRELATIONS

Surface	C	n	L,cm
Vertical	0.13	1/3	220.0
Horizontal-heated surface facing up	0.14	1/3	220.0
Horizontal-heated surface facing down	0.27	1/4	220.0
Vertical fins	0.32	1/4	3.5
Horizontal fins	0.32	1/4	3.5

Modeling Uncertainties

Typical spent fuel storage casks are large and complex thermal hydraulic systems, and some uncertainty about how best to construct an accurate overall model will always be present. These uncertainties lead inevitably to approximations, some of which may be difficult to quantify. Most uncertainties may be placed within one of three broad catagories:

- basic information that is application-specific and measurable (e.g., cask dimensions, heat generation rates, ambient conditions)

- information generic to most applications (e.g., property values, correlations)

- decisions about how to achieve the best match between a particular code and the application (e.g., computational mesh, internal algorithms).

An expanded indication of some of the more important factors falling within the above categories follows.

- The information shown on cask drawings may not entirely reflect the as-built cask geometry. Design information, not as-built information, was normally used as HYDRA input.

- Dimensional tolerances may be particularly significant when they influence small gaps with important thermal resistances. The input to HYDRA specified nominal dimensions.

- Potential eccentricities, such as the actual location of the basket within the cask cavity, are a source of uncertainty. Other eccentricities, such as the location of a fuel assembly within a basket fuel tube, are certain to occur and can substantially alter some thermal and flow resistances. The input to HYDRA specified no eccentricities.

- The total decay heat generation rate and the corresponding assembly axial profile have a direct impact on predicted cladding temperatures. Both the total heat generation rate and the axial profile are amenable to experimental determination, and that is the preferred approach. Predicted values were used as input to HYDRA.

- All material property values possess a range of uncertainties, although the range for most well-characterized materials is usually not significant. Exceptions include the emittance of some material surfaces, especially if the surface has been altered by some process (e.g., corrosion, crud, oxidation, or sandblasting). The HYDRA input file specified values believed to be typical. The consequences that a range of emittance values might have on predicted temperatures have not been investigated.

- Convection heat transfer coefficients as employed on the outside surface of the cask are known to result in approximate local heat transfer rates. The HYDRA input file specifies heat transfer coefficients based on information obtained in the open literature for conditions similar, but not identical, to the cask surfaces.

- Some boundary conditions may be difficult to determine. An example is the heat loss from the cask bottom to the rail car structure upon which it rested. The HYDRA input file specifies a relatively small rate of heat loss.

- Some uncertainties are inherent in the use of discrete solution methods. An example is the trade-off between mesh coarseness and accuracy. The conservation equations have been formulated within

HYDRA in an entirely consistent fashion. This means that desired numerical accuracy may be achieved by using a sufficiently large number of computational cells. The practical trade-off is between accuracy and computer time and costs. The optimum is difficult to determine a priori.

- Another source of uncertainty results from limitations of models constructed internal to the code. Thermal radiation models are a good example. All radiation enclosures within the cask are three-dimensional. Radiation models that are two-dimensional are used extensively within HYDRA for practicality. The errors associated with this approximation can be reduced, but not eliminated, by careful selection of a computational mesh.

- Finally, there is a fourth category of uncertainty not mentioned previously--human error. The internal coding or input specifications intended may not be what is actually present. This situation is at its worst when the offending mistake results in an error that is both significant and unobtrusive.

PREDICTIONS COMPARED TO DATA

Pretest and post-test predictions of temperatures are compared to experimentally measured test data in this section. All pretest predictions were conducted "pre-look"; that is, the modelers did not have access to the experimental results (except cask internal gas pressure and the ambient temperature) and had not previously modeled the CASTOR-V/21 cask. The post-test prediction results, which conclude this section, are much improved over pretest predictions and are in substantial agreement with test data.

The post-test predictions benefitted from the availability of measured temperature data and post-test observations of the cask and basket assembly. Three modifications to the code input files were found to be uniformly warranted and are briefly mentioned now as an aid to interpreting the pretest predictions.

- The convection heat transfer coefficient on the exterior surface was increased.

- The gap between the basket and the cask inner wall was reduced in accordance with post-test visual observations.

- Drag coefficients for the flow channels exterior to basket fuel tubes, omitted in the pretest analysis, were added.

The extent to which each of the three modifications impacts the predictions does depend on the particular experimental test run being considered.

Pretest Temperature Predictions Compared to Test Data

This subsection begins with a summary of comparisons of peak guide tube temperature predictions with data for all five test runs. Following this summary, selected predicted axial and radial temperature profiles are compared graphically with data for each run.

One of the factors of particular interest in cask heat transfer performance is peak cladding temperature. By means of a bar chart, Figure 5-3 illustrates comparisons of predicted and measured peak guide tube temperatures and temperature differences between the ambient and peak temperature for each run. The ambient temperature for all runs was approximately 25°C, reflecting the indoor environment of the performance test. Peak guide tube temperatures occurred in the center fuel assembly for all test runs.

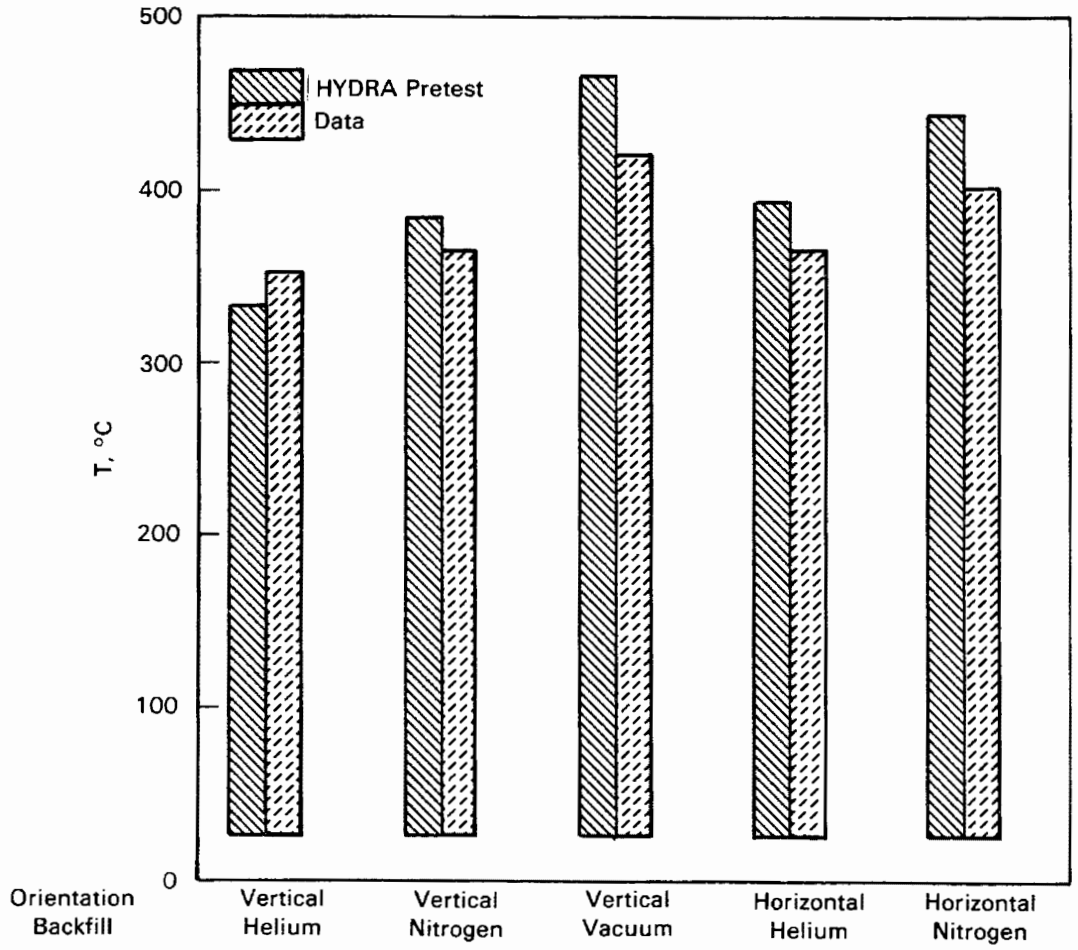

Figure 5-3. Pretest Predictions Compared to Peak Guide Tube and Ambient-to-Peak Guide Tube Temperature Difference Data

The axial location is quite variable depending on cask orientation, backfill gas, and pressure. These locations are best seen in subsequent figures that illustrate axial and radial temperature profiles.

The largest discrepancies between predicted and measured peak guide tube temperatures occur for the vertical vacuum and horizontal nitrogen runs; these discrepancies were 48°C and 42°C, respectively. This reflects agreement between predicted and measured peak guide tube temperatures of 12% or better. It will subsequently be shown that the major reason for the discrepancies associated with these two runs is the assumed presence of a 1.5-mm gap between the basket and the cask inner wall. In any event, the discrepancies shown for all runs are considered significant, and the explanations will be taken up in detail when post-test simulations are discussed.

Predicted axial temperature profiles for vertical, helium, nitrogen, and vacuum test runs are compared to test data in Figures 5-4, 5-5, and 5-6. Figure 5-4 shows predictions compared to data for the vertical, helium test run. Temperatures on the exterior surface of the cask are overpredicted. It will be seen in subsequent figures that this overprediction occurred for all test runs. An adjustment to the external heat transfer coefficient was made for post-test predictions and corrected this discrepancy.

Also shown in Figure 5-4 are axial temperature profiles for an outer fuel assembly and the center fuel assembly. The agreement between predictions and data is good for the outer assembly, but differences between predictions and data exist for the center assembly. Center fuel assembly temperatures are underpredicted by as much as 35°C, but the predicted profile indicates the influence of convection, as shown by hotter temperatures in the upper regions of the assemblies and cooler temperatures in the lower regions.

Figure 5-5 shows predictions compared to data for the vertical, nitrogen test run. As indicated previously, external cask surface temperatures are overpredicted. The replacement of helium with nitrogen gas results in overpredictions of temperatures of as much as 45°C in both the outer and center fuel assemblies. The resistance to heat flow between the assemblies and the cask body is apparently much less in the cask under test conditions than in the HYDRA model. The influence of upward convection, especially in the center fuel assembly, is again indicated.

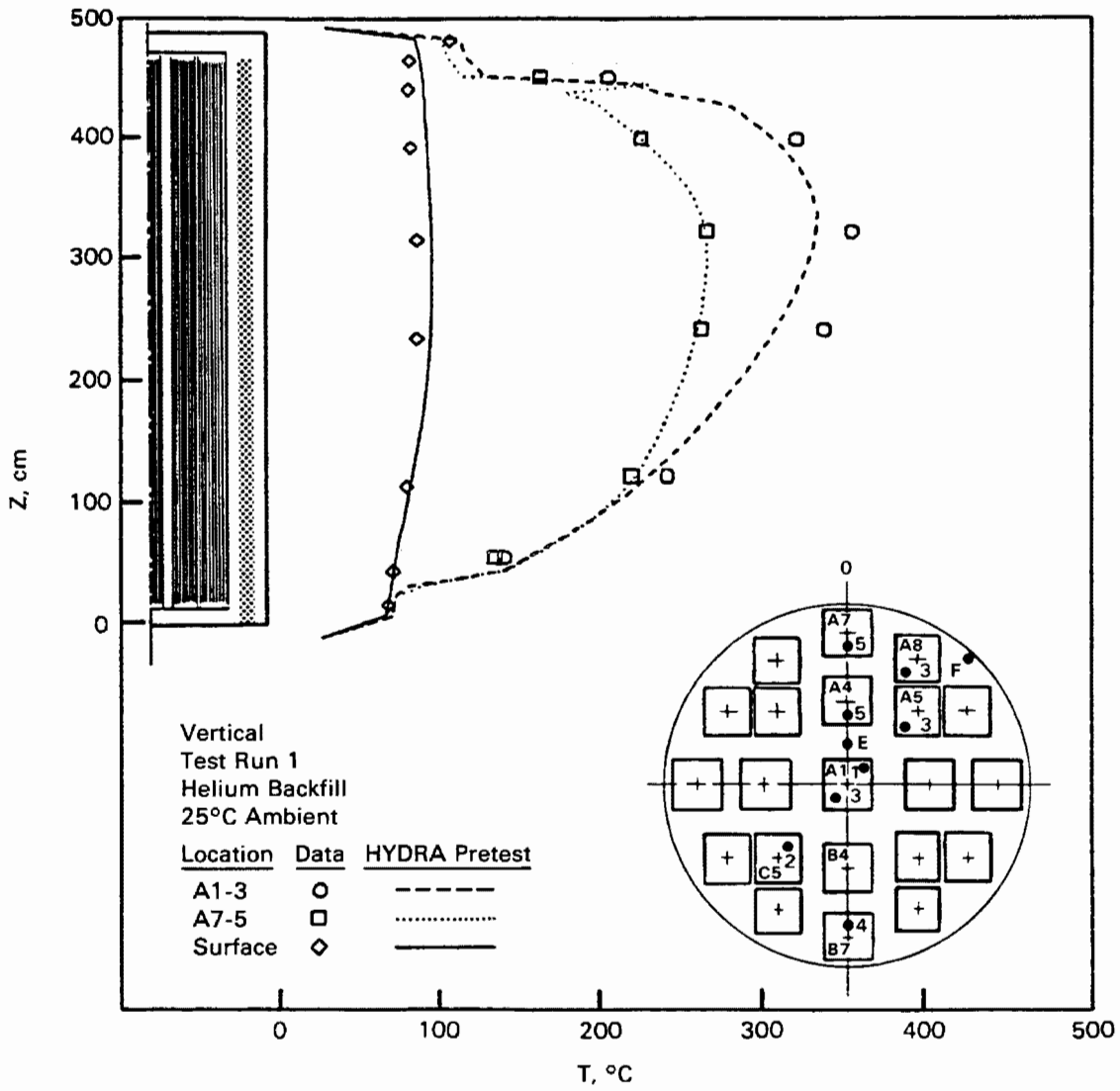

Figure 5-4. Pretest Axial Temperature Profile Predictions Compared to Vertical, Helium Test Data

Figure 5-6 shows predictions compared to data for the vertical, vacuum test run. The lack of significant convection in this test run results in peak temperatures being located near the axial elevation of assembly peak power generation. As in the vertical, nitrogen test run, the temperatures are similarly overpredicted by as much as 60°C.

Figure 5-7 shows predictions compared to data for an outer fuel assembly generating 1.8 kW of heat for the three vertical test runs. The trend established in the three previous figures continues, with the helium data being somewhat underpredicted

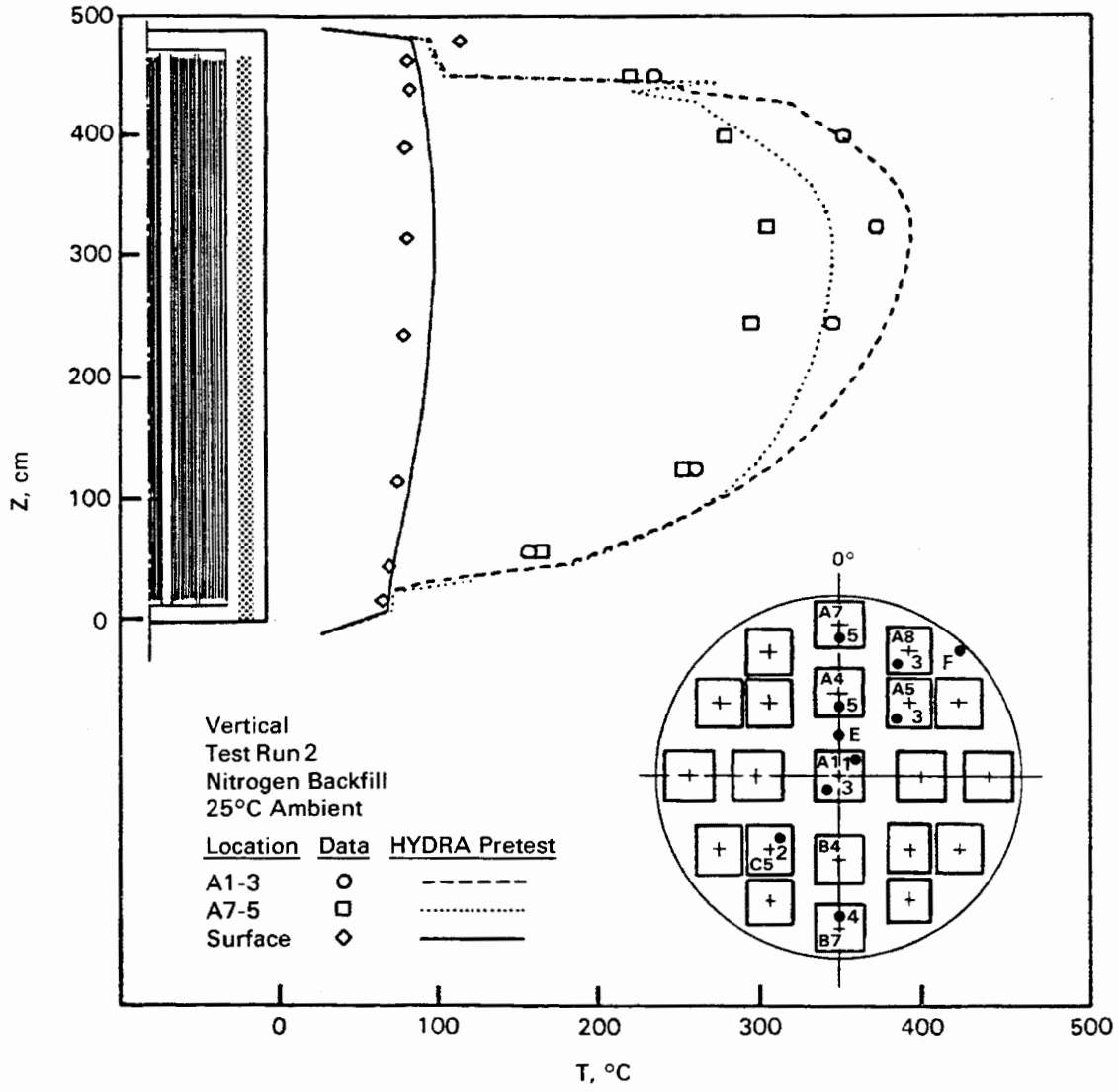

Figure 5-5. Pretest Axial Temperature Profile Predictions Compared to Vertical, Nitrogen Test Data

(20°C) and the nitrogen and vacuum data being overpredicted (45°C). The effect of convection is seen in the helium and nitrogen data/predictions, but not in the vacuum data/predictions.

Radial temperature profiles for the three vertical test runs from the center fuel assembly out to the cask surface are shown in Figure 5-8. The profiles are for the respective axial planes of peak cladding temperatures. Again, it can be seen that the helium test data are underpredicted near the center of the cask and the nitrogen

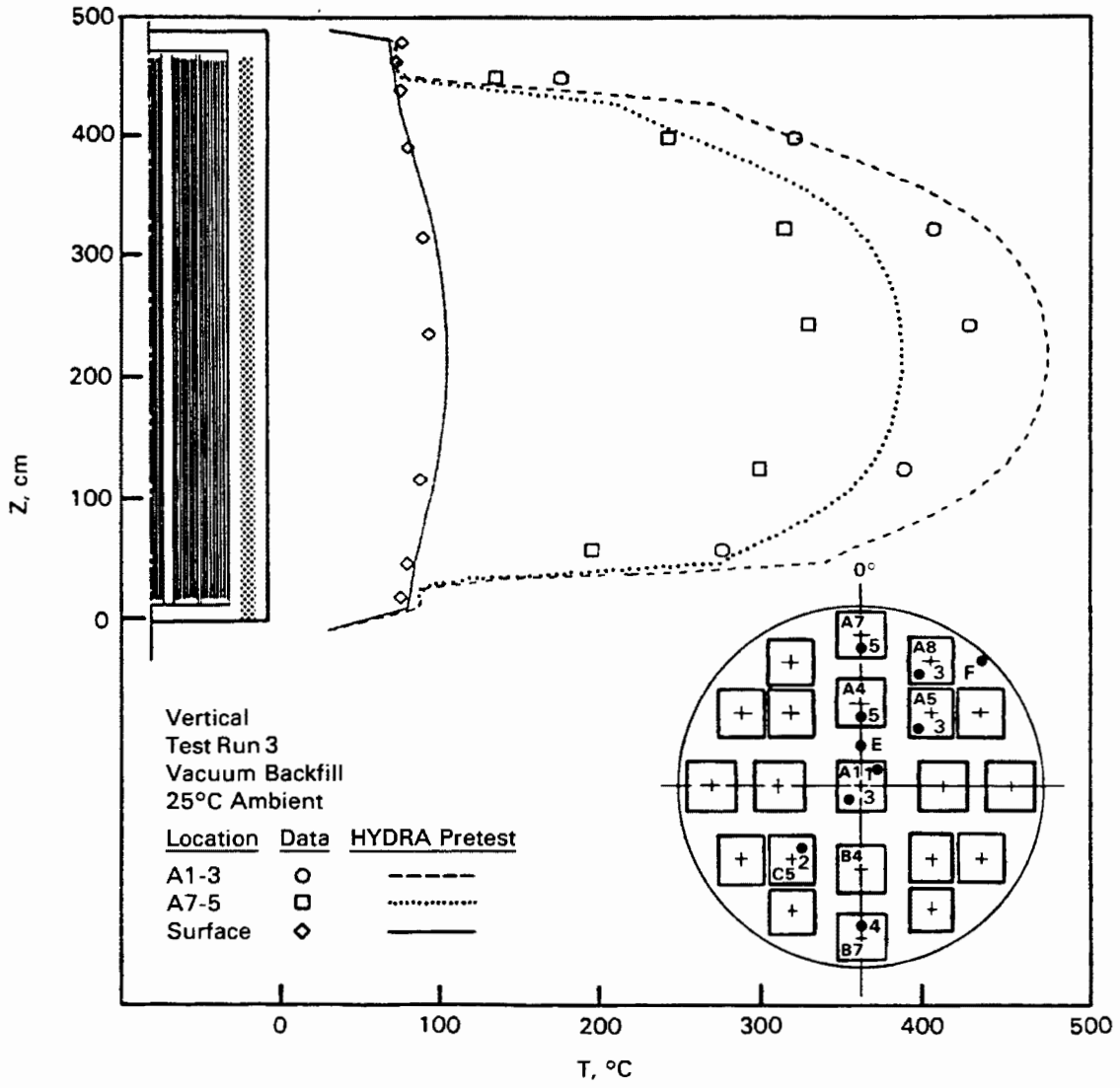

Figure 5-6. Pretest Axial Temperature Profile Predictions Compared to Vertical, Vacuum Test Data

and vacuum data are overpredicted. Temperatures of the gas between assemblies A1 and A4 were overpredicted in the vacuum run and underpredicted in the nitrogen and helium runs. However, HYDRA did predict that nitrogen temperatures would be less than helium temperatures, as indicated by the data. Large temperature differences (150°C to 200°C) were predicted to exist between the outer assembly and the inner cask wall.

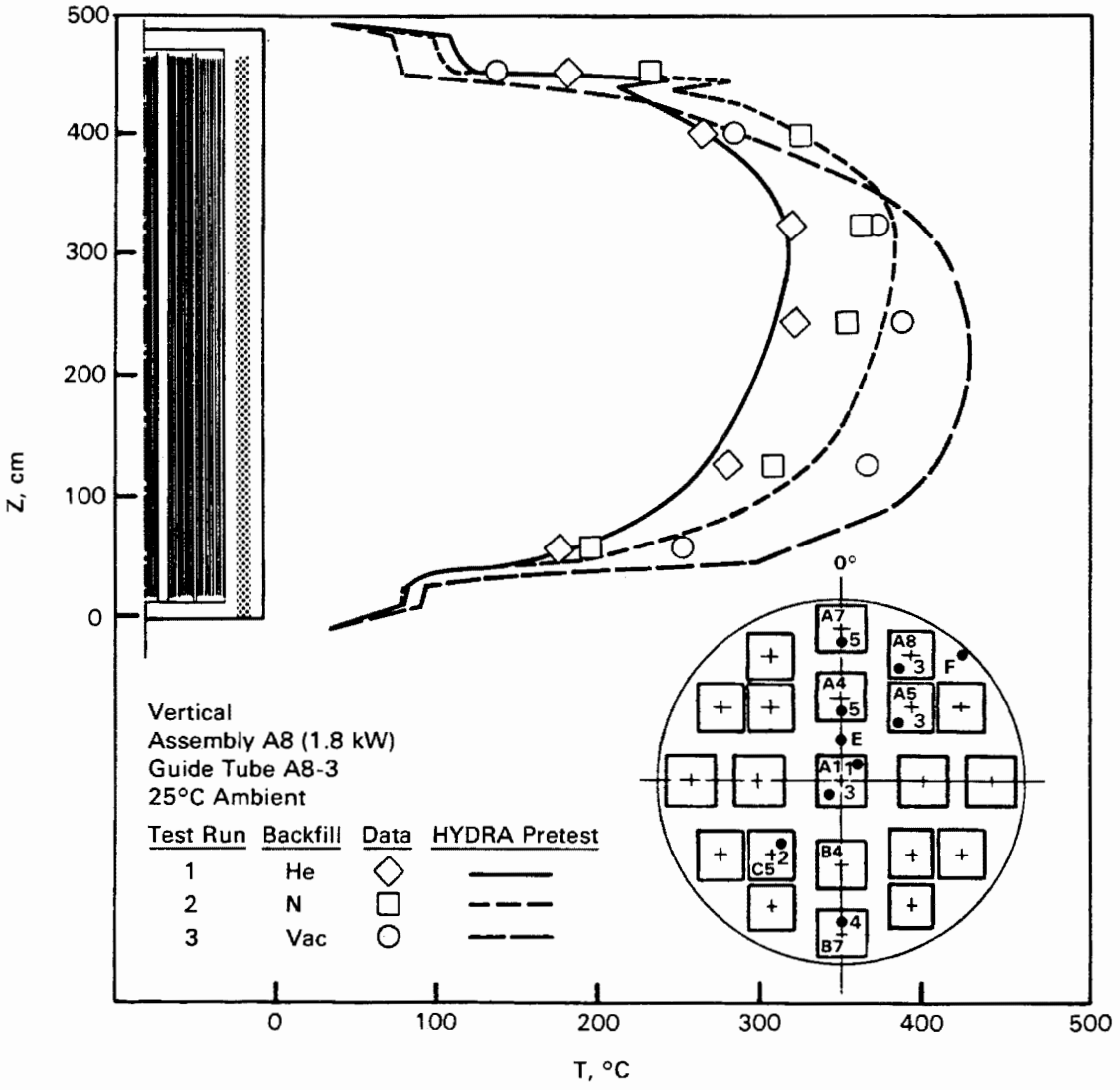

Figure 5-7. Pretest Axial Temperature Profile Predictions Compared to Vertical, Helium, Nitrogen, and Vacuum 1.8-kW Outer Fuel Assembly Test Data

Figures 5-9 and 5-10 show predictions of axial temperature profiles compared to data for the two horizontal test runs. The effects of axial convection are much reduced compared to those displayed for the corresponding vertical test runs as indicated by the symmetry of profiles about the axial centerline of the fuel assemblies. Predicted temperatures in the axial center region for the helium test run are too high (up to 35°C) due mainly to an overprediction of the cask surface temperature. The predicted temperatures for the nitrogen test run are also too high, even after adjusting for the surface temperature discrepancy. Temperature profiles in both backfills are predicted reasonably well.

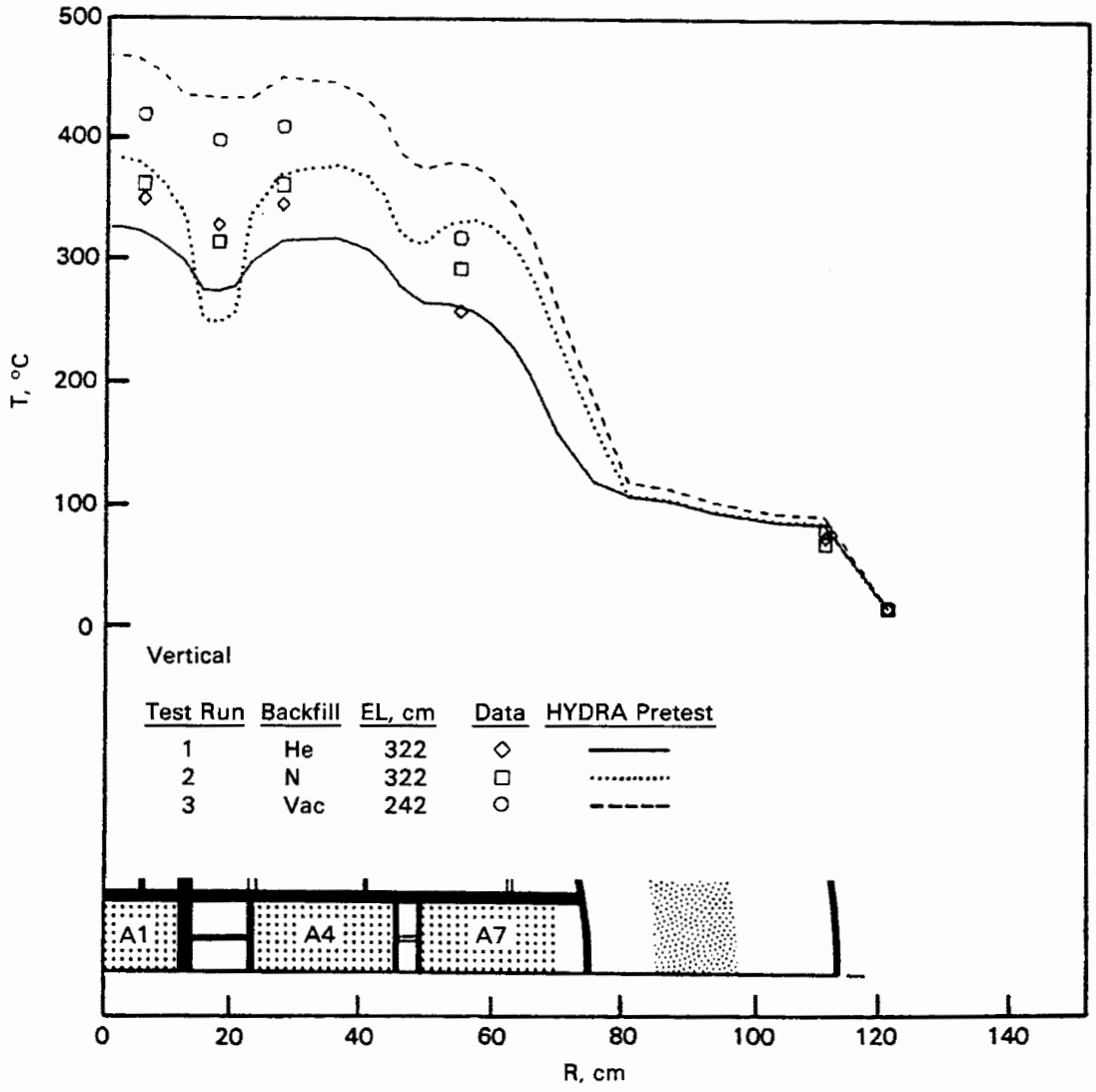

Figure 5-8. Pretest Radial Temperature Profile Predictions Compared to Vertical, Helium, Nitrogen, and Vacuum Test Data at Axial Planes of Peak Guide Tube Temperatures

Radial temperature profiles for a horizontal cask from cask surface-to-surface along the vertical diameter are compared in Figure 5-11 at the axial planes of peak cladding temperatures. The diameter is used because side-to-side symmetry is not present in a horizontal orientation. The predicted and measured profiles, however, show very little asymmetry, suggesting the relative importance of conduction and radiation heat transfer compared to convection. The predicted profiles are higher than the data, but both profiles are reasonably uniform in the center region of the basket like the data indicate. Large temperature differences (150°C to 200°C) are again predicted between the outer assembly and the inner cask wall.

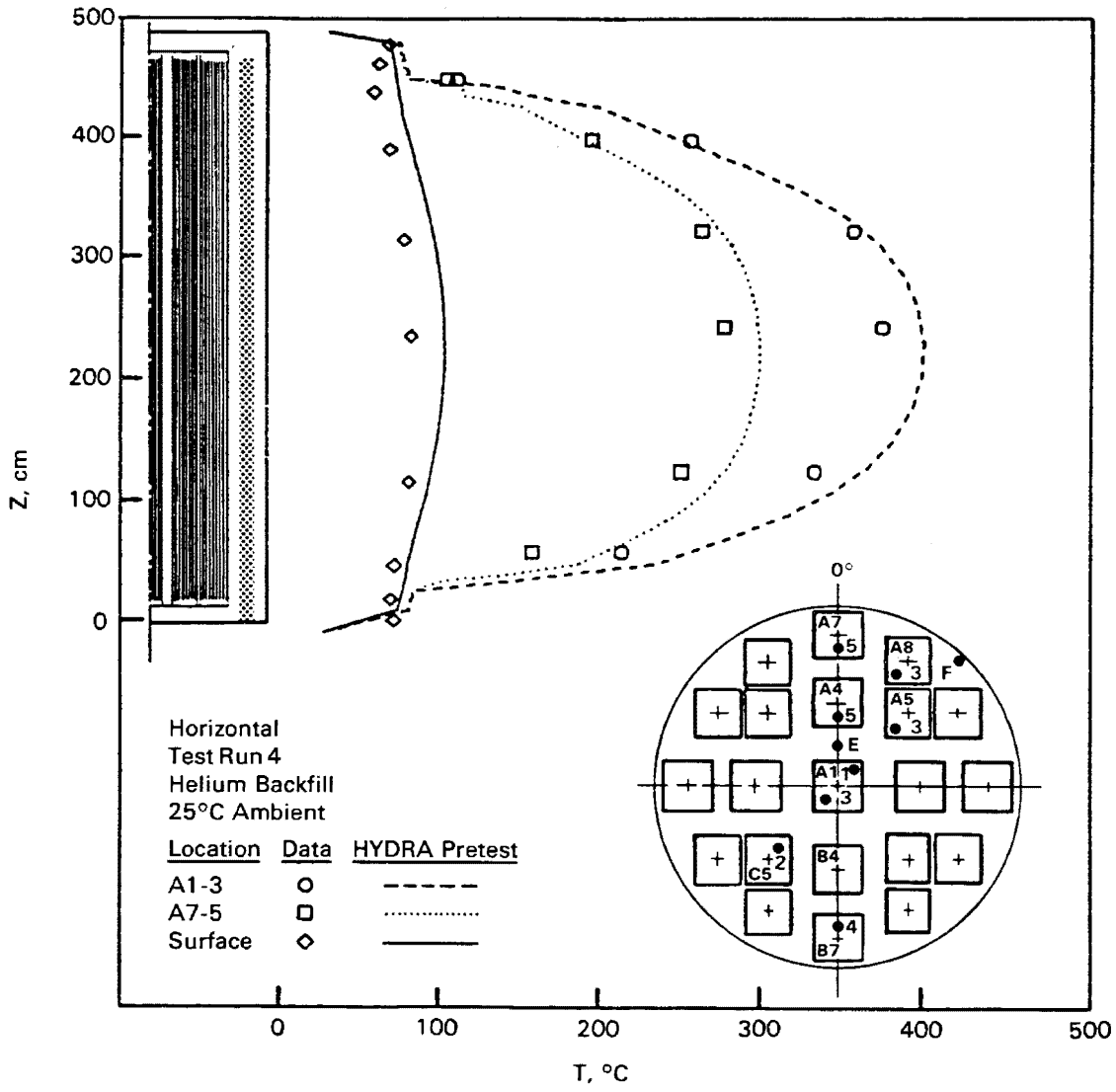

Figure 5-9. Pretest Axial Temperature Profile Predictions Compared to Horizontal, Helium Test Data

Three significant conclusions can be drawn from the results presented in Figures 5-3 through 5-11:

- The heat transfer from the side of the cask to the ambient is actually greater than predicted.
- The heat transfer from the fuel assemblies to the cask surface is better than predicted for test runs with nitrogen or vacuum backfills. The gap between the basket and cask inner wall can account for a substantial heat transfer resistance with nitrogen or vacuum.

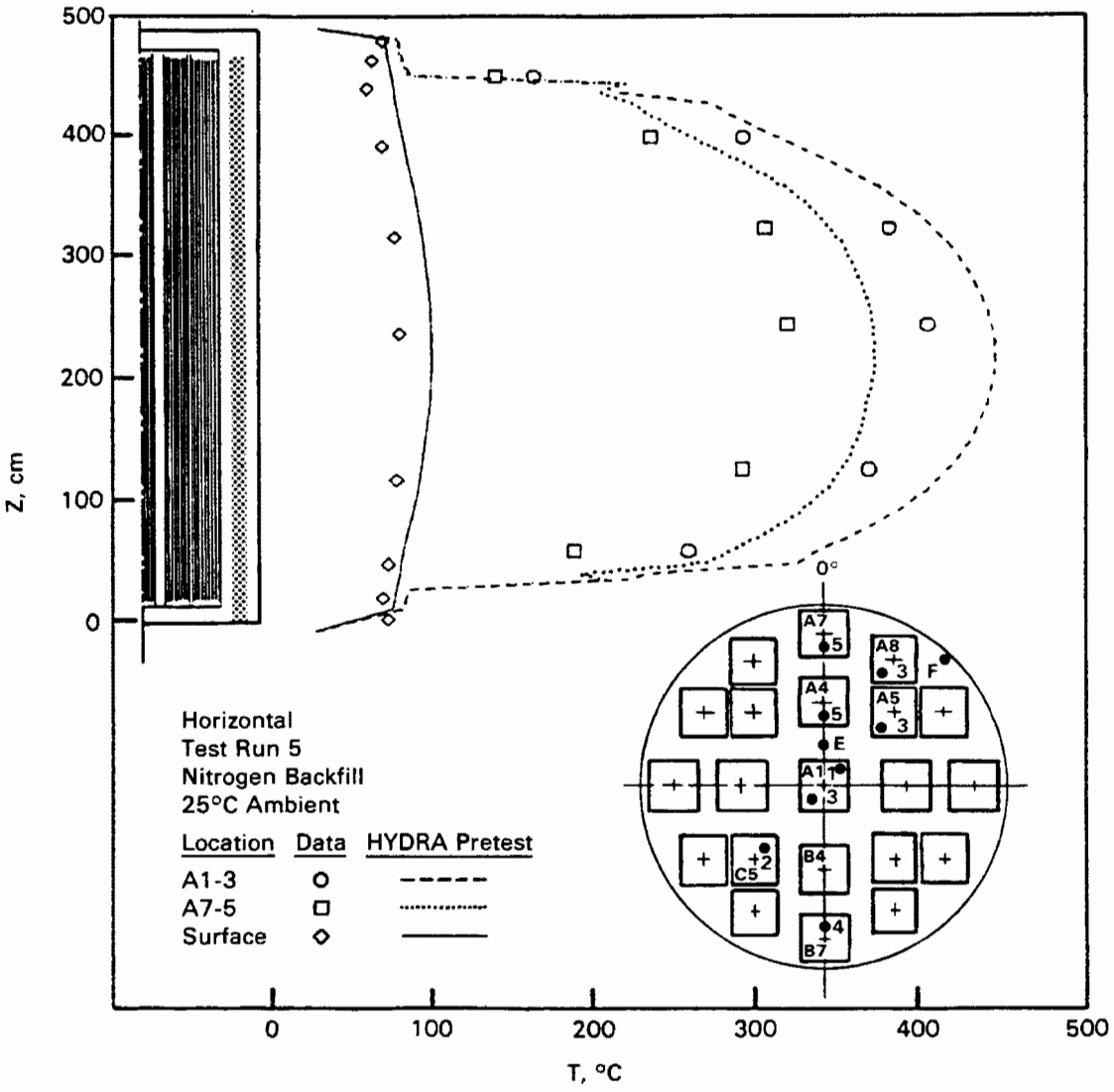

Figure 5-10. Pretest Axial Temperature Profile Predictions Compared to Horizontal, Nitrogen Test Data

- Finally, it can be seen that, after accounting for the above two effects, discrepancies between predictions and data will still remain for some of the test runs.

Clearly, one or more phenomena are not properly accounted for in the mathematical description of the physical cask if it is tacitly assumed that no serious experimental data problems exist. This matter will be pursued in the subsection on post-test simulations that follows.

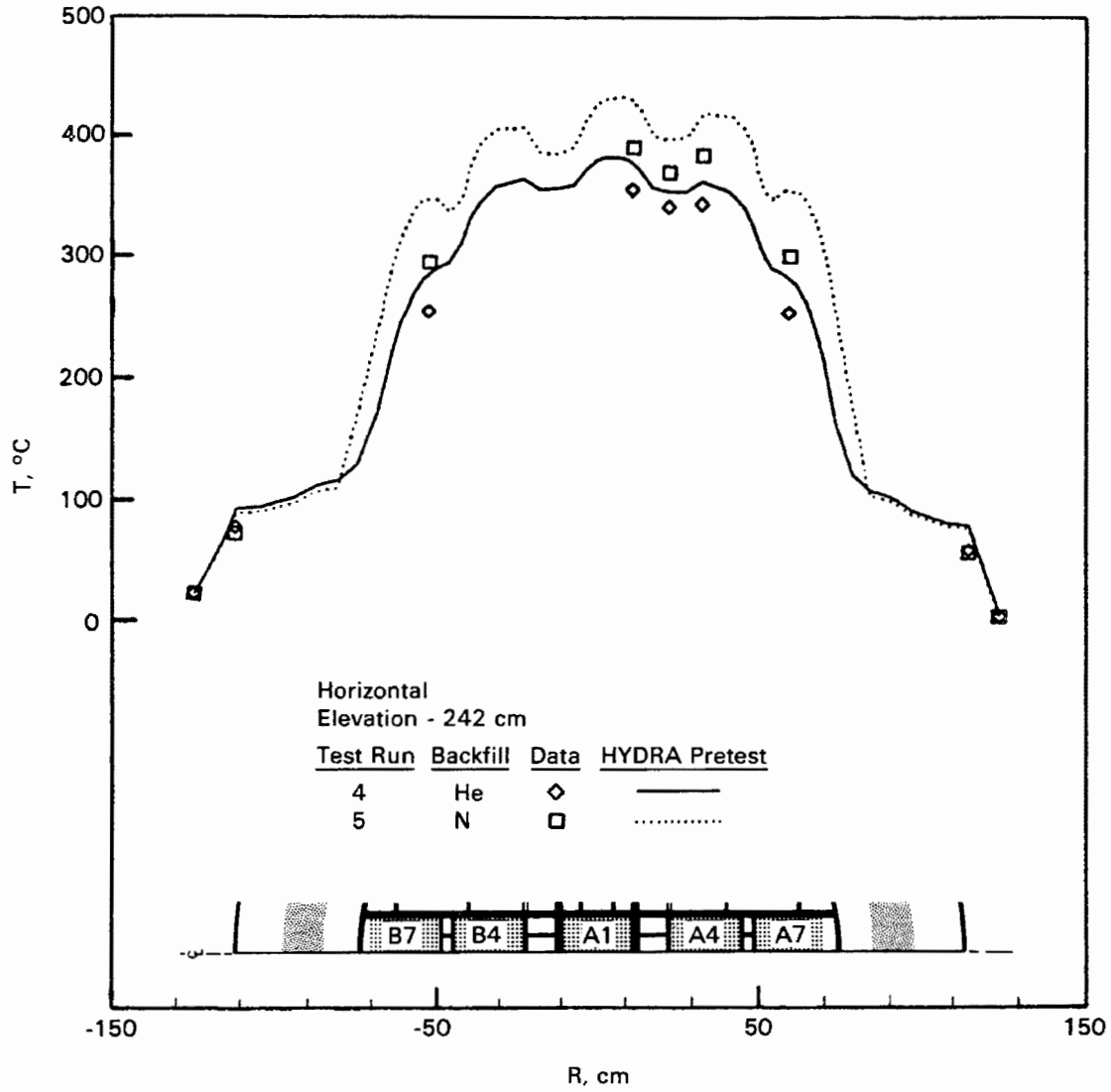

Figure 5-11. Pretest Radial Temperature Profile Predictions Compared to Horizontal, Helium, and Nitrogen Test Data at Axial Planes of Peak Guide Tube Temperatures

Post-Test Predictions Compared to Data

This subsection begins with a statement and explanation of three input file modifications applied to all five test runs. Figures showing post-test comparisons are presented next as counterparts to those displayed previously for pretest comparisons. This subsection concludes with graphic displays of selected heat flux and mass flux flow patterns intended to provide additional insight into CASTOR-V/21 cask performance.

Refinements to Pretest Analysis. After the experimental data were made available and compared to predictions, a careful review of data accuracy, the HYDRA code, and HYDRA input files was undertaken. The experimental procedures were examined for deficiencies that could result in errors in the reported temperatures or pressure. None was found to account for the general magnitude of disagreement between predictions and data. The code itself was reviewed, and no evidence could be found to support a change. Refinements to the code input files could, however, be supported.

Three refinements to the input files were found to be uniformly warranted. Mentioned briefly at the beginning of this section, they are restated here with amplification:

1. The exterior cask surface convection heat transfer coefficient was increased.
2. The gap between the basket and the cask inner wall was reduced.
3. Drag coefficients for flow channels between basket fuel tubes were added.

Each of the three refinements is discussed in turn.

The exterior convection heat transfer correlations used in the pretest simulations were obtained from commonly available open literature. Past experience has shown that they can often be improved upon for application to large casks. The coefficient for the finned surface of the side was adjusted for the post-test simulations. The correlation used has the form

$$Nu = C[Ra(L)]^n \qquad (5\text{-}6)$$

The values of C, n, and the significant length, L, are listed in Table 5-3.

Table 5-3

CONVECTION HEAT TRANSFER CORRELATIONS

Surface	C		n	L,cm
	Pretest	Post-Test		
Vertical fins	0.32	0.6	1/4	3.5
Horizontal fins	0.32	0.45	1/4	3.5

After the fifth test run (horizontal, nitrogen) was completed and the lid removed, cracks were observed at several weld locations in the top of the basket assembly (see Section 4 for a detailed discussion of this observation). It was concluded that inadequate clearance between the basket and cask cavity had not been allowed for the test basket. The gap between basket and cavity used in all pretest simulations was 1.5 mm. This gap was reduced to 0.01 mm for all post-test simulations.

The importance of this gap may, especially in the cases of nitrogen and vacuum backfills, have a significant effect on internal cask temperatures. The approximate temperature gradients in helium and nitrogen/vacuum are, respectively, 8°C/mm and 48°C/mm. These gradients are for 28 kW total decay heat generation rate and are based on the average heat flux at the axial elevation of peak cladding temperature. The gradients at most other axial elevations are less.

A review of the input files revealed that some drag coefficients had been omitted--most notably those relating to the angle support plates between basket fuel tubes. The effect of these drag coefficients is to reduce the magnitude of convection. The temperatures for the vacuum simulation were unaffected by this modification, the temperatures for the two horizontal simulations were slightly affected, and the temperatures for the vertical helium and vertical nitrogen simulations were markedly changed. Graphic displays of selected flow fields will be shown later in this subsection.

Post-Test Temperature Predictions Compared to Test Data. The presentation of comparisons of post-test predictions with temperature data and pretest predictions begins with a summary of peak cladding temperature comparisons for all five test runs. This summary is followed by comparisons of selected axial and radial temperature profile predictions with test data.

Pretest and post-test predictions of peak guide tube temperatures and ambient-to-peak guide tube temperature differences are compared to test data in the bar charts of Figure 5-12. The agreement between post-test predictions and test data is much improved over pretest predictions. A maximum discrepancy of 8°C between post-test predictions and data exists for the vertical and horizontal helium test runs. Therefore, peak guide tube temperatures were predicted within 3% or better.

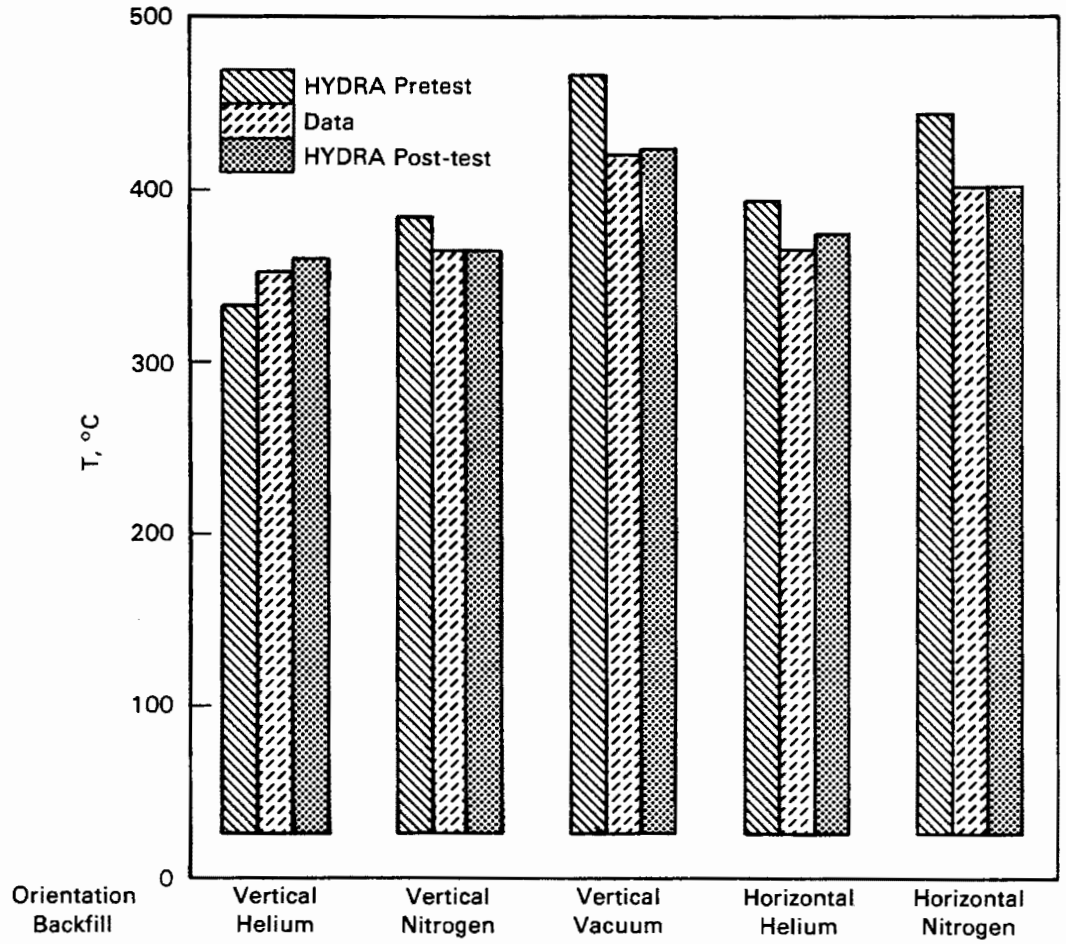

Figure 5-12. Post-Test Predictions Compared to Peak Guide Tube and Ambient-to-Peak Guide Tube Temperature Difference Data

Axial temperature profile predictions are compared to data for the vertical, helium test run in Figure 5-13. Temperatures on the exterior surface of the cask are now satisfactorily predicted. It will be seen in subsequent figures that satisfactory surface temperature predictions occur for all test runs. An adjustment to the exterior surface heat transfer coefficient was made as shown in Table 5-3.

Also shown in Figure 5-13 are the axial temperature profiles for an outer fuel assembly and the center fuel assembly. The agreement between predictions and data is good (15°C) for the outer assembly, and much improved (25°C) for the center assembly. Predicted center fuel assembly temperatures are increased over pretest predictions because of reduced convection, but the axial profile still indicates the influence of convection, i.e., hotter temperatures occurred in upper regions of the assemblies and cooler temperatures occurred in lower regions.

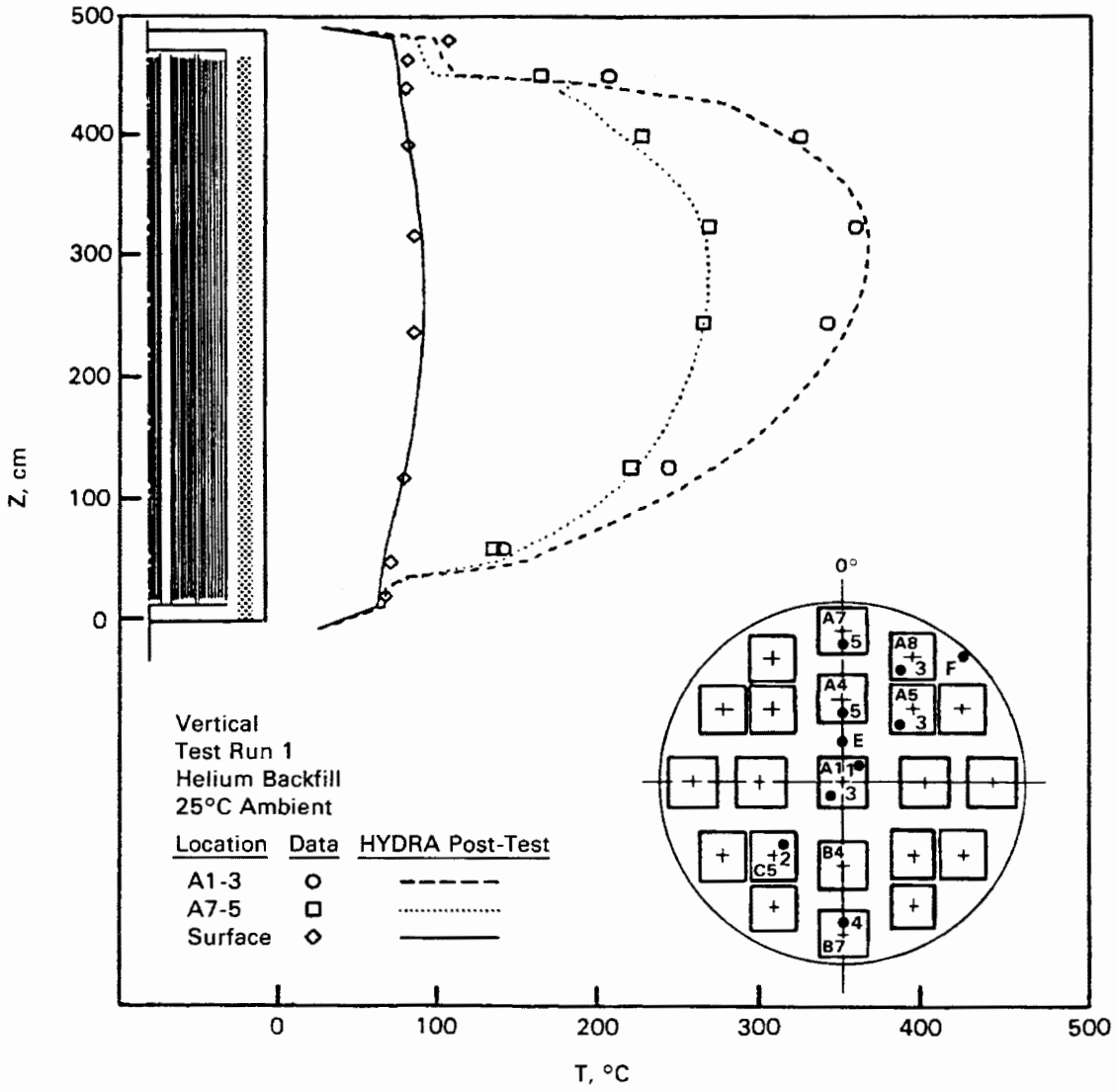

Figure 5-13. Post-Test Axial Temperature Profile Predictions Compared to Vertical, Helium Test Data

It can be seen in Figure 5-13 that temperatures at locations below the peak are slightly overpredicted and temperatures at locations above the peak are slightly underpredicted. It is speculated that the predicted axial decay heat generation rate profile is in error for some or all of the fuel assemblies. This source of uncertainty has been encountered in previous comparisons with cask data and could be reduced by experimental measurement (14, 15). This trend is common to all axial profile predictions presented in this section.

Figure 5-14 shows axial temperature profile predictions compared to data for the vertical, nitrogen test run. The reduced gap between the basket and the cask inner wall results in satisfactory predictions of temperatures (15°C) in the fuel assemblies. The influence of upward convection in the fuel assemblies is again indicated.

Figure 5-15 shows axial temperature profile predictions compared to data for the vertical, vacuum test run. The lack of significant convection for this test run results in peak temperatures being located near the axial elevation of peak decay

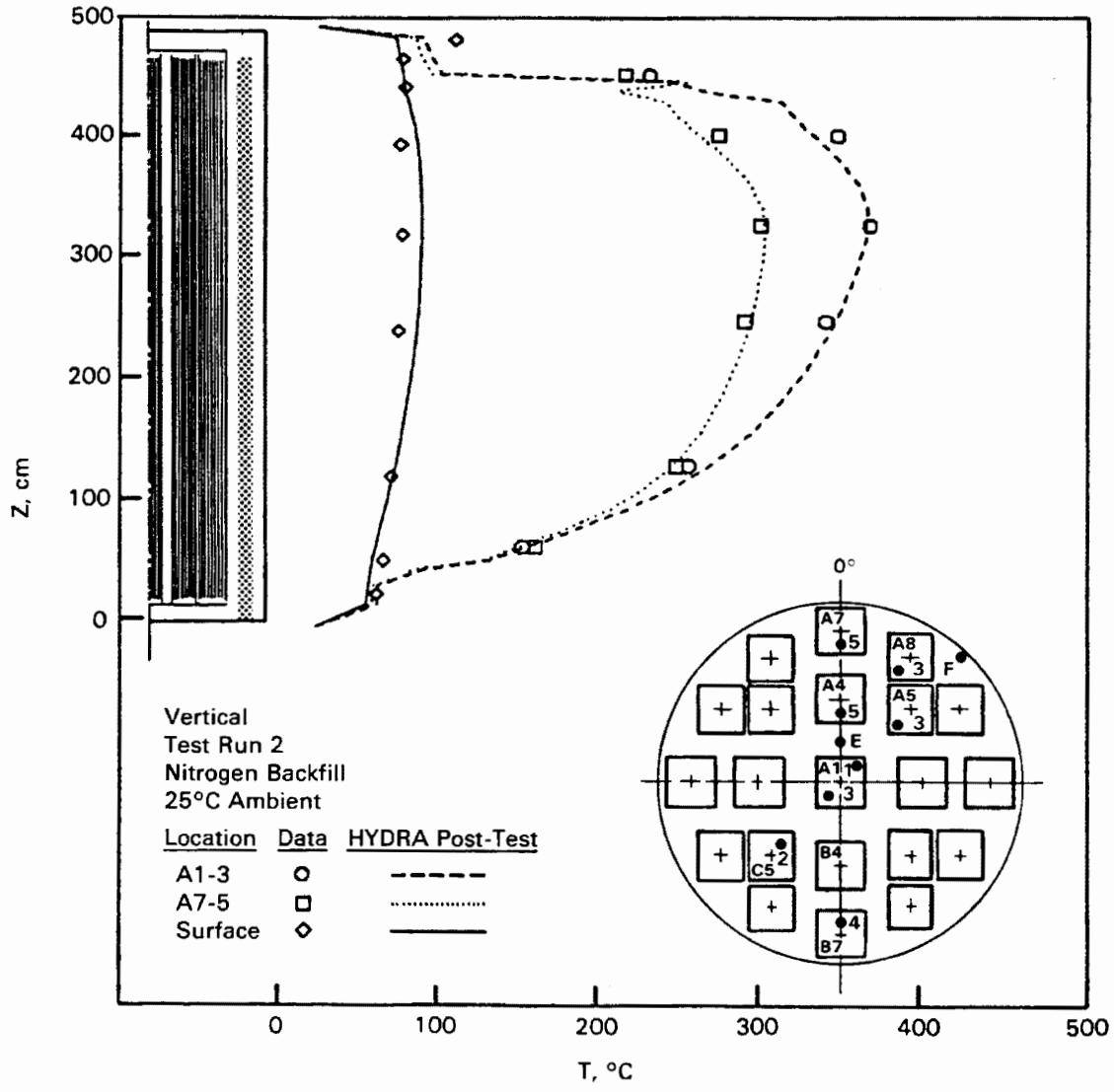

Figure 5-14. Post-Test Axial Temperature Profile Predictions Compared to Vertical, Nitrogen Test Data

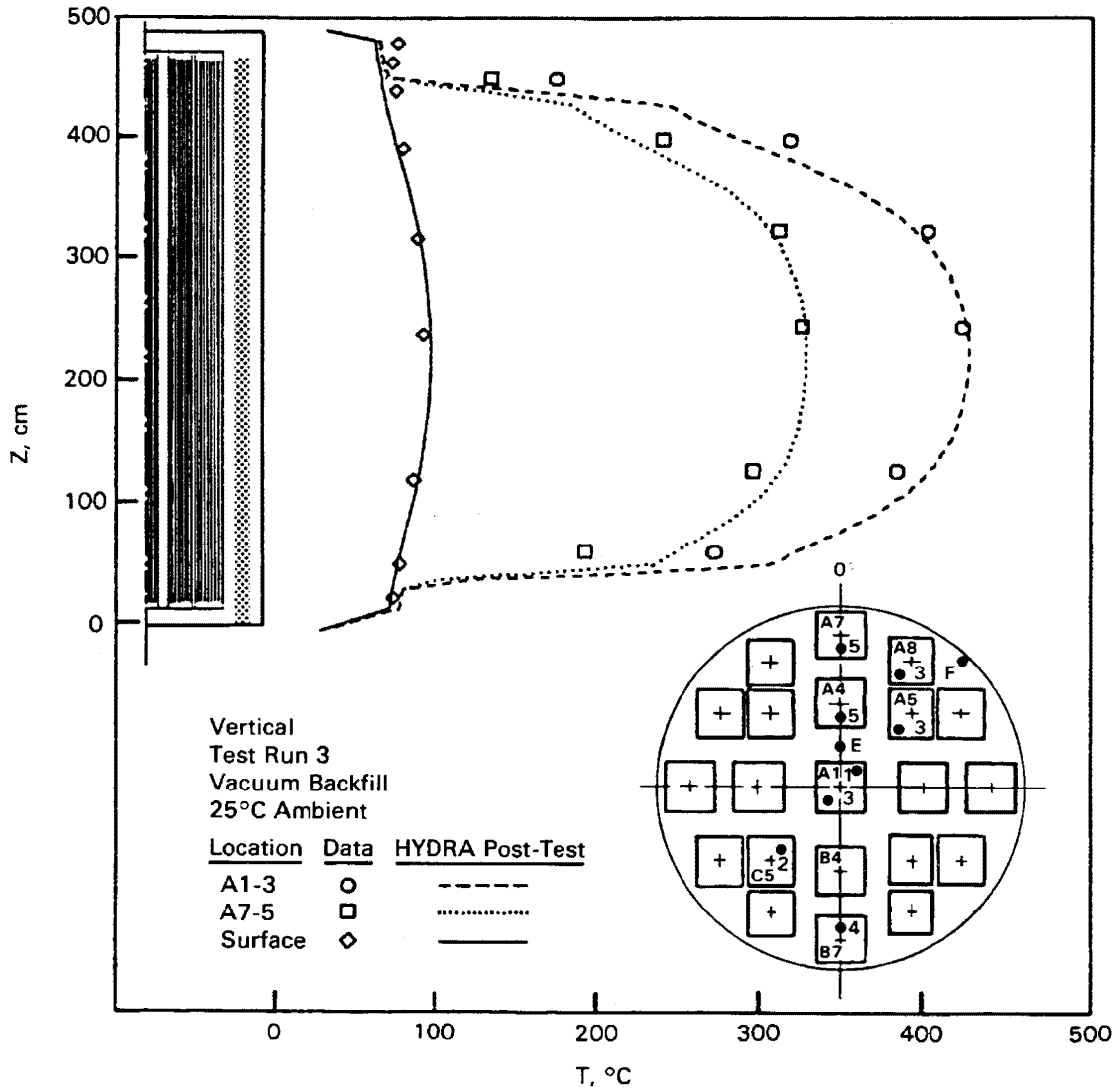

Figure 5-15. Post-Test Axial Temperature Profile Predictions Compared to Vertical, Vacuum Data

heat generation. As in the vertical, nitrogen test run, the temperatures in the outer fuel assembly are now accurately predicted.

Figure 5-16 shows axial temperature profile predictions compared to data for an outer fuel assembly generating 1.8 kW of heat. The results for the three vertical test runs are presented for comparison. Predictions agree exceptionally well with data for all three backfills. The effect of convection is seen in the helium and nitrogen test runs, but not in the vacuum run.

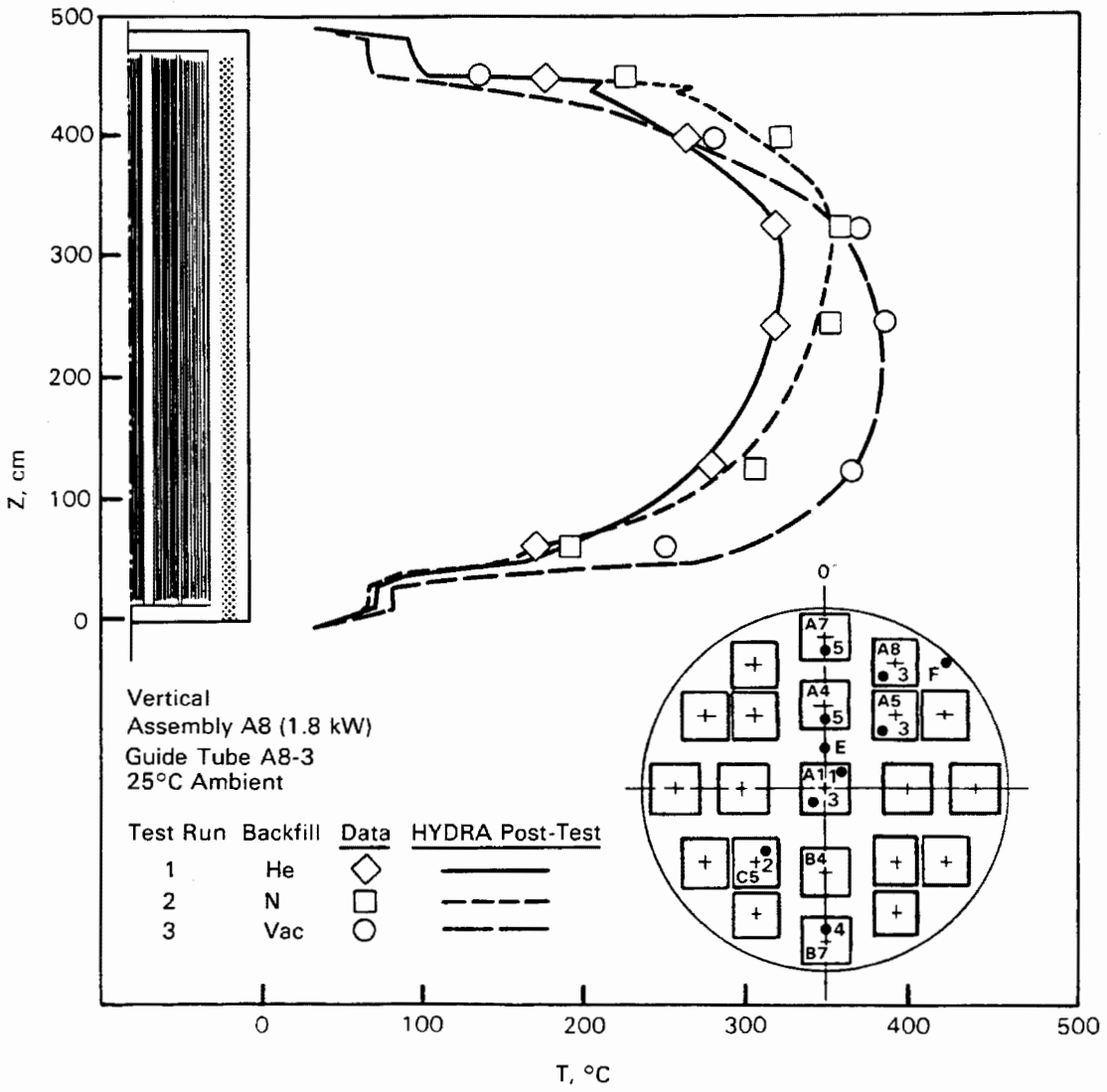

Figure 5-16. Post-Test Axial Temperature Profile Predictions Compared to Vertical, Helium, Nitrogen, and Vacuum 1.8-kW Outer Fuel Assembly Data

Figure 5-17 shows selected temperatures seen previously in Figures 5-13 and 5-16. The axial temperature profiles in the center fuel assembly (1.0 kW) and in one of the outer fuel assemblies generating 1.8 kW of heat are compared for the vertical, helium backfill test run. The peak temperatures in the 1.8-kW assembly are seen to be less than those in the 1.0-kW assembly. The 1.8-kW assembly is, of course, much closer to the relatively cool cask body. The upward mass fluxes in both assemblies are approximately the same, but the effect of convection compared to conduction and radiation heat transfer is more apparent in the center assembly. The conduction and

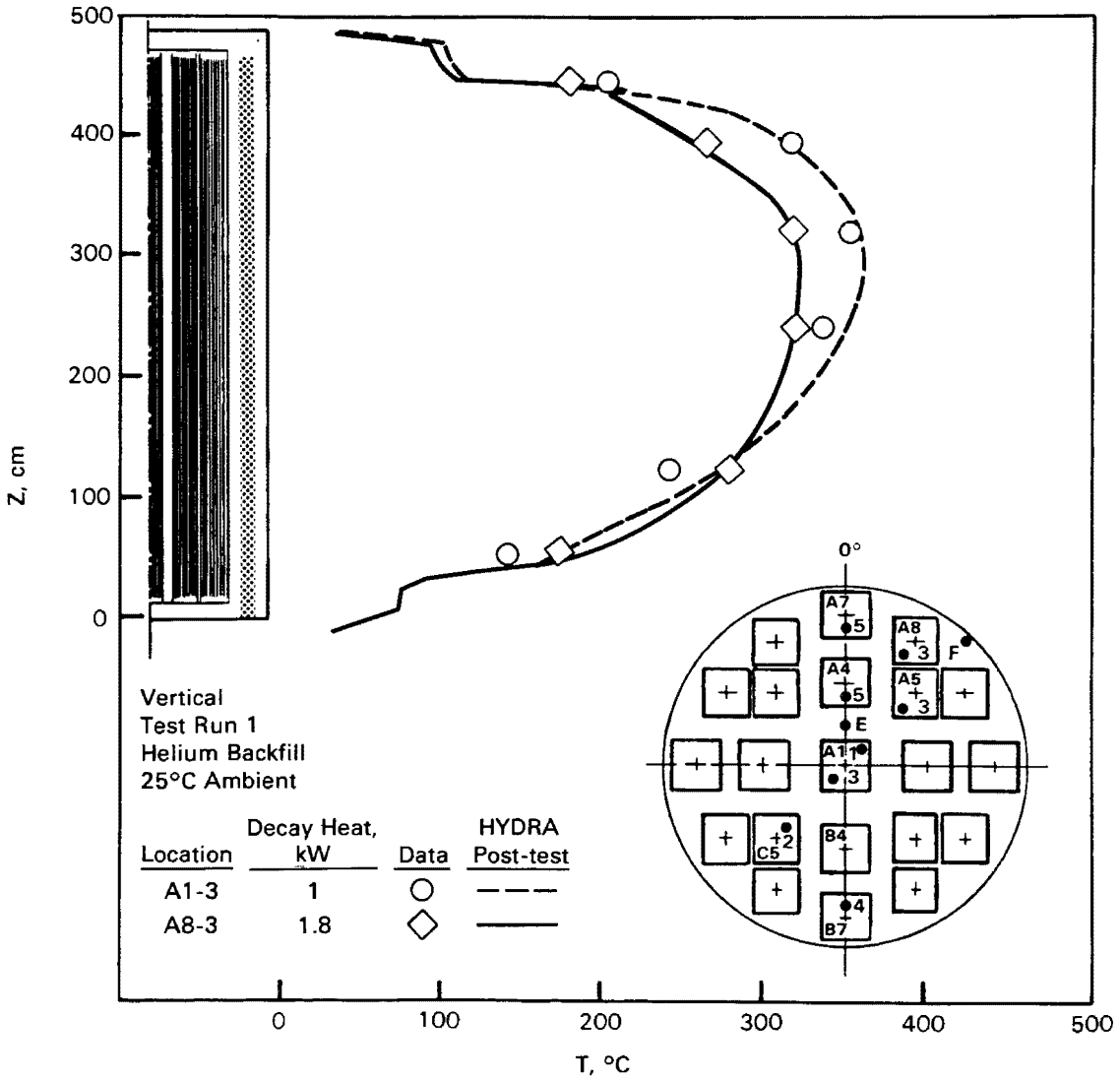

Figure 5-17. Post-Test Axial Temperature Profile Predictions Compared to Vertical, Helium, Test Data in Center 1-kW Assembly and Outer 1.8-kW Assembly

radiation heat transfer paths from the center assembly to the cask body are longer (more resistive) than for the 1.8-kW outer assembly.

Radial temperature profiles for the three vertical test runs from the center fuel assembly out to the cask surface are shown at the respective axial planes of peak guide tube temperature in Figure 5-18. Again, it can be seen collectively that the predicted and measured temperatures in the fuel assemblies are in good agreement. The disagreement between predicted and measured gas temperatures between assemblies A1 and A4 is probably caused by the uncertain location of the TC lances. The

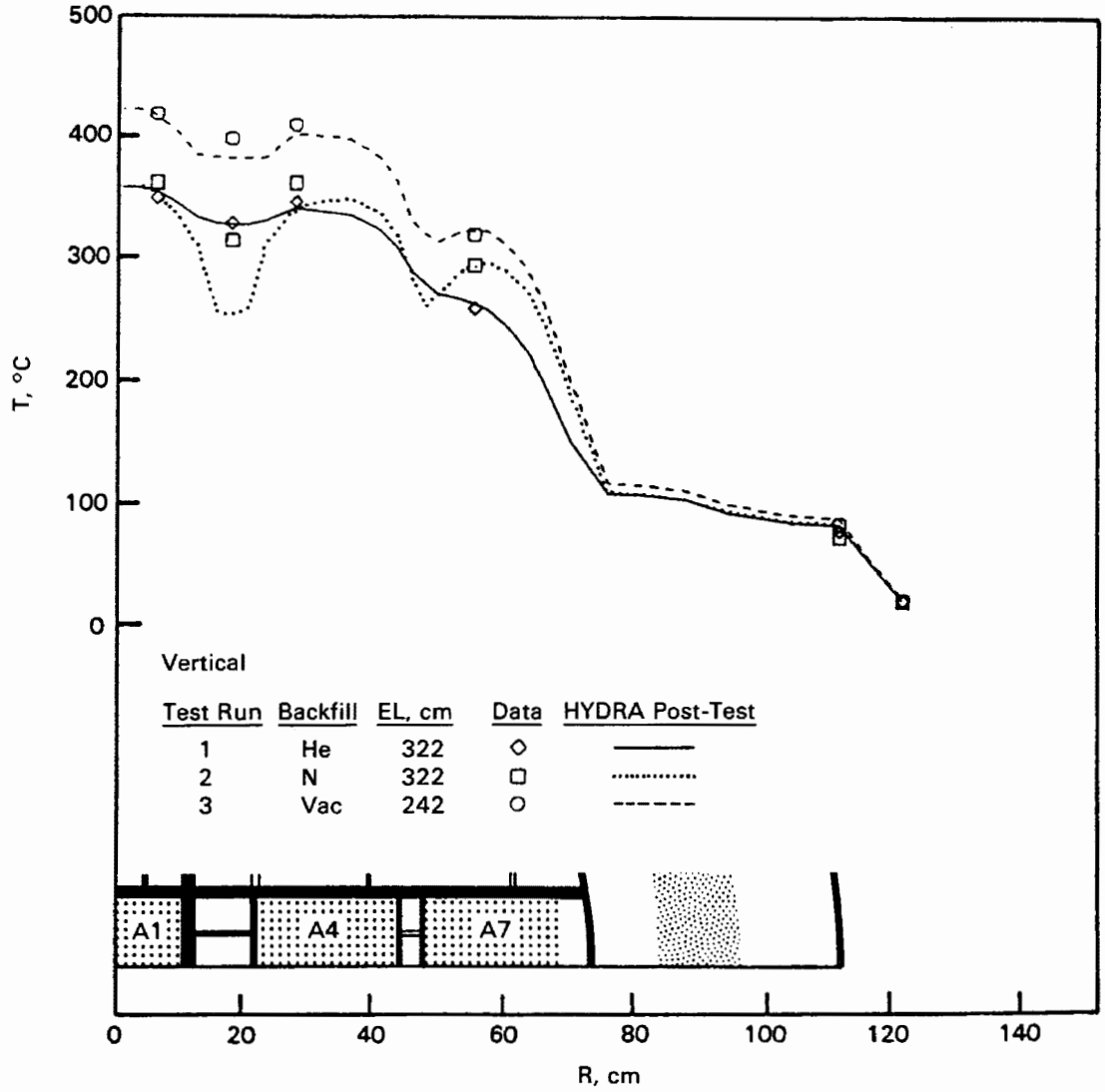

Figure 5-18. Post-Test Radial Temperature Profile Predictions Compared to Vertical, Helium, Nitrogen, and Vacuum Data at Axial Planes of Peak Guide Tube Temperatures

lances may be touching the basket, resulting in measured temperatures being greater than predicted temperatures. Even though the basket-to-inner wall gap was reduced from 1.5 mm to 0.01 mm for the post-test predictions, significant temperature differences (150°C to 200°C) are still predicted from the outer assembly to the inner cask wall.

Figures 5-19 and 5-20 show axial temperature profile predictions compared to data for the two horizontal test runs. The effects of axial convection are much reduced compared to those displayed for the corresponding vertical test runs as indicated by

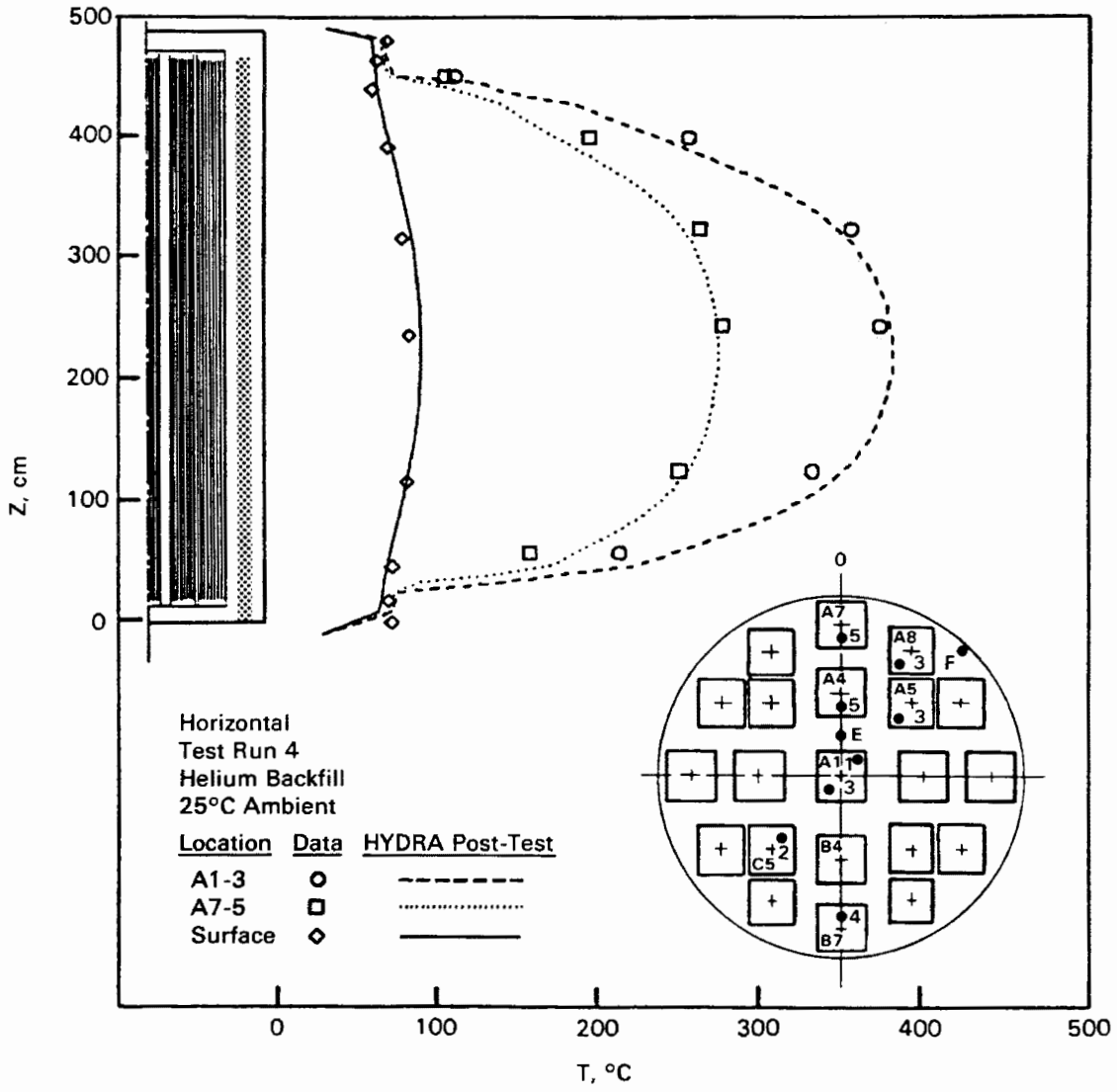

Figure 5-19. Post-Test Axial Temperature Profile Predictions Compared to Horizontal, Helium Data

the symmetry of the profiles about the axial assembly centerline. Predicted temperatures for the helium test run are now satisfactory (15°C), primarily because of an improved prediction of the cask surface temperature. The predicted temperatures for the nitrogen test run are also good (15°C).

Radial temperature profiles for the two horizontal test runs from cask surface-to-surface along the vertical diameter are illustrated at the respective axial planes of peak guide tube temperatures in Figure 5-21. The diameter is used because side-to-side symmetry is not present in a horizontal orientation. The two curves in

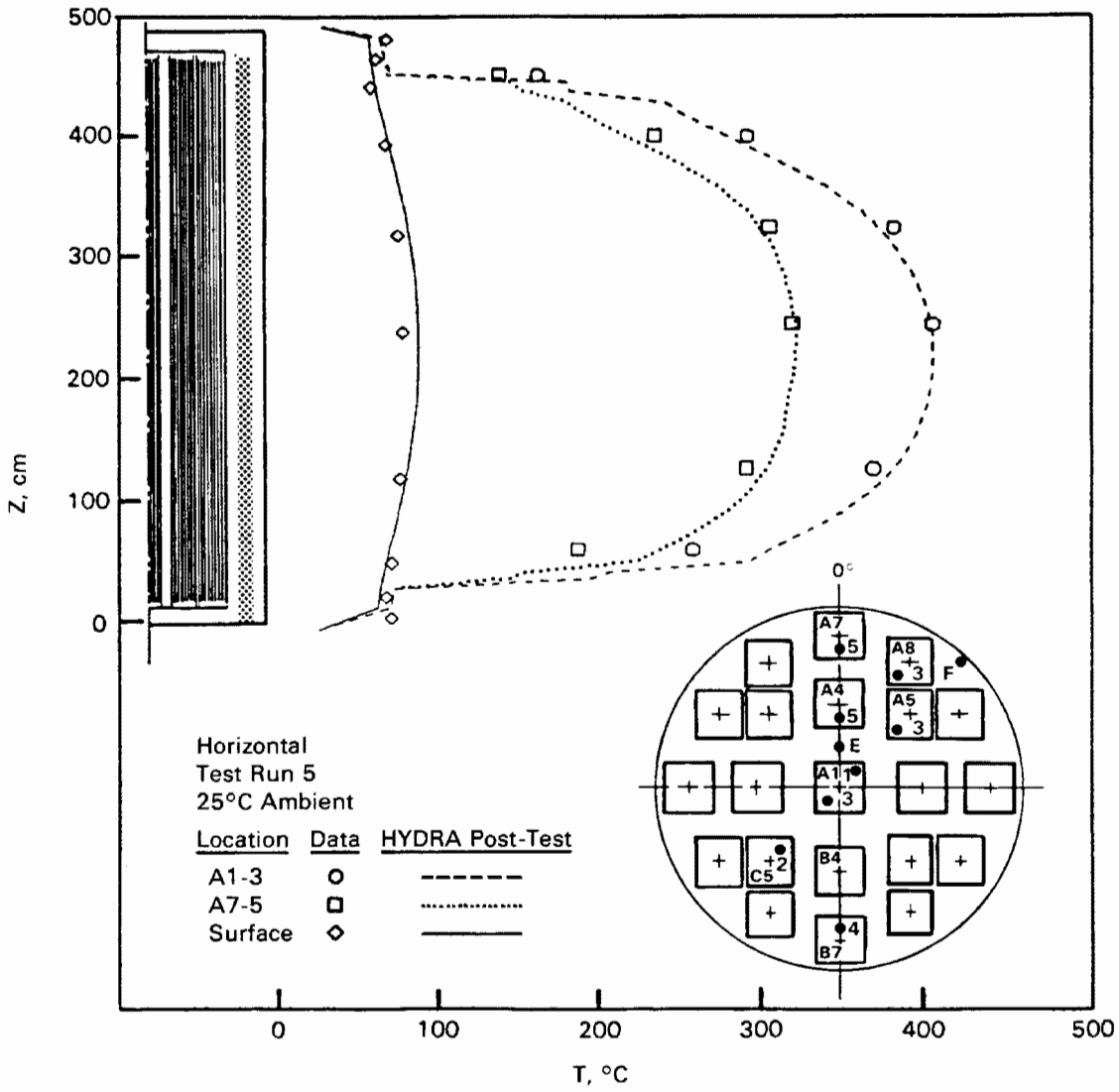

Figure 5-20. Post-Test Axial Temperature Profile Predictions Compared to Horizontal, Nitrogen Data

Figure 5-21 do, however, show very little asymmetry, suggesting the relative importance of conduction and radiation heat transfer compared to convection. Large temperature differences (150°C to 200°C) are again shown to be predicted between the outer assembly and the inner cask wall.

Some important observations should be pointed out regarding the pretest and post-test simulations before continuing with additional post-test results. Earlier in this section, in the subsection titled Modeling Uncertainties, a list of potential

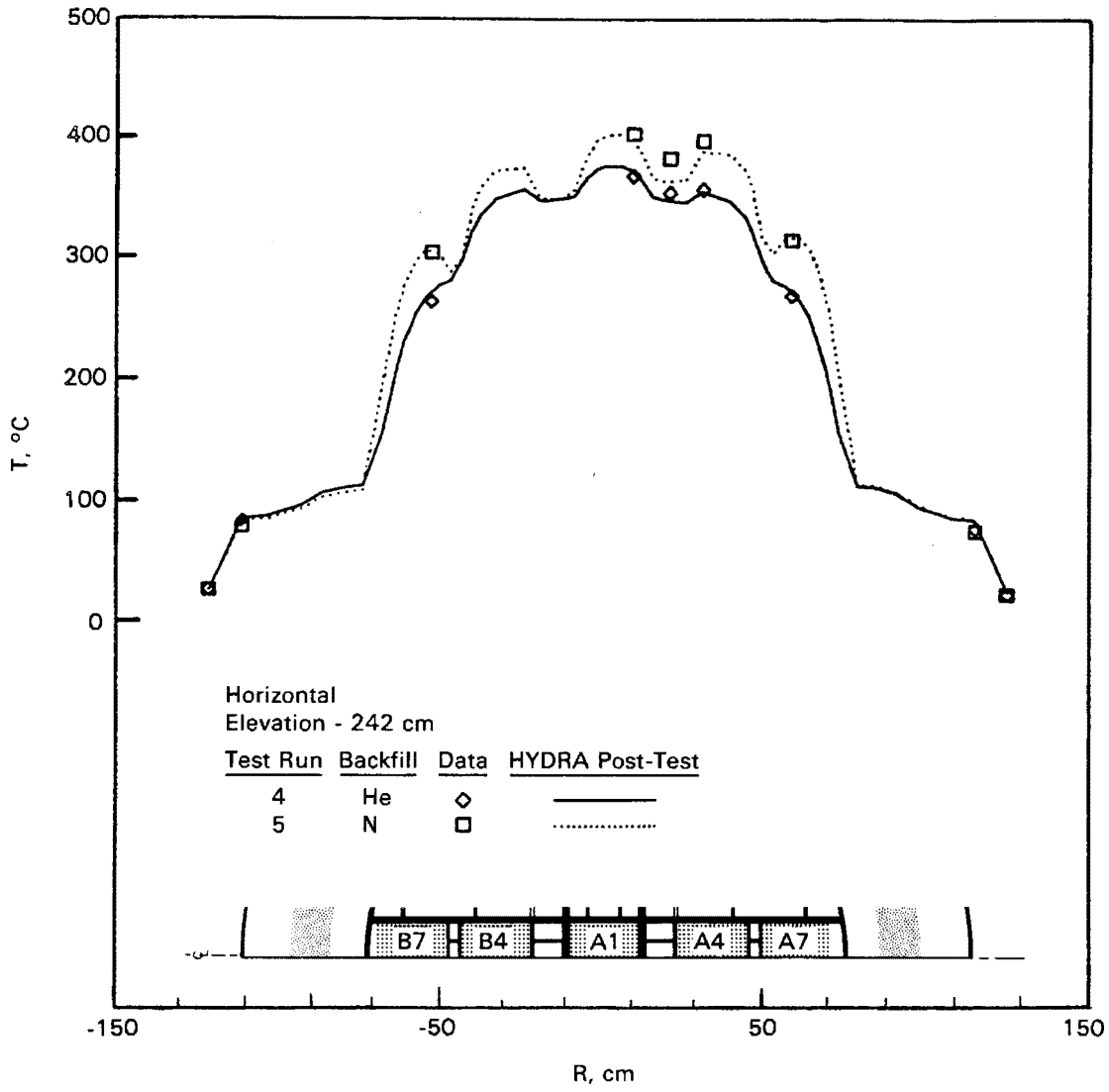

Figure 5-21. Post-Test Radial Temperature Profile Predictions Compared to Horizontal, Helium, and Nitrogen Data at Axial Planes of Peak Guide Tube Temperatures

uncertainties applicable to any HYDRA application was presented. Those that were encountered in this HYDRA analysis of the CASTOR-V/21 cask are presented for emphasis:

- Dimensional tolerances may be particularly significant when they influence small gaps with important thermal resistances. The input to HYDRA specified nominal dimensions.
- The total decay heat generation rate and the axial decay heat generation rate profile have a direct impact on predicted temperatures.

Both the total heat generation rate and the axial profile are amenable to experimental determination, and that is the preferred approach. Values used in HYDRA input were predictions from ORIGEN2 (Section 3).

- Convection heat transfer coefficients employed on the outside surface of the cask are known to result in approximate local heat transfer rates. The HYDRA input file specifies heat transfer coefficients based on information obtained in the open literature for conditions similar, but not identical, to surfaces of large casks.

- Finally, concerning the issue of human error, important flow resistances of support plates between the basket fuel tubes were unintentionally omitted from the pretest HYDRA input file.

Post-Test Predictions of Mass Fluxes. This subsection presents graphic displays of selected mass fluxes. These are helpful in interpreting the heat transfer performance of the CASTOR-V/21 cask. Mass fluxes rather than velocities are presented because the former are more directly related to convection heat transfer.

Figure 5-22 shows axial mass fluxes at the plane of peak guide tube temperature for the vertical, nitrogen test run. Relatively high flows are seen in the channels adjacent to the basket fuel tubes. Flow is generally upward in the interior regions of the basket and downward near the inner cask wall. A peak mass flux of approximately 0.03 g/sec-cm^2 can be seen from Figure 5-22 to be flowing down the cavity wall. The corresponding velocity is approximately 60 cm/sec. Upward mass fluxes in the fuel assemblies are approximately 0.001 g/sec-cm^2 with corresponding average assembly velocities being 2 cm/sec. A display of mass fluxes for the vertical, helium test run looks qualitatively similar to Figure 5-22 except that the mass fluxes are about an order of magnitude less. The convection flow in the vertical, vacuum test run also has a similar appearance, but the negligibly low mass fluxes are of no consequence to the temperature field.

Figure 5-23 shows a vector plot of mass fluxes for the vertical, nitrogen test run. The X-Z plane selected is one of the channels adjacent to basket fuel tubes and is identified in Figure 5-23. There is a general mass flow upward in the interior of the basket and downward next to the inner wall. The largest mass fluxes in this plane are horizontal and occur at the bottom of the cavity.

Figure 5-24 shows the flow pattern across the bottom of the cavity for the vertical, nitrogen test run. The largest mass flux is approximately 0.03 g/sec-cm^2. The results for helium are qualitatively similar but smaller by about an order of magnitude.

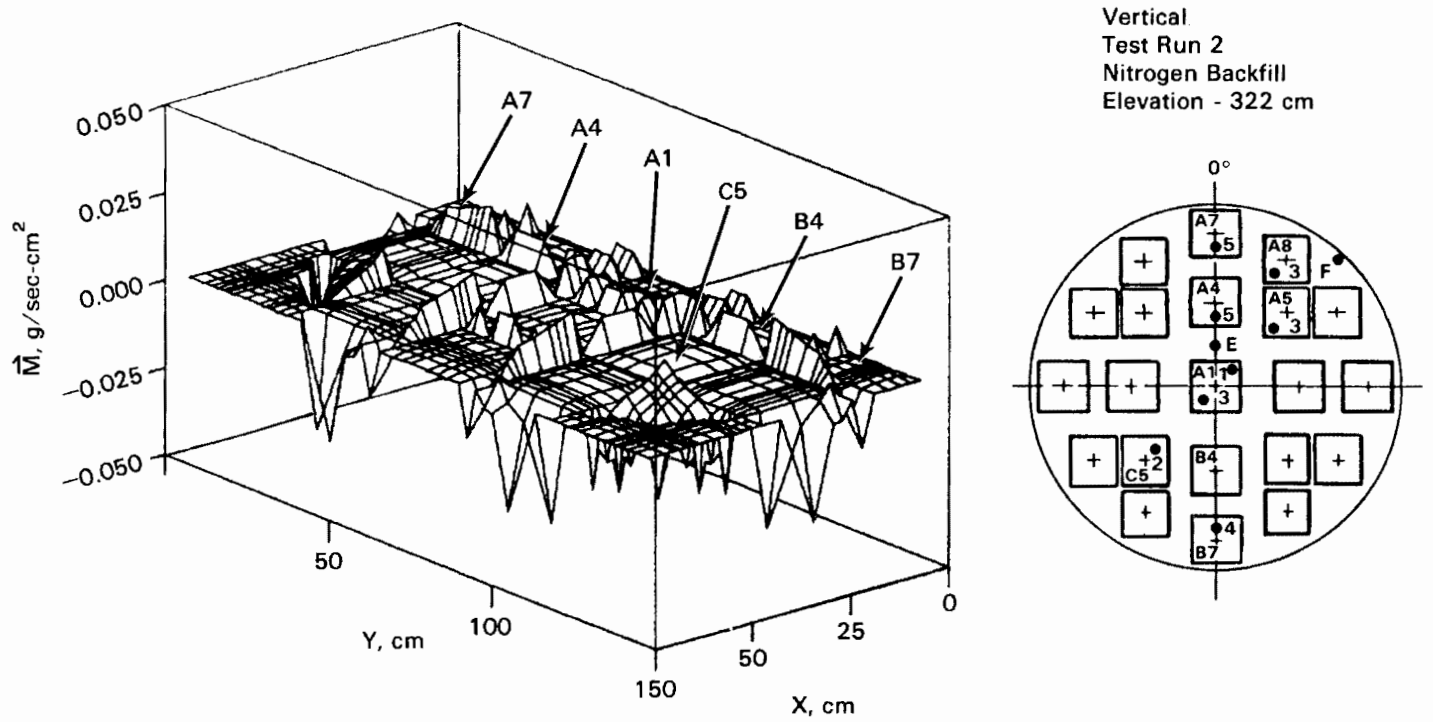

Figure 5-22. Axial Mass Fluxes at Plane of Peak Guide Tube Temperature for Vertical, Nitrogen Test Run

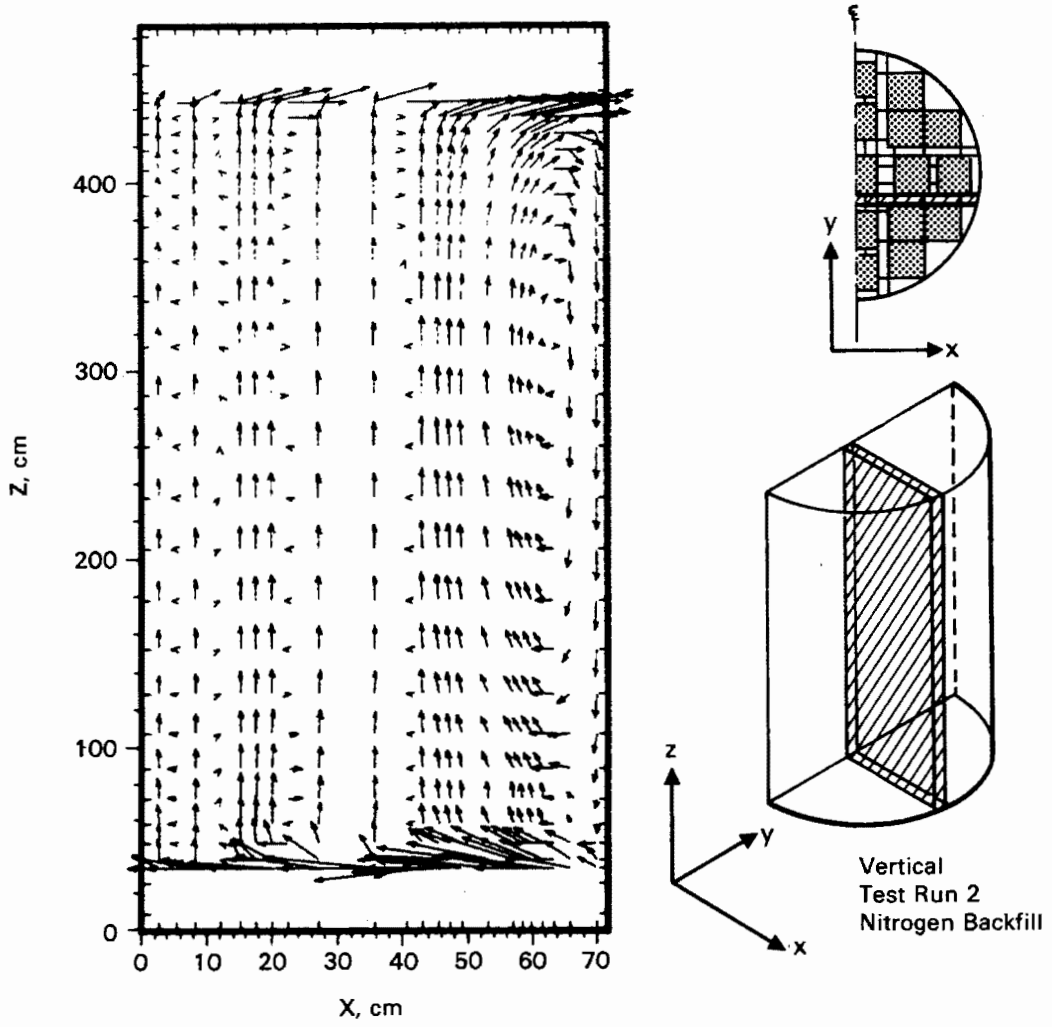

Figure 5-23. Vector Plot of Mass Fluxes in X-Z Plane for Vertical, Nitrogen Test Run

Figures 5-25 and 5-26 reflect flow patterns when the cask is horizontal and back-filled with nitrogen. Figure 5-25 depicts flow in a vertical Y-Z plane in a channel between basket fuel tubes. A number of recirculation cells are noticeable. There appears to be little or no axial end-to-end circulation, but rather a line of near-zero axial flow at an axial distance of about 220 cm. The largest fluxes are those at the cavity end shown in Figure 5-26 and are approximately 0.04 g/sec-cm^2. The largest fluxes for helium backfill at corresponding locations are about an order of magnitude less.

The mass flux maps presented in this subsection were constructed from local vector components in the respective planes. Mass flux maps of local vector components for

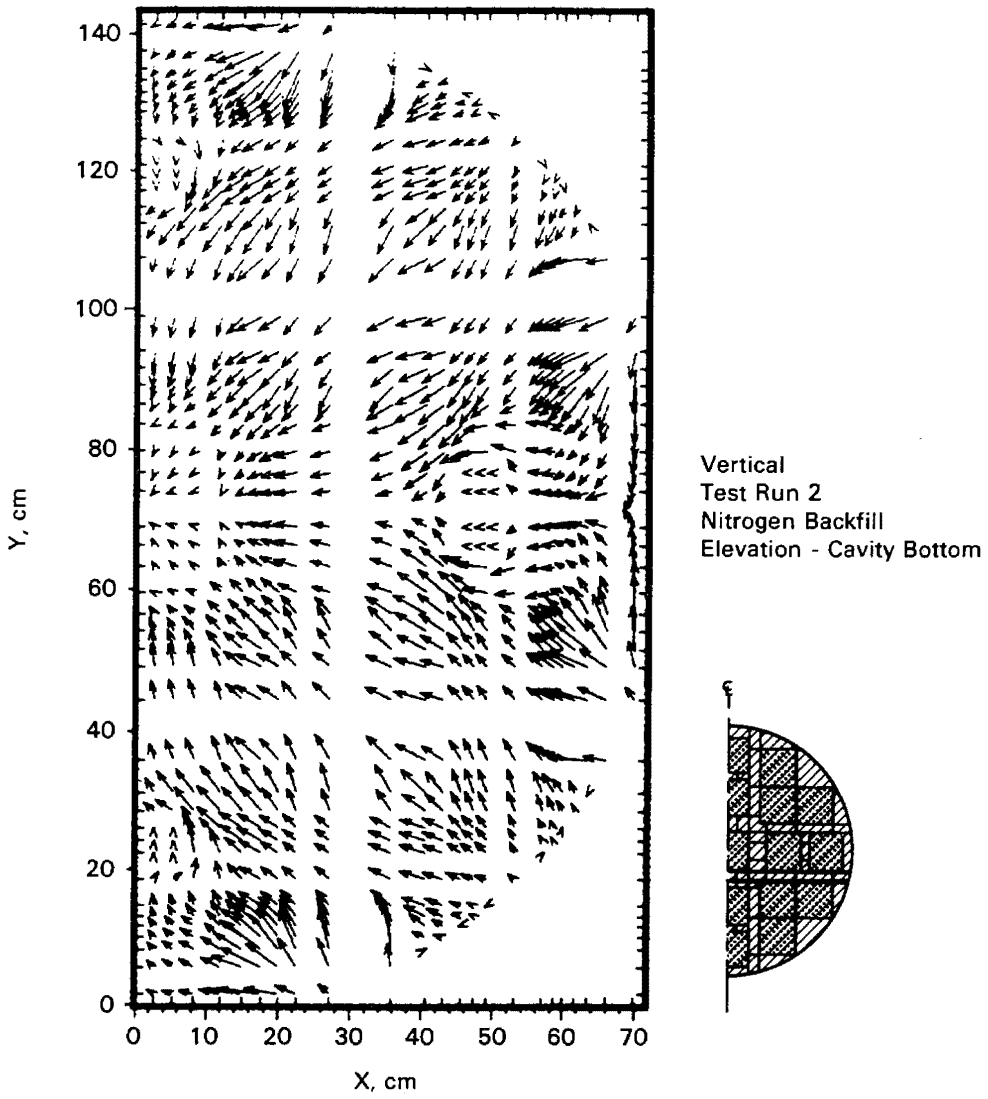

Figure 5-24. Vector Plot of Mass Fluxes in X-Y Plane at Bottom of Cavity for Vertical, Nitrogen Test Run

the entire cask inner cavity flow channels are available in HYDRA output. These vector plots (maps) can be appropriately selected to clearly indicate both local and global mass fluxes necessary to obtain a better understanding of cask performance and to identify promising approaches to cask optimization.

Post-Test Predictions of Heat Fluxes. This subsection presents graphic displays of selected heat fluxes to help interpret the heat transfer performance of the cask. Heat flux maps identify major heat transfer paths and paths that do not effectively transfer heat.

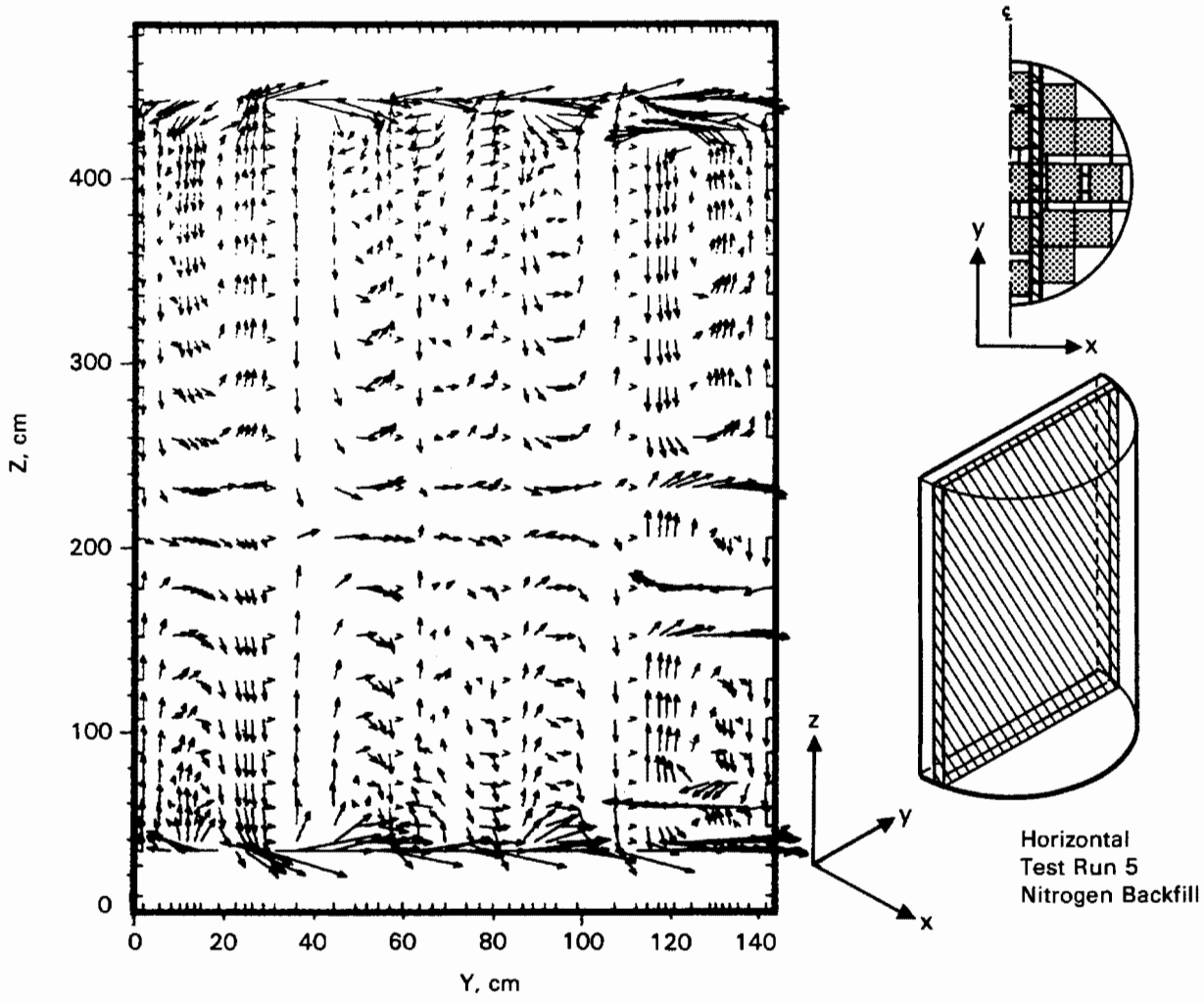

Figure 5-25. Vector Plot of Mass Fluxes in Y-Z Plane for Horizontal, Nitrogen Test Run

Heat fluxes in the X-Y plane at the axial location of peak guide tube temperature for the vertical, helium test runs are shown in Figure 5-27. The highest heat fluxes are directed along the solid borated stainless steel basket members next to the inner cask wall. Their magnitude is approximately 1.0 W/cm^2. Heat fluxes in the two large channels next to the inner cask wall are seen to be directed inward (at this axial plane). This reflects convection heat transfer. A vector plot of heat fluxes for the vertical, nitrogen test run is qualitatively similar.

Finally, Figure 5-28 shows heat fluxes in the vertical x-y plane at the axial location of peak guide tube temperature for the horizontal, nitrogen test run. Heat fluxes directed outward along the borated stainless steel basket members are

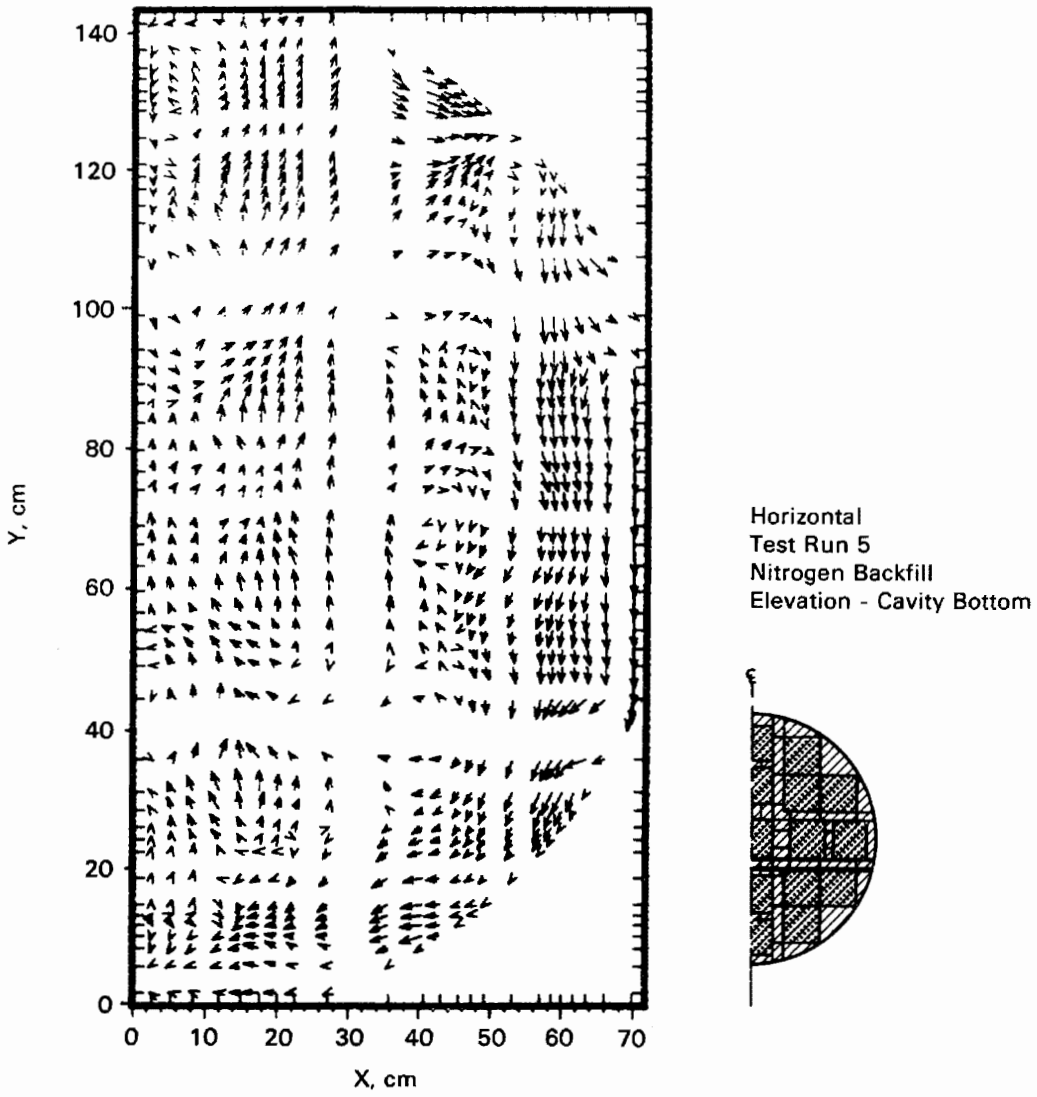

Figure 5-26. Vector Plot of Mass Fluxes in X-Y Plane at Bottom of Cavity for Horizontal, Nitrogen Test Run

approximately 2.0 W/cm^2 near the inner cask wall. Strong recirculation is indicated in the two large channels near the inner cask wall for the horizontal orientation. Magnitudes of heat fluxes approach 2.0 W/cm^2. A vector plot for the horizontal, helium test run appears qualitatively similar.

The heat flux maps presented in this subsection were constructed from local vector components in the respective planes. Heat flux maps of local vector components for the entire cask are available in HYDRA output. These vector plots (maps) can be appropriately selected to provide a clear indication of both local and global heat

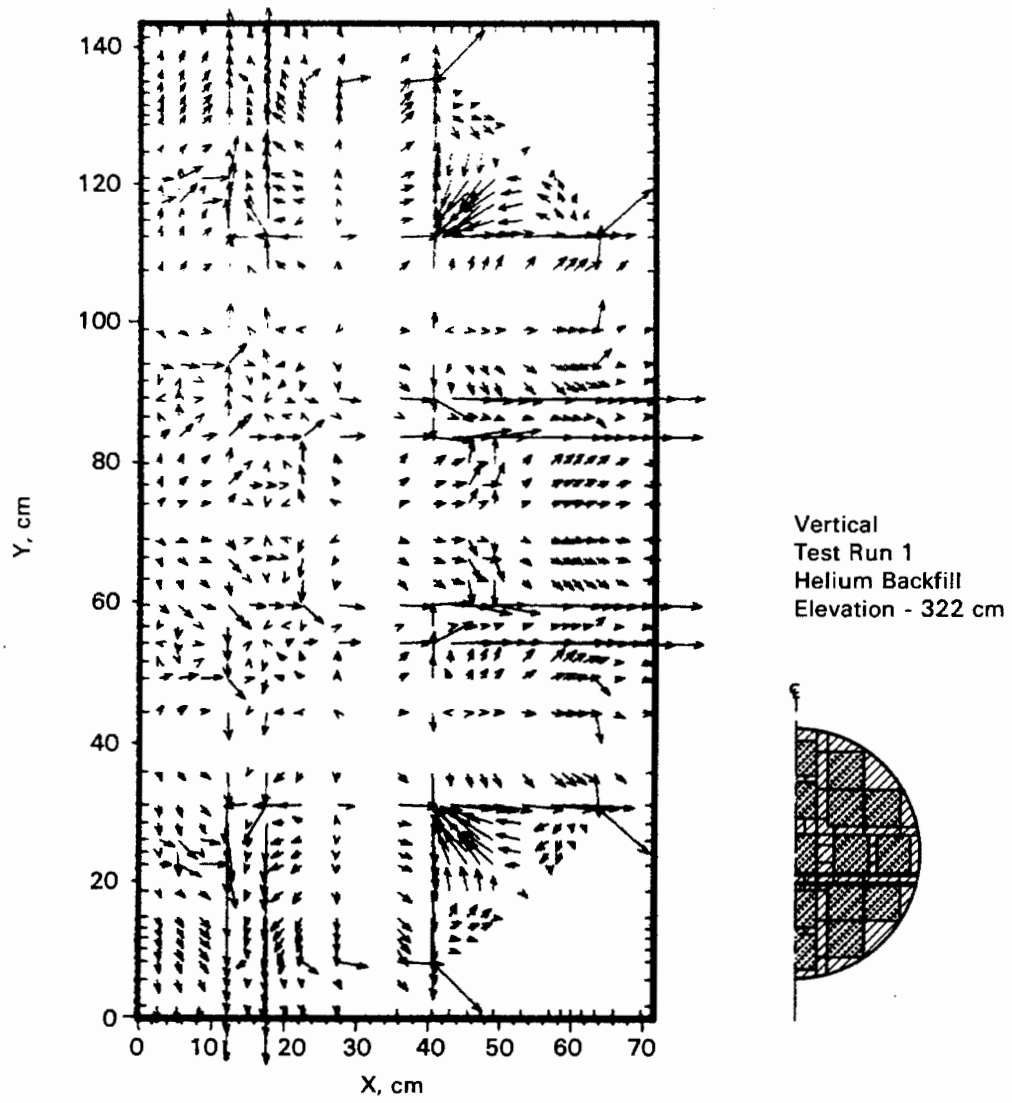

Figure 5-27. Vector Plot of Heat Fluxes in X-Y Plane at Axial Position of Peak Guide Tube Temperature for Vertical, Helium Test Run

fluxes necessary to obtain a better understanding of cask performance and to identify promising approaches to cask optimization.

PREDICTIONS OF CASK HEAT DISSIPATION LIMITS

The results of two additional simulations are presented in this section. The purpose of these simulations was to predict the total decay heat the cask can dissipate for a peak cladding temperature of approximately 370°C with each fuel assembly generating an equal amount of heat.

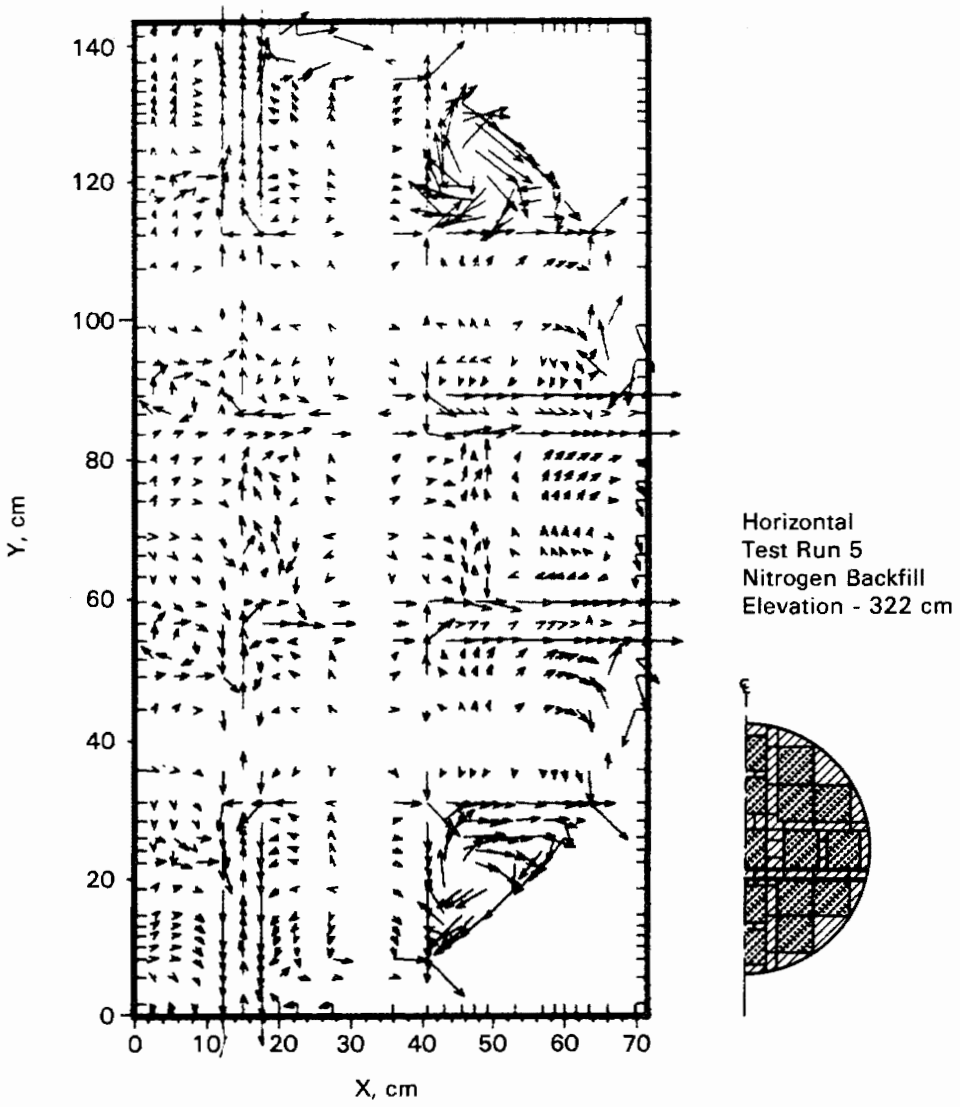

Figure 5-28. Vector Plot of Heat Fluxes in X-Y Plane at Axial Position of Peak Guide Tube Temperature for Horizontal, Nitrogen Test Run

The simulations were for a vertical cask with both helium and nitrogen backfills. Special features of both simulations are:

- 1-mm (0.039-in.) gap between basket and cask inner wall
- uniform fuel assembly decay heat generation rates
- 38°C ambient temperature
- 380°C allowable cladding temperature
- 0.6-bar backfill pressure.

All other specifications were the same as used for the post-test simulations.

Results of HYDRA predictions are presented in Table 5-4 and in Figures 5-29 and 5-30. As indicated in Table 5-4, cask decay heat dissipation limits predicted for a vertical cask with helium and nitrogen backfills were approximately 25 kW and 22 kW, respectively. Peak cladding temperatures of 369°C in helium and 375°C in nitrogen were predicted to result.

Figures 5-29 and 5-30 show the center assembly cladding temperature versus axial position for the two simulations. Also shown for comparison are the post-test predictions of the vertical helium and the vertical nitrogen test runs. When comparing decay heat dissipation limit predictions to post-test predictions, it should be kept in mind that post-test fuel assembly decay heat generation rates were not uniformly identical and that the ambient temperatures are not equal. Comparisons of the data and the two sets of predictions in each figure lead to the conclusion that predicted cask heat dissipation limits will be reasonably correct.

Table 5-4

PREDICTED CASK DECAY HEAT DISSIPATION LIMITS

Backfill Gas	Peak Cladding Temperature, °C	Total Decay Heat, kW
Helium	369	25.2
Nitrogen	375	21.8

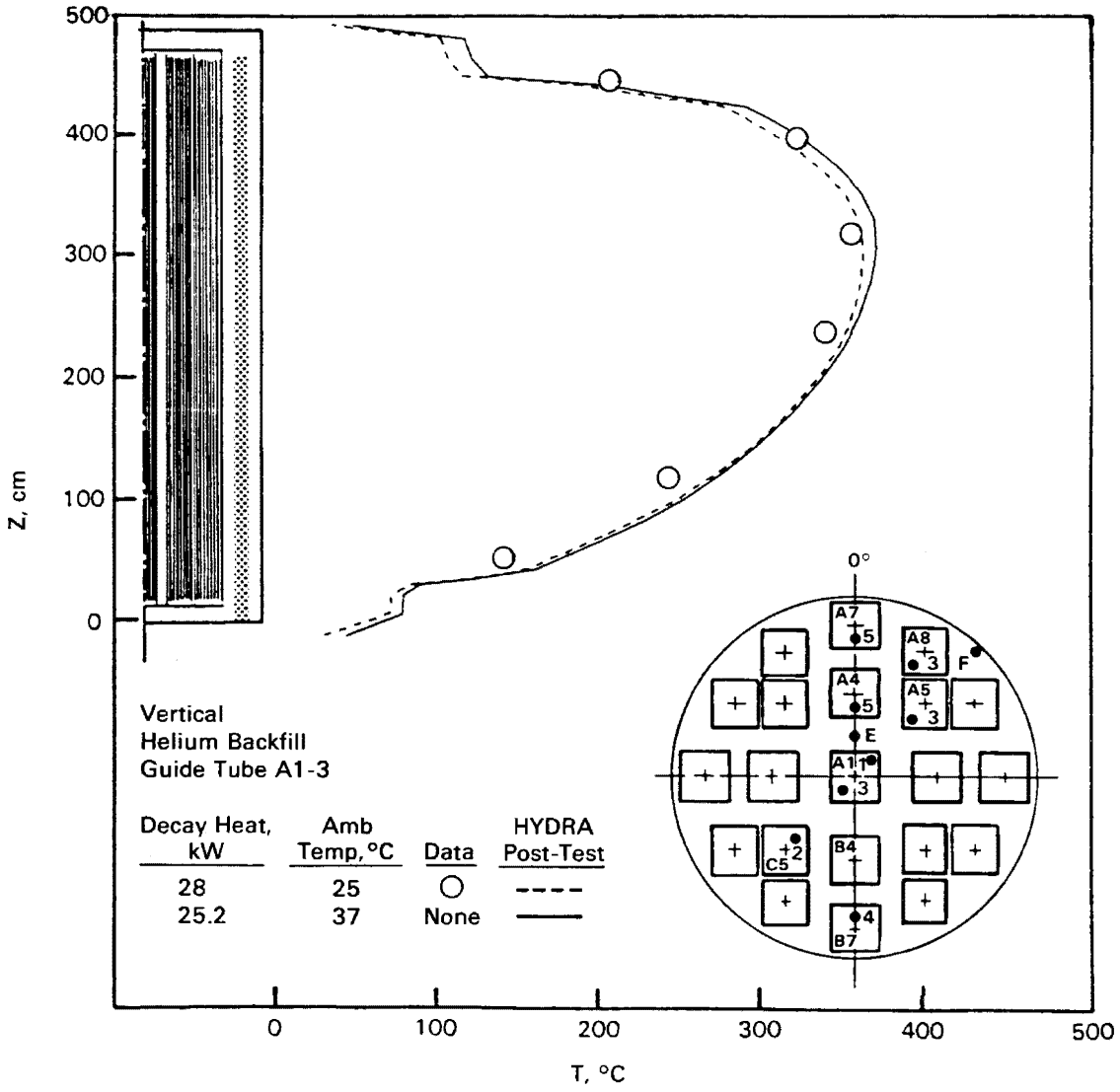

Figure 5-29. Axial Temperature Profile Prediction for 25.2 kW Total Uniform Heat Dissipation Compared to Vertical, Helium Test Data and Post-Test Prediction for 28 kW Total Heat Dissipation

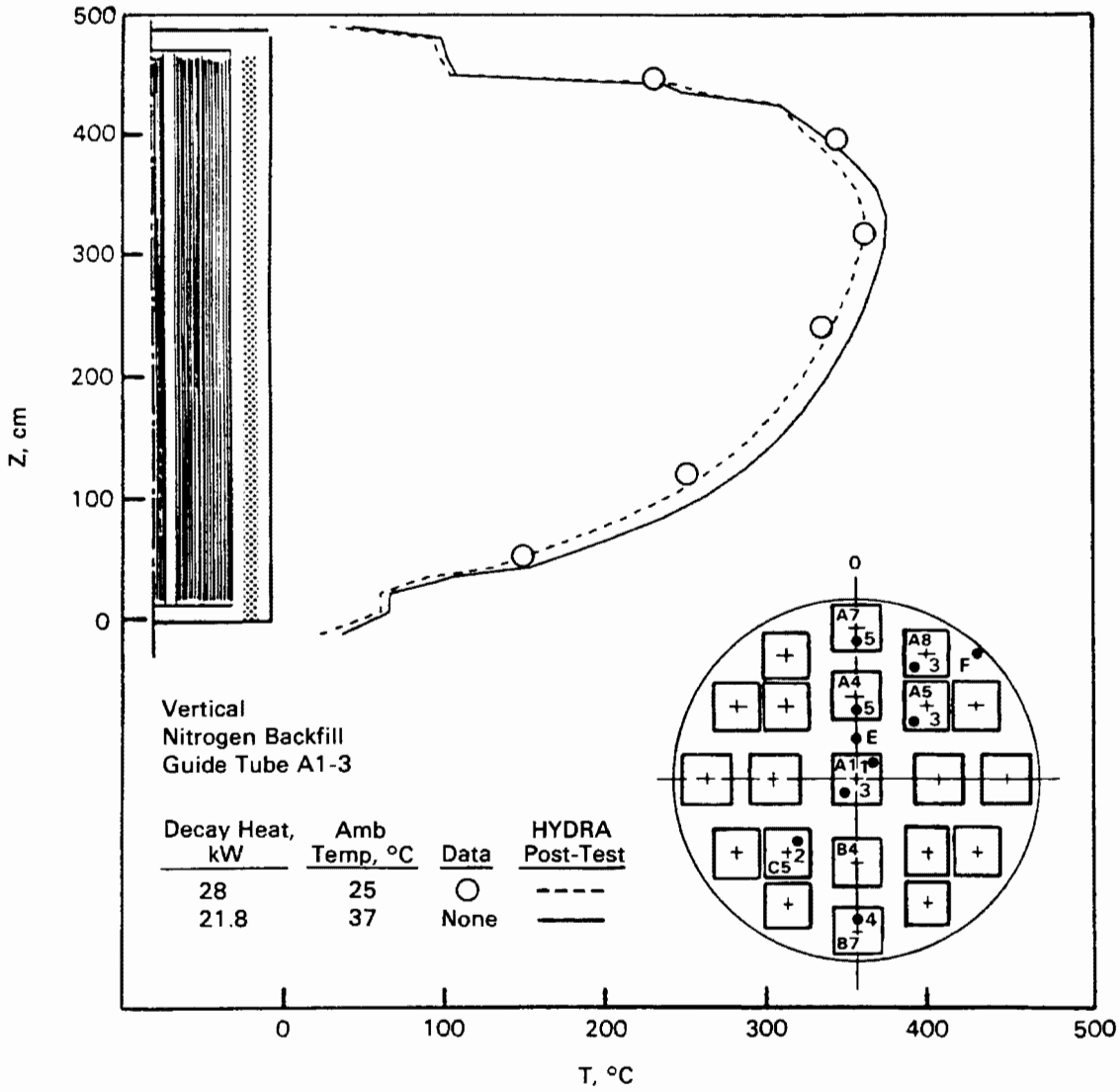

Figure 5-30. Axial Temperature Profile Predictions for 21.8-kW Total Uniform Heat Dissipation Compared to Vertical, Nitrogen Test Data and Post-Test Prediction for 28 kW Total Heat Dissipation

Section 6

REFERENCES

1. U.S. Department of Energy. Spent Fuel Storage Requirements. Richland, Washington: Richland Operations Office, 1985. DOE/RL-85-2.

2. General Nuclear Services, Inc. Topical Safety Analysis Report for the CASTOR-V/21 Cask Independent Spent Fuel Storage Installation (Dry Storage). Washington, D.C.: U.S. Nuclear Regulatory Commission, 1985. U.S. NRC Project Docket M-37.

3. K. R. Kingsley and V. J. Barnhart. CASTOR-V/21 Spent Fuel Dry Storage Cask Technical and Operations Manual. Avon, Connecticut: General Nuclear Services, Inc., 1985.

4. M. A. McKinnon, J. W. Doman, J. E. Tanner, R. J. Guenther, J. M. Creer, and C. E. King. BWR Spent Fuel Storage Cask Performance Test: Volume I - Cask Handling Experience and Decay Heat, Heat Transfer, and Shielding Data. Richland, Washington: Pacific Northwest Laboratory, 1986. PNL-5777 Vol. I.

5. F. M. Cummings. TACI-A Code for Interactive Analysis of Neutron Data Produced by a Tissue Equivalent Proportional Counter. Richland, Washington: Pacific Northwest Laboratory, 1984. PNL-5136.

6. A. G. Croff. ORIGEN-2--A Revised and Updated Version of the Oak Ridge Isotope Generation and Depletion Code. Oak Ridge, Tennessee: Oak Ridge National Laboratory, 1980. ORNL-5621.

7. W. D. Leggett III and L. D. Eisenhart. "INCORE Code." Richmond, Virginia: Virginia Power Company, 1967. WCAP-7149.

8. T. K. Ross. "NEWTOTE Code." Richmond, Virginia: Virginia Power Company, 1984. NFD-CCR-6, Rev. 8.

9. A. B. Johnson, Jr., and E. R. Gilbert. Technical Basis for Storage of Zircaloy Clad Fuel in Inert Gases. Richland, Washington: Pacific Northwest Laboratory, 1983. PNL-4835.

10. R. B. Davis. Data Report for the Nondestructive Examination of Turkey Point Spent Fuel Assemblies B02, B03, B17, B41, and B43. Richland, Washington: Hanford Engineering Development Laboratory, 1980. HEDL-TME-79-68.

11. R. Gunnink and J. B. Niday. Computerized Quantitative Analysis of Gamma Ray Spectrometry. Livermore, California: University of California Research Laboratory, 1972. UCRL-51061.

12. Keithly DAS Series 500 Measurement and Control System. Solon, Ohio: Keithly DAC Division and Control, 1984. Document No. 500-904-01B.

13. E. R. Gilbert, C. A. Knox, and G. D. White. "Behavior of Spent LWR Fuel in Nitrogen and in Air." In Proceedings, Third International Spent Fuel Storage Technology Symposium/Workshop, Vol. I, 1986, pp. S263-S278.

14. J. M. Creer. "Decay Heat and Heat Transfer Predictions for Spent Fuel Storage Systems." In Proceedings, Second International Irradiated Fuel Storage Operating Experience and Development Program Workshop, 1984, pp. 157-209.

15. D. R. Rector, R. A. McCann, U. P. Jenquin, C. M. Heeb, J. M. Creer, and C. L. Wheeler. CASTOR-1C Spent Fuel Storage Cask Decay Heat, Heat Transfer, and Shielding Analyses. Richland, Washington: Pacific Northwest Laboratory, 1986. PNL-XXXX.

16. General Nuclear Services, Inc. Evaluation of a CASTOR-V/21 Fuel Basket Subjected to a Dry Spent Fuel Storage Demonstration Test at Idaho National Engineering Laboratory. Washington, D.C.: U.S. Nuclear Regulatory Commission, 1985. U.S. NRC Project Docket M-37.

17. L. E. Wiles, N. J. Lombardo, C. M. Heeb, U. P. Jenquin, T. E. Michener, C. L. Wheeler, J. M. Creer, and R. A. McCann. BWR Spent Fuel Storage Cask Performance Test: Volume II - Pre- and Post-Test Decay Heat, Heat Transfer, and Shielding Analyses. Richland, Washington: Pacific Northwest Laboratory, 1986. PNL-5777 Vol. II.

18. C. L. Wheeler, R. A. McCann, N. J. Lombardo, D. R. Rector, and T. E. Michener. "HYDRA and COBRA-SFS Temperature Calculations for CASTOR-1C, REA 2023, CASTOR-V/21, and TN-24P Casks." In Proceedings, Third International Spent Fuel Storage Technology Symposium/Workshop, Vol. I, 1986, pp. S77-S98.

19. S. V. Patankar. Numerical Heat Transfer and Fluid Flow. Washington, D.C.: Hemisphere, 1980.

20. J. Douglas and J. Gunn. "A General Formulation of Alternating Direction Methods." I. Numer. Math., Vol. 6, 1964, p. 428.

21. G. D. Raithby and G. E. Schneider. "Numerical Solution of Problems in Incompressible Fluid Flow: Treatment of Velocity-Pressure Coupling." Numer. Heat Transfer, Vol. 2, 1979, pp. 417-440.

22. G. D. Raithby and G. E. Schneider. "Erratum." Numer. Heat Transfer, Vol. 3, 1980, p. 513.

23. Y. S. Touloukian and C. Y. Ho. Thermophysical Properties of Matter. Lafayette, Indiana: Thermophysical Properties Research Center, Purdue University, 1970.

24. L. E. Sissom and D. R. Pitts. Elements of Heat Transfer Phenomena. New York: McGraw-Hill, 1972.

25. J. B. Chaddock. "Free Convection Heat Transfer from Vertical Rectangular Fin Arrays." ASHRAE Journal, August 1970, pp. 53-60.

Appendix A

FUEL ASSEMBLY DATA

Table A-1

SURRY 2, CYCLE 3 REACTOR OPERATING HISTORY

Dates, mo/da/yr		Elapsed Time,	Reactor Power Level,
From	To	days	Fraction of 2441 MWth
06/10/76	06/10/76	1	0.200
06/11/76	06/12/76	2	0.755
06/13/76	07/29/76	47	0.991
07/30/76	07/30/76	1	0.283
07/31/76	08/02/76	3	0.0
08/03/76	08/03/76	1	0.684
08/04/76	08/14/76	42	0.986
08/15/76	08/15/76	1	0.541
08/16/76	12/18/76	94	0.0
12/19/76	12/19/76	1	0.098
12/20/76	12/21/76	2	0.960
12/22/76	12/22/76	1	0.658
12/23/76	12/25/76	3	0.0
12/26/76	12/26/76	1	0.201
12/27/76	12/29/76	3	0.974
12/30/76	12/31/76	2	0.815
01/01/77	02/09/77	40	0.978
02/10/77	02/10/77	1	0.594
02/11/77	04/10/77	59	0.0
04/11/77	04/11/77	1	0.569
04/12/77	07/10/77	90	0.992
07/11/77	07/11/77	1	0.813
07/12/77	07/23/77	12	0.0
07/24/77	07/24/77	1	0.315
07/25/77	08/12/77	19	0.998
08/13/77	08/13/77	1	0.002
08/14/77	08/14/77	1	0.646
08/15/77	09/08/77	25	0.999
09/09/77	09/09/77	1	0.874

Table A-2

SURRY 2, CYCLE 4 REACTOR OPERATING HISTORY

Dates, mo/da/yr		Elapsed Time,	Reactor Power Level,
From	To	days	Fraction of 2441 MWth
10/09/77	10/11/77	3	0.019
10/12/77	10/12/77	1	0.539
10/13/77	10/13/77	1	0.868
10/14/77	11/17/77	35	0.990
11/18/77	11/18/77	1	0.109
11/19/77	11/26/77	8	0.0
11/27/77	11/28/77	2	0.565
11/29/77	03/19/78	111	0.987
03/20/78	04/07/78	19	0.0
04/03/78	04/08/78	1	0.185
04/09/78	05/23/78	45	1.000
05/24/78	05/24/78	1	0.613
05/25/78	05/29/78	5	0.0
05/30/78	05/30/78	1	0.884
05/31/78	07/06/78	37	0.989
07/07/78	07/07/78	1	0.039
07/08/78	07/31/78	24	0.0
08/01/78	08/02/78	2	0.482
08/03/78	09/29/78	58	0.997
09/30/78	10/04/78	5	0.846
10/05/78	10/05/78	1	0.145
10/06/78	10/14/78	9	0.0
10/15/78	10/15/78	1	0.633
10/16/78	12/02/78	48	0.994
12/03/78	12/03/78	1	0.035
12/04/78	02/02/79	61	0.992
02/03/79	02/03/79	1	0.789
02/04/79	02/04/79	1	0.036

Table A-3

SURRY 2, CYCLE 5 REACTOR OPERATING HISTORY

Dates, mo/da/yr		Elapsed Time,	Reactor Power Level,
From	To	days	Fraction of 2441 MWth
08/17/80	08/19/80	3	0.077
08/20/80	08/22/80	3	0.455
08/23/80	08/23/80	1	0.128
08/24/80	08/26/80	3	0.427
08/27/80	08/28/80	2	0.287
08/29/80	08/30/80	2	0.466
08/31/80	09/01/80	2	0.624
09/02/80	09/30/80	2	0.936
09/04/80	09/08/80	5	0.653
09/09/80	10/31/80	53	0.997
11/01/80	11/02/80	2	0.592
11/03/80	03/20/81	138	0.999
03/21/81	03/22/81	2	0.461
03/23/81	04/05/81	14	0.996
04/06/81	04/06/81	1	0.683
04/07/81	04/17/81	11	0.995
04/18/81	04/18/81	1	0.064
04/19/81	04/27/81	9	0.0
04/28/81	04/28/81	1	0.758
04/29/81	05/04/81	6	0.998
05/05/81	05/06/81	2	0.573
05/07/81	06/28/81	53	0.998
06/29/81	06/30/81	2	0.795
07/01/81	07/16/81	16	0.998
07/17/81	07/18/81	2	0.556
07/19/81	08/12/81	25	0.998
08/13/81	08/13/81	1	0.779
08/14/81	09/02/81	20	0.995
09/03/81	09/09/81	7	0.0
09/10/81	09/10/81	1	0.629
09/11/81	10/10/81	30	0.993
10/11/81	10/12/81	2	0.793
10/13/81	11/06/81	25	0.996

Table A-4

SURRY 2, CYCLE 6 REACTOR OPERATING HISTORY

Dates, mo/da/yr		Elapsed Time,	Reactor Power Level,
From	To	days	Fraction of 2441 MWth
12/31/81	12/31/81	1	0.093
01/01/82	01/02/82	2	0.509
01/03/82	01/05/82	3	0.767
01/06/82	01/07/82	2	0.434
01/08/82	01/24/82	17	0.874
01/25/82	01/30/82	6	0.992
01/31/82	02/01/82	2	0.867
02/02/82	02/22/82	21	0.990
02/23/82	02/24/82	2	0.454
02/25/82	02/26/82	2	0.774
02/27/82	03/05/82	7	0.0
03/06/82	03/08/82	3	0.656
03/09/82	03/10/82	2	0.948
03/11/82	03/13/82	3	0.591
03/14/82	03/19/82	6	0.947
03/20/82	03/21/82	2	0.684
03/22/82	03/24/82	3	0.903
03/25/82	03/30/82	6	0.943
03/31/82	04/05/82	6	0.897
04/06/82	04/06/82	1	0.137
04/07/82	04/09/82	3	0.0
04/10/82	04/10/82	1	0.465
04/11/82	05/14/82	34	0.940
05/15/82	05/15/82	1	0.113
05/16/82	05/27/82	12	0.0
05/28/82	05/29/82	2	0.431
05/30/82	06/11/82	13	0.932
06/12/82	06/13/82	2	0.807
06/14/82	06/15/82	2	0.984
06/16/82	09/04/82	81	0.995
09/05/82	09/06/82	2	0.876
09/07/82	10/09/82	33	0.999
10/10/82	10/11/82	2	0.524
10/12/82	12/07/82	57	0.993
12/08/82	12/08/82	1	0.008
12/09/82	12/22/82	14	0.0
12/23/82	12/23/82	1	0.011
12/24/82	12/24/82	1	0.728
12/25/82	02/07/83	45	0.993
02/08/83	02/08/83	1	0.508

Table A-4

(CONTD)

Dates, mo/da/yr		Elapsed Time,	Reactor Power Level,
From	To	days	Fraction of 2441 MWth
02/09/83	03/03/83	23	0.996
03/04/83	03/07/83	4	0.931
03/08/83	03/16/83	9	0.996
03/17/83	03/18/83	2	0.844
03/19/83	04/11/83	24	0.991
04/12/83	04/13/83	2	0.499
04/14/83	04/15/83	2	0.996
04/16/83	04/16/83	1	0.040
04/17/83	04/24/83	8	0.0
04/25/83	04/25/83	1	0.299
04/26/83	06/19/83	55	0.997
06/20/83	06/25/83	6	0.657
06/26/83	06/29/83	4	0.885
06/30/83	06/30/83	1	0.012

Table A-5

FUEL ASSEMBLY DATA

Fuel Assembly ID No.	V05	T11	V04	T12	V08	T13	V24
Fuel Assembly ANSI No.	LM0425	LM02JR	LM041F	LM02JP	LM0428	LM02JY	LM042G
Initial Enrichment, wt%	2.91	3.11	2.91	3.11	2.91	3.11	2.91
Initial U Content, kg U	457.5	457.1	457.5	457.1	457.5	457.1	457.5
Active Fuel Length, in.	144	144	144	144	144	144	144
Burnup, MWd/MTU	31,511	35,722	31,146	35,722	31,146	35,722	31,146
Decay Heat, W[a]	1,108	1,202	1,088	1,202	1,088	1,202	1,088
Cooling Time, d[a]	1,301	1,301	1,301	1,301	1,301	1,301	1,301
Cycles Irradiated	S2C4	S2C3	S2C4	S2C3	S2C4	S2C3	S2C4
	S2C5	S2C4	S2C5	S2C4	S2C5	S2C4	S2C5
		S2C5		S2C5		S2C5	

Fuel Assembly ID No.	T03	V27	V14	T07	V11	V01	T16
Fuel Assembly ANSI No.	LM02JJ	LM0416	LM041L	LM02JL	LM042A	LM041D	LM02JN
Initial Enrichment, wt%	3.11	2.91	2.91	3.11	2.91	2.91	3.11
Initial U Content, kg U	457.1	457.5	457.5	457.1	457.5	457.5	457.1
Active Fuel Length, in.	144	144	144	144	144	144	144
Burnup, MWd/MTU	35,722	30,214	29,823	35,722	29,823	30,214	35,722
Decay Heat, W[a]	1,202	2,120	2,076	1,202	2,076	2,120	1,202
Cooling Time, d[a]	1,301	700	700	1,301	700	700	1,301
Cycles Irradiated	S2C3	S2C4	S2C4	S2C3	S2C4	S2C4	S2C3
	S2C4	S2C6	S2C6	S2C4	S2C6	S2C6	S2C4
	S2C5			S2C5			S2C5

Fuel Assembly ID No.	T08	V09	V13	T09	V25	V15	V12
Fuel Assembly ANSI No.	LM02JM	LM0423	LM0413	LM02JU	LM040H	LM042D	LM042C
Initial Enrichment, wt%	3.11	2.91	2.91	3.11	2.91	2.91	2.91
Initial U Content, kg U	457.1	457.5	457.5	457.1	457.5	457.5	457.5
Active Fuel Length, in.	144	144	144	144	144	144	144
Burnup, MWd/MTU	35,722	30,214	29,823	35,722	30,214	29,823	31,146
Decay Heat, W[a]	1,202	2,120	2,076	1,202	2,120	2,076	1,088
Cooling Time, d[a]	1,301	700	700	1,301	700	700	1,301
Cycles Irradiated	S2C3	S2C4	S2C4	S2C3	S2C4	S2C4	S2C4
	S2C4	S2C6	S2C6	S2C4	S2C6	S2C6	S2C5
	S2C5			S2C5			

[a]As of June 1, 1985.

Appendix B

TEMPERATURE AND PRESSURE MEASUREMENT UNCERTAINTIES

Appendix B

TEMPERATURE AND PRESSURE MEASUREMENT UNCERTAINTIES

Temperature measurement uncertainty is produced by the thermocouples, extension wires, and data acquisition system. Each component in the temperature measurement chain adds to the overall uncertainty. The measurement chain is shown below:

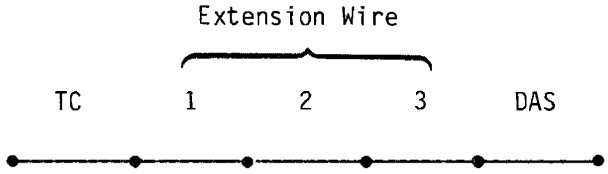

Following the derivation of Schenck (1), the overall uncertainty is equal to the square root of the sum of the squares of the individual temperature measurement uncertainties. The individual uncertainties are:

Lance Thermocouples

$T = 0.989 * T_m - 1.45$, $\sigma = \pm 0.38°C$

Vendor Specification for External Thermocouples

σ equals the maximun of $\pm 2.2°C$ or 0.75%. Because the maximum surface temperature was less than 100°C, $\sigma = \pm 2.2°C$.

Extension Wire - three segments were used for each thermocouple

σ equals the maximun of $\pm 2.2°C$ or 0.75%. Because the extension wire was near 25°C, $\sigma = \pm 2.2°C$.

Data Acquisition System

σ was estimated to be less than $\pm 1°C$.

Taking the square root of the sum of the squares of the deviations led to the following estimates of uncertainty for temperature measurements:

For the lance thermocouples,

$\sigma = \pm 4°C$

For the surface thermocouples,

$\sigma = \pm 4.5°C$.

Pressure measurements were obtained from a Leybold Heraeus model MAC 2000 pressure transducer with a 4- to 20-milliampere output. The 4- to 20-milliampere signal was fed through a precision resistor to create the signal processed by the data acquisition system. The pressure transducer was calibrated prior to use and had a precision of ±0.0112 amperes. The dropping resistor was measured to be a 249.2-ohm resistor with a precision of ±0.25 ohms. The equation relating the pressure reading from the data acquisition system to the output of the pressure transducer is of the form

$$P = 0.5017(I*R) - 500$$

where P = pressure
I = milliampere output of pressure transducer
R = resistance of dropping resistor.

Using the method of Schenck (1), the uncertainty of the pressure measurements is

$$\sigma_p^2 = (0.5017 \cdot 249.2)^2 (0.0112)^2 + (0.5017 \cdot I)^2 (0.25)^2$$

$$\sigma_p^2 = 1.9537 + 0.0157 (I^2)$$

which gives an uncertainty of ±1.5 mbar for vacuum measurements (near 0 mbar) and ±3 mbar for pressure readings in the vicinity of 600 mbar.

REFERENCE

1. H. Schenck, Jr. Theories of Engineering Experimentation. New York: McGraw-Hill, 1961, pp. 40-48

Appendix C

HEAT TRANSFER DATA

Table C-1

CORRECTED TEMPERATURE DATA FOR CASTOR-V/21 CASK PERFORMANCE TEST[a]

RUN No.	1	2	3	4	5
DATE: mo/da/yr	9/11/85	9/13/85	9/16/85	9/20/85	9/23/85
TIME: hr/min/sec	7/07/37	14/07/41	5/07/43	9/08/06	8/08/00
Orientation	Vertical	Vertical	Vertical	Horizontal	Horizontal
Backfill	Helium	Nitrogen	Vacuum	Helium	Nitrogen
PRES. mBar	488.5	558.6	2.5	549.5	579.7

Thermocouple	Temperature, °C					Elevation[b] or Radius,[c] cm	Angle, degrees[d]	Location[e]
TC1	127.7	154.5	184.5	148.7	178.4	55		A7-5
TC2	211.4	239.2	286.3	238.7	282.3	122		
TC3	254.5	280.9	316.1	264.5	309.0	242		
TC4	257.7	291.2	301.4	250.5	295.9	322		
TC5	216.5	265.8	230.2	183.0	225.5	397		
TC6	154.2	208.1	125.3	96.1	133.3	447		
TC7	119.4	126.9	252.2	198.1	235.6	55		E
TC8	196.9	178.0	352.6	306.5	325.8	122		
TC9	300.5	279.4	393.2	347.6	375.2	242		
TC10	325.4	312.3	371.6	322.6	352.1	322		
TC11	317.3	316.2	286.6	238.4	266.0	397		
TC12	246.8	251.8	156.2	111.3	166.1	447		
TC13	143.3	155.1	250.6	201.3	241.3	55		A4-5
TC14	248.1	256.5	365.7	314.0	349.2	122		

[a]Calibration equation $T_{corr} = 0.989T_{meas} - 1.8$ was used to correct lance TC readings.

[b]From exterior bottom of cask.

[c]From cask centerline.

[d]From 0° orientation mark.

[e]See Figure 3.17 for TC lance locations.

Table C-1

(CONTD)

Thermocouple	Temperature, °C					Elevation[b] or Radius,[c] cm	Angle, degrees[d]	Location[e]
TC15	328.5	332.6	403.9	350.1	388.3	242		A4-5
TC16	342.3	357.0	383.7	330.6	370.0	322		
TC17	297.0	326.5	292.6	239.9	283.9	397		
TC18	224.0	246.3	155.6	116.5	168.0	447		
TC19	163.6	182.8	243.0	184.9	237.4	55		A8-3
TC20	271.0	299.3	357.9	292.2	347.2	122		
TC21	312.8	346.2	379.7	315.0	369.2	242		
TC22	312.1	353.4	363.4	299.7	356.1	322		
TC23	256.8	316.1	274.6	214.2	268.7	397		
TC24	170.5	221.3	126.5	115.6	168.3	447		
TC25	85.4	115.8	124.3	119.6	168.0	55		F
TC26	144.3	192.1	208.2	178.8	243.9	122		
TC27	176.6	222.5	234.6	182.0	220.5	242		
TC28	140.2	214.6	218.1	171.4	223.5	322		
TC29	155.3	225.3	167.0	133.8	174.6	397		
TC30	142.8	205.1	106.5	97.0	145.3	447		
TC31	154.3	161.5	254.7	196.8	245.0	55		A5-3
TC32	265.4	271.6	371.1	313.1	352.5	122		
TC33	328.8	338.7	399.9	342.9	384.1	242		
TC34	335.4	358.0	380.4	321.8	364.7	322		
TC35	286.9	333.4	290.4	231.9	275.9	397		

[a]Calibration equation $T_{corr} = 0.989T_{meas} - 1.8$ was used to correct lance TC readings.

[b]From exterior bottom of cask.

[c]From cask centerline.

[d]From 0° orientation mark.

[e]See Figure 3.17 for TC lance locations.

Table C-1

(CONTD)

Thermocouple	Temperature, °C					Elevation[b] or Radius,[c] cm	Angle, degrees[d]	Location[e]
TC36	194.8	257.9	144.8	96.2	162.4	447		A5-3
TC37	133.4	146.4	263.3	202.8	249.2	55		A1-3
TC38	233.6	247.3	374.6	319.4	350.8	122		
TC39	329.5	330.9	414.1	360.5	394.5	242		
TC40	346.8	358.0	391.9	336.2	370.2	322		
TC41	313.2	337.4	306.6	243.5	282.2	397		
TC42	195.9	223.2	164.8	102.1	155.3	447		
TC43	133.5	144.1	263.1	206.9	252.6	55		A1-1
TC44	229.3	236.9	368.0	316.3	348.1	122		
TC45	323.7	323.1	408.2	356.4	391.4	242		
TC46	343.7	351.0	385.2	333.9	369.4	322		
TC47	309.7	331.1	299.0	242.9	283.3	397		
TC48	196.3	236.8	164.7	125.6	160.7	447		
TC49	150.3	157.5	253.1	195.9	239.7	55		C5-2
TC50	258.7	265.5	364.7	309.1	345.1	122		
TC51	324.8	335.8	399.5	342.7	380.4	242		
TC52	333.5	356.8	380.4	321.8	357.5	322		
TC53	285.7	331.8	289.9	225.2	267.1	397		
TC54	200.7	260.7	137.5	97.7	128.5	447		
TC55	129.9	157.3	190.4	151.1	183.8	55		B7-4

[a]Calibration equation $T_{corr} = 0.989T_{meas} - 1.8$ was used to correct lance TC readings.

[b]From exterior bottom of cask.

[c]From cask centerline.

[d]From 0° orientation mark.

[e]See Figure 3.17 for TC lance locations.

Table C-1

(CONTD)

Thermocouple	Temperature, °C					Elevation[b] or Radius,[c] cm	Angle, degrees[d]	Location[e]
TV56	212.4	239.2	289.6	235.4	273.5	122		B7-4
TC57	256.7	280.2	317.5	257.6	296.2	242		↓
TC58	258.6	292.6	302.0	243.0	277.6	322		
TC59	213.9	265.9	230.8	169.9	204.5	397		
TC60	153.9	215.5	123.0	85.5	107.3	447		
TC61	64.6	61.3	69.9	66.0	67.8	175	0	SIDE
TC62	68.3	64.7	73.9	68.0	69.9	460	353	↓
TC63	75.5	70.1	82.1	76.5	76.9	1148	0	
TC64	71.7	65.8	79.4	72.2	73.5	1130	↓	
TC65	81.6	74.1	86.8	77.5	77.5	2348		
TC66	74.8	69.0	79.2	71.4	72.0	2330		
TC67	81.7	76.1	82.9	73.3	73.0	3148		
TC68	74.7	68.0	75.8	67.6	66.9	3130		
TC69	78.1	74.9	74.0	64.4	66.6	3898		
TC70	76.5	77.9	68.5	54.4	56.7	4380		
TC71	76.6	75.5	66.8	57.3	59.1	4621		
TC72	72.1	65.9	77.6	66.0	67.1	1148	45	
TC73	78.2	69.9	78.2	62.4	60.2	2348	↓	
TC74	79.2	79.0	73.0	62.2	62.0	3898		
TC75	75.8	66.7	81.2	73.7	71.1	1148	180	↓

[a]Calibration equation $T_{corr} = 0.989T_{meas} - 1.8$ was used to correct lance TC readings.

[b]From exterior bottom of cask.

[c]From cask centerline.

[d]From 0° orientation mark.

[e]See Figure 3.17 for TC lance locations.

Table C-1

(CONTD)

Thermocouple	Temperature, °C					Elevation[b] or Radius,[c] cm	Angle, degrees[d]	Location[e]
TC76	84.6	75.9	88.2	80.7	75.9	2348	180	SIDE
TC77	79.5	72.1	83.0	76.3	71.5	2330	↓	↓
TC78	81.6	75.7	75.5	64.1	61.3	3880	↓	↓
TC79	78.5	68.4	74.3	65.5	61.3	2348	225	↓
TC80	93.3	69.4	87.1	78.7	74.1	3898	225	↓
TC81	71.2	63.1	78.6	69.5	67.9	1148	270	↓
TC82	81.4	61.1	86.1	73.4	71.5	2348	↓	↓
TC83	78.9	68.6	77.7	65.2	63.7	3898	↓	↓
TC84	97.5	102.3	69.1	66.4	70.2	487	0	LID
TC85	74.1	78.0	65.3	51.2	52.8	1100	0	↓
TC86	102.9	111.7	73.4	60.1	64.8	487	90	↓
TC87	74.5	77.6	65.8	51.2	50.9	1100	90	↓
TC88	105.3	108.8	67.9	63.5	69.0	0	↓	↓
TC89	43.1	77.2	65.6	51.3	49.9	1100	180	↓
TC90	24.9	24.8	23.8	68.2	69.7	487	0	BOTTOM
TC91	26.5	23.6	24.8	62.9	66.8	1100	0	↓
TC92	--	--	--	69.2	68.9	487	90	↓
TC93	--	--	--	24.2	63.9	1100	90	↓
TC94	--	--	--	68.4	69.0	0	↓	↓
TC95	--	--	--	65.0	66.6	1100	180	↓
TC96	28.2	24.0	26.0	23.9	23.9		↓	AMBIENT

[a]Calibration equation $T_{corr} = 0.989T_{meas} - 1.8$ was used to correct lance TC readings.

[b]From exterior bottom of cask.

[c]From cask centerline.

[d]From 0° orientation mark.

[e]See Figure 3.17 for TC lance locations.

Appendix D

DOSE RATE DATA

Table D-1

DOSIMETER RADIATION MEASUREMENTS FROM CASTOR-V/21 CASK PERFORMANCE TEST

Location				
Angle,[a] degrees	Elevation[b] or Radius,[c] mm	Exposure Time, hr	TLD Dose Rate,[d] mR/hr	TED Dose Rate,[e] mrem/hr
SIDE				
45	175	41.77	23.0	2.1
↓	480	41.77	140.0	21.0[f]
	1048	41.73	36.0	9.7
	1597	41.73	38.0	11.5
	2149	41.73	38.0	12.0
	2701	41.73	37.0	10.6
	3298	41.73	39.0	10.3
	3850	41.72	28.0	7.0
	4350	41.72	22.0	5.3
	4400	41.72	118.0	15.0
	4450	41.70	68.0	9.7
	4500	41.70	26.0	7.3
	4550	41.70	9.4	5.6
	4600	41.70	4.3	3.8
	4650	41.70	2.5	3.8
	4700	41.65	1.6	2.1
	4750	41.63	1.1	2.6
↓	4800	41.63	0.7	1.5
60	2701	41.62	31.0	13.0
75	2701	41.62	23.0	11.0
90	175	41.50	26.0	1.5
↓	480	41.50	125.0	3.5
	1048	41.48	25.0	8.7
	1597	41.48	21.0	15.0
	2149	41.45	21.0	12.0
	2701	41.43	24.0	16.0
	3298	41.43	22.0	13.0
	3850	41.43	70.0	9.8
↓	4350	41.42	79.0	11.5

[a]From 0° orientation mark.

[b]From exterior bottom of cask.

[c]From cask centerline.

[d]Gamma.

[e]Neutron.

[f]Problem with processing dosimeter.

[g]High dose rates caused by special test instrumentation.

Table D-1

(CONTD)

Location				
Angle,[a] degrees	Elevation[b] or Radius,[c] mm	Exposure Time, hr	TLD Dose Rate,[d] mR/hr	TED Dose Rate,[e] mrem/hr
90	4400	41.40	134.0	13.0
↓	4450	41.38	81.0	10.0
	4500	41.38	33.0	4.7
	4550	41.37	12.0	6.9
	4600	41.35	5.0	3.5
	4650	41.33	3.1	8.8
	4700	41.32	1.9	3.8
	4750	41.32	1.3	0.9
↓	4800	41.32	1.2	0.7
105	2701	41.33	24.0	14.0
120	2701	41.30	31.0	9.3
72, 73	2149	21.23	23.0	15.0
73, 74	2149	21.23	24.0	17.0
74, 75	2149	21.23	23.0	14.0
75, 76	2149	21.23	22.0	11.0
76, 77	2149	21.23	25.0	13.0
77, 78	2149	21.23	24.0	7.0
Trunnion, 90	--	17.50	19.0	8.1
Trunnion, 90	--	17.48	42.0	27.0
TOP				
45	203	41.30	32.5	44.0
↓	406	41.28	43.0	35.0
	585	41.20	26.0	32.0
	928	41.20	6.4	5.1
↓	1100	41.18	1.0	1.3
90	170	41.18	30.0	44.0
↓	340	41.17	36.0	36.0
	487	41.15	29.5	32.0
↓	634	41.12	29.0	27.0

[a]From 0° orientation mark.

[b]From exterior bottom of cask.

[c]From cask centerline.

[d]Gamma.

[e]Neutron.

[f]Problem with processing dosimeter.

[g]High dose rates caused by special test instrumentation.

Table D-1

(CONTD)

Location		Exposure Time, hr	TLD Dose Rate,[d] mR/hr	TED Dose Rate,[e] mrem/hr
Angle,[a] degrees	Elevation[b] or Radius,[c] mm			
90	706	41.05	22.0	19.0
↓	780	41.07	56.0	16.0
	854	41.07	9.2	2.3
	928	41.07	2.5	3.1[f]
	985	41.05	3.1	0.2
	1042	41.03	1.6	0.7
	1100	40.95	1.0	1.4
↓	0	40.95	40.0	44.0
Fill valve	--	17.57	196.0	30.0
Hole at 180	--	17.52	32.0	13.0
BOTTOM				
90	0	23.53	22.0	41.0
45	203	23.53	17.5	33.0
↓	406	23.48	25.0	22.0
	585	23.45	25.0	19.0
	928	23.42	18.0	3.1
↓	1100	23.40	3.4	--
90	170	23.42	18.0	31.0
↓	340	23.40	24.0	25.0
	487	23.40	22.0	23.0
	634	23.38	20.0	21.0
	928	23.30	26.0	--
↓	1100	23.30	7.0	1.6

[a]From 0° orientation mark.

[b]From exterior bottom of cask.

[c]From cask centerline.

[d]Gamma.

[e]Neutron.

[f]Problem with processing dosimeter.

[g]High dose rates caused by special test instrumentation.

Table D-2

PNL RADIATION SURVEY INSTRUMENT MEASUREMENTS
FROM CASTOR-V/21 CASK PERFORMANCE TEST

Location		Exterior Surface Dose Rates, mrem/hr	
Angle,[a] degrees	Elevation[b] or Radius,[c] mm	Gamma[d]	Neutron[e]
SIDE			
90	175	5	1
↓	480	110	1
	1048	25	6
	1597	26	8
	2149	22	8
	2701	22	9
	3298	21	7
	3850	60	11
	4400	11	12
↓	4800	4	9
45	2701	34	8
60	↓	31	6
75		24	7
105		23	8
120	↓	31	7
TOP			
	centerline	37	45
45	406	36	--
45	1100	12	--
90	340	35	40
90	634	29	30
90	1100	18	5
BOTTOM			
	centerline	21	50
45	406	24	40
45	1100	14	4
90	340	24	40
90	634	21	20
90	1100	18	5

[a] From 0° orientation mark.

[b] From exterior bottom of cask.

[c] From cask centerline.

[d] With an Eberline RO-3B.

[e] With a SNOOPY.

Table D-3

INEL RADIATION SURVEY INSTRUMENT MEASUREMENTS
FROM CASTOR-V/21 CASK PERORMANCE TEST

Location		Dose Rate, mrem/hr	
Angle,[a] degrees	Elevation[b] or Radius,[c] mm	Gamma[d]	Neutron[e]
SIDE			
45	175	60	3
↓	480	140	3
	1048	40	4
	1597	44	5
	2149	45	10
	2701	45	15
	3298	44	10
	3850	32	10
	4350	22	15
	4400	110	15
	4450	110	15
	4500	110	15
	4550	18	15
	4600	18	15
	4650	18	15
	4700	3	15
	4750	3	15
↓	4800	3	15
60	2701	35	10
75	2701	29	10
90	175	70	3
↓	480	140	3
	1048	30	10
	1597	25	10
	2149	40	20
	2701	28	20
	3298	28	15
	3850	8	10
↓	4350	80	20

[a]From 0° orientation mark.

[b]From exterior bottom of cask.

[c]From cask centerline.

[d]With an Eberline RO-3A.

[e]With an Eberline PNR-4.

Table D-3

(CONTD)

Location		Dose Rate, mrem/hr	
Angle,[a] degrees	Elevation[b] or Radius,[c] mm	Gamma[d]	Neutron[e]
90	4400	38	18
↓	4450	16	15
	4500	10	15
	4550	6	10
	4600	27	15
	4650	27	15
	4700	27	15
	4750	3	15
↓	4800	3	15
105	2701	31	12
120	2701	41	20
LID			
45	203	44	45
↓	406	42	45
	585	35	45
	928	15	20
↓	1100	4	15
90	170	37	50
↓	340	40	50
	487	34	40
	634	30	40
	706	25	40
	780	30	40
	854	8	10
	928	8	10
	985	3	10
	1042	3	10
	1100	2	5
↓	centerline	40	70

[a] From 0° orientation mark.

[b] From exterior bottom of cask.

[c] From cask centerline.

[d] With an Eberline RO-3A.

[e] With an Eberline PNR-4.

Table D-3

(CONTD)

Location		Dose Rate, mrem/hr	
Angle,[a] degrees	Elevation[b] or Radius,[c] mm	Gamma[d]	Neutron[e]
BOTTOM			
	centerline	26	70
45	203	22	50
↓	406	30	50
↓	585	29	45
↓	928	13	25
↓	1100	8	5
90	170	25	55
↓	340	30	50
↓	487	25	40
↓	634	22	35
↓	928	20	4
↓	1100	9	4

[a]From 0° orientation mark.

[b]From exterior bottom of cask.

[c]From cask centerline.

[d]With an Eberline RO-3A.

[e]With an Eberline PNR-4.

Table D-4

INEL RADIATION SURVEY INSTRUMENT MEASUREMENTS AT THE CASTOR-V/21 SURFACE AND 1 M AND 2 M FROM THE CASK

Location		Dose Rate, mrem/hr					
		Surface		1 m		2 m	
Angle,[a] degrees	Elevation or Radius	Gamma[d]	Neutron[e]	Gamma[d]	Neutron[e]	Gamma[d]	Neutron[e]
SIDE							
0	L/2[b]	15	20	2	10	1	6
45		5	34	3	14	3	7
90		15	20	4	11	2	6
180		5	20	3	12	2	7
225		4	34	4	14	2	9
270		5	18	3	10	2	7
LID							
--	centerline	40	290	15	160	3	60
--	R/2[c]	30	38	15	25	3	45
--	R	10	3	5	8	3	7

[a]From 0° orientation mark.

[b]L - CASTOR-V/21 cask total length.

[c]R - CASTOR-V/21 cask outer radius excluding fins.

[d]With an Eberline RO-3A.

[e]With an Eberline PNR-4.

[f]High dose rates caused by special test instrumentation.